Current data are consistent with flat spatial hypersurfaces in the ΛCDM cosmological model but favor more lensing than the model predicts

Javier de Cruz Pérez,[1,*] Chan-Gyung Park,[2,†] and Bharat Ratra[1,‡]

[1]Department of Physics, Kansas State University, 116 Cardwell Hall, Manhattan, Kansas 66506, USA
[2]Division of Science Education and Institute of Science Education, Jeonbuk National University, Jeonju 54896, Republic of Korea

(Received 8 November 2022; accepted 14 February 2023; published 17 March 2023)

We study the performance of three pairs of tilted, and a pair of untilted, Λ cold dark matter (ΛCDM) cosmological models, with three of these four pairs allowing for nonflat spatial hypersurfaces, against cosmic microwave background (CMB) temperature and polarization power spectrum data (P18), measurements of the Planck 2018 lensing potential power spectrum (lensing), and a large compilation of non-CMB data (non-CMB). For the eight models, we measure cosmological parameters and study whether or not pairs of the datasets (as well as subsets of them) are mutually consistent in these models. Half of these models allow the lensing consistency parameter A_L, which rescales the gravitational potential power spectrum, to be an additional free parameter to be determined from data, while the other three have $A_L = 1$ which is the theoretically expected value. The pair of untilted nonflat ΛCDM models are incompatible with P18 data. The tilted spatially flat models assume the usual primordial spatial inhomogeneity power spectrum that is a power law in wave number. The tilted nonflat models assume either the primordial power spectrum used in the Planck group analyses [Planck $P(q)$], which has recently been numerically shown to be a good approximation to what is quantum-mechanically generated from a particular choice of closed inflation model initial conditions, or a recently computed power spectrum [new $P(q)$] that quantum-mechanically follows from a different set of nonflat inflation model initial conditions. In the tilted nonflat models with $A_L = 1$, we find differences between P18 data and non-CMB data cosmological parameter constraints, which are large enough to rule out the Planck $P(q)$ model at 3σ but not the new $P(q)$ model. No significant differences are found when cosmological parameter constraints obtained with two different datasets are compared within the standard tilted flat ΛCDM model. While both P18 data and non-CMB data separately favor a closed geometry, with spatial curvature density parameter $\Omega_k < 0$, when P18 + non-CMB data are jointly analyzed the evidence in favor of nonflat hypersurfaces subsides. Differences between P18 data and non-CMB data cosmological constraints subside when A_L is allowed to vary. From the most restrictive P18 + lensing + non-CMB data combination, we get almost model-independent constraints on the cosmological parameters and find that the $A_L > 1$ option is preferred over the $\Omega_k < 0$ one, with the A_L parameter, for all models, being larger than unity by $\sim 2.5\sigma$. According to the deviance information criterion, in the P18 + lensing + non-CMB analysis, the varying A_L option is on the verge of being strongly favored over the $A_L = 1$ one, which could indicate a problem for the standard tilted flat ΛCDM model. These data are consistent with flat spatial hypersurfaces but more and better data could improve the constraints on Ω_k and might alter this conclusion. Error bars on some cosmological parameters are significantly reduced when non-CMB data are used jointly with P18 + lensing data. For example, in the tilted flat ΛCDM model for P18 + lensing + non-CMB data, the Hubble constant $H_0 = 68.09 \pm 0.38$ km s^{-1} Mpc^{-1}, which is consistent with that from a median statistics analysis of a large compilation of H_0 measurements, as well as with a number of local measurements of the cosmological expansion rate. This H_0 error bar is 31% smaller than that from P18 + lensing data alone.

DOI: 10.1103/PhysRevD.107.063522

I. INTRODUCTION

General relativity is the current best description of gravity on cosmological scales. In general relativity, gravity is responsible for the observed expansion of the Universe and can be sourced by nonrelativistic (cold dark and baryonic) matter, relativistic radiation/matter, a

*decruz@phys.ksu.edu
†park.chan.gyung@gmail.com
‡ratra@phys.ksu.edu

cosmological constant (or a dynamical dark energy density), and the curvature of space. In an influential 1932 paper, Einstein and de Sitter [1] noted that available data then were unable to measure spatial curvature and so decided to study whether a spatially flat cosmological model was observationally consistent. They acknowledged that the cosmological model had to be dynamical, so Einstein's original argument for a cosmological constant —to make the Universe static—was no longer valid, and so the cosmological constant did not have to be included in this Einstein–de Sitter model. They ignored relativistic radiation/matter in this model (which was not under discussion then and is known to be negligible at late times when the model was meant to be applicable). This Einstein–de Sitter model only included nonrelativistic (and then only baryonic) matter.

A little over half a century later, motivated by observations indicating a lower than critical nonrelativistic matter energy density and the first inflation model, an improved standard model, the spatially flat Λ cold dark matter (ΛCDM) model, was proposed [2]. In this model, the cosmological constant Λ, which has a time- and space-independent energy density, is the dominant contributor to the current cosmological energy budget, followed by nonrelativistic nonbaryonic cold dark matter (CDM), and then nonrelativistic baryonic matter. Like the Einstein–de Sitter model, the standard spatially flat ΛCDM model assumes vanishing spatial curvature, motivated by early models of spatially flat inflation [3–6]. Soon after, spatially nonflat, open, and closed inflation models were developed [7–9].

A decade and a half later, the observed currently accelerated cosmological expansion, discovered from type Ia supernova (SNIa) measurements [10,11], greatly strengthened support for a cosmological constant or a dynamical dark energy density that slowly varied in time and space [12,13]—if general relativity is an accurate model for gravity on cosmological length scales—and for the spatially flat ΛCDM model or a model close to it. For reviews of the current situation, see Refs. [14–16].

A half-decade prior to the first SNIa observations indicating currently accelerated cosmological expansion, evidence for a lower than critical value of nonrelativistic matter density, along with the development of an open inflation model [7], led to some discussion of an open CDM model [17–23]. However, with cosmic microwave background (CMB) observations indicating that space curvature had to be a subdominant contributor to the current cosmological energy budget [24,25] and with SNIa observations favoring a significant contribution to the energy budget from a cosmological constant, interest in open CDM models soon faded.

More recently, especially because of results from Planck CMB anisotropy data [25], there has been renewed interest in nonflat models. In these models, the current cosmological energy budget is dominated by Λ, to be consistent with the observed currently accelerated cosmological expansion, but they now have very mildly closed spatial hypersurfaces instead of open ones. This is because, from an analysis of the final Planck 2018 TT, TE, EE + lowE (hereafter P18) data that makes use of a specific primordial power spectrum (see below for a fuller discussion of these data and the power spectrum they use in this analysis), they find a spatial curvature energy density parameter value $\Omega_k = -0.044^{+0.018}_{-0.015}$ that is closed and 2.7σ away from flat [25] when Ω_k is included as an additional free parameter in the analysis. We note that, from a combination of Atacama Cosmology Telescope (ACT) and Wilkinson Microwave Anisotropy Probe CMB anisotropy data, the authors of Ref. [26] find $\Omega_k = -0.001^{+0.014}_{-0.010}$, which is 2.1σ from the P18 value and consistent with flat spatial hypersurfaces, while the South Pole Telescope (SPT) CMB anisotropy data results in $\Omega_k = 0.001^{+0.018}_{-0.019}$ [27], which is 1.7σ from the P18 value and also consistent with flat spatial hypersurfaces. Both these analyses use the primordial power spectrum used in the P18 analysis.

The above result led to the study of the so-called lensing anomaly. The trajectory of CMB photons are bent by the gravitational effect of inhomogeneities present in the mass distribution along their way to us. This statistical phenomenon, predicted by general relativity, is known as weak gravitational lensing of the CMB. When computing the predicted CMB temperature and polarization spectra in a cosmological model that are to be compared to the observed spectra, it is important to account for this effect and compute what are known as lensed CMB spectra. If we use the tilted flat ΛCDM model to measure cosmological parameter values from Planck CMB data, we can use this model, with these parameter values, to compute the expected amount of CMB weak gravitational lensing [28]. Incorrectly predicting the amount of weak lensing present in the CMB power spectra would indicate an inconsistency in the standard model when it is used to fit Planck CMB temperature and polarization anisotropy data. It turns out that this is actually the case, since an excess of CMB weak lensing is observed in the CMB power spectra, compared to what is expected in the standard model with parameter values determined from CMB data [25,29]. This is known as the lensing anomaly, since the effect is not yet thought to be statistically significant enough to reject the standard spatially flat ΛCDM model.

A number of solutions have been proposed, with two being more widely debated. The first of these is related to the aforementioned nonzero value for Ω_k in the P18 data analysis, which favors closed spatial hypersurfaces, when Ω_k is taken to be an additional free parameter, e.g., [25,30–33]. Because of the excess of CMB weak lensing found, it is desirable to have a higher value of the nonrelativistic matter energy density parameter Ω_m in order to increase the amount of gravitational lensing of CMB photons. Because of the tight constraints imposed by CMB data on this parameter, there is no room within the tilted flat ΛCDM model to do this.

By allowing nonflat spatial hypersurfaces, a closed model with $\Omega_k < 0$ can resolve this problem, since the CMB power spectra are affected by the combination $(\Omega_m + \Omega_k)h^2$, where h is the Hubble constant H_0 in units of 100 km s^{-1} Mpc^{-1}; this can be held constant by making Ω_k slightly more negative, while slightly increasing Ω_m to give more CMB weak lensing, and also slightly adjusting h. Cosmological distances also depend on spatial curvature; therefore in a nonflat cosmological model the positions of the acoustic peaks are shifted relative to the flat model case. This would not be a welcome change, since the constraints from the observed CMB power spectra are tight. This can be resolved by reducing the value of h which shifts the acoustic peaks in the opposite direction. The fact that almost the same temperature and polarization power spectra can be produced with different combinations of the cosmological parameter values points to a geometrical degeneracy between these three parameters H_0-Ω_m-Ω_k.

While the first of the more widely debated resolutions is based on a change of more conventional cosmological parameters, the second one is more phenomenological, e.g., [25,31,32,34,35]. Reference [29] introduces the lensing consistency parameter A_L, which rescales the gravitational potential power spectrum in such a way that when $A_L = 1$ we recover the theoretically predicted amount of weak lensing. If A_L is allowed to vary in the analysis, to be determined from data, when $A_L > 1$ the predicted amount of lensing is greater than the case when $A_L = 1$. In Ref. [25] when P18 data are used to analyze the tilted flat $\Lambda\text{CDM} + A_L$ model, the result is $A_L = 1.180 \pm 0.065$, which represents a 2.8σ deviation from the theoretically expected value $A_L = 1$. We emphasize, however, that the measured Planck lensing likelihood is consistent with $A_L = 1$; see Fig. 3 of Ref. [25] and Ref. [36]. We also note that from ACT CMB anisotropy data $A_L = 1.01 \pm 0.11$ [26], consistent with $A_L = 1$ and 1.3σ smaller than the P18 value, while from SPT CMB anisotropy data $A_L = 0.81 \pm 0.14$ [34], 1.4σ smaller than $A_L = 1$, and 2.4σ smaller than the P18 value.

To analyze CMB anisotropy data, one must assume a form for the primordial power spectrum of spatial inhomogeneities as a function of wave number. In the inflation scenario, zero-point quantum-mechanical fluctuations during inflation generate the spatial inhomogeneities [37–41]. In spatially flat inflation models, if the inflaton field slowly rolls down an almost flat potential energy density, the scale factor increases exponentially with time and the primordial power spectrum is almost scale invariant with hardly any tilt [42–44]. A steeper inflaton potential energy density makes the inflaton evolve more rapidly, can cause the scale factor to grow only as a power of time, and will increase the power spectral tilt [45–47].

There has been much less study of the quantum-mechanical generation of spatial inhomogeneities in nonflat inflation models. Power spectra have been derived in spatially open and closed inflation models [7–9], with a slow-rolling inflation potential energy density [18,48], but these are untilted power spectra. The power spectrum assumed in the nonflat analyses of Refs. [25,30,31] is tilted but was not derived from an inflation model computation. Very recently, a numerical study in closed inflation models that computes primordial power spectra generated for a few different, initially slow-roll, inflation initial conditions finds that it is possible to generate, in the closed case, a tilted power spectrum very close to that used in Refs. [25,30,31,49]. Also recently, a different set of initial conditions in closed and open inflation models were used to compute a different tilted power spectrum [50].

In this paper we consider cosmological models with four different power spectra. In the tilted flat ΛCDM model, we use the usual spatially flat inflation model tilted power spectrum. In the untilted nonflat ΛCDM model, we use the untilted nonflat inflation model power spectrum [18,48]. In the two different tilted nonflat ΛCDM models, we use the power spectrum assumed in Refs. [25,30,31]—which we call the Planck $P(q)$—as well as the power spectrum computed in Ref. [50], which we call the new $P(q)$. See Sec. III below for a fuller description of the four power spectra we use.

We emphasize that we use only nonflat inflation model power spectra that can be derived using a straightforward extension of the spatially flat inflation model initial conditions to the nonflat inflation case. The issue of nonflat inflation model initial conditions is more complex than the flat inflation case (see discussion in Ref. [50]), so we focus on the simplest physically consistent options, which also makes the analysis tractable. We note that a number of other power spectra have been considered in closed cosmological models, see Refs. [51–58].

A desire to measure the spatial curvature energy density parameter Ω_k provides part of the motivation for our work. The CMB anisotropy data are currently the most restrictive cosmological data, but to use these to measure Ω_k requires assumption of a primordial power spectrum for spatial inhomogeneities. Other, less-restrictive data that do not require assuming a power spectrum can also be used to measure Ω_k. These include better-established lower redshift data (that reach to $z \sim 2.3$), such as SNIa, Hubble parameter as a function of redshift $[H(z)]$, and (non-growth-rate) baryon acoustic oscillation (BAO) measurements [59–61], as well as emerging probes that reach to higher z, such as HII starburst galaxy apparent magnitude observations as a function of z that reach to $z \sim 2.5$ [62–66], quasar angular size measurements that reach to $z \sim 2.7$ [67–70], Mg II and C IV reverberation measured quasar data that reach to $z \sim 3.4$ [71–77], possibly quasar flux measurements that reach to $z \sim 7.5$ [78–87], and gamma-ray burst data that reach to $z \sim 8.2$ [88–98]. Individually these low- and intermediate-redshift datasets are only able to provide relatively weaker constraints on cosmological parameters in general, and specifically on Ω_k, compared to those from

CMB data. However, when many (or all) low- and intermediate-redshift data are analyzed jointly, they provide useful constraints on Ω_k—currently still not nearly as restrictive as the CMB ones—favoring flat spatial hypersurfaces but still allowing a small amount of spatial curvature energy density [99–101]. For other recent discussions of constraints on spatial curvature, see Refs. [102–109] and references therein, and see Refs. [110–112] and references therein for recent, more general discussions of nonflat cosmological models.

While the standard spatially flat ΛCDM cosmological model is attractive because of its simplicity—the model only has six free cosmological parameters—it is not straightforward to understand how to consistently generalize the current quantum-mechanical standard model of particle physics to one that accommodates the cosmological constant that is part of the standard ΛCDM model. Nonetheless, the standard cosmological model is consistent with a wide variety of measurements, including CMB anisotropy measurements [25], SNIa apparent magnitude observations [59], BAO data [61], $H(z)$ observations [60], and measurements of the growth of structure as a function of redshift ($f\sigma_8$). It is important to bear in mind that these data do not rule out mild evolution of the dark energy density [63,70,75,90,93,95,100,113–127] or, as discussed in detail above, mildly curved spatial hypersurfaces. These extensions, among others, might alleviate some of the issues affecting the standard spatially flat ΛCDM model, such as differences in H_0 and σ_8 values determined using different techniques [14–16]. In this paper, however, we focus our efforts on the study of the lensing anomaly and on the measurement of Ω_k.

In this paper, we study eight cosmological models (six of them are tilted models and two untilted), namely, the tilted flat ΛCDM ($+A_L$) models, the untilted nonflat ΛCDM ($+A_L$) models, the tilted nonflat ΛCDM ($+A_L$) Planck $P(q)$ models, and the tilted nonflat ΛCDM($+A_L$) new $P(q)$ models. Six of these are nonflat models, characterized by three different primordial power spectra (see Sec. III for the form of the power spectra). By using a number of cosmological models with compilations of observational data to test how well the models fit these data and to constrain the cosmological parameters of the models, we can measure, among other things, Ω_k and also determine whether the cosmological parameter constraints set by different data are model dependent or not. The datasets we employ in this work are P18 data, Planck 2018 CMB weak lensing data, non-growth-factor BAO (BAO′) data, BAO (including growth-factor) data, and non-CMB data [composed of BAO, $f\sigma_8$, $H(z)$, and SNIa data]. These data are described in more detail in Sec. II.

A brief summary of the more significant results we find follows. These assume that the datasets we use are correct and do not have unaccounted for systematic errors. The untilted nonflat ΛCDM model with and without a varying A_L parameter is not able to properly fit the P18 CMB anisotropy power spectra, due to the lack of the tilt (n_s) degree of freedom. Consequently, its performance in comparison with the tilted models turns out to be very poor. Significant evidence in favor of a closed Universe is found when P18 data are considered alone and the tilted nonflat models better fit these data than does the standard tilted flat ΛCDM model. There are disagreements between P18 data cosmological constraints and non-CMB data cosmological constraints in the context of the tilted nonflat models with $A_L = 1$, with the tilted nonflat ΛCDM Planck $P(q)$ model ruled out at 3σ. These tensions completely fade when the A_L parameter is allowed to vary. On the other hand, no significant tension is found when the cosmological parameter constraints obtained with two different datasets are compared within the standard tilted flat ΛCDM model. The most-restrictive P18 + lensing + non-CMB dataset clearly favors the varying A_L option (with $A_L > 1$) over the $A_L = 1$ one—which could be a problem for the standard tilted flat ΛCDM model—and when this dataset is utilized we get almost model-independent cosmological parameter constraints. These data are consistent with flat spatial hypersurfaces, so we conclude that current data do not favor curved geometry—but more and better data could improve the constraints on Ω_k and might alter this conclusion. We note that, even though both P18 data and non-CMB data favor closed geometry, the larger H_0 and smaller Ω_m values favored by non-CMB data (compared to those favored by P18 data) result in P18 + lensing + non-CMB data favoring flat spatial hypersurfaces. The Hubble constant value measured using these data in the tilted flat ΛCDM model is $H_0 = 68.09 \pm 0.38$ km s^{-1} Mpc^{-1}, which is consistent with that from a median statistics analysis of a large compilation of Hubble constant measurements, as well as with a number of local measurements of the cosmological expansion rate. This H_0 error bar is 31% smaller than that from P18 + lensing data alone; similarly augmenting the P18 + lensing data with our non-CMB data compilation reduces the Ω_m error bar by 33% and also reduces error bars on all the other cosmological parameters by smaller amounts.

The layout of our paper is as follows. In Sec. II, we detail the observational datasets we employ to test the different cosmological models. In Sec. III, we describe the cosmological models and primordial power spectra we study and summarize the methods we use in our analyses. We dedicate Sec. IV to discuss in detail the results obtained by testing the different cosmological models against the several datasets we consider. In this section we also utilize different statistical estimators to compare the performance of the models in fitting data and to study possible tensions between different datasets in a given model. In Sec. V, we summarize the more significant results of the previous (long) section. Finally, in Sec. VI, we deliver our conclusions.

II. DATA

We use CMB anisotropy data and non-CMB data to constrain cosmological parameters, to determine how well the cosmological models we study fit these data, and to study how mutually consistent these datasets are in each of the cosmological models. We now list the datasets we use.

A. P18

Planck 2018 CMB temperature anisotropy data together with polarization data and their corresponding cross-spectra (TT, TE, EE + lowE) [25], which contain TT power spectra at low ℓ ($2 \leq \ell \leq 29$) and high ℓ ($30 \leq \ell \leq 2508$) —where ℓ is multipole number, TE data at high ℓ ($30 \leq \ell \leq 1996$), and EE data at low ℓ ($2 \leq \ell \leq 29$) and high ℓ ($30 \leq \ell \leq 1996$). We use the Planck 2018 baseline `Plik` $\ell \geq 30$ likelihood, which is described in Sec. 2.2.1 of Ref. [25].

B. (P18) lensing

Planck 2018 lensing potential power spectrum, see Sec. 2.3 of Ref. [25] or Sec. 2 of Ref. [36] for more details.

C. BAO′

Twelve BAO data points from both anisotropic and isotropic BAO estimators that probe the redshift range $0.122 \leq z \leq 2.334$ [128–134]. These are BAO data with growth rates excluded from the original papers and are listed, along with the appropriate covariance matrices, in Sec. 3 of Ref. [101].

D. BAO

An extension of the BAO′ data described above that also probe the redshift range $0.122 \leq z \leq 2.334$, but now include the correlated growth rate ($f\sigma_8$) data points provided in Refs. [128–131]. Table I lists these BAO data points.

The quantities listed in Table I include transverse comoving distance at redshift z,

$$D_M(z) = (1+z)D_A(z), \tag{1}$$

where $D_A(z)$ is the angular size distance at z,

TABLE I. BAO measurements.[a]

$z_{\rm eff}$	Measurement	References
0.122	$D_V(r_{d,\rm fid}/r_d)\,(\rm Mpc) = 539 \pm 17\,(\rm Mpc)$	[132]
0.38	$D_M/r_d = 10.274 \pm 0.151$	[128]
0.38	$D_H/r_d = 24.888 \pm 0.582$	[128]
0.51	$D_M/r_d = 13.381 \pm 0.179$	[128]
0.51	$D_H/r_d = 22.429 \pm 0.482$	[128]
0.38	$f\sigma_8 = 0.49729 \pm 0.04508$	[128]
0.51	$f\sigma_8 = 0.45902 \pm 0.03784$	[128]
0.698	$D_M/r_d = 17.646 \pm 0.302$	[128,129]
0.698	$D_H/r_d = 19.770 \pm 0.469$	[128,129]
0.698	$f\sigma_8 = 0.47300 \pm 0.04429$	[128,129]
0.81	$D_A/r_d = 10.75 \pm 0.43$	[133]
1.48	$D_M/r_d = 30.21 \pm 0.79$	[130,131]
1.48	$D_H/r_d = 13.23 \pm 0.47$	[130,131]
1.48	$f\sigma_8 = 0.462 \pm 0.045$	[130,131]
2.334	$D_M/r_d = 37.5^{+1.2}_{-1.1}$	[134]
2.334	$D_H/r_d = 8.99^{+0.20}_{-0.19}$	[134]

[a]Note: For the data point at $z = 0.122$ the sound horizon size (at the drag epoch) of the fiducial model is $r_{d,\rm fid} = 147.5$ Mpc [132].

$$D_H(z) = \frac{c}{H(z)}, \tag{2}$$

where $H(z)$ is the Hubble parameter and c is the speed of light, and the angle-averaged distance

$$D_V(z) = [czD_M^2(z)/H(z)]^{1/3}. \tag{3}$$

The measurements are provided as relative distances with respect to the radius of the sound horizon at the drag epoch redshift z_d,

$$r_d = \int_{z_d}^{\infty} \frac{c_s(z)dz}{H(z)}, \tag{4}$$

where $c_s(z)$ is the speed of sound in the photon-baryon fluid.

For BAO data from Ref. [128], the appropriate covariance matrix is now

$$\begin{pmatrix} 0.022897 & -0.02007 & 0.0026481 & 0.013487 & -0.0081402 & 0.0010292 \\ -0.02007 & 0.33849 & -0.0085213 & -0.016024 & 0.13652 & -0.0038002 \\ 0.0026481 & -0.0085213 & 0.0020319 & 0.001325 & -0.0023012 & 0.000814158 \\ 0.013487 & -0.016024 & 0.001325 & 0.032158 & -0.020091 & 0.0026409 \\ -0.0081402 & 0.13652 & -0.0023012 & -0.020091 & 0.23192 & -0.0055377 \\ 0.0010292 & -0.0038002 & 0.000814158 & 0.0026409 & -0.0055377 & 0.0014322 \end{pmatrix}, \tag{5}$$

while the covariance matrix for BAO data from Refs. [128,129] is

$$\begin{pmatrix} 0.09114 & -0.033789 & 0.0024686 \\ -0.033789 & 0.22009 & -0.0036088 \\ 0.0024686 & -0.0036088 & 0.0019616 \end{pmatrix}, \quad (6)$$

and that for BAO data from Refs. [130,131] is

$$\begin{pmatrix} 0.6227 & 0.01424 & 0.02257 \\ 0.01424 & 0.2195 & -0.007315 \\ 0.02257 & -0.007315 & 0.002020 \end{pmatrix}. \quad (7)$$

E. $f\sigma_8$

$f\sigma_8$ data points, in addition to those correlated with BAO data that are listed in Table I. These independent $f\sigma_8$ measurements are obtained either from peculiar velocity data [135–137] or from redshift space distortion analyses [138–142]. These are listed in Table II.

The combination $f(z)\sigma_8(z)$ is used to quantify the growth rate of the matter density perturbation. Here, the growth rate

$$f(z) = -(1+z)\frac{d\ln D(z)}{dz}, \quad (8)$$

where $D(z)$ is the growth function. The other function involved, $\sigma_8(z)$, is the root mean square of matter fluctuations smoothed over spheres of radius $R_8 = 8h^{-1}$ Mpc at a given value of the redshift. It is computed as

$$\sigma_8^2(z) = \int \frac{d^3k}{(2\pi)^3} P_m(z,\vec{k}) W^2(kR_8), \quad (9)$$

where $P_m(z,\vec{k})$ is the matter power spectrum and $W(kR_8)$ is the window function.

TABLE II. $f\sigma_8$ measurements.

$z_{\rm eff}$	$f\sigma_8$	References
0.02	0.398 ± 0.065	[135,136]
0.035	0.338 ± 0.027	[137]
0.1	0.376 ± 0.038	[138]
0.18	0.29 ± 0.10	[139]
0.38	0.44 ± 0.06	[140]
0.6	0.49 ± 0.12	[141]
0.86	0.46 ± 0.09	[141]
1.36	0.482 ± 0.116	[142]

F. SNIa

Apparent magnitude as a function of redshift measurements for 1048 Pantheon SNIa [59], probing the redshift range $0.01 < z < 2.3$, and 20 compressed data points, spanning the redshift range $0.015 \leq z \leq 0.7026$, representing 207 DES 3 yr SNIa [143]. The Pantheon and DES 3 yr data are independent of each other, but the data points within each sample are correlated and we account for the corresponding covariance matrices in our analyses.

G. $H(z)$

Hubble parameter measurements over the redshift range $0.070 \leq z \leq 1.965$ obtained using the differential age technique. The 31 data points employed are listed in Table 2 of Ref. [144].

Hereafter, we denote the combination of BAO, $f\sigma_8$, SNIa, and $H(z)$ datasets as the non-CMB dataset.

III. METHODS

We apply the Markov chain Monte Carlo (MCMC) method, implemented in the CAMB/CosmoMC package (version of October 2018) [145–147], to explore the parameter space of the different models under study. The CAMB program computes the matter and CMB power spectra based on the evolution of density perturbations of the matter and radiation components, and the CosmoMC program uses the MCMC method to estimate the parameter constraints that are favored by the given observational datasets. We have performed cross-checks using the CLASS/MontePython package [148,149]. In general, a good agreement between the results is obtained unless significant degeneracies between some of the fitting parameters are present. When this happens, differences in the central values are found, but the two sets of results remain compatible at 1σ due to large error bars. The inclusion of more data breaks the aforementioned degeneracies and the two sets of results then agree really well.

In this paper, we consider eight cosmological models: the tilted flat, (two) tilted nonflat, and the untilted nonflat ΛCDM models, as well as their extensions through the inclusion of the A_L parameter, for a total of eight cases. A_L is a phenomenological parameter that scales the theoretical prediction of the gravitational potential power spectrum, with its theoretical expected value being $A_L = 1$, see Ref. [29]. $A_L > 1$ causes the smoothing of acoustic peaks in the CMB angular power spectrum, and Planck CMB data tend to prefer $A_L > 1$ [25].

The tilted flat ΛCDM model is characterized by six cosmological parameters ($\Omega_b h^2$, $\Omega_c h^2$, $\theta_{\rm MC}$, τ, A_s, n_s), where Ω_b and Ω_c are the current values of nonrelativistic baryonic and cold dark matter density parameters, $\theta_{\rm MC}$ is the angular size of the sound horizon at recombination defined in the CAMB/CosmoMC program, τ is the reionization optical depth, and A_s and n_s are the amplitude and the

spectral index of the primordial scalar-type energy density perturbation power spectrum

$$P_\delta(k) = A_s\left(\frac{k}{k_0}\right)^{n_s}, \tag{10}$$

where k is wave number and the pivot scale for A_s is $k_0 = 0.05\ \mathrm{Mpc}^{-1}$. This power spectrum is generated by quantum-mechanical fluctuations during an early epoch of power-law inflation in an exponential potential energy density scalar field cosmological model with flat spatial hypersurfaces [45–47].

In the nonflat very-slow-roll (so untilted) inflation ΛCDM model, the presence of nonzero spatial curvature determines a new length scale, and the power-law part of the primordial power spectrum is not relevant. Thus, this model still has six cosmological parameters, with the spectral index n_s being replaced by the current value of the spatial curvature density parameter Ω_k. For very-slow-roll inflation in this nonflat inflation mode, the primordial power spectrum is [18,48]

$$P_\delta(q) \propto \frac{(q^2-4K)^2}{q(q^2-K)}, \tag{11}$$

where $q = \sqrt{k^2+K}$ is the wave number in a model with nonzero spatial curvature $K = -(H_0^2/c^2)\Omega_k$, and A_s is defined to be the amplitude of the power spectrum at the pivot scale k_0. This power spectrum form holds in both the open ($\Omega_k > 0$) and closed ($\Omega_k < 0$) cases, with $q|K|^{-1/2} \geq 0$ and continuous in the open case, and $q|K|^{-1/2} = 3, 4, 5\ldots$ in the closed case. It is the power spectrum used in the nonflat model analyses in Refs. [118,144,150–154].

For the tilted nonflat ΛCDM model, there are seven cosmological parameters, with Ω_k added to the six of the tilted flat ΛCDM model. In this model, it has been usual to assume, e.g., [25], a primordial power spectrum of the form

$$P_\delta(q) \propto \frac{(q^2-4K)^2}{q(q^2-K)}\left(\frac{k}{k_0}\right)^{n_s-1}, \tag{12}$$

where q (and A_s) is defined in the previous paragraph. The above expression, which we refer to as the Planck $P(q)$, is a phenomenologically modified version of the nonflat very-slow-roll untilted primordial density perturbation, given in Eq. (11), to now also allow for tilt [155]. It assumes that tilt in a nonflat space works in a way similar to how it does in flat space. This expression was known to be physically reasonable in the cases when $K = 0$ or $n_s = 1$, since Eqs. (10) and (11) are recovered, respectively, and these two expressions hold in physically consistent inflation models. Very recently, a numerical study in closed inflation models that computes primordial power spectra generated for a few different, initially slow-roll inflation initial conditions finds that it is possible to generate, in the closed case, a power spectrum very close to that given in Eq. (12) [49].

In this paper, we also study another not-necessarily very-slow-rolling nonflat (closed and open) inflation model [50]. These tilted nonflat inflation models result in a primordial power spectrum that differs from that of Eq. (12) and assumes a different inflation initial condition than those studied in Ref. [49]. For the closed and open inflation models, the resulting power spectrum

$$P_\delta(q) \propto (q^2-4K)^2|P_\zeta(A)|, \tag{13}$$

where $P_\zeta(A)$ is different in the closed and open cases. For the closed inflation model,

$$\sqrt{|P_\zeta(A)|} = \left(\frac{16\pi}{m_p^2}\right)^{1/2} Q^{1/p}\frac{(2+q_s)p}{\sqrt{\pi q_s}}\left|-1+\frac{W(A)}{p}\right|\frac{2^{-(6-4q_s+2A-W(A))/p}}{\sqrt{A}(A-1)(A+3)}\left|\frac{\Gamma(1+W(A)/p)\Gamma((2+q_s)/(2p))}{\Gamma((2+W(A))/p)}\right|, \tag{14}$$

with

$$W(A) = \sqrt{-8-4q_s+q_s^2+4A(A+2)}, \tag{15}$$

and

$$A = \frac{q}{\sqrt{|K|}} - 1. \tag{16}$$

While for the open inflation model,

$$\sqrt{|P_\zeta(A)|} = \left(\frac{16\pi}{m_p^2}\right)^{1/2} Q^{1/p}\frac{(2+q_s)p}{\sqrt{\pi q_s}}\left|-1+\frac{W(A)}{p}\right|\frac{2^{-(6-4q_s)/p+\mathrm{Re}(W(A)/p)}}{\sqrt{A}(A^2+4)}\left|\frac{\Gamma(1+W(A)/p)\Gamma((2+q_s)/(2p))}{\Gamma((2+W(A))/p)}\right|, \tag{17}$$

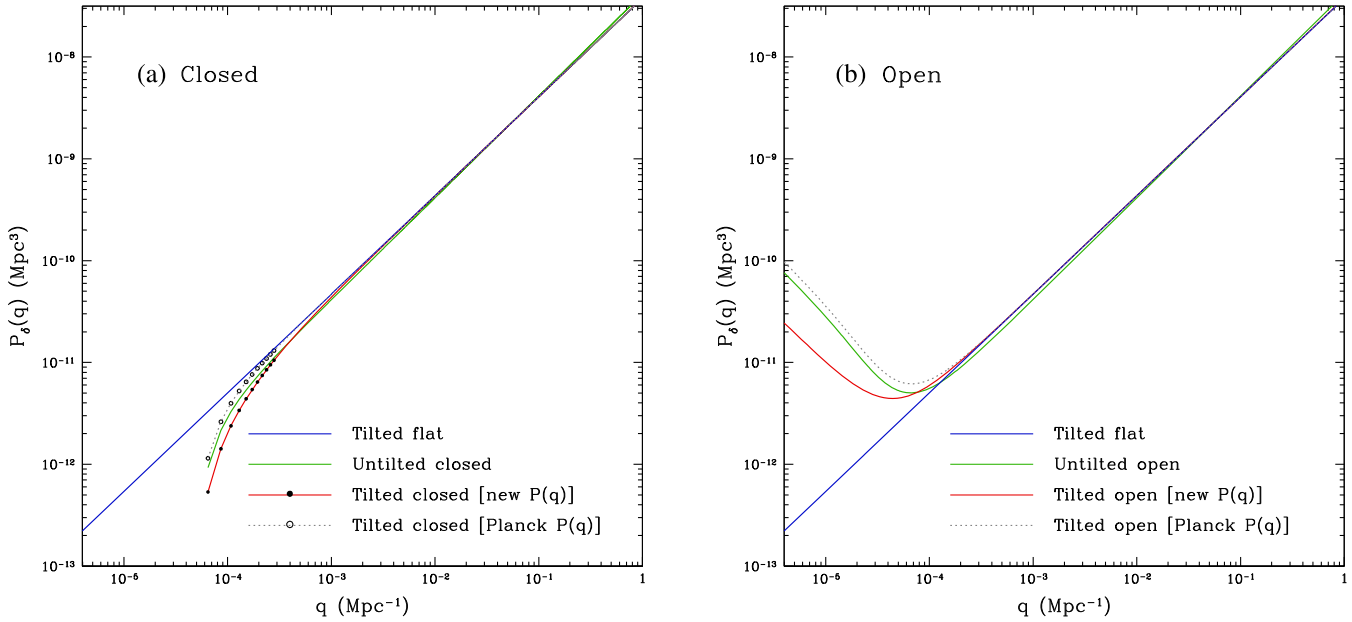

FIG. 1. Initial scalar-type perturbation power spectra of the tilted flat, untilted nonflat, and two tilted nonflat ΛCDM models [(a) for closed and (b) for open models]. For the tilted nonflat closed models, the cosmological parameters of the tilted nonflat ΛCDM model with Planck $P(q)$ constrained by using P18 + lensing data (including $\Omega_k = -0.0103$) are used (see Table VI). For closed models, the same value of A_s was assumed for all models and the same value of n_s was assumed for all tilted models. The powers at the first 11 large-scale wave numbers are indicated by the filled (open) circles for the tilted closed model with the new (Planck) $P(q)$. For open nonflat models, $\Omega_k = +0.0103$ was assumed. For the tilted flat model, the generalized wave number q is equivalent to k.

with

$$W(A) = \sqrt{-12 - 4q_s + q_s^2 - 4A^2}, \tag{18}$$

and

$$A = \frac{q}{\sqrt{|K|}}. \tag{19}$$

In these equations, $\Gamma(x)$ is the Gamma function, m_p is the Planck mass, Q is a normalization constant, $q_s = (2 - 2n_s)/(3 - n_s)$, and finally $p = 2 - q_s$. In both the closed and open inflation models, $0 < q_s < 2$, so $-\infty < n_s < 1$. In these equations, the large vertical bars indicate that we take the absolute value of the enclosed functions. In this paper, we refer to the power spectrum in this tilted nonflat ΛCDM as the new $P(q)$, which is shown in Eq. (13), and following the procedure applied to the other power spectra, A_s gives the amplitude of the new $P(q)$ at the pivot scale k_0.

Figures 1(a) and 1(b) compares the initial scalar-type perturbation spectra of the tilted flat, untilted nonflat, and two tilted nonflat models with the Planck $P(q)$ and the new $P(q)$. In this figure, we set the values of the cosmological parameters, for all the models, to the mean values of the tilted nonflat ΛCDM model with Planck $P(q)$ constrained by the P18 + lensing data (see Table VI for the parameters), except in Fig. 1(b) for the open models, where we change the sign of Ω_k.

In the cases where we include the A_L parameter in the analysis, this increases by one the number of cosmological model parameters to be determined from data; so depending on the model, we then have either seven or eight cosmological model parameters in these cases.

At the background level, the evolution of the scale factor a in all models we study is described by the Hubble function

$$H^2(a) = H_0^2[\Omega_\gamma a^{-4} + (\Omega_b + \Omega_c)a^{-3} + \Omega_k a^{-2} + \Omega_\nu(a) + \Omega_\Lambda]. \tag{20}$$

Here $a = 1/(1+z)$ is the cosmic scale factor normalized to unity at present, Ω_Λ represents the cosmological constant dark energy density parameter, Ω_γ is the current value of the CMB photon energy density parameter, and $\Omega_\nu(a)$ represents the contribution of the massless and massive neutrinos, for which it is not possible to get an analytical expression. In all cases we study, we determine the contribution of photons and massless and massive neutrinos by assuming a present CMB temperature $T_0 = 2.7255$ K, the effective number of neutrino species $N_{\rm eff} = 3.046$, and a single massive neutrino species with neutrino mass 0.06 eV. During parameter exploration using the MCMC method, we set wide flat priors on parameters in order that they do

TABLE III. Flat priors of the fitting parameters.[a]

Parameters	Our	Handley	Handley + Ω_k
$\Omega_b h^2$	[0.005, 0.1]	[0.019, 0.025]	[0.019, 0.025]
$\Omega_c h^2$	[0.001, 0.99]	[0.095, 0.145]	[0.095, 0.145]
$100\theta_{\rm MC}$	[0.5, 10]	[1.03, 1.05]	[1.03, 1.05]
τ	[0.01, 0.8]	[0.01, 0.4]	[0.01, 0.4]
Ω_k	$[-0.5, 0.5]$	$[-0.1, 0.05]$	$[-0.3, 0.15]$
n_s	[0.8, 1.2]	[0.885, 1.04]	[0.885, 1.04]
$\ln(10^{10}A_s)$	[1.61, 3.91]	[2.5, 3.7]	[2.5, 3.7]
A_L	[0, 10]	…	…

[a]Note: In almost all the computations reported in this paper we use the priors listed in the "Our" column in this table. A general exception is that, in almost all the computations in the tilted nonflat ΛCDM model with the new $P(q)$, we use a more restrictive prior range for the spectral index $0.8 \leq n_s < 1$. In addition to these choices, in all cases, for the derived parameter H_0 we restrict its range of variation to $0.2 \leq h \leq 1$. In Table XXI when only lensing data are used, in order to test the impact of different choices of priors, we also provide results for the narrower priors employed in Ref. [30] (listed in the Handley column above). The Handley + Ω_k column priors above differ from Handley priors by allowing for a broader prior for the Ω_k parameter.

not affect the parameter estimation; these priors are listed in Table III.

Because of the lack of constraining power of some of the datasets, when they are considered alone, we have to fix the values of some of the cosmological parameters in the analyses of these datasets. In BAO′, BAO, (P18) lensing, or non-CMB data alone analyses, we set the values of τ and n_s to those obtained in the P18 data alone analysis for each model. Additionally, in BAO′ data alone analyses we also fix the value of $\ln(10^{10}A_s)$, again, to the corresponding P18 data analysis value. Finally, in Sec. IV A 7, when we compare the constraints obtained from P18 + lensing data and non-CMB data, in the non-CMB data analyses the values of τ and n_s are fixed to the ones we get in the P18 + lensing data analysis for each model.

We use the converged MCMC chains to compute mean values, their confidence limits, and the posterior distributions of the model parameters with the GetDist code [156]. The MCMC chains are considered to converge when the Gelman and Rubin R statistic provided by CosmoMC becomes $R - 1 < 0.01$.

In addition to using the various combinations of datasets (see Sec. II) for constraining cosmological parameters in the models we study, we want to also determine which of these models better fit the datasets we study. For a fair comparison between competing cosmological models with different numbers of free parameters, it is necessary to be able to conveniently penalize for extra degrees of freedom. In this work, we employ two different statistical criteria that differently penalize for extra degrees of freedom to compare the performance of the models.

The first one we use is the Akaike information criterion (AIC) [157], which is defined as

$$\mathrm{AIC} = \chi^2_{\rm min} + 2n. \tag{21}$$

Here n is the number of independent cosmological parameters θ and $\chi^2_{\rm min} \equiv \chi^2(\hat{\theta}) = -2\ln\mathcal{L}(\hat{\theta})$ is the minimum value of $\chi^2(\theta) = -2\ln\mathcal{L}(\theta)$ evaluated at the best-fit cosmological parameter values $\hat{\theta}$, where $\mathcal{L}(\theta)$ is the likelihood function.

The expression in Eq. (21) is valid only for a large number of data points. According to Ref. [158], when the number of data points N obeys $N/n < 40$, the expression in Eq. (21) should be replaced by

$$\mathrm{AIC}_c = \mathrm{AIC} + \frac{2n(n+1)}{N-n-1} = \chi^2_{\rm min} + \frac{2nN}{N-n-1}. \tag{22}$$

Note that when N is large compared to n we have $N/(N-n-1) \simeq 1$ and then $\mathrm{AIC}_c \simeq \mathrm{AIC}$. This is the case for P18 data and non-CMB data but not for the BAO, BAO′, and lensing datasets. In particular, for BAO data $N = 16$, for BAO′ data $N = 12$, for the lensing dataset $N = 9$, and in all three cases $N/n < 40$ so $\mathrm{AIC}_c \neq \mathrm{AIC}$.

The second one we use is the deviance information criterion (DIC) [159], which is defined as

$$\mathrm{DIC} = \chi^2(\hat{\theta}) + 2p_D, \tag{23}$$

where $p_D = \overline{\chi^2} - \chi^2(\hat{\theta})$ is the penalization for those models with more degrees of freedom. Here an overbar represents the mean value of the corresponding quantity. Unlike the AIC, the DIC is computed from Monte Carlo posterior samples and also uses the effective number of constrained parameters by taking into account whether or not a parameter is unconstrained by data, see Refs. [159,160]. Therefore, we may say that the DIC is more reliable than the AIC.

We mostly use the differences in the AIC_c and DIC values that are defined as

$$\Delta\mathrm{AIC}_c \equiv \mathrm{AIC}_{c,\mathrm{X}} - \mathrm{AIC}_{c,\mathrm{Y}}, \tag{24}$$

$$\Delta\mathrm{DIC} \equiv \mathrm{DIC}_{\mathrm{X}} - \mathrm{DIC}_{\mathrm{Y}}. \tag{25}$$

Here Y represents the tilted flat ΛCDM model and X represents the model under study. When $-2 \leq \Delta\mathrm{AIC}_c$, $\Delta\mathrm{DIC} < 0$ there is weak evidence in favor of the model under study relative to the tilted flat ΛCDM model. If $-6 \leq \Delta\mathrm{AIC}_c, \Delta\mathrm{DIC} < -2$ there is positive evidence, whereas if $-10 \leq \Delta\mathrm{AIC}_c, \Delta\mathrm{DIC} < -6$ there is strong evidence for the model under study. Finally, if $\Delta\mathrm{AIC}_c$, $\Delta\mathrm{DIC} < -10$ there is very strong evidence in favor of the

model under study relative to the tilted flat ΛCDM model. This scale also holds when $\Delta\mathrm{AIC}_c$ and ΔDIC are positive, and then favors the tilted flat ΛCDM model over the model under study.

We also want to determine whether some of the datasets we consider are mutually consistent (or inconsistent) in a specified cosmological model, and also whether or not the dataset consistency (inconsistency) is model dependent. We utilize two different statistical estimators for this purpose. The first one makes use of DIC values and is presented in Sec. 2.1.7 of Ref. [161]. This estimator is based on

$$\mathcal{I}(D_1, D_2) \equiv \exp\left(-\frac{\mathcal{G}(D_1, D_2)}{2}\right), \tag{26}$$

where

$$\mathcal{G}(D_1, D_2) = \mathrm{DIC}(D_1 \cup D_2) - \mathrm{DIC}(D_1) - \mathrm{DIC}(D_2). \tag{27}$$

Here D_1 and D_2 represent the two datasets under comparison, $\mathrm{DIC}(D_1)$ and $\mathrm{DIC}(D_2)$ are the DIC values that result when datasets D_1 and D_2, respectively, are individually used to constrain cosmological parameters of the specified cosmological model, and $\mathrm{DIC}(D_1 \cup D_2)$ is the DIC value that results when datasets D_1 and D_2 are jointly used to constrain cosmological parameters of the specified model. The intuitive idea behind this estimator is that if two datasets are mutually consistent in a given cosmological model, which means that the cosmological parameter best-fit values determined from each dataset are approximately similar, we would have $\chi^2_{\mathrm{min}}(D_1 \cup D_2) \simeq \chi^2_{\mathrm{min}}(D_1) + \chi^2_{\mathrm{min}}(D_2)$. This would lead to negative values of $\mathcal{G}(D_1, D_2)$ [see Eq. (23)], which in turn would lead to $\mathcal{I}(D_1, D_2) > 1$. However, if $\chi^2_{\mathrm{min}}(D_1 \cup D_2) > \chi^2_{\mathrm{min}}(D_1) + \chi^2_{\mathrm{min}}(D_2)$ and is large enough, then we would find $\mathcal{I}(D_1, D_2) < 1$. Therefore, $\log_{10}\mathcal{I} > 0$ when the two datasets are mutually consistent and when $\log_{10}\mathcal{I} < 0$ the two datasets are mutually inconsistent in the cosmological model under study. Applying the Jeffreys scale, the level of consistency or inconsistency between the two datasets is substantial if $|\log_{10}\mathcal{I}| > 0.5$, is strong if $|\log_{10}\mathcal{I}| > 1$, and is decisive if $|\log_{10}\mathcal{I}| > 2$ [161].

We now summarize the second statistical estimator we utilize to determine whether two datasets are mutually consistent (or inconsistent) in a specified cosmological model. This is described in Refs. [30,55,162], also see references therein. Given a dataset D and a given model M, we can express the posterior distribution for the independent model parameters θ through the Bayes theorem

$$p(\theta|D, M) = \frac{p(D|\theta, M)p(\theta|M)}{p(D|M)}. \tag{28}$$

In the above expression $\mathcal{L}_D(\theta) \equiv p(D|\theta, M)$ is the likelihood function, $\pi(\theta) \equiv p(\theta|M)$ are the priors for the model parameters θ, $\mathcal{Z}_D \equiv p(D|M)$ represents the evidence, and $\mathcal{P}_D(\theta) \equiv p(\theta|D, M)$ is the posterior distribution. Taking advantage of the fact that $\mathcal{P}_D(\theta)$ is a probability distribution function in θ, which means that $\int \mathcal{P}_D(\theta)d\theta = 1$, we can express the evidence as

$$\mathcal{Z}_D = \int \mathcal{L}_D(\theta)\pi(\theta)d\theta. \tag{29}$$

For numerical computation of the Bayesian evidence, we apply the method described in Ref. [163]. We are interested in quantifying the tension between two independent datasets D_1 and D_2. The total likelihood from a joint analysis of both these datasets is the product of the likelihoods for each dataset, $\mathcal{L}_{12} = \mathcal{L}_1\mathcal{L}_2$. Consequently, $\mathcal{Z}_{12} = \int \mathcal{L}_1(\theta)\mathcal{L}_2(\theta)\pi(\theta)d\theta$. Here and in what follows we index quantities with "1" or "2" when they have been computed using dataset D_1 or D_2 respectively, and we use index "12" when the two datasets are jointly used. We define the Bayes ratio as

$$R_D \equiv \frac{\mathcal{Z}_{12}}{\mathcal{Z}_1\mathcal{Z}_2}. \tag{30}$$

This statistic is constructed in such a way that when $R_D \gg 1$ we can say that datasets D_1 and D_2 are consistent in the context of the particular model, while if $R_D \ll 1$ the two datasets are inconsistent. However, R_D is strongly prior dependent and to avoid this problem we instead use the suspiciousness S_D [30,55,162], which we define in the following.

To define S_D we will need the Shannon information [164],

$$\mathcal{I}_{S,D}(\theta) = \ln\frac{\mathcal{P}_D(\theta)}{\pi(\theta)}, \tag{31}$$

which is a measure of the amount of information about the parameters θ that has been gained when moving from the priors to the posterior. The average value over the posterior of the Shannon information,

$$\mathcal{D}_D = \int \mathcal{P}_D(\theta)\mathcal{I}_{S,D}(\theta)d\theta \equiv \langle\mathcal{I}_{S,D}\rangle_{\mathcal{P}_D}, \tag{32}$$

is known as the Kullback-Leibler divergence and measures how data compresses from prior to posterior. The suspiciousness S_D is defined in terms of the Bayes ratio R_D and the information ratio I_D,

$$S_D = \frac{R_D}{I_D}, \tag{33}$$

where

$$\ln(I_D) = \mathcal{D}_1 + \mathcal{D}_2 - \mathcal{D}_{12}. \quad (34)$$

By considering a Gaussian analogy, we can turn $\ln(S_D)$ into the tension probability p of two datasets being inconsistent [30,55,162],

$$p = \int_{d-2\ln(S_D)}^{\infty} \chi^2_d(x)dx = \int_{d-2\ln(S_D)}^{\infty} \frac{x^{d/2-1}e^{-x/2}}{2^{d/2}\Gamma(d/2)}dx, \quad (35)$$

where d is the Bayesian model dimensionality,

$$d = \tilde{d}_1 + \tilde{d}_2 - \tilde{d}_{12}, \quad \tilde{d}/2 = \langle \mathcal{I}^2_{S,D}\rangle_{\mathcal{P}_D} - \langle \mathcal{I}_{S,D}\rangle^2_{\mathcal{P}_D}. \quad (36)$$

If $p \lesssim 0.05$ the datasets are in moderate tension, whereas if $p \lesssim 0.003$ they are in strong tension. The value of p can be converted into a "sigma value" using the Gaussian formula

$$\sigma = \sqrt{2}\mathrm{Erfc}^{-1}(p), \quad (37)$$

where Erfc^{-1} is the inverse complementary error function. In particular, $p \lesssim 0.05$ and $p \lesssim 0.003$ correspond to 2σ and 3σ Gaussian standard deviation, respectively.

In Sec. IV C we use both these statistical estimators to examine the consistency of five pairs of data, namely, P18 and lensing, P18 and BAO, P18 and BAO′, P18 and non-CMB, and P18 + lensing and non-CMB, in the context of different cosmological models. We shall see in Sec. IV A that, when A_L is allowed to vary, error bars and two-dimensional cosmological constraint contours determined from each dataset broaden (compared to the $A_L = 1$ case) and so are mutually consistent between different datasets (even if they are not mutually consistent when $A_L = 1$). We find, in Sec. IV C, a similar improvement in consistency when A_L is allowed to vary (compared to the $A_L = 1$ case).

IV. RESULTS

A. Cosmological parameters

The cosmological parameter mean values and error bars favored by the P18, P18 + lensing, and P18 + lensing + non-CMB datasets are summarized in Tables IV–VII for the tilted flat ΛCDM ($+A_L$) models, the untilted nonflat ΛCDM ($+A_L$) models, the tilted nonflat ΛCDM ($+A_L$) models with the Planck $P(q)$, and the tilted nonflat ΛCDM ($+A_L$) models with the new $P(q)$, respectively. Likelihood distributions of cosmological parameters of the four models with $A_L = 1$ are shown in Figs. 2–4 for the P18, P18 + lensing, and P18 + lensing + non-CMB datasets, respectively. The likelihood results for these four models, but now with A_L allowed to vary, are shown in Figs. 5–7. Figures 8–15 show, in each of the eight cosmological

TABLE IV. Mean and 68.3% confidence limits of tilted flat ΛCDM ($+A_L$) model parameters constrained by TT, TE, EE + lowE (P18), P18 + lensing, and P18 + lensing + non-CMB datasets. H_0 has units of km s^{-1} Mpc^{-1}.

	Tilted flat ΛCDM model		
Parameter	P18	P18 + lensing	P18 + lensing + non-CMB
$\Omega_b h^2$	0.02236 ± 0.00015	0.02237 ± 0.00014	0.02250 ± 0.00013
$\Omega_c h^2$	0.1202 ± 0.0014	0.1200 ± 0.0012	0.11838 ± 0.00083
$100\theta_{\rm MC}$	1.04090 ± 0.00031	1.04091 ± 0.00031	1.04110 ± 0.00029
τ	0.0542 ± 0.0079	0.0543 ± 0.0073	0.0569 ± 0.0071
n_s	0.9649 ± 0.0043	0.9649 ± 0.0041	0.9688 ± 0.0036
$\ln(10^{10}A_s)$	3.044 ± 0.016	3.044 ± 0.014	3.046 ± 0.014
H_0	67.28 ± 0.61	67.34 ± 0.55	68.09 ± 0.38
Ω_m	0.3165 ± 0.0084	0.3155 ± 0.0075	0.3053 ± 0.0050
σ_8	0.8118 ± 0.0074	0.8112 ± 0.0059	0.8072 ± 0.0058
	Tilted flat ΛCDM + A_L model		
Parameter	P18	P18 + lensing	P18 + lensing + non-CMB
$\Omega_b h^2$	0.02259 ± 0.00017	0.02251 ± 0.00017	0.02258 ± 0.00014
$\Omega_c h^2$	0.1180 ± 0.0015	0.1183 ± 0.0015	0.11747 ± 0.00091
$100\theta_{\rm MC}$	1.04114 ± 0.00032	1.04109 ± 0.00032	1.04118 ± 0.00029
τ	0.0496 ± 0.0082	0.0487 ± 0.0087	0.0476 ± 0.0085
n_s	0.9710 ± 0.0050	0.9695 ± 0.0048	0.9715 ± 0.0038
$\ln(10^{10}A_s)$	3.030 ± 0.017	3.028 ± 0.018	3.023 ± 0.018
A_L	1.181 ± 0.067	1.073 ± 0.041	1.089 ± 0.035
H_0	68.31 ± 0.71	68.14 ± 0.69	68.52 ± 0.42
Ω_m	0.3029 ± 0.0093	0.3048 ± 0.0091	0.2998 ± 0.0053
σ_8	0.7997 ± 0.0088	0.7996 ± 0.0089	0.7955 ± 0.0075

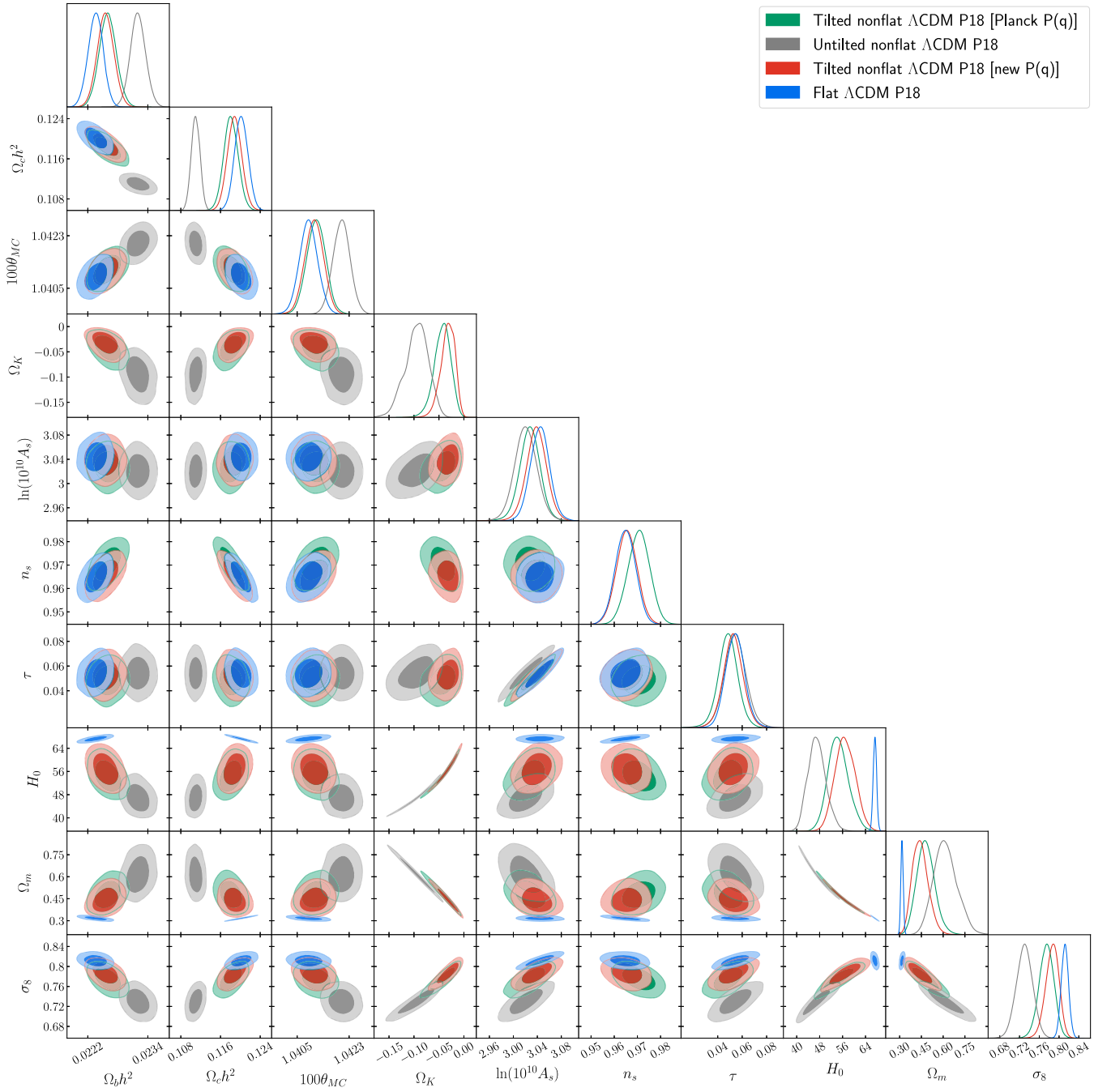

FIG. 2. Planck 2018 TT, TE, EE + lowE (P18) data likelihood distributions of parameters of the tilted nonflat ΛCDM model with the new initial power spectrum [new $P(q)$] (red contours), of the tilted nonflat ΛCDM model with the Planck team's initial spectrum [Planck $P(q)$] (green), of the untilted nonflat ΛCDM model (gray), and of the tilted flat ΛCDM model (blue contours).

models we study, the cosmological parameter constraints for P18, P18 + lensing, and P18 + lensing + non-CMB data, to illustrate how the cosmological parameter constraints change as we include more data. These results are discussed in Secs. IV A 1–IV A 4. In the third paragraph of Sec. IV C, we briefly discuss some cosmological parameter constraints from (P18) lensing only data and in Sec. V we discuss whether P18, P18 + lensing, P18 + non-CMB, and P18 + lensing + non-CMB data cosmological parameter constraints are model independent or not.

Our results may indicate tensions between some of the CMB datasets and some non-CMB low-redshift data in the context of the nonflat models. Tension between P18 data and BAO′/BAO data in the tilted nonflat ΛCDM Planck $P(q)$ model has been noted in Refs. [30,31,165] (our updated BAO′/BAO data differ from those used in these

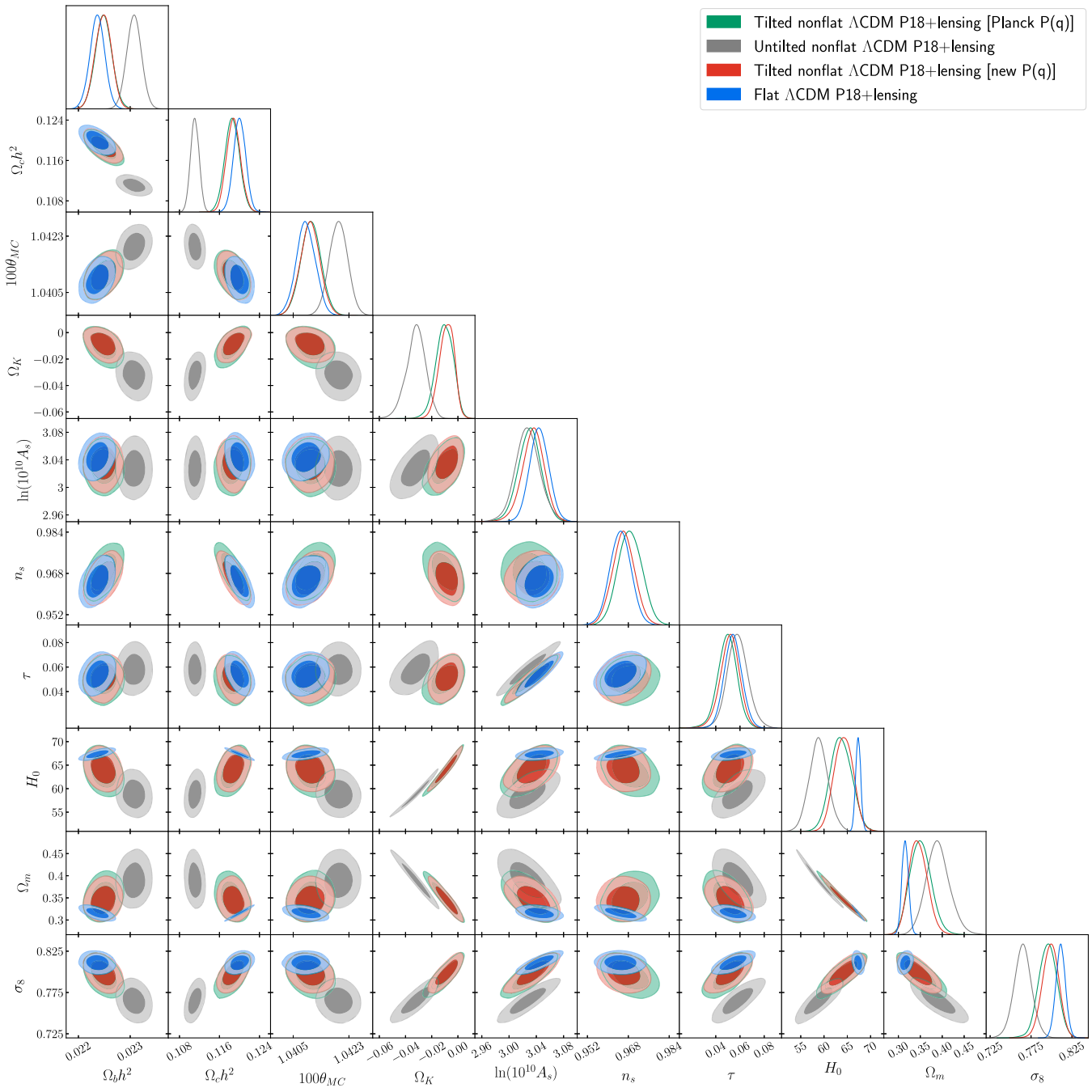

FIG. 3. P18 + lensing data likelihood distributions of parameters of the tilted nonflat ΛCDM model with the new initial power spectrum [new $P(q)$] (red contours), of the tilted nonflat ΛCDM model with the Planck team's initial spectrum [Planck $P(q)$] (green), of the untilted nonflat ΛCDM model (gray), and of the tilted flat ΛCDM model (blue contours).

references, see Sec. II). Here we want to check whether this tension is observed for our updated BAO′/BAO data, whether it is observed in the context of the other models we study, and how this tension is affected when we allow the A_L parameter to vary. In addition to the P18 vs BAO′/BAO comparison, we also compare P18 data and non-CMB data, as well as P18 + lensing and non-CMB data. These comparisons are discussed in Sec. IV A 5–IV A 7.

We now discuss the results obtained from the different datasets we consider.

1. P18 data cosmological constraints

In the case of the tilted flat ΛCDM model, with just six primary (not derived) cosmological parameters, and with $\Omega_k = 0$, from P18 data alone (see Table IV, Figs. 2 and 5) the derived parameters $\Omega_m = 0.3165 \pm 0.0084$ and

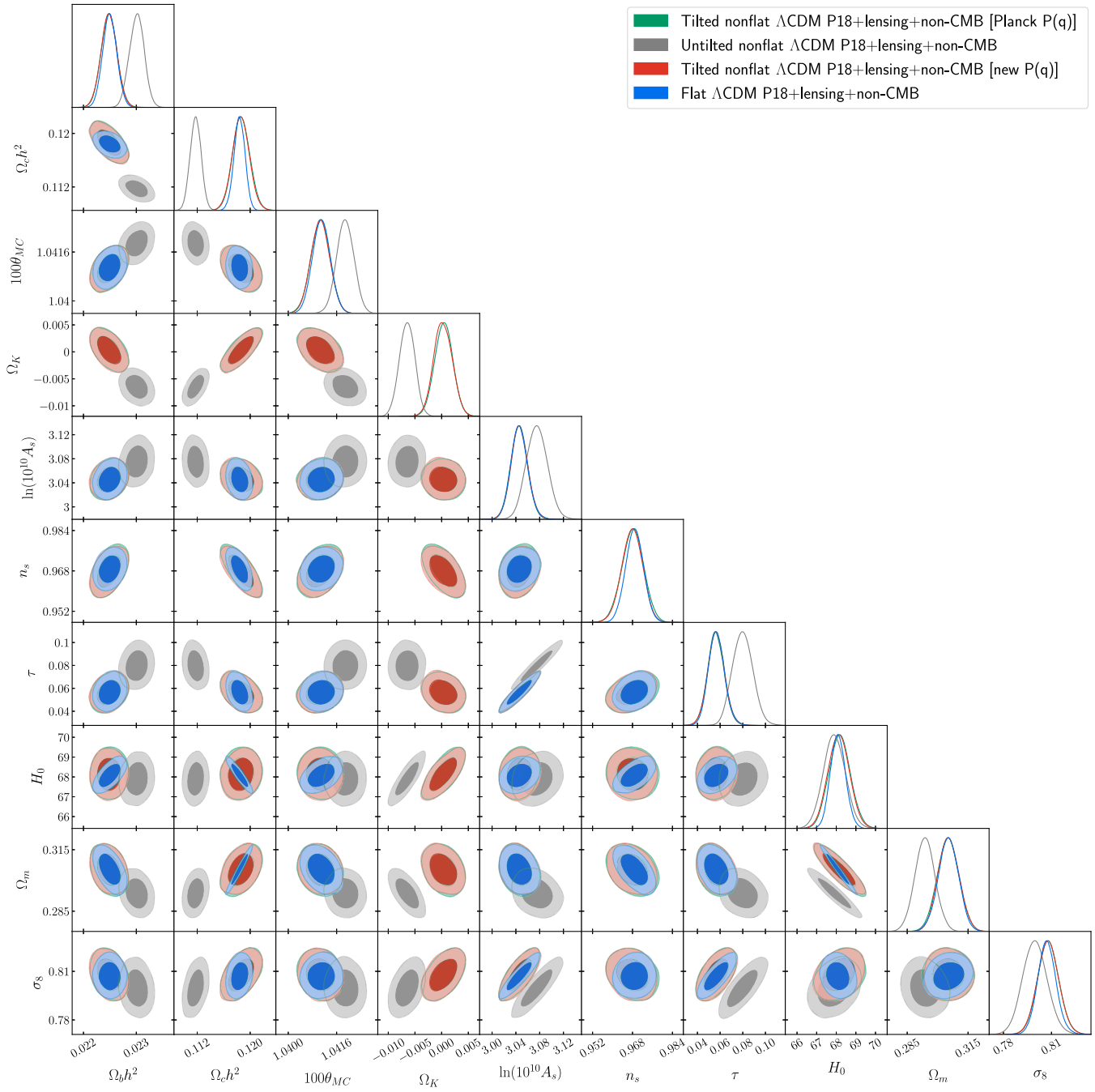

FIG. 4. P18 + lensing + non-CMB data likelihood distributions of parameters of the tilted nonflat ΛCDM model with the new initial power spectrum [new $P(q)$] (red contours), of the tilted nonflat ΛCDM model with the Planck team's initial spectrum [Planck $P(q)$] (green), of the untilted nonflat ΛCDM model (gray), and of the tilted flat ΛCDM model (blue contours).

$H_0 = 67.28 \pm 0.61$ km s^{-1} Mpc^{-1}, which are consistent with many other measurements of these quantities and which differ from the low-redshift data measurements of Ref. [101], $\Omega_m = 0.295 \pm 0.017$ and $H_0 = 69.7 \pm 1.2$ km s^{-1} Mpc^{-1}, by 1.1σ and 1.8σ.

The improvement in the fit to P18 data when the A_L parameter is allowed to vary, in the tilted flat ΛCDM + A_L model, is positive, according to the statistical DIC described in Sec. III (see the results in Sec. IV B). This fact is reflected in the measured (from P18 data) value of this phenomenological parameter $A_L = 1.181 \pm 0.067$, which differs from the theoretically expected $A_L = 1$ by 2.7σ. The inclusion of the A_L parameter, introduced to deal with the lensing anomaly, does not significantly affect the values of the other six primary parameters, leaving them close to the values found for the six-parameter ($\Omega_k = 0$) tilted flat

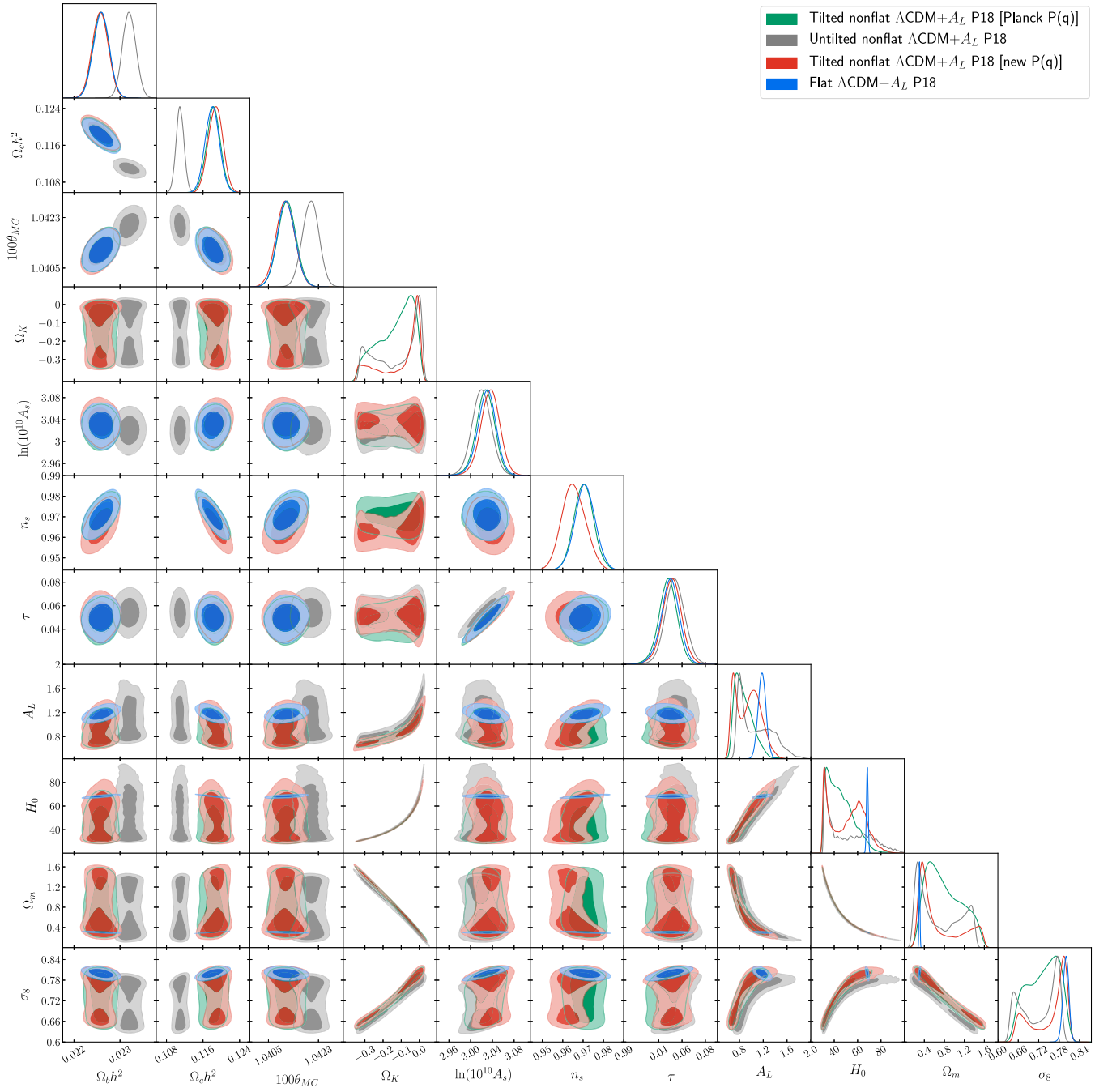

FIG. 5. Planck 2018 TT, TE, EE + lowE (P18) data likelihood distributions of parameters of the tilted nonflat ΛCDM + A_L model with the new initial power spectrum [new $P(q)$] (red contours), of the tilted nonflat ΛCDM + A_L model with the Planck team's initial spectrum [Planck $P(q)$] (green), of the untilted nonflat ΛCDM + A_L model (gray), and of the tilted flat ΛCDM + A_L model (blue contours).

ΛCDM model with $A_L = 1$ (the largest difference is for $\Omega_c h^2$, where it is 1.1σ of the quadrature sum of the two error bars); it does, however, increase the error bars somewhat, with the largest increase being 16% for n_s. In addition, in the case when A_L is allowed to vary, the derived parameters Ω_m and H_0 (as well as σ_8) error bars mildly increase, by 11% and 16%, resulting in (for P18 data) $\Omega_m = 0.3029 \pm 0.0093$ and $H_0 = 68.31 \pm 0.71\,\mathrm{km\,s^{-1}\,Mpc^{-1}}$, which are consistent with many other measurements of these quantities, now differing only by 0.41σ and 1.0σ, respectively, from those of Ref. [101]. These derived Ω_m and H_0 parameter values in the A_L-varying case also differ from those in the $A_L = 1$ case by at most 1.1σ.

The addition of the Ω_k parameter to the six primary cosmological parameters of the tilted flat ΛCDM model introduces a strong degeneracy between increasing Ω_m and

TABLE V. Mean and 68.3% confidence limits of untilted nonflat ΛCDM ($+A_L$) model parameters constrained by TT, TE, EE + lowE (P18), P18 + lensing, and P18 + lensing + non-CMB datasets. H_0 has units of km s^{-1} Mpc^{-1}.

	Untilted nonflat ΛCDM model		
Parameter	P18	P18 + lensing	P18 + lensing + non-CMB
$\Omega_b h^2$	0.02320 ± 0.00015	0.02307 ± 0.00014	0.02301 ± 0.00014
$\Omega_c h^2$	0.11098 ± 0.00088	0.11108 ± 0.00086	0.11176 ± 0.00083
$100\theta_{\rm MC}$	1.04204 ± 0.00030	1.04196 ± 0.00029	1.04189 ± 0.00029
τ	0.0543 ± 0.0091	0.0580 ± 0.0087	0.0799 ± 0.0089
Ω_k	-0.095 ± 0.024	-0.0322 ± 0.0075	-0.0065 ± 0.0014
$\ln(10^{10} A_s)$	3.021 ± 0.019	3.027 ± 0.018	3.075 ± 0.018
H_0	47.1 ± 3.2	58.9 ± 2.1	67.90 ± 0.56
Ω_m	0.617 ± 0.082	0.390 ± 0.027	0.2938 ± 0.0049
σ_8	0.730 ± 0.017	0.765 ± 0.011	0.7997 ± 0.0076
	Untilted nonflat ΛCDM + A_L model		
Parameter	P18	P18 + lensing	P18 + lensing + non-CMB
$\Omega_b h^2$	0.02320 ± 0.00015	0.02312 ± 0.00014	0.02310 ± 0.00014
$\Omega_c h^2$	0.11097 ± 0.00087	0.11092 ± 0.00087	0.11100 ± 0.00085
$100\theta_{\rm MC}$	1.04202 ± 0.00030	1.04193 ± 0.00029	1.04195 ± 0.00030
τ	0.0540 ± 0.0087	0.0554 ± 0.0097	0.0566 ± 0.0083
Ω_k	-0.12 ± 0.12	0.0161 ± 0.0094	-0.0060 ± 0.0014
$\ln(10^{10} A_s)$	3.020 ± 0.018	3.021 ± 0.020	3.024 ± 0.017
A_L	1.08 ± 0.27	1.44 ± 0.15	1.162 ± 0.036
H_0	52 ± 18	85.7 ± 8.5	68.48 ± 0.58
Ω_m	0.70 ± 0.42	0.190 ± 0.043	0.2874 ± 0.0050
σ_8	0.721 ± 0.053	0.7805 ± 0.0094	0.7764 ± 0.0078

decreasing H_0. The nonflat models also show some degeneracy between Ω_m and Ω_k, as well as between H_0 and Ω_k. These degeneracies can be seen in the corresponding panels in Fig. 2. In the tilted nonflat ΛCDM models (see Tables VI and VII and Fig. 2), we see that P18 data alone are unable to break the strong geometrical degeneracy between Ω_m, H_0, and Ω_k. For the Planck $P(q)$ and the new $P(q)$, the measured values (from P18 data) $\Omega_m = 0.481 \pm 0.062$ and 0.444 ± 0.055, as well as $H_0 = 54.5 \pm 3.6$ and 56.9 ± 3.6 km s^{-1} Mpc^{-1}, respectively, are in conflict with most other measurements of these parameters; for example, see the low-redshift data measurements of Ref. [101] in the paragraph before last. Note that, even though the values of, and error bars on, the six primary cosmological parameters in common between the two tilted nonflat models and the tilted flat model are very similar [the largest difference is 1.1σ for $\Omega_b h^2$ between the tilted flat and the tilted nonflat Planck $P(q)$ models, and the biggest increase, 13%, in the error bars is also for $\Omega_b h^2$, in both tilted nonflat models relative to the tilted flat model], the additional primary cosmological parameter Ω_k in the two tilted nonflat models is relatively poorly constrained; the derived cosmological parameters Ω_m and H_0 error bars in the two tilted nonflat ΛCDM models are approximately factors of 7 and 6 larger than those in the tilted flat ΛCDM model (and Ω_m and H_0 in these tilted nonflat models differ by between 2.3σ and 3.5σ from the tilted flat model values). The evidence in favor of $\Omega_k < 0$ is significant in both of the tilted nonflat ΛCDM models. For the Planck $P(q)$ case, we find $\Omega_k = -0.043 \pm 0.017$, while for the new $P(q)$ case $\Omega_k = -0.033 \pm 0.014$, being 2.5σ and 2.4σ away from flat hypersurfaces respectively. In both cases, there is clear preference for a closed over an open spatial geometry. And we shall see in Sec. IV B, the P18 data DIC strongly favors both tilted nonflat models over the tilted flat ΛCDM model.

Allowing the A_L parameter to vary in the nonflat models introduces an additional strong degeneracy between Ω_k, Ω_m, H_0, and A_L; compare the corresponding panels in Figs. 2 and 5. In the tilted nonflat ΛCDM + A_L models with the Planck $P(q)$ and with the new $P(q)$, where the A_L parameter is allowed to vary (see Tables VI and VII and Fig. 5), P18 data alone are unable to break the strong geometrical degeneracy between Ω_m, H_0, Ω_k, and A_L. [In the tilted nonflat ΛCDM + A_L new $P(q)$ model, some parameters have a somewhat bimodal distribution for P18 data, see the one-dimensional posterior distributions in Fig. 5. This is not the case for the tilted nonflat ΛCDM + A_L Planck $P(q)$ model.] Like in the tilted flat ΛCDM case discussed in the paragraph before last, the extra A_L

parameter does not significantly affect any of the (primary, not derived) cosmological parameter constraints, compared to the $A_L = 1$ case, except, because of the additional $\Omega_k - A_L$ degeneracy, the Ω_k constraints, which are now $\Omega_k = -0.130 \pm 0.095$ for the Planck $P(q)$ case and $\Omega_k = -0.10 \pm 0.11$ for the new $P(q)$, being only 1.4σ and 0.91σ, respectively, away from flat spatial hypersurfaces, with the Ω_k error bars now being factors of 6 and 8, respectively, larger than those in the $A_L = 1$ case. Also, unlike the tilted flat ΛCDM case of the paragraph before last, we measure, from the P18 data, $A_L = 0.88 \pm 0.15$ and 0.94 ± 0.20, which differ from the theoretically expected $A_L = 1$ by only 0.80σ and 0.30σ. We will see in Sec. IV B that in both these models the fit to P18 data is weakly or positively better when $A_L = 1$ compared to the case when the A_L parameter is allowed to vary. However, when A_L varies, the DIC weakly favors (positively disfavors) the tilted nonflat Planck $P(q)$ [new $P(q)$] model over the tilted flat $\Lambda\text{CDM} + A_L$ model. In addition, in both these cases, when A_L is allowed to vary, the Ω_m and H_0 (as well as σ_8) error bars significantly increase, resulting in (for P18 data) $\Omega_m = 0.80 \pm 0.35$ and 0.70 ± 0.43, as well as $H_0 = 45 \pm 11$ and 51 ± 14 km s^{-1} Mpc^{-1}, which are consistent with many other measurements of these quantities. Again, the error bars on $\Omega_b h^2$, $\Omega_c h^2$, $\theta_{\rm MC}$, τ, n_s, and A_s are similar in the two tilted nonflat $\Lambda\text{CDM} + A_L$ models and the tilted flat $\Lambda\text{CDM} + A_L$ model; however, the A_L error bars are approximately a factor of 2.5 larger in the tilted nonflat models, with the introduction of the seventh primary cosmological parameter Ω_k (that is poorly constrained) also resulting in the Ω_m error bars being a factor ∼42 larger and the H_0 error bars being a factor ∼18 larger in the tilted nonflat $\Lambda\text{CDM} + A_L$ models compared to the tilted flat $\Lambda\text{CDM} + A_L$ model.

The restriction that $n_s = 1$ in the untilted nonflat ΛCDM ($+A_L$) models is an unwelcome feature when fitting the P18 CMB anisotropy spectra, according to the statistical criteria outlined in Sec. IV B. Because of this, we will focus less attention on the untilted nonflat ΛCDM model compared to the two tilted nonflat models. Despite the poor performance of the untilted nonflat ΛCDM model in this case (which also affects what happens when additional data are jointly analyzed with P18 data), the model shares some features with the two tilted nonflat ΛCDM models (see Table V and Fig. 2), namely, the evidence in favor of closed spatial geometry, now with $\Omega_k = -0.095 \pm 0.024$ (4.0σ) and the presence of the aforementioned geometrical degeneracy between Ω_m, H_0, and Ω_k. Also, as in the two tilted nonflat models, in the untilted nonflat case the measured values (from P18 data) $\Omega_m = 0.617 \pm 0.082$ and $H_0 = 47.1 \pm 3.2$ km s^{-1} Mpc^{-1} are in conflict with most other measurements of these parameters.

In the untilted nonflat $\Lambda\text{CDM} + A_L$ model where the A_L parameter is allowed to vary (see Table V and Fig. 5) P18 data alone is again unable to break the larger geometrical degeneracy between Ω_m, H_0, Ω_k, and A_L. Like in the tilted flat and nonflat ΛCDM cases discussed earlier, the extra A_L parameter does not significantly affect any of the (primary, not derived) cosmological parameter constraints in the untilted nonflat model, compared to the $A_L = 1$ case, except, because of the additional $\Omega_k - A_L$ degeneracy, for the Ω_k constraint, which is now $\Omega_k = -0.12 \pm 0.12$ and only 1.0σ away from flat spatial hypersurfaces. Also, unlike the tilted flat ΛCDM case, but like the tilted nonflat cases of the paragraph before last, we measure, from the P18 data, $A_L = 1.08 \pm 0.27$, which differs from the theoretically expected value of $A_L = 1$ by only 0.30σ. We will see in Sec. IV B that in this model the fit to P18 data is slightly better when $A_L = 1$ compared to the case when the A_L parameter is allowed to vary. Similar to the two tilted nonflat models of the paragraph before last, when A_L is allowed to vary in the untilted nonflat model, the Ω_m and H_0 (as well as σ_8) error bars significantly increase, resulting in (for P18 data) $\Omega_m = 0.70 \pm 0.42$ and $H_0 = 52 \pm 18$ km s^{-1} Mpc^{-1}, which are consistent with most other measurements of these quantities.

In Fig. 2 we provide the 2σ contour plots for all four of the $A_L = 1$ models. The contours for the untilted nonflat ΛCDM model overlap minimally or even do not overlap at all with those corresponding to the other models. This is likely due to the lack of the degree of freedom encapsulated in n_s in the untilted nonflat model, which greatly hinders the fit of the CMB anisotropy power spectra and causes the other parameters to shift from the ranges preferred in the context of the other three models. As for the other three cosmological models, there is a significant overlap of contours, except when Ω_m or H_0 (or less so σ_8) is involved, which can even lead to the contours not overlapping at all. This is presumably related to the geometrical degeneracy previously mentioned.

The corresponding plots for the four models now including allowing A_L to vary are in Fig. 5. Allowing A_L to vary broadens the contours, and for some parameters there are two disconnected 1σ regions. While the untilted nonflat model contours still do not overlap in many cases with those of the other three models, in the other three models the contours overlap even when Ω_m or H_0 or σ_8 is involved.

2. P18 + lensing *data cosmological constraints*

Constraints on primary parameters derived from joint analyses of P18 and lensing data are quite similar to those derived from P18 data alone (see Tables IV–VII, Figs. 3 and 6), except for Ω_k and A_L constraints. On the other hand, constraints on derived parameters Ω_m and H_0 are, in most nonflat cases, greatly affected by lensing data. In this subsubsection we discuss parameter constraints from jointly analyzed P18 and lensing data and compare these to the P18 data alone constraints.

Ideally, one would like to establish that cosmological parameter constraints derived from P18 data and from lensing data are mutually consistent, prior to using

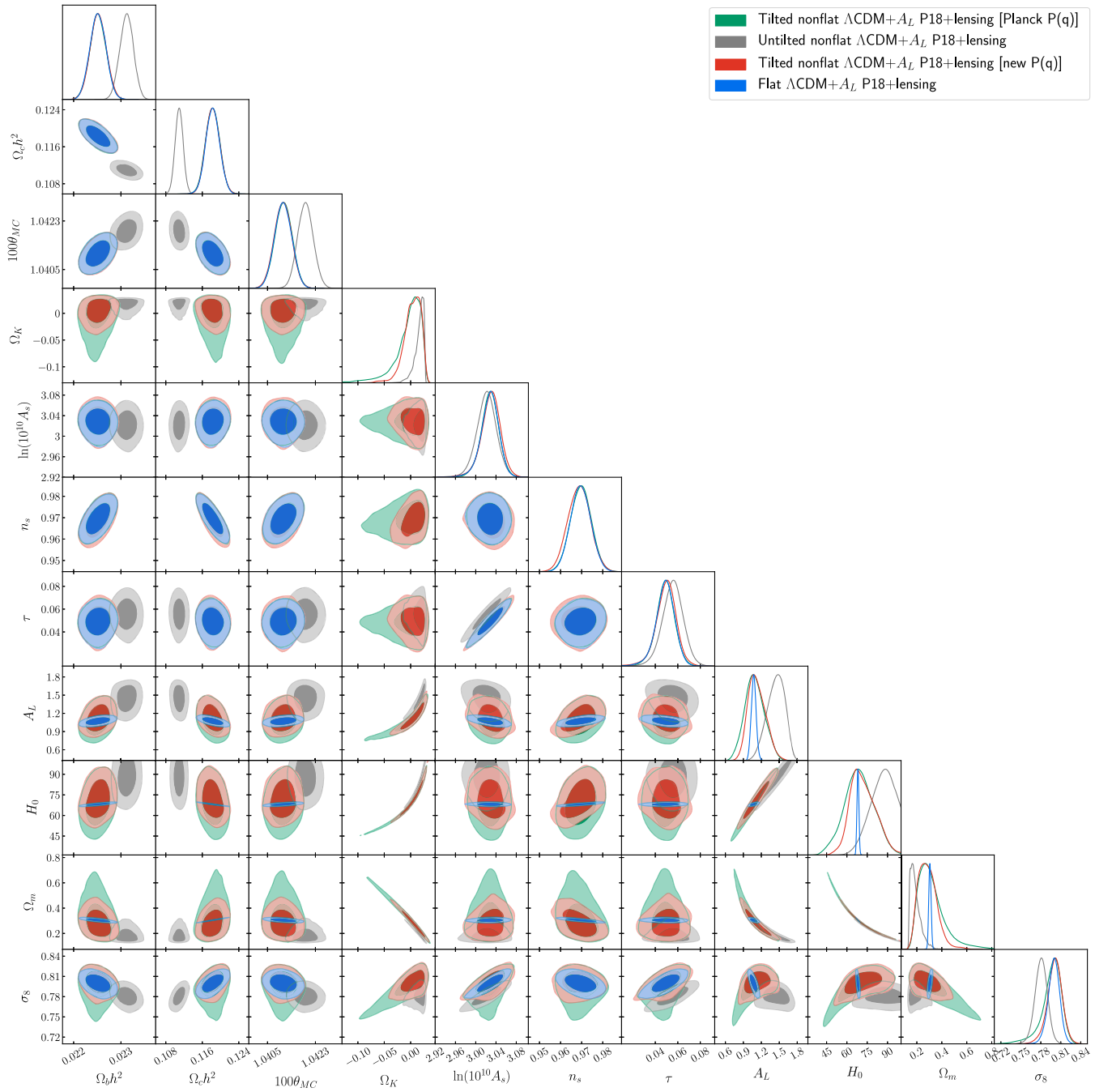

FIG. 6. P18 + lensing data likelihood distributions of parameters of the tilted nonflat ΛCDM + A_L model with the new initial power spectrum [new $P(q)$] (red contours), of the tilted nonflat ΛCDM + A_L model with the Planck team's initial spectrum [Planck $P(q)$] (green), of the untilted nonflat ΛCDM + A_L model (gray), and of the tilted flat ΛCDM + A_L model (blue contours).

P18 + lensing data in joint analyses. While it is not straightforward to derive (P18) lensing data alone cosmological parameter constraints for the wide flat priors in the Our column of Table III, we shall see, in Sec. IV C (where we do briefly discuss some of these cosmological constraints), that P18 data and lensing data are not significantly mutually inconsistent. This is also consistent with the results we discuss in this subsubsection.

Comparing the six-parameter tilted flat ΛCDM primary cosmological parameter constraints for P18 data and P18 + lensing data, shown in the upper half of Table IV, we see that there are no significant changes in parameter values (the largest change is that $\Omega_c h^2$ is 0.11σ smaller in the P18 + lensing case) with all but the $\theta_{\rm MC}$ error bars being smaller in the P18 + lensing case (the $\theta_{\rm MC}$ error bar is unchanged and the largest decrease is 14% for the $\Omega_c h^2$

error bar). For the derived parameters, the largest change is the 0.089σ decrease in Ω_m relative to the P18 data value and the 20% smaller σ_8 error bar. For P18 + lensing data, we find $\Omega_m = 0.3155 \pm 0.0075$ and $H_0 = 67.34 \pm 0.55$ km s^{-1} Mpc^{-1}, which are consistent with many other measurements of these quantities and 1.1σ larger and 1.8σ lower than the low-redshift data measurements of Ref. [101].

Comparing the seven-parameter tilted flat $\Lambda\text{CDM} + A_L$ primary cosmological parameter constraints for P18 data and P18 + lensing data, shown in the lower half of Table IV, we see more significant changes in the parameter values (the largest change is that A_L is 1.4σ smaller in the P18 + lensing case, with the next largest being $\Omega_b h^2$, which is 0.33σ smaller) with some of the error bars being larger in the P18 + lensing case [the largest increase is 6% for the τ and $\ln(10^{10}A_s)$ error bars] and some of the error bars being smaller (the largest decrease is 39% for A_L). The reason the error bars of τ and $\ln(10^{10}A_s)$ increase, contrary to the common expectation that the error bars of the parameters will become smaller as more data are added, appears to be that the degeneracy between parameters is only partially broken by the lensing data. Interestingly, these characteristics are common to all other A_L-varying models (see Tables V–VII). For the derived parameters, the largest change is the 0.17σ decrease in H_0 relative to the P18 data value and the 3% smaller H_0 error bar. For P18 + lensing data in the varying A_L case, we measure $\Omega_m = 0.3048 \pm 0.0091$ and $H_0 = 68.14 \pm 0.69$ km s^{-1} Mpc^{-1}, which are consistent with many other measurements of these quantities and 0.51σ larger and 1.1σ lower than the low-redshift data measurements of Ref. [101].

The improvement in the fit to P18 + lensing data when the A_L parameter is allowed to vary, in the tilted flat $\Lambda\text{CDM} + A_L$ model, is only weak, as discussed in Sec. IV B. We now find $A_L = 1.073 \pm 0.041$, which is 1.8σ away from the theoretically expected $A_L = 1$. While there is still a deviation from the predicted value, the tendency of the lensing data is to push A_L closer to 1, resulting in a smaller deviation than the 2.7σ one found for $A_L = 1.181 \pm 0.067$ from P18 data in the tilted flat $\Lambda\text{CDM} + A_L$ model. The inclusion of the A_L parameter does not significantly affect the values of the other six primary parameters, leaving them close to the values found for the six-parameter tilted flat ΛCDM model with $A_L = 1$ (the largest difference is for $\Omega_c h^2$, where it is 0.88σ of the quadrature sum of the two error bars); it does, however, increase the error bars, more than what happens in the P18 alone data case discussed in Sec. IV A 1, with largest increase being 29% for $\ln(10^{10}A_s)$. In addition, in the case when A_L is allowed to vary, the derived parameters change somewhat and their error bars increase, with the largest changes associated with σ_8, where it is now 1.1σ smaller with a 51% larger error bar.

In the six-parameter untilted nonflat ΛCDM model, including lensing data in the mix results in a reduction in the size of the cosmological parameter error bars relative to those from P18 data (see Table V and Fig. 3). The most affected parameters are the primary parameter Ω_k, whose error bars decrease by 69%, and the derived parameters H_0, Ω_m, and σ_8, for which we observe a shrinkage of the error bars by 34%, 67%, and 35%, respectively. As happens in the tilted flat ΛCDM model, here also there are no significant changes in the values of the primary parameters, with the exception of the curvature parameter Ω_k. This is not true for two of the derived parameters, H_0 and Ω_m, which together with the curvature parameter are involved in the Ω_m-H_0-Ω_k geometrical degeneracy. From P18 + lensing data, we find $\Omega_k = -0.095 \pm 0.024$, $H_0 = 47.1 \pm 3.2$ km s^{-1} Mpc^{-1}, and $\Omega_m = 0.390 \pm 0.027$. These values differ by 2.5σ, 3.1σ, and 2.6σ, respectively, from the corresponding values obtained in the P18 data alone analysis.

From the results obtained for the untilted nonflat $\Lambda\text{CDM} + A_L$ model (see Table V and Fig. 6), we observe significant changes in the values of the primary parameters Ω_k and A_L, as well as in the derived parameters H_0 and Ω_m. For the P18 + lensing dataset, we get $\Omega_k = 0.0161 \pm 0.0094$ (1.7σ away from flat) and $A_L = 1.44 \pm 0.15$ (2.9σ away from $A_L = 1$). These values differ by 1.1σ and 1.2σ, respectively, from the corresponding values obtained in the P18 data alone analysis. For the derived parameters, from P18 + lensing data we find $H_0 = 85.7 \pm 8.5$ km s^{-1} Mpc^{-1} and $\Omega_m = 0.190 \pm 0.043$, which differ by 1.7σ and 1.2σ from the corresponding P18 data alone values.

Joint analyses of the P18 and lensing data in the tilted nonflat models result in constraints that differ more from those derived using just P18 data compared to what happens in the tilted flat model case (see Tables VI and VII and Fig. 3). This is because lensing data partially break the Ω_m-H_0-Ω_k geometrical P18 alone data degeneracy of the tilted nonflat models (compare the corresponding panels in Figs. 2 and 3).

Comparing the seven-parameter tilted nonflat ΛCDM Planck $P(q)$ and new $P(q)$ primary cosmological parameter constraints for P18 data and P18 + lensing data, shown in the upper halves of Tables VI and VII, we see that aside from Ω_k (discussed next) there are no significant changes in parameter values [the largest change is that $\Omega_b h^2$ is 0.47σ (0.30σ) smaller in the P18 + lensing case, for the Planck (new) $P(q)$] with some of the error bars being smaller in the P18 + lensing case [leaving aside Ω_k (discussed next) the largest decrease is 6% (7%) for the $\Omega_b h^2$ ($\Omega_c h^2$) error bar, for the Planck (new) $P(q)$]. On the other hand, Ω_k changes significantly when lensing data are added to the mix, becoming 1.8σ (1.6σ) larger and closer to flat for the Planck (new) $P(q)$, with 61% (59%) smaller error bars, still favoring closed geometry over flat but only by 1.6σ (1.5σ), respectively. For the derived parameters, the largest change is the 2.2σ (1.8σ) increase in H_0 relative to the P18 data value for the Planck (new) $P(q)$, with 61% (62%) smaller error bars for Ω_m. For P18 + lensing data, we find $\Omega_m = 0.351 \pm 0.024$ (0.345 ± 0.021) and

TABLE VI. Mean and 68.3% confidence limits of Planck-$P(q)$-based tilted nonflat ΛCDM ($+A_L$) model parameters constrained by TT, TE, EE + lowE (P18), P18 + lensing, and P18 + lensing + non-CMB datasets. H_0 has units of km s^{-1} Mpc^{-1}.

	Tilted nonflat ΛCDM model [Planck $P(q)$]		
Parameter	P18	P18 + lensing	P18 + lensing + non-CMB
$\Omega_b h^2$	0.02260 ± 0.00017	0.02249 ± 0.00016	0.02249 ± 0.00015
$\Omega_c h^2$	0.1181 ± 0.0015	0.1186 ± 0.0015	0.1187 ± 0.0013
$100\theta_{\rm MC}$	1.04116 ± 0.00032	1.04107 ± 0.00032	1.04106 ± 0.00031
τ	0.0483 ± 0.0083	0.0495 ± 0.0082	0.0563 ± 0.0073
Ω_k	-0.043 ± 0.017	-0.0103 ± 0.0066	0.0004 ± 0.0017
n_s	0.9706 ± 0.0047	0.9687 ± 0.0046	0.9681 ± 0.0044
$\ln(10^{10} A_s)$	3.027 ± 0.017	3.030 ± 0.017	3.046 ± 0.014
H_0	54.5 ± 3.6	63.7 ± 2.3	68.17 ± 0.55
Ω_m	0.481 ± 0.062	0.351 ± 0.024	0.3051 ± 0.0053
σ_8	0.775 ± 0.015	0.796 ± 0.011	0.8080 ± 0.0066
	Tilted nonflat ΛCDM + A_L model [Planck $P(q)$]		
Parameter	P18	P18 + lensing	P18 + lensing + non-CMB
$\Omega_b h^2$	0.02258 ± 0.00017	0.02251 ± 0.00017	0.02259 ± 0.00016
$\Omega_c h^2$	0.1183 ± 0.0015	0.1183 ± 0.0015	0.1173 ± 0.0014
$100\theta_{\rm MC}$	1.04116 ± 0.00033	1.04110 ± 0.00032	1.04118 ± 0.00032
τ	0.0478 ± 0.0081	0.0489 ± 0.0085	0.0479 ± 0.0085
Ω_k	-0.130 ± 0.095	-0.005 ± 0.027	-0.0002 ± 0.0017
n_s	0.9704 ± 0.0048	0.9696 ± 0.0049	0.9718 ± 0.0045
$\ln(10^{10} A_s)$	3.027 ± 0.017	3.028 ± 0.018	3.024 ± 0.017
A_L	0.88 ± 0.15	1.09 ± 0.16	1.090 ± 0.036
H_0	45 ± 11	69 ± 11	68.49 ± 0.56
Ω_m	0.80 ± 0.35	0.32 ± 0.11	0.2998 ± 0.0055
σ_8	0.733 ± 0.045	0.796 ± 0.016	0.7952 ± 0.0085

$H_0 = 63.7 \pm 2.3$ (64.2 ± 2.0) km s^{-1} Mpc^{-1} for the Planck (new) $P(q)$, which are consistent with many other measurements of these quantities and 1.9σ (1.9σ) larger and 2.3σ (2.4σ) lower, respectively, than the low-redshift data measurements of Ref. [101].

Comparing the eight-parameter tilted nonflat ΛCDM + A_L Planck (new) $P(q)$ primary cosmological parameter constraints for P18 data and P18 + lensing data, shown in the lower half of Table VI (Table VII), we see that there are smaller differences compared to the tilted flat ΛCDM + A_L case. For the Planck $P(q)$ case, we mostly find less significant changes (the largest changes are that Ω_k and A_L are 1.3σ and 0.95σ larger in the P18 + lensing case, with the next largest being $\Omega_b h^2$, which is 0.29σ smaller) with some of the error bars being larger in the P18 + lensing case (the largest increase is 7% for the A_L error bar, and this is the only model where the A_L error bar is larger for P18 + lensing data than for P18 data) and some of the error bars being smaller (the largest decrease is 72% for Ω_k). In the new $P(q)$ case, we find roughly half the parameters change more significantly (the largest changes again are that Ω_k and A_L are 0.93σ and 0.76σ larger in the P18 + lensing case, with the next largest being n_s, which is 0.44σ larger) with some of the error bars being larger in the P18 + lensing case (the largest increase is 8% for the τ error bar) and some of the error bars being smaller (the largest decrease is 85% for Ω_k). From the P18 + lensing analyses, we measure $\Omega_k = -0.005 \pm 0.027$ for the Planck $P(q)$ case and $\Omega_k = 0.003 \pm 0.016$ for the new $P(q)$, both being only 0.19σ away from flat spatial hypersurfaces, very different from the P18 data alone results. For the derived parameters, the largest change is the 1.5σ (1.3σ) increase in H_0 relative to the P18 data value for the Planck (new) $P(q)$, with 69% (82%) smaller error bars for Ω_m. For P18 + lensing data, we find $\Omega_m = 0.32 \pm 0.11$ (0.287 ± 0.076) and $H_0 = 69 \pm 11$ (72.0 ± 9.2) km s^{-1} Mpc^{-1} for the Planck (new) $P(q)$, which are consistent with many other measurements of these quantities and 0.22σ larger (0.10σ smaller) and 0.063σ lower (0.25σ higher), respectively, than the low-redshift data measurements of Ref. [101]. [Note that the P18 + lensing data Planck $P(q)$ H_0 error bar is unchanged, ± 11 km s^{-1}, from the P18 data value, and this is the only model where this happens.]

We will see in Sec. IV B that in both tilted nonflat ΛCDM + A_L models the fit to P18 + lensing data is weakly better when $A_L = 1$ compared to the case when

TABLE VII. Mean and 68.3% confidence limits of new-$P(q)$-based tilted nonflat ΛCDM ($+A_L$) model parameters constrained by TT, TE, EE + lowE (P18), P18 + lensing, and P18 + lensing + non-CMB datasets. H_0 has units of km s^{-1} Mpc^{-1}.

	Tilted nonflat ΛCDM model [new $P(q)$]		
Parameter	P18	P18 + lensing	P18 + lensing + non-CMB
$\Omega_b h^2$	0.02255 ± 0.00017	0.02248 ± 0.00016	0.02248 ± 0.00015
$\Omega_c h^2$	0.1188 ± 0.0015	0.1188 ± 0.0014	0.1186 ± 0.0013
$100\theta_{\rm MC}$	1.04109 ± 0.00032	1.04104 ± 0.00032	1.04106 ± 0.00031
τ	0.0525 ± 0.0083	0.0515 ± 0.0081	0.0566 ± 0.0074
Ω_k	-0.033 ± 0.014	-0.0086 ± 0.0057	0.0003 ± 0.0017
n_s	0.9654 ± 0.0045	0.9661 ± 0.0043	0.9679 ± 0.0042
$\ln(10^{10} A_s)$	3.039 ± 0.017	3.035 ± 0.016	3.046 ± 0.014
H_0	56.9 ± 3.6	64.2 ± 2.0	68.13 ± 0.54
Ω_m	0.444 ± 0.055	0.345 ± 0.021	0.3054 ± 0.0051
σ_8	0.786 ± 0.014	0.799 ± 0.010	0.8079 ± 0.0067
	Tilted nonflat ΛCDM + A_L model [new $P(q)$]		
Parameter	P18	P18 + lensing	P18 + lensing + non-CMB
$\Omega_b h^2$	0.02257 ± 0.00017	0.02252 ± 0.00017	0.02260 ± 0.00016
$\Omega_c h^2$	0.1187 ± 0.0016	0.1183 ± 0.0015	0.1174 ± 0.0013
$100\theta_{\rm MC}$	1.04111 ± 0.00033	1.04108 ± 0.00032	1.04118 ± 0.00032
τ	0.0512 ± 0.0086	0.0495 ± 0.0093	0.0486 ± 0.0086
Ω_k	-0.10 ± 0.11	0.003 ± 0.016	-0.0002 ± 0.0017
n_s	0.9654 ± 0.0057	0.9688 ± 0.0053	0.9713 ± 0.0042
$\ln(10^{10} A_s)$	3.036 ± 0.018	3.030 ± 0.019	3.025 ± 0.017
A_L	0.94 ± 0.20	1.13 ± 0.15	1.088 ± 0.035
H_0	51 ± 14	72.0 ± 9.2	68.48 ± 0.56
Ω_m	0.70 ± 0.43	0.287 ± 0.076	0.2999 ± 0.0055
σ_8	0.752 ± 0.052	0.801 ± 0.011	0.7956 ± 0.0082

the A_L parameter is allowed to vary; this differs from what happens in the tilted flat ΛCDM + A_L model. Also, unlike the tilted flat ΛCDM + A_L P18 + lensing case, we measure, from P18 + lensing data, $A_L = 1.089 \pm 0.16$ and 1.13 ± 0.15, for the Planck $P(q)$ and the new $P(q)$, respectively, which differ from the theoretically expected $A_L = 1$ by only 0.56σ and 0.87σ. The inclusion of the A_L parameter does not significantly affect the values of the other seven primary parameters, leaving them close to the values found for the seven-parameter tilted nonflat ΛCDM models with $A_L = 1$ [the largest difference is for Ω_k, where it is 0.19σ (0.68σ) for the Planck (new) $P(q)$]; it does, however, increase the error bars, but less than what happens in the P18 alone data case discussed in Sec. IV A 1, with largest factor being 4 (3) for Ω_k for the Planck (new) $P(q)$. In addition, in the case when A_L is allowed to vary, the derived parameters change somewhat and their error bars increase, with the largest changes associated with H_0, where it is now 0.47σ (0.83σ) larger for the Planck (new) $P(q)$ with a factor of 5 (5) larger error bar.

From the discussion above in this subsubsection, the fact that the cosmological constraint contours displayed in Fig. 3 for the three tilted models overlap should not come as a surprise. Unlike in the previous P18 data alone case, the P18 + lensing data contours that involve Ω_m, H_0, or Ω_k now overlap for the tilted models, indicating that the geometrical degeneracy is, at least, partially broken. Figure 6 shows the results when the A_L parameter is included in the analysis. While the overlap already found in the P18 data alone analysis (see Fig. 5) remains, the bimodal 1σ regions of that plot have now disappeared.

3. P18 + lensing + non-CMB *data cosmological constraints*

In this subsubsection, we comment on the results obtained from a joint analysis of the P18 + lensing + non-CMB dataset and how the cosmological constraints change when compared to those obtained using P18 + lensing data. As outlined in Sec. II, non-CMB data we use here is composed of BAO, $f\sigma_8$, SNIa, and $H(z)$ data, all of which provide useful information on the late-time Universe.

Ideally, one would like to establish that cosmological parameter constraints derived from P18 + lensing data and from non-CMB data are mutually consistent, prior to using P18 + lensing + non-CMB data in joint analyses. Given

that P18 data dominate the P18 + lensing data compilation, it is instructive to also study whether P18 data cosmological constraints are consistent with those from non-CMB data. We shall see in Sec. IV A 5 that, in some of the models we study here, cosmological constraints from BAO′ and BAO data, the dominant part of the non-CMB data compilation, are somewhat inconsistent with those derived using P18 data. This is also consistent with the results we discuss in this subsubsection, as well as with the results presented in Sec. IV A 6, where we compare the cosmological parameter values obtained using P18 data and using non-CMB data. In Sec. IV A 7, we compare P18 + lensing data cosmological constraints and non-CMB data cosmological constraints and find similar tensions. In addition, in Sec. IV C, we study tensions between some of the CMB datasets and some of the low-redshift datasets, including the case of P18 + lensing data vs non-CMB data, by using the two statistical estimators presented in Sec. III.

Comparing the six-parameter tilted flat ΛCDM primary cosmological parameter constraints for P18 + lensing data and P18 + lensing + non-CMB data, shown in the upper half of Table IV, we see that there are no significant changes in parameter values (the largest change is that $\Omega_c h^2$ is 1.1σ smaller in the P18 + lensing + non-CMB case) with all but the $\ln(10^{10}A_s)$ error bars being smaller in the P18 + lensing + non-CMB case [the $\ln(10^{10}A_s)$ error bar is unchanged and the largest decrease is 31% for the $\Omega_c h^2$ error bar]. For the derived parameters, the largest changes are the 1.1σ decrease in Ω_m and the 1.1σ increase in H_0 relative to the P18 + lensing data values and the 33% (31%) smaller Ω_m (H_0) error bar. For P18 + lensing + non-CMB data, we find $\Omega_m = 0.3053 \pm 0.0050$ and $H_0 = 68.09 \pm 0.38$ km s^{-1} Mpc^{-1}, which are consistent with many other measurements of these quantities and 0.58σ larger and 1.3σ lower than the low-redshift data measurements of Ref. [101].

Comparing the seven-parameter tilted flat ΛCDM + A_L primary cosmological parameter constraints for P18 + lensing data and P18 + lensing + non-CMB data, shown in the lower half of Table IV, we see smaller changes in the parameter values (the largest change is that $\Omega_c h^2$ is 0.47σ smaller in the P18 + lensing + non-CMB case, with the next largest being n_s, which is 0.33σ larger) with all but the $\ln(10^{10}A_s)$ error bars being smaller in the P18 + lensing + non-CMB case [the $\ln(10^{10}A_s)$ error bar is unchanged and the largest decrease is 39% for the $\Omega_c h^2$ error bars]. For the derived parameters, the largest changes are the 0.47σ increase in H_0 and the 0.47σ decrease in Ω_m relative to the P18 + lensing data values and the 42% smaller Ω_m error bar. For P18 + lensing + non-CMB data in the varying A_L case, we measure $\Omega_m = 0.2998 \pm 0.0053$ and $H_0 = 68.52 \pm 0.42$ km s^{-1} Mpc^{-1}, which are consistent with many other measurements of these quantities and 0.27σ larger and 0.93σ lower than the low-redshift data measurements of Ref. [101].

The improvement in the fit to P18 + lensing + non-CMB data when the A_L parameter is allowed to vary, in the tilted flat ΛCDM + A_L model, is positive, as discussed in Sec. IV B. We now find $A_L = 1.089 \pm 0.035$, which is now 2.5σ away from the theoretically expected $A_L = 1$, larger than the 1.8σ deviation for the P18 + lensing case of Sec. IV A 2; the tendency of the non-CMB data is to push A_L farther away from 1. The inclusion of the A_L parameter does not significantly affect the values of the other six primary parameters, leaving them close to the values found for the six-parameter tilted flat ΛCDM model with $A_L = 1$ [the largest difference is for $\ln(10^{10}A_s)$, where it is 1.0σ lower]; it does, however, increase the error bars, comparable to what happens in the P18 + lensing data case discussed in Sec. IV A 2, with largest increase being 29% for $\ln(10^{10}A_s)$. In addition, in the case when A_L is allowed to vary, the derived parameters change somewhat and their error bars increase, with the largest changes associated with σ_8, where it is now 1.2σ smaller with a 29% larger error bar.

Adding non-CMB data to P18 + lensing data strongly suppresses P18 + lensing data support for nonzero spatial curvature (see Tables VI and VII), except in the case of the untilted nonflat ΛCDM model, for which $\Omega_k = -0.0065 \pm 0.0014$ (4.6σ away from flat) and also for the untilted nonflat ΛCDM + A_L model where $\Omega_k = -0.0060 \pm 0.0014$ (4.3σ away from flat) (see Table V).

Comparing the seven-parameter tilted nonflat ΛCDM Planck $P(q)$ and new $P(q)$ primary cosmological parameter constraints for P18 + lensing data and P18 + lensing + non-CMB data, shown in the upper halves of Tables VI and VII, we see that aside from Ω_k (discussed next) there are no significant changes in parameter values [the largest change is that $\ln(10^{10}A_s)$ is 0.73σ (0.52σ) larger in the P18 + lensing + non-CMB case, for the Planck (new) $P(q)$] with all of the error bars being smaller in the P18 + lensing + non-CMB case [leaving aside Ω_k (discussed next) the largest decrease is 18% (13%) for the $\log(10^{10}A_s)$ error bar, for the Planck (new) $P(q)$]. On the other hand, Ω_k changes significantly when non-CMB data are added to the mix, becoming 1.6σ (1.5σ) larger and closer to flat for the Planck (new) $P(q)$, with 74% (70%) smaller error bars, now favoring open geometry over flat but only by 0.24σ (0.18σ), respectively. For the derived parameters, the largest changes are the 1.9σ (1.9σ) increase in H_0 and the 1.9σ (1.8σ) decrease in Ω_m relative to the P18 + lensing data values for the Planck (new) $P(q)$, with 78% (76%) smaller error bars for Ω_m and 76% (73%) smaller error bars for H_0. For P18 + lensing + non-CMB data, we find $\Omega_m = 0.3051 \pm 0.0053$ (0.3054 ± 0.0051) and $H_0 = 68.17 \pm 0.55$ (68.13 ± 0.54) km s^{-1} Mpc^{-1} for the Planck (new) $P(q)$, which are consistent with many other measurements of these quantities and 0.57σ (0.59σ) larger and 1.2σ (1.2σ) lower, respectively, than the low-redshift data measurements of Ref. [101].

Comparing the eight-parameter tilted nonflat ΛCDM + A_L Planck (new) $P(q)$ primary cosmological parameter constraints for P18 + lensing data and P18 + lensing + non-CMB data, shown in the lower half of Table VI (Table VII), we see that there are approximately comparable differences to the tilted flat ΛCDM + A_L case. For the Planck (new) $P(q)$ case, the largest change is that $\Omega_c h^2$ is 0.49σ (0.45σ) smaller in the P18 + lensing + non-CMB case, with the next largest being $\Omega_b h^2$ (n_s), which is 0.34σ (0.37σ) smaller, with most of the error bars being smaller in the P18 + lensing + non-CMB case [the largest decreases are 94% (89%) for Ω_k and 77% (77%) for A_L]. From the P18 + lensing + non-CMB analyses, we measure $\Omega_k = -0.0002 \pm 0.0017$ for both $P(q)$ cases, both being only 0.12σ away from flat spatial hypersurfaces, very different from the P18 data alone results. For the derived parameters,

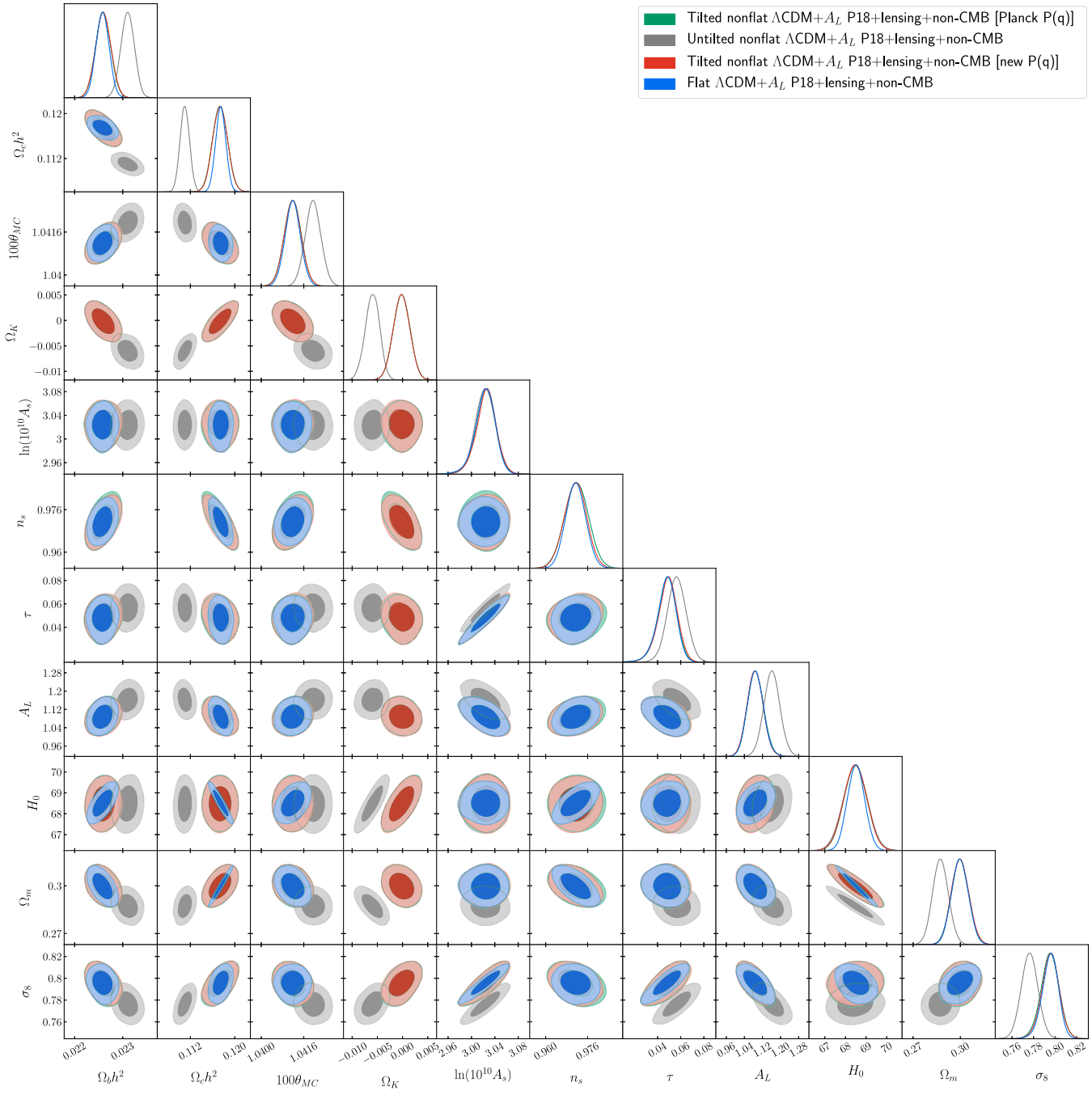

FIG. 7. P18 + lensing + non-CMB data likelihood distributions of parameters of the tilted nonflat ΛCDM + A_L model with the new initial power spectrum [new $P(q)$] (red contours), of the tilted nonflat ΛCDM + A_L model with the Planck team's initial spectrum [Planck $P(q)$] (green), of the untilted nonflat ΛCDM + A_L model (gray), and of the tilted flat ΛCDM + A_L model (blue contours).

the largest change is the 0.18σ (0.39σ) decrease in Ω_m (σ_8) relative to the P18 + lensing data value for the Planck (new) $P(q)$, with 95% (93%) smaller error bars for Ω_m and 95% (94%) smaller error bars for H_0. For P18 + lensing + non-CMB data, we find $\Omega_m = 0.2998 \pm 0.0055$ (0.2999 ± 0.0055) and $H_0 = 68.49 \pm 0.56$ (68.48 ± 0.56) km s^{-1} Mpc^{-1} for the Planck (new) $P(q)$, which are consistent with many other measurements of these quantities and 0.27σ (0.27σ) larger and 0.91σ (0.92σ) lower, respectively, than the low-redshift data measurements of Ref. [101].

We will see in Sec. IV B that in both tilted nonflat $\Lambda\text{CDM} + A_L$ models the fit to P18 + lensing + non-CMB data is positively better when the A_L parameter is allowed to vary compared to the $A_L = 1$ case; this is similar to what happens in the tilted flat $\Lambda\text{CDM} + A_L$ model. Also, like the tilted flat $\Lambda\text{CDM} + A_L$ P18 + lensing + non-CMB case, we measure, from P18 + lensing + non-CMB data,

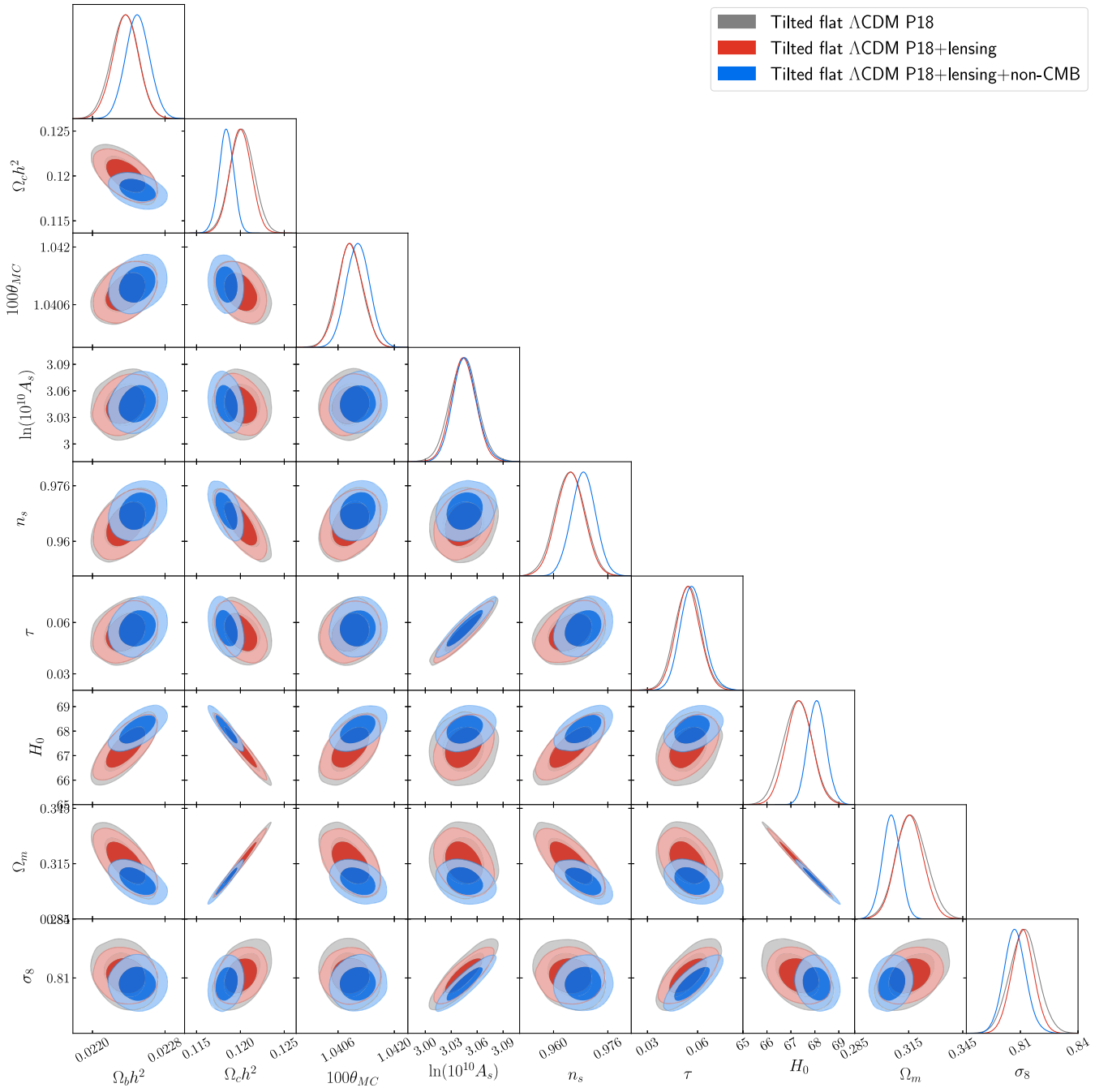

FIG. 8. Likelihood distributions of tilted flat ΛCDM model parameters constrained by P18 (gray contours), P18 + lensing (red contours), P18 + lensing + non-CMB (blue contours) datasets.

$A_L = 1.090 \pm 0.036$ and 1.088 ± 0.035, for the Planck $P(q)$ and the new $P(q)$, respectively, which both differ from the theoretically expected $A_L = 1$ by 2.5σ. The inclusion of the A_L parameter does not significantly affect the values of the other seven primary parameters, leaving them close to the values found for the seven-parameter tilted nonflat ΛCDM models with $A_L = 1$ [the largest difference is for $\ln(10^{10}A_s)$, where it is 1.0σ (0.95σ) smaller for the Planck (new) $P(q)$]; it does, however, increase the error bars, but less than what happens in the P18 alone and P18 + lensing data cases discussed in Secs. IV A 1 and IV A 2, with the largest increase being 21% for $\ln(10^{10}A_s)$ for both $P(q)$ cases. In addition, in the case when A_L is allowed to vary, the derived parameters change somewhat and their error bars increase, with the largest changes associated with σ_8, where it is now 1.3σ (1.2σ) smaller for the Planck (new) $P(q)$ with a 21% (22%) larger error bar.

When non-CMB data (that include $f\sigma_8$ data) are added to the mix and the A_L parameter is allowed to vary, $A_L > 1$ is favored and there is a decrease in the value of σ_8 compared to the $A_L = 1$ case, which helps to alleviate the corresponding tension. Since $A_L > 1$ helps to resolve the lensing anomaly, there is less or no need to increase the value of Ω_m to predict more lensing. A lower value of Ω_m means less structure formation in the past, consequently slightly alleviating the σ_8 tension. While Ω_k plays a role at both early and late times, the A_L parameter only has an impact on CMB data. Since, as we shall see in Sec. IV A 6, non-CMB data prefer a flatter geometry than do P18 data, it is possible to understand why the evidence in favor of $\Omega_k \neq 0$ subsides, while the evidence for $A_L > 1$ does not, when non-CMB data are added to the mix. A fairly large negative value of Ω_k is required to resolve the P18 data lensing anomaly, thus improving upon the performance shown by the tilted flat ΛCDM model; however, such a large value of the curvature parameter is not supported by lensing data or by non-CMB data. This fact raises the issue of whether it is consistent to jointly use P18, lensing, and non-CMB datasets in the context of the nonflat models. We try to answer this question through the use of different statistical criteria, in Sec. IV C. Note that Figs. 4 and 7 show that when P18 + lensing + non-CMB data are used it is not necessary to consider $A_L \neq 1$ in order to make the three sets of tilted model contours overlap.

4. Comparing P18, P18 + lensing, *and* P18 + lensing + non-CMB *data cosmological constraints for each model*

Cosmological parameter contour plots allow us to easily see the degree of correlation between the two variables. If the two variables are more correlated then the corresponding constraint contours are more linelike, on the other hand, if they are less correlated the contours are broader and enclose two-dimensional areas. In this subsubsection, we comment on how the constraint contours for each cosmological model change depending on whether we consider P18, P18 + lensing, or P18 + lensing + non-CMB data. Figures 8–15 show, for each of the eight cosmological models we study, the cosmological parameter constraints for P18, P18 + lensing, and P18 + lensing + non-CMB data. The constraint contours shrink as more data are included in the analysis used to determine them.

From Fig. 8, for the six-parameter tilted flat ΛCDM, we see that there are significant overlaps between the contours obtained in the three datasets considered. Along with the results discussed in Secs. IV A 2 and IV A 3 this is an indication that there is not significant tension between P18, P18 + lensing, and P18 + lensing + non-CMB data when these data are analyzed in the tilted flat ΛCDM model. The Ω_m-H_0 panel contours indicate that these two parameters are strongly correlated. The inclusion of lensing data and/or non-CMB data, which provide information about the late-time Universe, partially breaks this correlation and induces a shift in the one-dimensional posterior distributions of not only these two parameters but also other parameters. Non-CMB data cause a larger shift.

For the six-parameter untilted nonflat ΛCDM model (see Fig. 9), constraint contours determined from the three different datasets overlap only for some parameters. In particular, for constraint contours in panels that involve Ω_k, Ω_m, or H_0 there is no overlap between those determined using P18 data and those determined using P18 + lensing + non-CMB data (there are larger than 2σ differences between these contours when one of these three parameters are involved and the differences are larger when two of these three parameters are involved), and there is only a slight amount of overlap between the P18 data contours and the P18 + lensing data contours. The Ω_m-H_0-Ω_k geometrical degeneracy is prominent for P18 data and is clearly seen in the Ω_k-Ω_m, Ω_k-H_0, and Ω_m-H_0 panels, as these three parameters are strongly correlated. Including lensing data and/or non-CMB data partially breaks this degeneracy, causing significant shifts in the one-dimensional posterior distributions of not only these three parameters but also other parameters. The shifts are bigger here than in the tilted flat ΛCDM model and indicate significant tension between the datasets, especially between the P18 and P18 + lensing + non-CMB datasets, when they are analyzed in the untilted nonflat ΛCDM model. Non-CMB data again appear to cause the larger shift. As discussed in more detail in Sec. IV C, these shifts mean that P18 and non-CMB data are mutually inconsistent in the untilted nonflat ΛCDM model and so cannot be jointly used to derive cosmological parameter constraints in this model.

Similar, but quantitatively less discrepant, results are obtained for the seven-parameter tilted nonflat ΛCDM Planck $P(q)$ and the tilted nonflat ΛCDM new $P(q)$ models (see Figs. 10 and 11). The differences between the untilted nonflat and tilted nonflat results is likely a consequence of the additional n_s parameter in the tilted nonflat models. In the tilted nonflat models, the more-discrepant P18 and

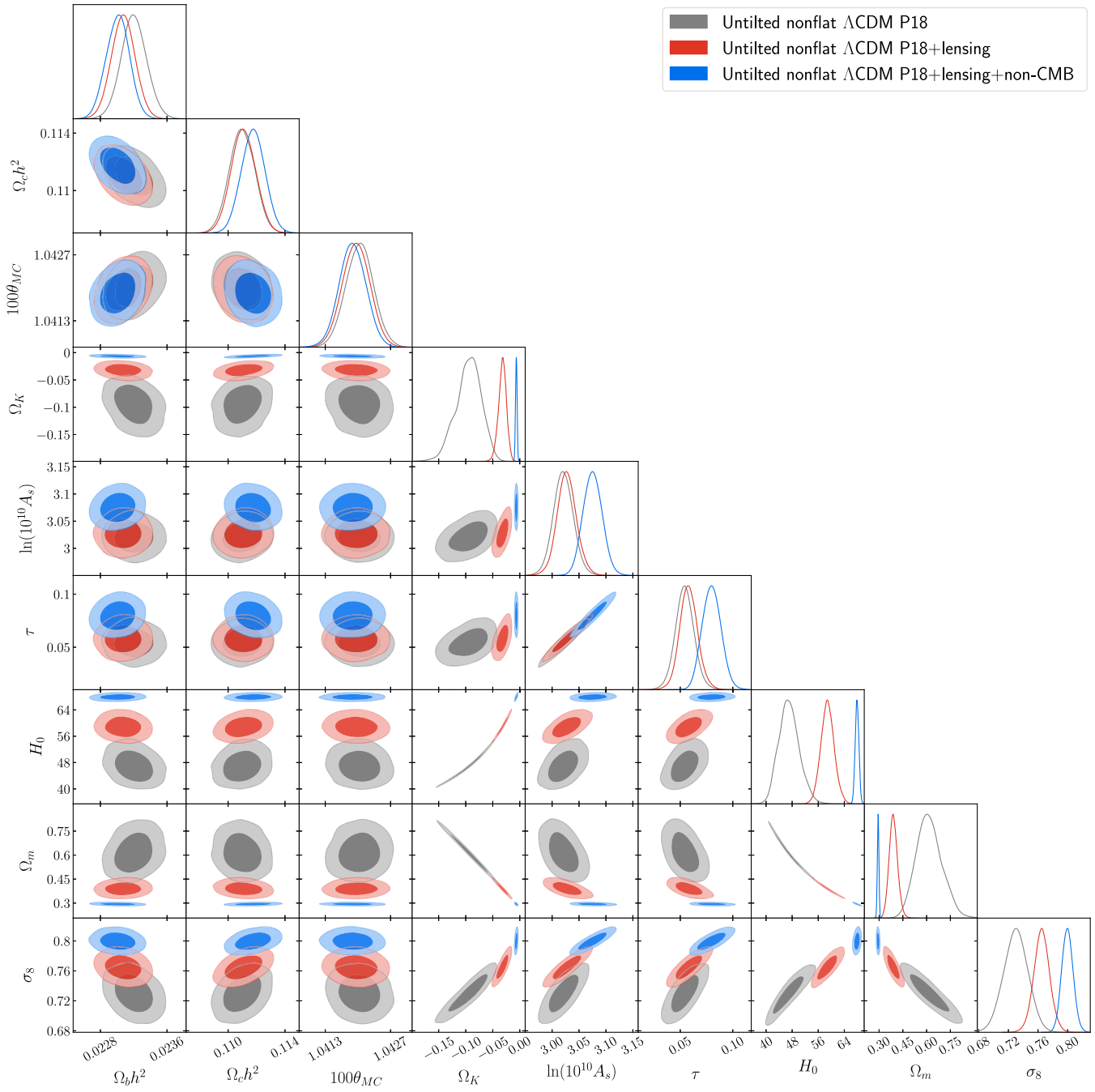

FIG. 9. Likelihood distributions of untilted nonflat ΛCDM model parameters constrained by P18 (gray contours), P18 + lensing (red contours), P18 + lensing + non-CMB (blue contours) datasets.

P18 + lensing + non-CMB data constraint contours overlap in all panels for pairs of the six primary cosmological parameters excluding the Ω_k parameter, as well as the derived Ω_m and H_0 parameters. The differences are larger in the Planck $P(q)$ case than in the new $P(q)$ case, largest for H_0, smallest for Ω_m, with Ω_k being in between. In the new $P(q)$ case, the 2σ contours overlap for Ω_m and almost overlap for Ω_k. These results may be an indication of the tension found, in the context of the tilted nonflat models, between P18 data and the BAO dataset. We shall study this tension in more detail in Sec. IV C. As in the untilted nonflat ΛCDM model, the geometrical degeneracy between Ω_m, H_0, and Ω_k affects the tilted nonflat models. Again, including lensing data and/or non-CMB data partially breaks this degeneracy, causing significant shifts in the one-dimensional posterior distributions of not only these three parameters but also other parameters. The shifts are bigger here than in the tilted flat ΛCDM model and but

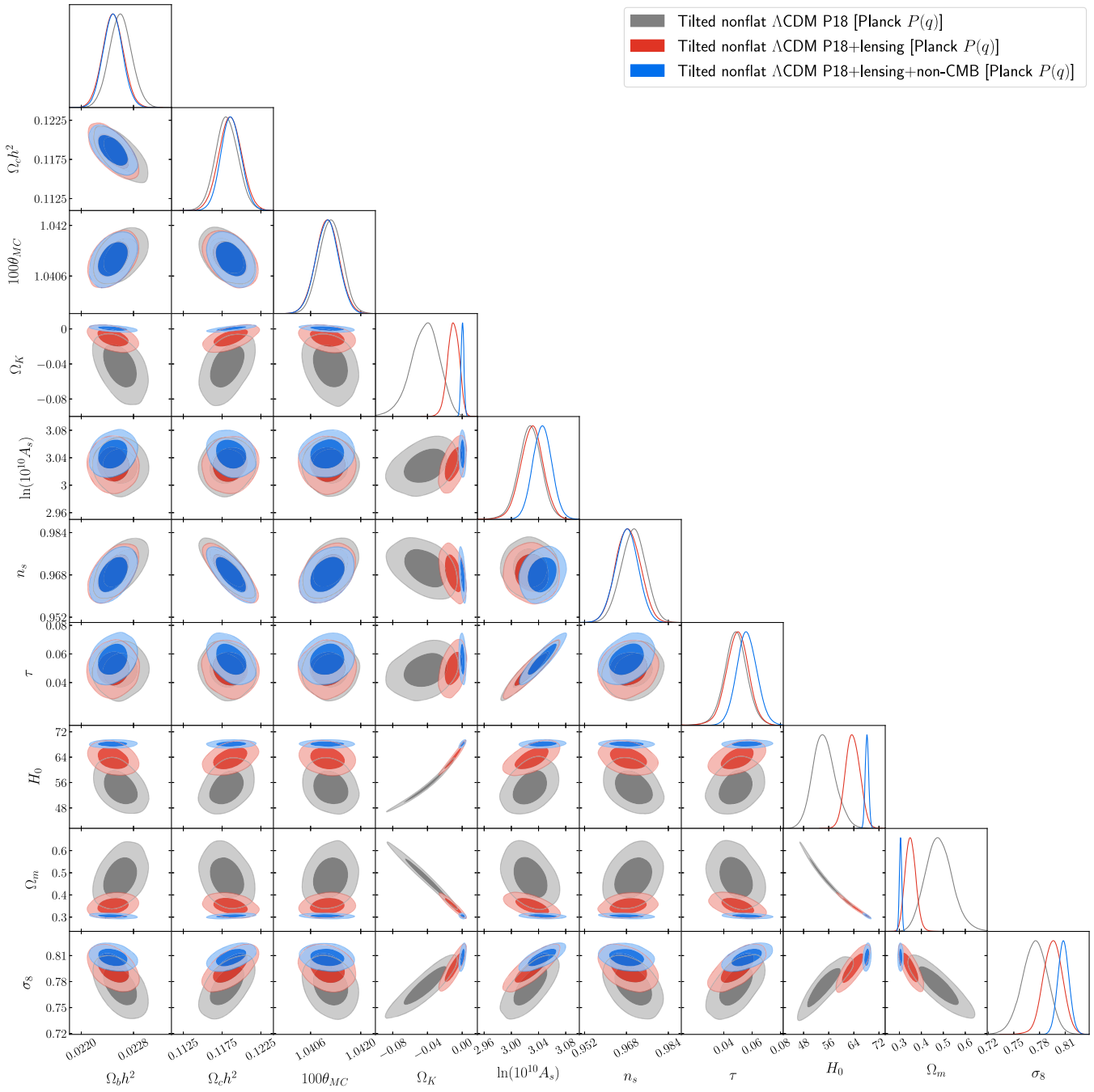

FIG. 10. Likelihood distributions of tilted nonflat ΛCDM model parameters with the Planck team's initial power spectrum [Planck $P(q)$] constrained by P18 (gray contours), P18 + lensing (red contours), P18 + lensing + non-CMB (blue contours) datasets.

smaller than in the untilted nonflat ΛCDM model, but still indicate some tension between the datasets, especially between the P18 and P18 + lensing + non-CMB datasets, especially when they are analyzed in the tilted nonflat ΛCDM Planck $P(q)$ model. Non-CMB data again appear to cause the larger shift.

When the A_L parameter is allowed to vary, the three different sets of constraint contours overlap in all four models (see Figs. 12–15). In the nonflat models there now is a bigger degeneracy between the cosmological parameters Ω_m, H_0, Ω_k, and A_L, which causes the constraint contours to expand relative to the $A_L = 1$ case, especially for P18 data. For some parameters in the untilted nonflat ΛCDM model and the tilted nonflat ΛCDM new $P(q)$ model, we observe a bimodal distribution when only P18 data are used, and the same parameters in the tilted nonflat ΛCDM Planck $P(q)$ model have an almost bimodal distribution for P18 data. These bimodalities are

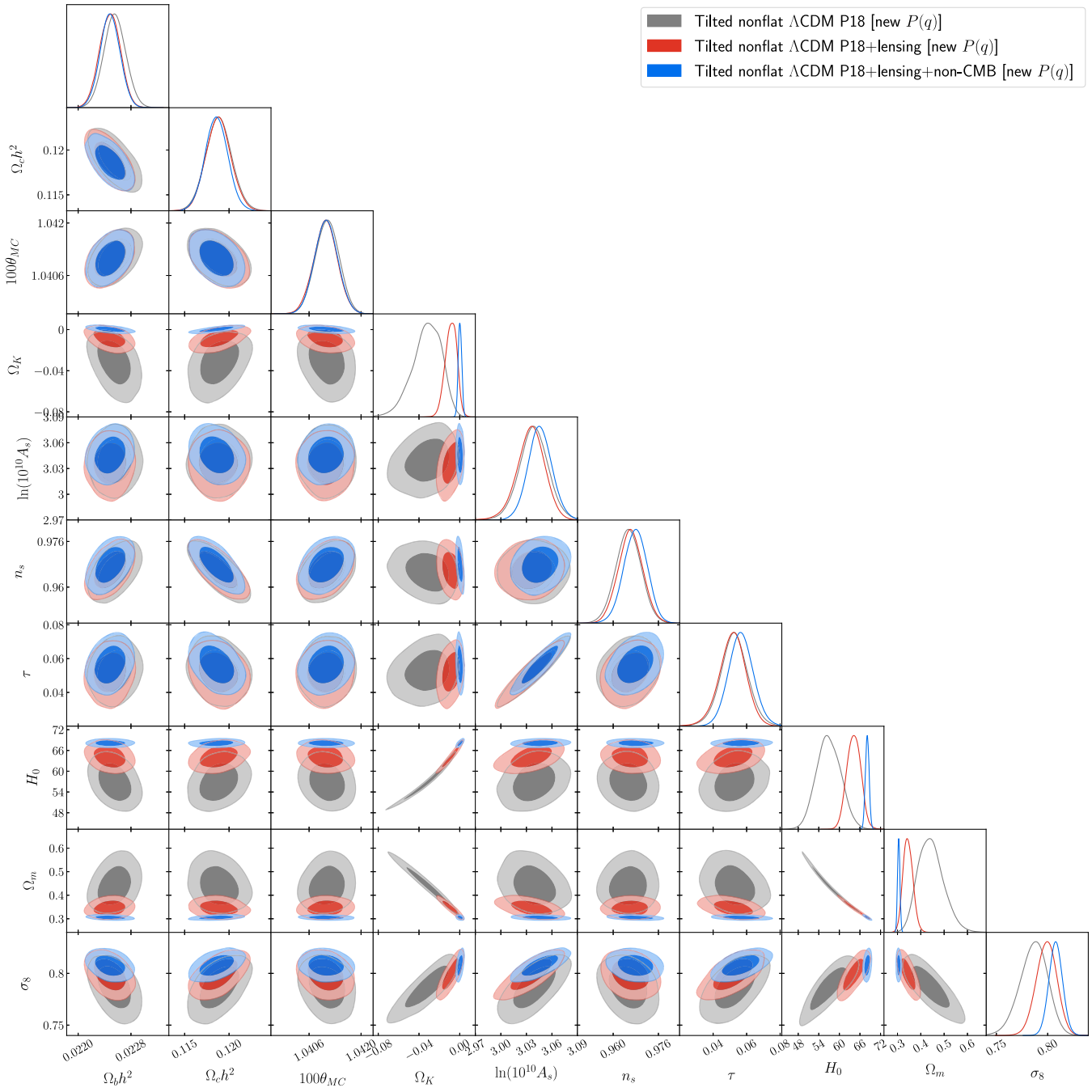

FIG. 11. Likelihood distributions of tilted nonflat ΛCDM model parameters with the new initial power spectrum [new $P(q)$] constrained by P18 (gray contours), P18 + lensing (red contours), P18 + lensing + non-CMB (blue contours) datasets.

likely a consequences of the above-mentioned geometrical degeneracy.

5. *Comparing P18 data and* BAO/BAO′ *data cosmological constraints*

In this subsubsection, we compare BAO and BAO′ data cosmological constraints to those obtained from P18 data. Prior to jointly analyzing P18 + BAO/BAO′ data, we need to determine whether P18 and BAO/BAO′ data cosmological constraints are mutually consistent. In Sec. IV C, we use two other statistical estimators to examine whether or not P18 and BAO/BAO′ data are in tension.

The cosmological parameter mean values and error bars favored by the P18, BAO, BAO′, P18 + BAO, and P18 + BAO′ datasets are summarized in Tables VIII–XI for the tilted flat ΛCDM ($+A_L$) models, the untilted nonflat ΛCDM ($+A_L$) models, the tilted nonflat ΛCDM ($+A_L$)

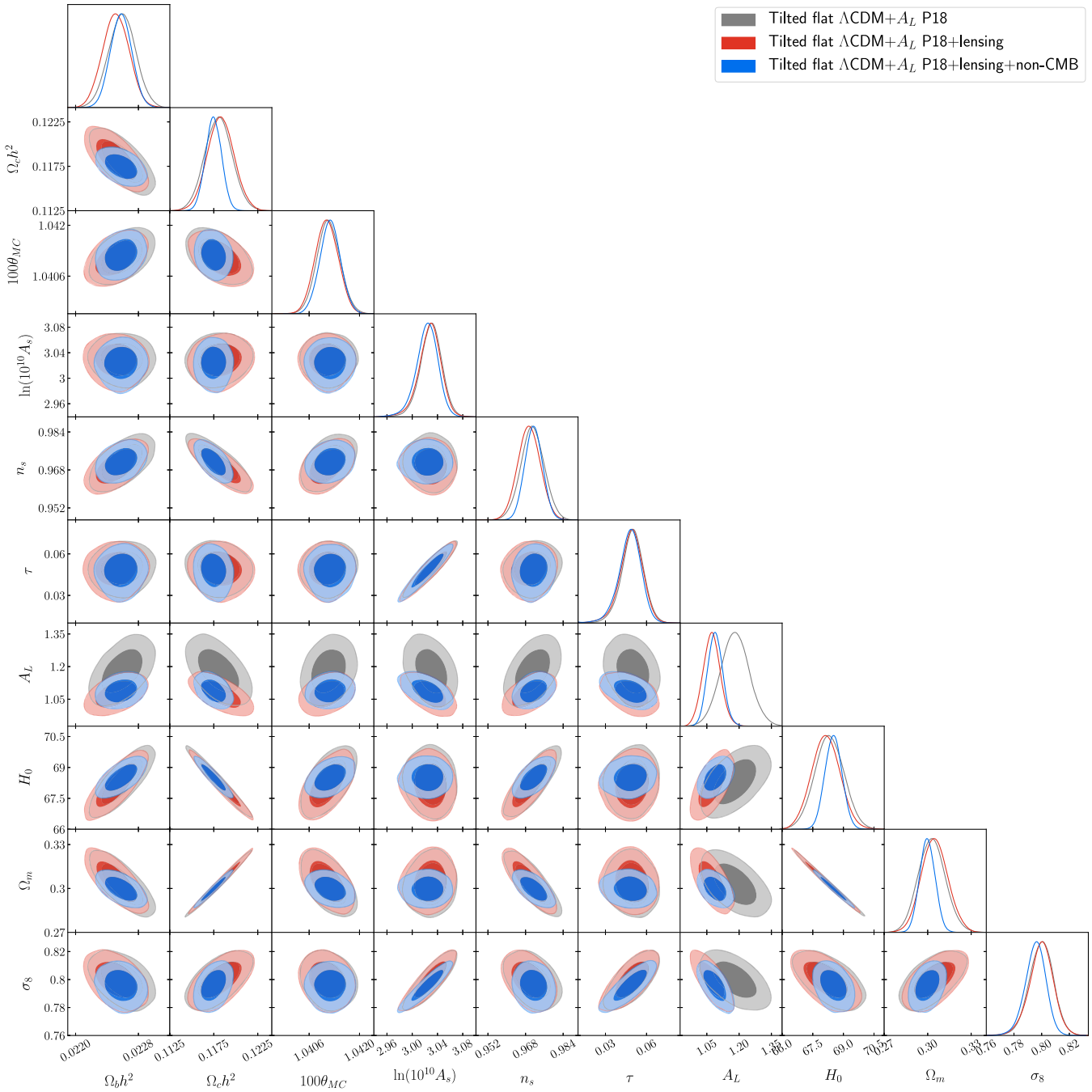

FIG. 12. Likelihood distributions of tilted flat ΛCDM + A_L model parameters constrained by P18 (gray contours), P18 + lensing (red contours), P18 + lensing + non-CMB (blue contours) datasets.

models with the Planck $P(q)$, and the tilted nonflat ΛCDM ($+A_L$) models with the new $P(q)$, respectively. Likelihood distributions of cosmological parameters of the four models with $A_L = 1$ and A_L varying are shown in Figs. 16–23 for the P18, BAO, BAO′, P18 + BAO, and P18 + BAO′ datasets.

Since neither BAO′ nor BAO data have the ability to constrain τ or n_s or A_L, we set their values to those found in the corresponding P18 data analysis. In addition, for the same reason, in the BAO′ data analyses, we also set the value of $\ln(10^{10}A_s)$ to that found in the corresponding P18 data analysis. We see from the upper and lower panels of Tables VIII–XI that the BAO and BAO′ data results for the $A_L = 1$ and A_L-varying cases are similar, even though the fixed τ and n_s [and $\ln(10^{10}A_s)$] values are slightly different for the $A_L = 1$ and A_L-varying cases.

From Tables VIII–XI we see that, in the six nonflat ΛCDM ($+A_L$) models, the constraints set by BAO′/BAO

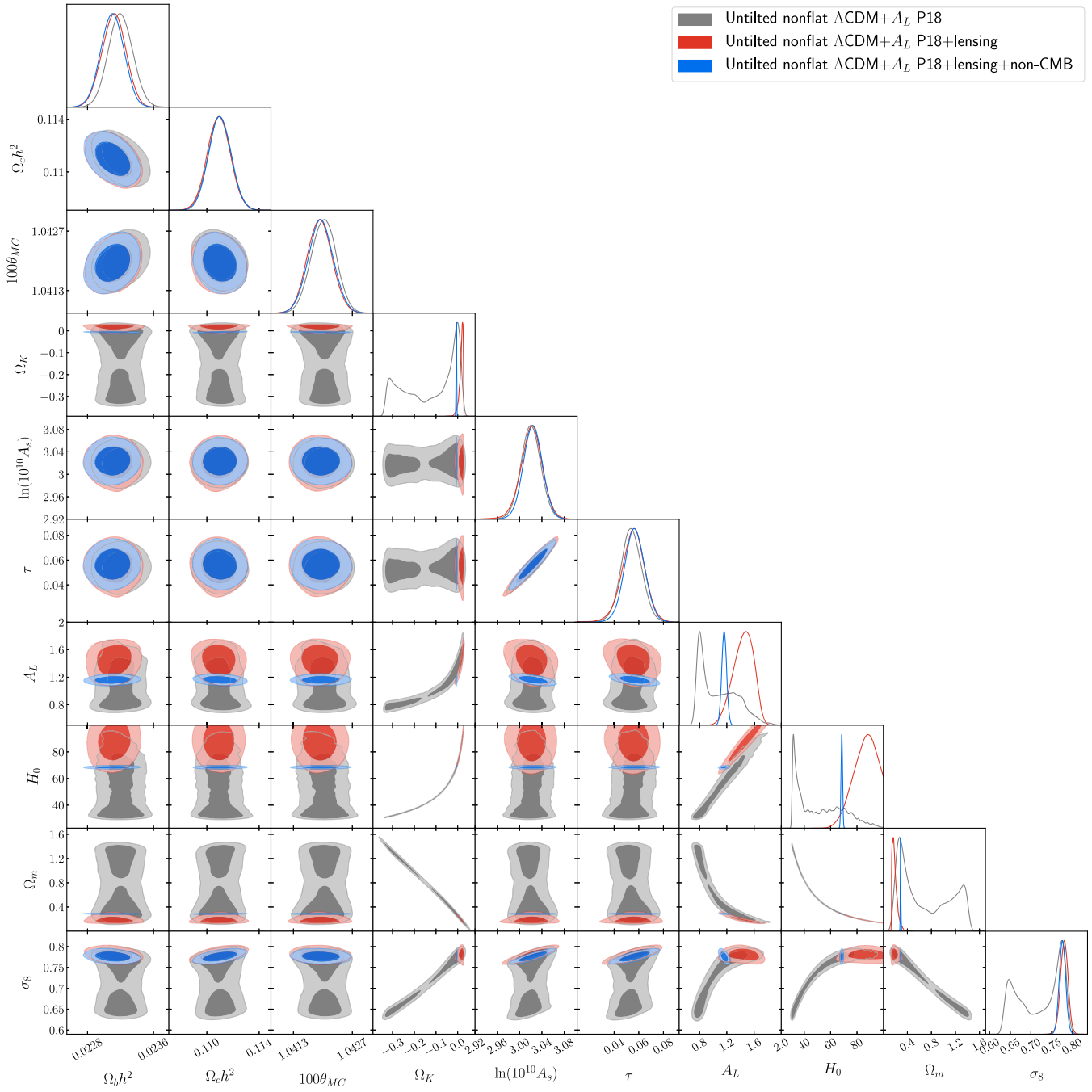

FIG. 13. Likelihood distributions of untilted nonflat ΛCDM + A_L model parameters constrained by P18 (gray contours), P18 + lensing (red contours), P18 + lensing + non-CMB (blue contours) datasets.

data on Ω_m are tighter than the ones imposed by P18 data, and in the three nonflat ΛCDM + A_L models the constraints set by BAO′/BAO data on Ω_k are tighter than the ones imposed by P18 data. P18 data more restrictively constrain all other parameters in all eight cosmological models.

As we discuss below, there is a significant level of disagreement in the nonflat models between P18 data cosmological constraints and BAO′/BAO data cosmological constraints, in most cases. From Tables IX–XI we see that all three datasets, P18, BAO′, and BAO, favor negative values of the curvature parameter, with BAO′ and BAO data favoring closed geometry only weakly, at 0.48σ to 0.96σ. However, we should take into account the geometrical degeneracy between H_0, Ω_k, and Ω_m and note that both BAO′ and BAO data favor higher values of H_0 and lower values of Ω_m than do P18 data, and this is what causes the P18 and BAO/BAO′ cosmological constraint differences.

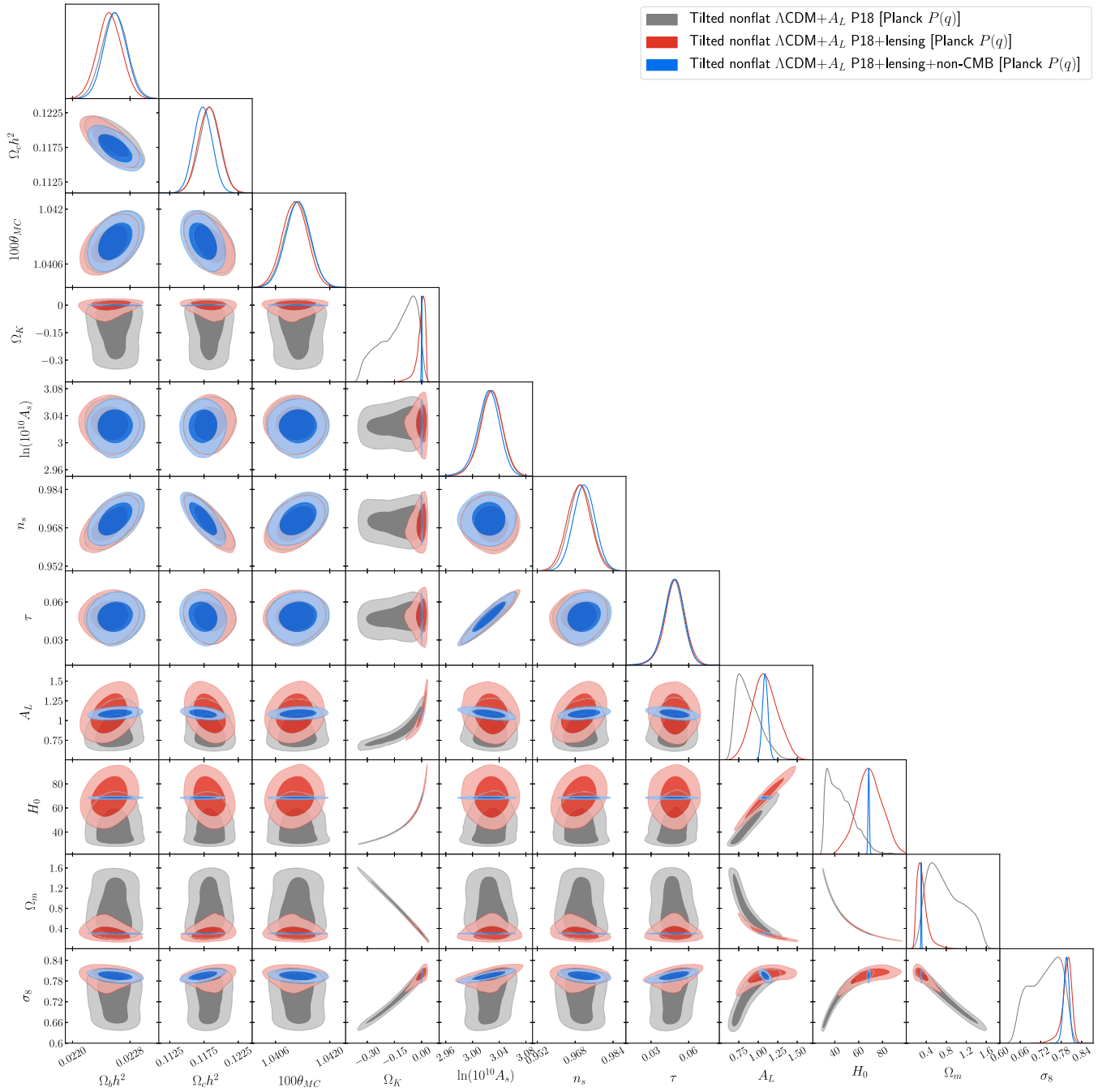

FIG. 14. Likelihood distributions of tilted nonflat ΛCDM + A_L model parameters with the Planck team's initial power spectrum [Planck $P(q)$] constrained by P18 (gray contours), P18 + lensing (red contours), P18 + lensing + non-CMB (blue contours) datasets.

We first discuss BAO′ data results (BAO′ data do not include $f\sigma_8$ data points, see Sec. II) and then consider results from BAO data. This will allow us to test the impact of some $f\sigma_8$ data on the cosmological constraints.

Comparing the six- and the three-parameter tilted flat ΛCDM model primary cosmological parameter constraints for P18 and BAO′ data, shown in the upper half of Table VIII, we see that the values of $\Omega_b h^2$ and $\Omega_c h^2$ are in mild disagreement, at 1.3σ and 1.1σ, respectively. We also observe a similar 1.3σ level of tension in the derived H_0 values, whereas the other two derived parameters, Ω_m and σ_8, show a better agreement, disagreeing by only 0.91σ and 0.90σ, respectively.

Comparing the seven- and the three-parameter tilted flat ΛCDM + A_L model primary cosmological parameter constraints for P18 and BAO′ data, shown in the lower half of Table VIII, we see that the values of $\Omega_b h^2$, $\Omega_c h^2$, and $100\theta_{\rm MC}$ are in 1.7σ, 1.4σ, and 1.3σ tension, respectively.

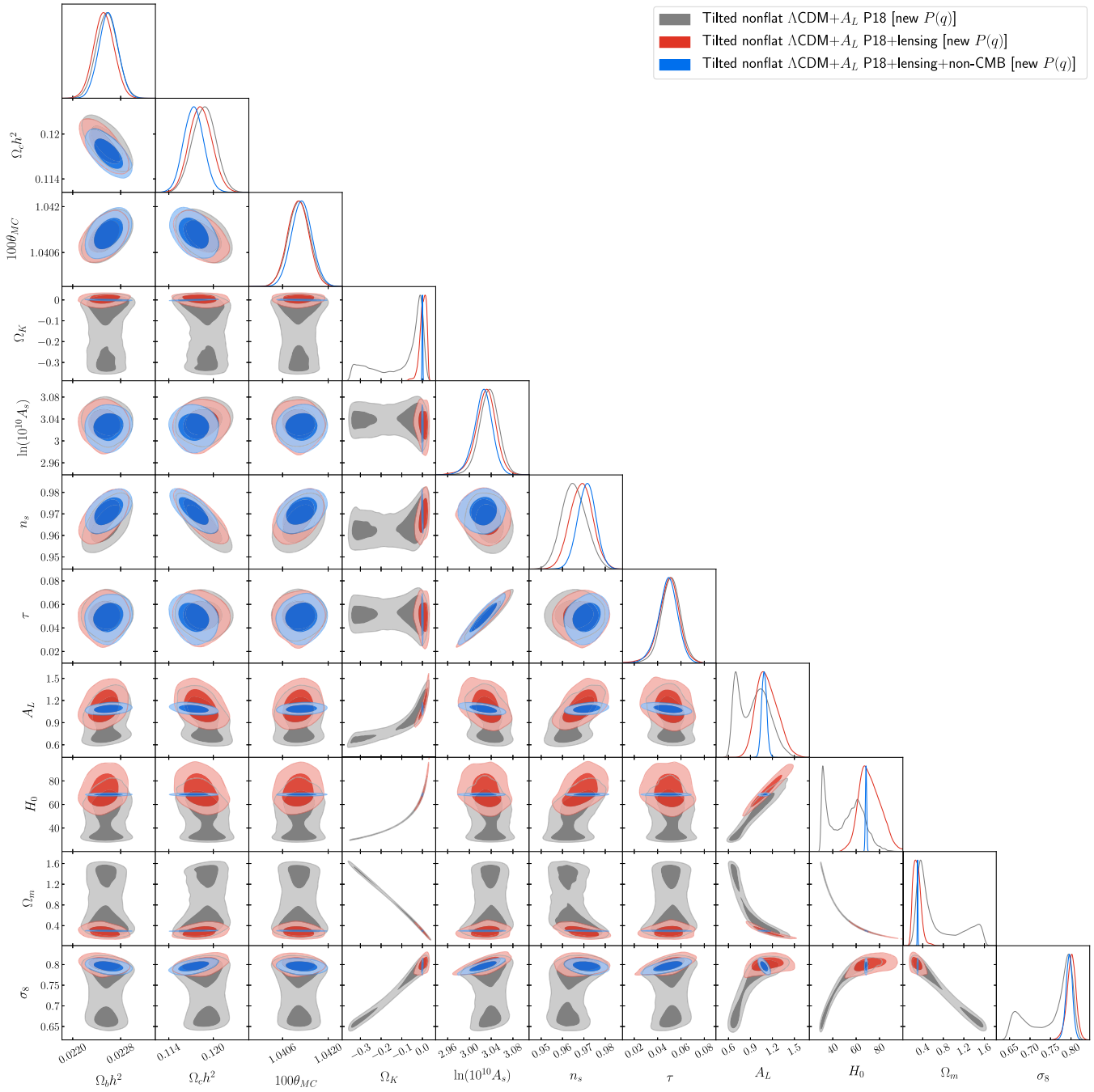

FIG. 15. Likelihood distributions of tilted nonflat ΛCDM + A_L model parameters with the new initial power spectrum [new $P(q)$] constrained by P18 (gray contours), P18 + lensing (red contours), P18 + lensing + non-CMB (blue contours) datasets.

As for the derived parameters, we find H_0 and σ_8 values are in 1.7σ and 1.2σ disagreement, while Ω_m values differ by only 0.046σ. This means that only for the Ω_m parameter does the inclusion of a varying A_L reduce the disagreement found in the $A_L = 1$ case, while increasing the disagreement for a number of other parameters.

P18 and BAO′ data results obtained for the six- and the three-parameter untilted nonflat ΛCDM model, shown in the upper half of Table IX, indicate more significant differences than found in the tilted flat ΛCDM model. The primary cosmological parameters $\Omega_b h^2$ and $\Omega_c h^2$ values disagree at 1.1σ and 1.4σ, while the primary spatial curvature parameter value is $\Omega_k = -0.034 \pm 0.057$ for BAO′ data, which is 0.60σ away from flat and in 0.99σ tension with the P18 value $\Omega_k = -0.095 \pm 0.024$, which is 4.0σ away from flat. Regarding the derived parameters, we find that Ω_m, H_0, and σ_8 values are in 3.7σ, 2.9σ, and 1.5σ disagreement. According to these results, P18 and BAO′

TABLE VIII. Mean and 68.3% confidence limits of tilted flat ΛCDM ($+A_L$) model parameters constrained by TT, TE, EE + lowE (P18), BAO, and BAO′ data. H_0 has units of km s^{-1} Mpc^{-1}.[a]

	Tilted flat ΛCDM model				
Parameter	P18	P18 + BAO	BAO	P18 + BAO′	BAO′
$\Omega_b h^2$	0.02236 ± 0.00015	0.02243 ± 0.00013	0.043 ± 0.016	0.02241 ± 0.00014	0.043 ± 0.016
$\Omega_c h^2$	0.1202 ± 0.0014	0.11926 ± 0.00097	0.163 ± 0.042	0.11946 ± 0.00098	0.168 ± 0.044
$100\theta_{\rm MC}$	1.04090 ± 0.00031	1.04102 ± 0.00029	1.054 ± 0.026	1.04099 ± 0.00029	1.059 ± 0.025
τ	0.0542 ± 0.0079	0.0581 ± 0.0081	0.0542	0.0555 ± 0.0077	0.0542
n_s	0.9649 ± 0.0043	0.9673 ± 0.0037	0.9649	0.9665 ± 0.0038	0.9649
$\ln(10^{10} A_s)$	3.044 ± 0.016	3.051 ± 0.017	3.01 ± 0.27	3.045 ± 0.016	3.044
H_0	67.28 ± 0.61	67.70 ± 0.43	83 ± 12	67.60 ± 0.44	83 ± 12
Ω_m	0.3165 ± 0.0084	0.3106 ± 0.0058	0.294 ± 0.015	0.3119 ± 0.0059	0.300 ± 0.016
σ_8	0.8118 ± 0.0074	0.8119 ± 0.0073	0.874 ± 0.037	0.8102 ± 0.0070	0.92 ± 0.12
$\chi^2_{\rm min}$ (total)	2765.80	2786.66	15.92	2777.75	10.98
$\chi^2_{\rm min}$ (BAO/BAO′)	⋯	20.22	15.92	11.61	10.98
$\chi^2_{\rm BAO/BAO'}$ (at P18 B-F)	⋯	22.24	22.24	12.58	12.58
DIC	2817.93	2839.25	21.93	2829.61	14.93
AIC$_c$	2819.80	2840.66	27.56	2831.75	19.98
	Tilted flat ΛCDM + A_L model				
Parameter	P18	P18 + BAO	BAO	P18 + BAO′	BAO′
$\Omega_b h^2$	0.02259 ± 0.00017	0.02258 ± 0.00015	0.043 ± 0.015	0.02256 ± 0.00014	0.045 ± 0.013
$\Omega_c h^2$	0.1180 ± 0.0015	0.1183 ± 0.0010	0.163 ± 0.042	0.1185 ± 0.0010	0.177 ± 0.042
$100\theta_{\rm MC}$	1.04114 ± 0.00032	1.04113 ± 0.00029	1.055 ± 0.024	1.04109 ± 0.00030	1.065 ± 0.018
τ	0.0496 ± 0.0082	0.0522 ± 0.0080	0.0496	0.0492 ± 0.0084	0.0496
n_s	0.9710 ± 0.0050	0.9705 ± 0.0038	0.9710	0.9698 ± 0.0039	0.9710
$\ln(10^{10} A_s)$	3.030 ± 0.017	3.036 ± 0.017	3.00 ± 0.27	3.030 ± 0.018	3.030
A_L	1.181 ± 0.067	1.170 ± 0.060	1.181	1.174 ± 0.061	1.181
H_0	68.31 ± 0.71	68.21 ± 0.46	83 ± 12	68.11 ± 0.47	85 ± 10
Ω_m	0.3029 ± 0.0093	0.3042 ± 0.0060	0.294 ± 0.015	0.3055 ± 0.0061	0.302 ± 0.017
σ_8	0.7997 ± 0.0088	0.8031 ± 0.0077	0.875 ± 0.037	0.8011 ± 0.0079	0.93 ± 0.11
$\chi^2_{\rm min}$ (total)	2756.12	2776.71	15.91	2767.77	10.98
$\chi^2_{\rm min}$ (BAO/BAO′)	⋯	20.47	15.91	11.37	10.98
$\chi^2_{\rm BAO/BAO'}$ (at P18 B-F)	⋯	20.78	20.78	11.88	11.88
DIC	2812.41	2832.92	21.83	2823.77	15.04
ΔDIC	−5.52	−6.33	−0.10	−5.90	0.11
AIC$_c$	2812.12	2832.71	27.55	2823.77	19.98
ΔAIC$_c$	−7.68	−7.95	−0.01	−7.98	0.00

[a]Note: ΔDIC (ΔAIC$_c$) indicates an excess value relative to that of the tilted flat ΛCDM model constrained with the same data. The number of free parameters of the tilted flat ΛCDM model is 27 for P18, P18 + BAO, and P18 + BAO′ datasets (including 21 internal calibration parameters), 4 for BAO data, and 3 for BAO′ data.

data probably should not be jointly analyzed in the context of the untilted nonflat ΛCDM model.

The results for the seven- and the three-parameter untilted nonflat ΛCDM + A_L model, obtained considering P18 and BAO′ data, are in the lower half of Table IX. While there is a slight increase in the disagreement between the values of the primary parameters $\Omega_b h^2$ (1.3σ) and $\Omega_c h^2$ (1.6σ), there are significant decreases for the derived parameters Ω_m and H_0, but not for σ_8, that now disagree by 0.93σ, 1.5σ, and 1.5σ, respectively. This is caused by the increase in the size of the error bars in the A_L-varying P18 case with respect to the corresponding values obtained with $A_L = 1$. For the BAO′ data primary spatial curvature parameter, we find $\Omega_k = -0.035 \pm 0.058$, which is 0.60σ away from flat hypersurfaces and only in 0.64σ tension with the P18 value $\Omega_k = -0.12 \pm 0.12$, which is now only 1.0σ away from flat. According to these results, unlike in the $A_L = 1$ case, in the A_L-varying case P18 and BAO′ data can probably be jointly analyzed in the context of the untilted

TABLE IX. Mean and 68.3% confidence limits of untilted nonflat ΛCDM ($+A_L$) model parameters constrained by TT, TE, EE + lowE (P18), BAO, and BAO′ data. H_0 has units of km s^{-1} Mpc^{-1}.[a]

	Untilted nonflat ΛCDM model				
Parameter	P18	P18 + BAO	BAO	P18 + BAO′	BAO′
$\Omega_b h^2$	0.02320 ± 0.00015	0.02298 ± 0.00014	0.040 ± 0.015	0.02299 ± 0.00014	0.040 ± 0.015
$\Omega_c h^2$	0.11098 ± 0.00088	0.11184 ± 0.00089	0.175 ± 0.046	0.11171 ± 0.00089	0.175 ± 0.047
$100\theta_{\rm MC}$	1.04204 ± 0.00030	1.04188 ± 0.00029	1.16 ± 0.13	1.04189 ± 0.00030	1.13 ± 0.12
τ	0.0543 ± 0.0091	0.077 ± 0.010	0.0543	0.073 ± 0.010	0.0543
Ω_k	-0.095 ± 0.024	-0.0066 ± 0.0015	-0.047 ± 0.059	-0.0074 ± 0.0016	-0.034 ± 0.057
$\ln(10^{10} A_s)$	3.021 ± 0.019	3.069 ± 0.021	2.70 ± 0.43	3.059 ± 0.021	3.021
H_0	47.1 ± 3.2	67.77 ± 0.60	84 ± 12	67.46 ± 0.63	83 ± 12
Ω_m	0.617 ± 0.082	0.2950 ± 0.0055	0.303 ± 0.019	0.2975 ± 0.0057	0.307 ± 0.019
σ_8	0.730 ± 0.017	0.7977 ± 0.0093	0.850 ± 0.048	0.7927 ± 0.0090	1.00 ± 0.18
$\chi^2_{\rm min}$ (total)	2789.77	2837.93	15.91	2828.81	10.67
$\chi^2_{\rm min}$ (BAO/BAO′)	⋯	20.34	15.91	11.68	10.67
$\chi^2_{\rm BAO/BAO'}$ (at P18 B-F)	⋯	1987.47	1987.47	1765.08	1765.08
DIC	2847.14	2895.04	24.31	2884.90	17.55
ΔDIC	29.21	55.79	2.38	55.29	2.62
AIC$_c$	2843.77	2891.93	31.91	2882.81	24.39
ΔAIC$_c$	23.97	51.27	4.35	51.06	4.41
	Untilted nonflat ΛCDM + A_L model				
Parameter	P18	P18 + BAO	BAO	P18 + BAO′	BAO′
$\Omega_b h^2$	0.02320 ± 0.00015	0.02318 ± 0.00015	0.041 ± 0.015	0.02320 ± 0.00015	0.042 ± 0.014
$\Omega_c h^2$	0.11097 ± 0.00087	0.11117 ± 0.00086	0.176 ± 0.045	0.11095 ± 0.00087	0.180 ± 0.044
$100\theta_{\rm MC}$	1.04202 ± 0.00030	1.04198 ± 0.00030	1.16 ± 0.13	1.04199 ± 0.00030	1.14 ± 0.12
τ	0.0540 ± 0.0087	0.0598 ± 0.0087	0.0540	0.0557 ± 0.0089	0.0540
Ω_k	-0.12 ± 0.12	-0.0064 ± 0.0015	-0.050 ± 0.060	-0.0073 ± 0.0015	-0.035 ± 0.058
$\ln(10^{10} A_s)$	3.020 ± 0.018	3.033 ± 0.018	2.68 ± 0.41	3.023 ± 0.019	3.020
A_L	1.08 ± 0.27	1.310 ± 0.062	1.08	1.319 ± 0.063	1.08
H_0	52 ± 18	68.27 ± 0.61	84 ± 12	67.93 ± 0.62	84 ± 11
Ω_m	0.70 ± 0.42	0.2897 ± 0.0054	0.304 ± 0.018	0.2921 ± 0.0055	0.307 ± 0.020
σ_8	0.721 ± 0.053	0.7799 ± 0.0083	0.848 ± 0.049	0.7750 ± 0.0085	1.01 ± 0.18
$\chi^2_{\rm min}$ (total)	2787.76	2809.82	15.89	2799.18	10.68
$\chi^2_{\rm min}$ (BAO/BAO′)	⋯	21.96	15.89	11.38	10.68
$\chi^2_{\rm BAO/BAO'}$ (at P18 B-F)	⋯	106.63	106.63	80.18	80.18
DIC	2846.45	2869.28	24.63	2857.90	17.89
ΔDIC	28.52	30.03	2.70	28.29	2.96
AIC$_c$	2843.76	2865.82	31.89	2855.18	24.39
ΔAIC$_c$	23.96	25.16	4.33	23.43	4.41

[a]Note: ΔDIC (ΔAIC$_c$) indicates an excess value relative to that of the tilted flat ΛCDM model constrained with the same data.

nonflat ΛCDM model. Note that in this case a joint analysis of P18 + BAO′ data favors closed geometry at 4.9σ, with $\Omega_k = -0.0073 \pm 0.0015$, although because of the lack of the tilt (n_s) degree of freedom, this untilted nonflat ΛCDM + A_L model does not provide a good fit to smaller-angular-scale P18 data, which is reflected in the large ΔDIC and ΔAIC$_c$ values for the P18 + BAO′ case in the lower half of Table IX.

Comparing the seven- and the four-parameter tilted nonflat ΛCDM Planck $P(q)$ model primary cosmological parameter constraints for P18 and BAO′ data, we see in the upper half of Table X that the values of $\Omega_b h^2$ and $\Omega_c h^2$ are both in 1.1σ disagreement. The BAO′ data primary spatial curvature parameter value $\Omega_k = -0.033 \pm 0.055$ is 0.6σ away from flat and only in 0.17σ tension with the P18 value $\Omega_k = -0.043 \pm 0.017$, which is 2.5σ in favor of closed geometry. The derived parameters Ω_m, H_0, and σ_8 are in 2.7σ, 2.3σ, and 1.2σ tension. These results reveal that P18 and BAO′ data cosmological constraints are somewhat inconsistent in the tilted nonflat ΛCDM Planck

TABLE X. Mean and 68.3% confidence limits of Planck-$P(q)$-based tilted nonflat ΛCDM ($+A_L$) model parameters constrained by TT, TE, EE + lowE (P18), BAO, and BAO′ data. H_0 has units of km s^{-1} Mpc^{-1}.[a]

	Tilted nonflat ΛCDM model [Planck $P(q)$]				
Parameter	P18	P18 + BAO	BAO	P18 + BAO′	BAO′
$\Omega_b h^2$	0.02260 ± 0.00017	0.02241 ± 0.00015	0.040 ± 0.015	0.02241 ± 0.00015	0.040 ± 0.016
$\Omega_c h^2$	0.1181 ± 0.0015	0.1195 ± 0.0014	0.174 ± 0.047	0.1195 ± 0.0014	0.172 ± 0.047
$100\theta_{\rm MC}$	1.04116 ± 0.00032	1.04099 ± 0.00032	1.15 ± 0.13	1.04099 ± 0.00032	1.13 ± 0.12
τ	0.0483 ± 0.0083	0.0578 ± 0.0077	0.0483	0.0550 ± 0.0078	0.0483
Ω_k	-0.043 ± 0.017	0.0005 ± 0.0018	-0.046 ± 0.060	-0.0001 ± 0.0018	-0.033 ± 0.055
n_s	0.9706 ± 0.0047	0.9667 ± 0.0045	0.9706	0.9666 ± 0.0044	0.9706
$\ln(10^{10}A_s)$	3.027 ± 0.017	3.051 ± 0.016	2.74 ± 0.43	3.044 ± 0.016	3.027
H_0	54.5 ± 3.6	67.83 ± 0.58	83 ± 12	67.58 ± 0.62	83 ± 12
Ω_m	0.481 ± 0.062	0.3100 ± 0.0060	0.303 ± 0.019	0.3122 ± 0.0063	0.306 ± 0.019
σ_8	0.775 ± 0.015	0.8130 ± 0.0079	0.850 ± 0.049	0.8099 ± 0.0081	0.98 ± 0.17
$\chi^2_{\rm min}$ (total)	2754.73	2786.20	15.88	2776.90	10.68
$\chi^2_{\rm min}$ (BAO/BAO′)	⋯	20.09	15.88	11.71	10.68
$\chi^2_{\rm BAO/BAO'}$ (at P18 B-F)	⋯	665.90	665.90	582.59	582.59
DIC	2810.59	2840.62	24.34	2832.28	17.58
ΔDIC	−7.34	1.37	2.41	2.67	2.65
AIC$_c$	2810.73	2842.20	31.88	2832.90	24.39
ΔAIC$_c$	−9.07	1.54	4.32	1.15	4.41
	Tilted nonflat ΛCDM + A_L model [Planck $P(q)$]				
Parameter	P18	P18 + BAO	BAO	P18 + BAO′	BAO′
$\Omega_b h^2$	0.02258 ± 0.00017	0.02260 ± 0.00017	0.041 ± 0.014	0.02262 ± 0.00017	0.044 ± 0.013
$\Omega_c h^2$	0.1183 ± 0.0015	0.1180 ± 0.0015	0.174 ± 0.045	0.1178 ± 0.0015	0.182 ± 0.043
$100\theta_{\rm MC}$	1.04116 ± 0.00033	1.04115 ± 0.00033	1.16 ± 0.14	1.04118 ± 0.00032	1.12 ± 0.11
τ	0.0478 ± 0.0081	0.0522 ± 0.0081	0.0478	0.0496 ± 0.0085	0.0478
Ω_k	-0.130 ± 0.095	-0.0004 ± 0.0018	-0.045 ± 0.063	-0.0012 ± 0.0018	-0.026 ± 0.054
n_s	0.9704 ± 0.0048	0.9712 ± 0.0047	0.9704	0.9716 ± 0.0047	0.9704
$\ln(10^{10}A_s)$	3.027 ± 0.017	3.035 ± 0.017	2.74 ± 0.45	3.029 ± 0.018	3.027
A_L	0.88 ± 0.15	1.170 ± 0.061	0.88	1.178 ± 0.061	0.88
H_0	45 ± 11	68.13 ± 0.60	84 ± 11	67.85 ± 0.61	85 ± 10
Ω_m	0.80 ± 0.35	0.3044 ± 0.0062	0.303 ± 0.019	0.3064 ± 0.0063	0.307 ± 0.019
σ_8	0.733 ± 0.045	0.8020 ± 0.0089	0.851 ± 0.048	0.7983 ± 0.0091	0.99 ± 0.16
$\chi^2_{\rm min}$ (total)	2754.99	2776.32	15.91	2767.04	10.73
$\chi^2_{\rm min}$ (BAO/BAO′)	⋯	20.38	15.91	11.22	10.73
$\chi^2_{\rm BAO/BAO'}$ (at P18 B-F)	⋯	593.77	593.77	518.08	518.08
DIC	2811.63	2835.10	24.31	2825.27	17.54
ΔDIC	−6.30	−4.15	2.38	−4.34	2.61
AIC$_c$	2812.99	2834.32	31.91	2825.04	24.45
ΔAIC$_c$	−6.81	−6.34	4.35	−6.71	4.47

[a]Note: ΔDIC (ΔAIC$_c$) indicates an excess value relative to that of the tilted flat ΛCDM model constrained with the same data.

$P(q)$ model and these data probably should not be used jointly to constrain this model.

Looking at the lower half of Table X, we can compare results obtained for the eight- and the four-parameter tilted nonflat ΛCDM + A_L Planck $P(q)$ model from P18 and BAO′ data, respectively. We observe that the primary parameters $\Omega_b h^2$ and $\Omega_c h^2$ are in 1.6σ and 1.5σ tension. For the BAO′ data primary spatial curvature parameter, we find $\Omega_k = -0.026 \pm 0.054$, which is only 0.48σ away from flat and in 0.95σ tension with the P18 value -0.130 ± 0.095, which is 1.4σ away from flat. Regarding the derived parameters, we find that Ω_m, H_0, and σ_8 are in 1.4σ, 2.7σ, and 1.6σ disagreement. Compared to the $A_L = 1$ case, in the A_L-varying case we find a significant reduction only in the Ω_m tension, with most of the other parameter disagreements being more significant, which again suggests that P18 and

TABLE XI. Mean and 68.3% confidence limits of tilted new-$P(q)$-based nonflat ΛCDM ($+A_L$) model parameters with the new $P(q)$ constrained by TT, TE, EE + lowE (P18), BAO, and BAO′ data. H_0 has units of km s^{-1} Mpc^{-1}.[a]

	Tilted nonflat ΛCDM model [new $P(q)$]				
Parameter	P18	P18 + BAO	BAO	P18 + BAO′	BAO′
$\Omega_b h^2$	0.02255 ± 0.00017	0.02242 ± 0.00015	0.039 ± 0.015	0.02243 ± 0.00016	0.041 ± 0.016
$\Omega_c h^2$	0.1188 ± 0.0015	0.1194 ± 0.0014	0.173 ± 0.048	0.1193 ± 0.0014	0.177 ± 0.048
$100\theta_{\rm MC}$	1.04109 ± 0.00032	1.04100 ± 0.00032	1.16 ± 0.14	1.04102 ± 0.00032	1.13 ± 0.12
τ	0.0525 ± 0.0083	0.0582 ± 0.0081	0.0525	0.0562 ± 0.0080	0.0525
Ω_k	-0.033 ± 0.014	0.0003 ± 0.0018	-0.051 ± 0.061	-0.0004 ± 0.0018	-0.032 ± 0.059
n_s	0.9654 ± 0.0045	0.9665 ± 0.0043	0.9654	0.9665 ± 0.0043	0.9654
$\ln(10^{10}A_s)$	3.039 ± 0.017	3.051 ± 0.016	2.72 ± 0.45	3.046 ± 0.016	3.039
H_0	56.9 ± 3.6	67.79 ± 0.59	83 ± 12	67.52 ± 0.61	83 ± 12
Ω_m	0.444 ± 0.055	0.3102 ± 0.0060	0.304 ± 0.019	0.3124 ± 0.0063	0.307 ± 0.020
σ_8	0.786 ± 0.014	0.8128 ± 0.0079	0.846 ± 0.048	0.8098 ± 0.0080	0.99 ± 0.18
$\chi^2_{\rm min}$ (total)	2757.38	2786.27	15.90	2777.01	10.67
$\chi^2_{\rm min}$ (BAO/BAO′)	⋯	20.66	15.90	11.82	10.67
$\chi^2_{\rm BAO/BAO'}$ (at P18 B-F)	⋯	278.54	278.54	236.71	236.71
DIC	2811.54	2840.16	24.57	2831.65	17.69
ΔDIC	−6.39	0.91	2.64	2.04	2.76
AIC$_c$	2813.38	2842.27	31.90	2833.01	24.39
ΔAIC$_c$	−6.42	1.61	4.34	1.26	4.41

	Tilted nonflat ΛCDM + A_L model [new $P(q)$]				
Parameter	P18	P18 + BAO	BAO	P18 + BAO′	BAO′
$\Omega_b h^2$	0.02257 ± 0.00017	0.02260 ± 0.00017	0.039 ± 0.015	0.02261 ± 0.00017	0.042 ± 0.015
$\Omega_c h^2$	0.1187 ± 0.0016	0.1180 ± 0.0014	0.174 ± 0.047	0.1178 ± 0.0015	0.177 ± 0.046
$100\theta_{\rm MC}$	1.04111 ± 0.00033	1.04117 ± 0.00033	1.17 ± 0.14	1.04117 ± 0.00032	1.13 ± 0.13
τ	0.0512 ± 0.0086	0.0532 ± 0.0081	0.0512	0.0495 ± 0.0084	0.0512
Ω_k	-0.10 ± 0.11	-0.0005 ± 0.0017	-0.055 ± 0.060	-0.0012 ± 0.0018	-0.035 ± 0.059
n_s	0.9654 ± 0.0057	0.9707 ± 0.0044	0.9654	0.9715 ± 0.0047	0.9654
$\ln(10^{10}A_s)$	3.036 ± 0.018	3.038 ± 0.017	2.69 ± 0.43	3.029 ± 0.018	3.036
A_L	0.94 ± 0.20	1.168 ± 0.061	0.94	1.176 ± 0.062	0.94
H_0	51 ± 14	68.09 ± 0.60	83 ± 12	67.85 ± 0.63	84 ± 11
Ω_m	0.70 ± 0.43	0.3048 ± 0.0062	0.304 ± 0.019	0.3065 ± 0.0065	0.306 ± 0.020
σ_8	0.752 ± 0.052	0.8026 ± 0.0086	0.844 ± 0.048	0.7982 ± 0.0092	0.99 ± 0.18
$\chi^2_{\rm min}$ (total)	2756.33	2776.32	15.90	2767.43	10.68
$\chi^2_{\rm min}$ (BAO/BAO′)	⋯	20.30	15.90	11.21	10.68
$\chi^2_{\rm BAO/BAO'}$ (at P18 B-F)	⋯	194.81	194.81	160.72	160.72
DIC	2814.83	2834.67	24.75	2824.97	17.76
ΔDIC	−3.10	−4.58	2.82	−4.64	2.83
AIC$_c$	2814.33	2834.32	31.90	2825.43	24.39
ΔAIC$_c$	−5.47	−6.34	4.34	−6.32	4.41

[a]Note: ΔDIC (ΔAIC$_c$) indicates an excess value relative to that of the tilted flat ΛCDM model constrained with the same data.

BAO′ data should not be jointly analyzed within the tilted nonflat ΛCDM + A_L Planck $P(q)$ model.

Comparing the seven- and the four-parameter tilted nonflat ΛCDM new $P(q)$ model primary cosmological parameter constraints for P18 and BAO′ data, from the upper half of Table XI we see that the values of $\Omega_b h^2$ and $\Omega_c h^2$ both disagree at 1.2σ. The BAO′ data primary spatial curvature parameter value is $\Omega_k = -0.032 \pm 0.059$, which is only a 0.54σ deviation from flat and, similar to the Planck $P(q)$ model, is only in 0.016σ disagreement with the P18 value -0.033 ± 0.014, which is 2.4σ away from flat. Regarding the derived parameters Ω_m, H_0, and σ_8, we find that their values disagree at 2.3σ, 2.1σ, and 1.1σ, respectively. While these disagreements are smaller than the ones found in the tilted nonflat ΛCDM Planck $P(q)$ model, they still are large enough to require we more

carefully test whether P18 and BAO′ data can be jointly used to constrain cosmological parameters in this cosmological model.

The results for the eight- and the four-parameter tilted nonflat ΛCDM + A_L new $P(q)$ model are in the lower half of Table XI, for P18 and BAO′ data, respectively. As happens in the Planck $P(q)$ model, when the A_L parameter is allowed to vary, the tensions found for the primary parameters $\Omega_b h^2$ and $\Omega_c h^2$ do not decrease (in fact, they slightly increase) with respect to the $A_L = 1$ case, both now being 1.3σ. For the BAO′ data primary spatial curvature parameter, we find $\Omega_k = -0.035 \pm 0.059$, which is 0.59σ away from flat hypersurfaces and only in 0.52σ tension with the P18 value $\Omega_k = -0.10 \pm 0.11$, which is 0.91σ away from flat. As for the value of the derived parameters Ω_m, H_0, and σ_8, we find disagreements at 0.92σ, 1.9σ, and 1.3σ, respectively. The tensions are reduced with respect to the case with $A_L = 1$, due to the increase of the error bars, but possibly still are not small enough to allow the joint use of P18 + BAO′ data for constraining tilted nonflat ΛCDM + A_L new $P(q)$ model cosmological parameters.

We now comment on the consistency between the cosmological constraints obtained using the BAO dataset (which contain some $f\sigma_8$ data points) and the P18 data cosmological constraints. Here we also have to deal with the σ_8 tension, namely, the discrepancy between the larger value for σ_8 obtained when P18 data are considered and the typically smaller values that one gets from low-redshift structure formation data (the $f\sigma_8$ data points we consider) or from weak lensing measurements. Note that since BAO data include some $f\sigma_8$ measurements we allow for $\ln(10^{10}A_s)$ to vary in the BAO data only analyses (unlike the BAO′ data only analyses where we fix the value of this parameter). We shall see that the tilted nonflat ΛCDM new $P(q)$ model is the model that best reconciles these measurements.

Comparing the six- and the four-parameter tilted flat ΛCDM primary cosmological parameter constraints for P18 and BAO data, shown in the upper half of Table VIII, we see that the values of $\Omega_b h^2$ and $\Omega_c h^2$ are in 1.3σ and 1.0σ tension, respectively. A similar level of disagreement is found if we look at the values of the derived parameters. In particular, for Ω_m, H_0, and σ_8 we find 1.3σ, 1.3σ, and 1.6σ disagreement. Here the greatest disagreement is that affecting σ_8, which has to do with the σ_8 tension mentioned above.

Considering the results presented in the lower half of Table VIII for the seven- and the four-parameter tilted flat ΛCDM + A_L model, obtained for P18 and BAO data, respectively, we find that including a varying A_L parameter does not decrease the primary parameter tensions found when $A_L = 1$. For $\Omega_b h^2$ and $\Omega_c h^2$, the disagreement is now 1.4σ and 1.1σ. On the other hand, for the derived Ω_m, H_0, and σ_8, we find that their corresponding values disagree at 0.50σ, 1.2σ, and 2.0σ. Once again, allowing A_L to vary reduces the Ω_m disagreement and the largest disagreement is between the σ_8 values.

Comparing the six- and the five-parameter untilted nonflat ΛCDM model primary cosmological parameter constraints for P18 and BAO data, provided in the upper half of Table IX, we observe that the values of $\Omega_b h^2$ and $\Omega_c h^2$ show a disagreement of 1.1σ and 1.4σ, respectively. The BAO data value for the primary spatial curvature parameter is $\Omega_k = -0.047 \pm 0.059$, which is 0.80σ away from flat hypersurfaces and in 0.75σ tension with the P18 value -0.095 ± 0.024, which represents a 4.0σ deviation from flat. The level of tension is worse for the derived parameters Ω_m, H_0, and σ_8, the disagreements now being 3.7σ, 3.0σ, and 2.4σ. We may say that P18 and BAO data should not be jointly used to constrain cosmological parameters in the untilted nonflat ΛCDM model.

Results for the seven- and the five-parameter untilted nonflat ΛCDM + A_L model for P18 and BAO data, respectively, can be seen in the lower half of Table IX. Again we do not observe a reduction in the tension for the primary parameters $\Omega_b h^2$ (1.2σ) and $\Omega_c h^2$ (1.4σ) compared with the results found for the $A_L = 1$ case. On the other hand, there is an important decrease for the derived parameters Ω_m, H_0, and σ_8, the disagreement now being 0.94σ, 1.5σ, and 1.8σ, respectively. This is probably caused by the increase in the size of the error bars in the A_L-varying P18 case, with respect to the corresponding values obtained with $A_L = 1$. For the BAO data primary spatial curvature parameter, we find $\Omega_k = -0.050 \pm 0.060$, which is 0.83σ away from flat and in 0.52σ tension with the P18 value $\Omega_k = -0.12 \pm 0.12$, which is 1.0σ in favor of a closed geometry.

Comparing the seven- and the five-parameter tilted nonflat ΛCDM Planck $P(q)$ model primary cosmological parameter constraints for P18 and BAO data, shown in the upper half of Table X, we see that the values of $\Omega_b h^2$ and $\Omega_c h^2$ are both in 1.2σ tension. The BAO data primary spatial curvature parameter $\Omega_k = -0.046 \pm 0.060$ is 0.77σ away from flat hypersurfaces and, as in the BAO′ case, in good agreement with, differing only by 0.048σ from, the P18 result -0.043 ± 0.017, which is 2.5σ away from flat. As for the derived parameters Ω_m, H_0, and σ_8, we observe disagreements of 2.7σ, 2.3σ, and 1.5σ. These results reveal an inconsistency between P18 and BAO cosmological constraints that probably mean P18 and BAO data should not be used to jointly constrain cosmological parameters in the tilted nonflat ΛCDM Planck $P(q)$ model.

We provide results for the eight- and the five-parameter tilted nonflat ΛCDM + A_L Planck $P(q)$ model, from P18 and BAO data, in the lower half of Table X. For the primary parameters $\Omega_b h^2$ and $\Omega_c h^2$, we find a tension between the P18 and BAO values of 1.3σ and 1.2σ, respectively. For the BAO data primary spatial curvature parameter, we find $\Omega_k = -0.045 \pm 0.063$, which represents a 0.71σ evidence in favor of closed geometry and is only in 0.75σ tension

with respect to the P18 value -0.130 ± 0.095, which represents a 1.4σ deviation from flat. Regarding the derived Ω_m, H_0, and σ_8 parameters, the observed disagreements are 1.4σ, 2.5σ, and 1.8σ. The tension for Ω_m has reduced significantly with respect to the $A_L = 1$ case, however, overall the disagreements are still large enough to not allow one to jointly analyze P18 and BAO data in this cosmological model.

Comparing the seven- and the five-parameter tilted nonflat ΛCDM new $P(q)$ model primary cosmological parameter constraints for P18 and BAO data, shown in the upper half of Table XI, we see that the values of $\Omega_b h^2$ and $\Omega_c h^2$ are both in 1.1σ disagreement. The BAO data value of the primary spatial curvature parameter is $\Omega_k = -0.051 \pm 0.061$, which represents a 0.84σ deviation from a flat geometry and is only in 0.29σ disagreement with the P18 value $\Omega_k = -0.033 \pm 0.014$, which is 2.4σ away from flat. Regarding the derived parameters Ω_m, H_0, and σ_8, we find 2.4σ, 2.1σ, and 1.2σ disagreements between the corresponding values. It is necessary to further study the possible tension between P18 and BAO within this model.

Results for the eight- and the five-parameter tilted nonflat ΛCDM + A_L new $P(q)$ model, obtained from P18 and BAO data, can be seen in the lower half of Table XI. For the primary parameters $\Omega_b h^2$ and $\Omega_c h^2$, the disagreement is at 1.1σ and 1.2σ, respectively. For the BAO data primary spatial curvature parameter, we find $\Omega_k = -0.055 \pm 0.060$, which represents 0.92σ evidence in favor of closed geometry and is in only 0.36σ disagreement with the P18 value -0.10 ± 0.11, which represents a 0.91σ deviation from flat. Regarding the derived parameters, Ω_m, H_0, and σ_8 we find 0.92σ, 1.7σ, and 1.3σ disagreements. The tensions for H_0 and Ω_m have reduced with respect to the case with $A_L = 1$, however, they are still large enough to wonder whether we can jointly analyze P18 and BAO data in the context of this model.

In Tables VIII–XI, $\chi^2_{\rm min}$ (BAO/BAO′) is the value of χ^2 for BAO or BAO′ data, respectively, at the best-fit position for BAO or BAO′ data, while $\chi^2_{\rm BAO/BAO'}$ (at P18 B-F) is the value of χ^2 for BAO or BAO′ data evaluated at the best-fit position for P18 data. The values of $\chi^2_{\rm min}$ (BAO/BAO′) and $\chi^2_{\rm BAO/BAO'}$ (at P18 B-F) give a qualitative indication of the agreement or disagreement in the values of the cosmological parameters obtained by considering P18 data and by considering BAO/BAO′ data. If the cosmological parameters agree, one might expect that $\chi^2_{\rm min}$ (BAO/BAO′) $\simeq \chi^2_{\rm BAO/BAO'}$ (at P18 B-F). We see that this is the case only for the tilted flat ΛCDM $(+A_L)$ models for the BAO′ data, but again emphasize that this is only a qualitative probe.

Figures 16–23 show one-dimensional likelihoods and two-dimensional contours for cosmological parameters obtained using P18, BAO′, BAO, P18 + BAO′, and P18 + BAO data. As mentioned above, BAO′ data constraints (shown in green) and BAO data constraints (shown in gray) are comparatively less restrictive than P18 constraints (shown in dark blue), are unable to put tight constraints on the primary cosmological parameters (except for Ω_k in the three nonflat ΛCDM + A_L models), in most cases overlap at 2σ with each other, and in many cases they also overlap with the P18 data constraints. Since the BAO dataset contains more measurements than the BAO′ dataset, the BAO constraints are typically more restrictive, and BAO data, which includes $f\sigma_8$ measurements, are much more effective at constraining σ_8 than are BAO′ data.

Figures 16 and 17 are for tilted flat ΛCDM $(+A_L)$ models. The $\sim 1\sigma$ disagreements between the BAO′/BAO constraints and those obtained with P18 data, discussed above, can be clearly seen in the contour plots. For the tilted flat ΛCDM model, the larger disagreements are in panels for derived cosmological parameters, with the largest for σ_8. Some of these disagreements decrease when the A_L parameter is allowed to vary.

Looking at the contour plots for the untilted nonflat ΛCDM $(+A_L)$ models (see Figs. 18 and 19), we observe nonoverlapping contours in those panels that involve the derived parameters Ω_m and H_0. These disagreements are smaller when A_L is allowed to vary. This may indicate that in the context of this cosmological model we may jointly analyze P18 data with BAO′/BAO data only when A_L is allowed to vary.

Figures 20 and 21 show cosmological parameter constraints for the tilted nonflat ΛCDM $(+A_L)$ Planck $P(q)$ models, while the ones for the tilted nonflat ΛCDM $(+A_L)$ new $P(q)$ models are displayed in Figs. 22 and 23. As expected, considering the results discussed above in this subsubsection, the contour plots for these tilted nonflat models are quite similar. We see in the panels that involve the primary cosmological parameters that there is overlap at 1σ, not only when A_L is allowed to vary but also when $A_L = 1$. When $A_L = 1$, for the Planck $P(q)$ model, some P18 and BAO′/BAO data constraint contours that involve Ω_m and H_0 do not overlap even at 2σ. This is not true for the new $P(q)$ model with $A_L = 1$, where overlap is reached at $< 2\sigma$. This may indicate that the new $P(q)$ model is better able to reconcile P18 and BAO′/BAO data.

In view of the results discussed in this subsubsection, further tests are needed to properly quantify the level of disagreement, in the context of nonflat models, between P18 data and BAO′/BAO data cosmological constraints. We return to this issue in Sec. IV C.

6. Comparing P18 data and non-CMB data cosmological constraints

In the previous subsubsection, we compared BAO and BAO′ data cosmological constraints to those obtained from P18 data. In the nonflat models with $A_L = 1$ there is somewhat significant disagreement between the values of the cosmological parameters (especially the derived

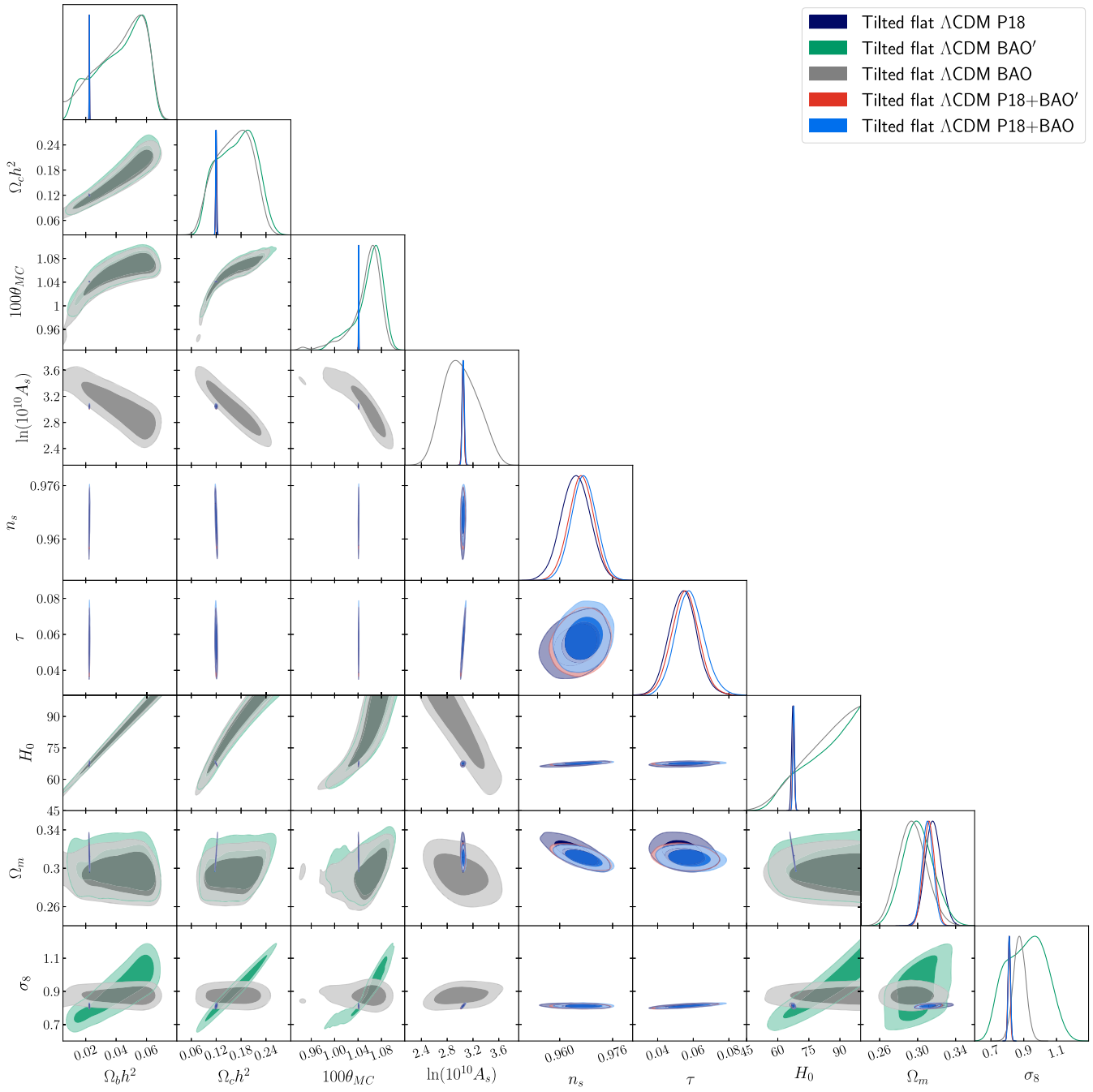

FIG. 16. Likelihood distributions constrained by the Planck 2018 TT, TE, EE + lowE (P18), BAO, and BAO′ datasets in the tilted flat ΛCDM model.

parameters Ω_m, H_0, and σ_8) determined using P18 data and those determined from BAO or BAO′ data. This disagreement motivates additional tests to decide whether P18 data and BAO′/BAO data can be used together to constrain parameters of the nonflat models. While both P18 data and BAO′/BAO data favor negative Ω_k values, BAO′/BAO data favor higher values of H_0 and lower values of Ω_m relative to the values obtained in the P18 analysis. Allowing for a varying A_L parameter resolves these tensions, which may indicate that we can only jointly analyze P18 data and BAO′/BAO data in the nonflat models when A_L is allowed to vary.

To further examine these inconsistencies, in this subsubsection we compare non-CMB data (which include BAO as well as BAO′ data) cosmological constraints to those obtained from P18 data. (Prior to jointly analyzing P18 + non-CMB data, we need to determine whether P18 and non-CMB data cosmological constraints are mutually

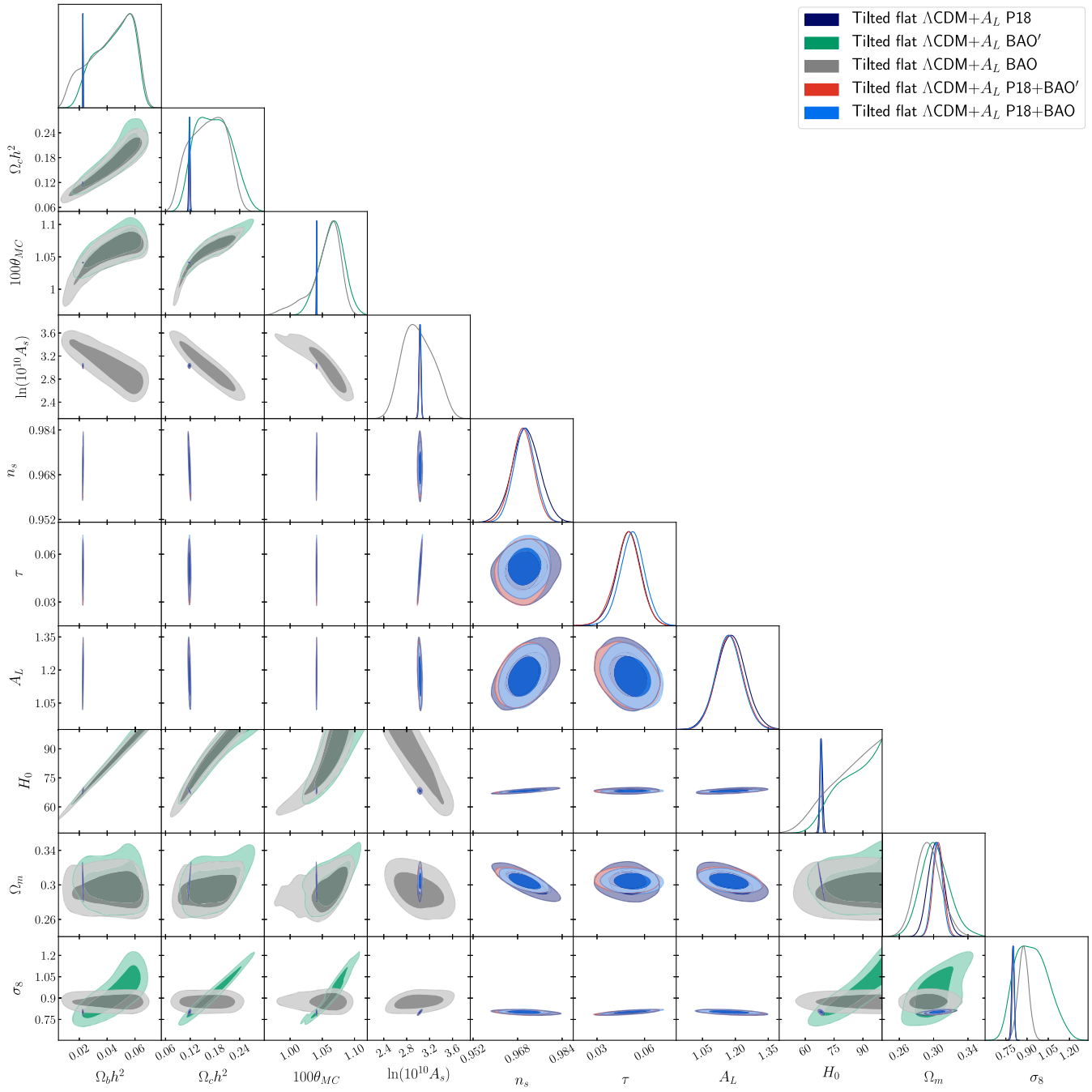

FIG. 17. Likelihood distributions constrained by the Planck 2018 TT, TE, EE + lowE (P18), BAO, and BAO′ datasets in the tilted flat ΛCDM + A_L model.

consistent.) This allows us to examine how the inclusion of SNIa, $H(z)$, and $f\sigma_8$ data affects the P18 data vs BAO′/BAO data conclusions of Sec. IV A 5 and provides a different, perhaps more expansive, test of the consistency of cosmological parameters obtained from high- and low-redshift data. In Sec. IV C, we use two other statistical estimators to examine whether or not P18 and non-CMB data are in tension.

The cosmological parameter mean values and error bars favored by the P18, non-CMB, and P18 + non-CMB datasets are summarized in Tables XII–XV for the tilted flat ΛCDM ($+A_L$) models, the untilted nonflat ΛCDM ($+A_L$) models, the tilted nonflat ΛCDM ($+A_L$) models with the Planck $P(q)$, and the tilted nonflat ΛCDM ($+A_L$) models with the new $P(q)$, respectively. Likelihood distributions of cosmological parameters of the four models

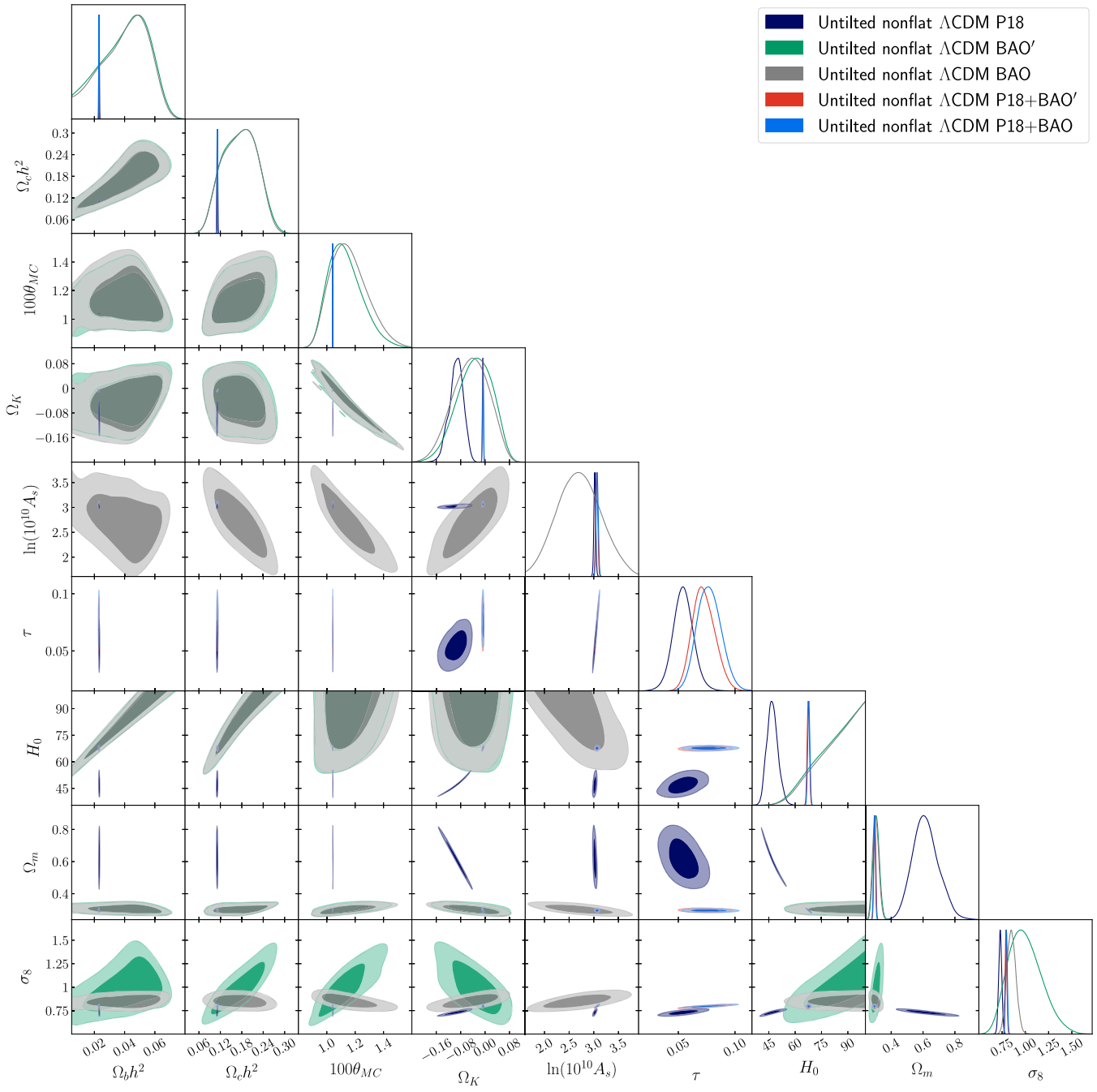

FIG. 18. Likelihood distributions constrained by the Planck 2018 TT, TE, EE + lowE (P18), BAO, and BAO′ datasets in the untilted nonflat ΛCDM model.

with $A_L = 1$ and with A_L varying are shown in Figs. 24–31 for the P18, non-CMB, and P18 + non-CMB datasets.

Since non-CMB data do not have the ability to constrain τ or n_s, we set their values to those found in the corresponding P18 data analysis. A_L does not affect predictions for the non-CMB measurements we study, so we do not include A_L in the non-CMB data analyses. (We saw, in Sec. IV A 5, that BAO′/BAO data constraints for $A_L = 1$ and for varying A_L were very similar, see Tables VIII–XI.)

From Tables XIII–XV, we see, in the six nonflat ΛCDM $(+A_L)$ models, that the constraints set by non-CMB data on H_0 and Ω_m are tighter than the ones imposed by P18 data, and in the three nonflat ΛCDM + A_L models that the constraints set by non-CMB data on Ω_k and σ_8 are tighter than the ones imposed by P18 data. P18 data more restrictively constrain all other parameters in all eight cosmological models.

As we discuss below, there is at least one parameter in the three nonflat models with $A_L = 1$ with a more than 3σ

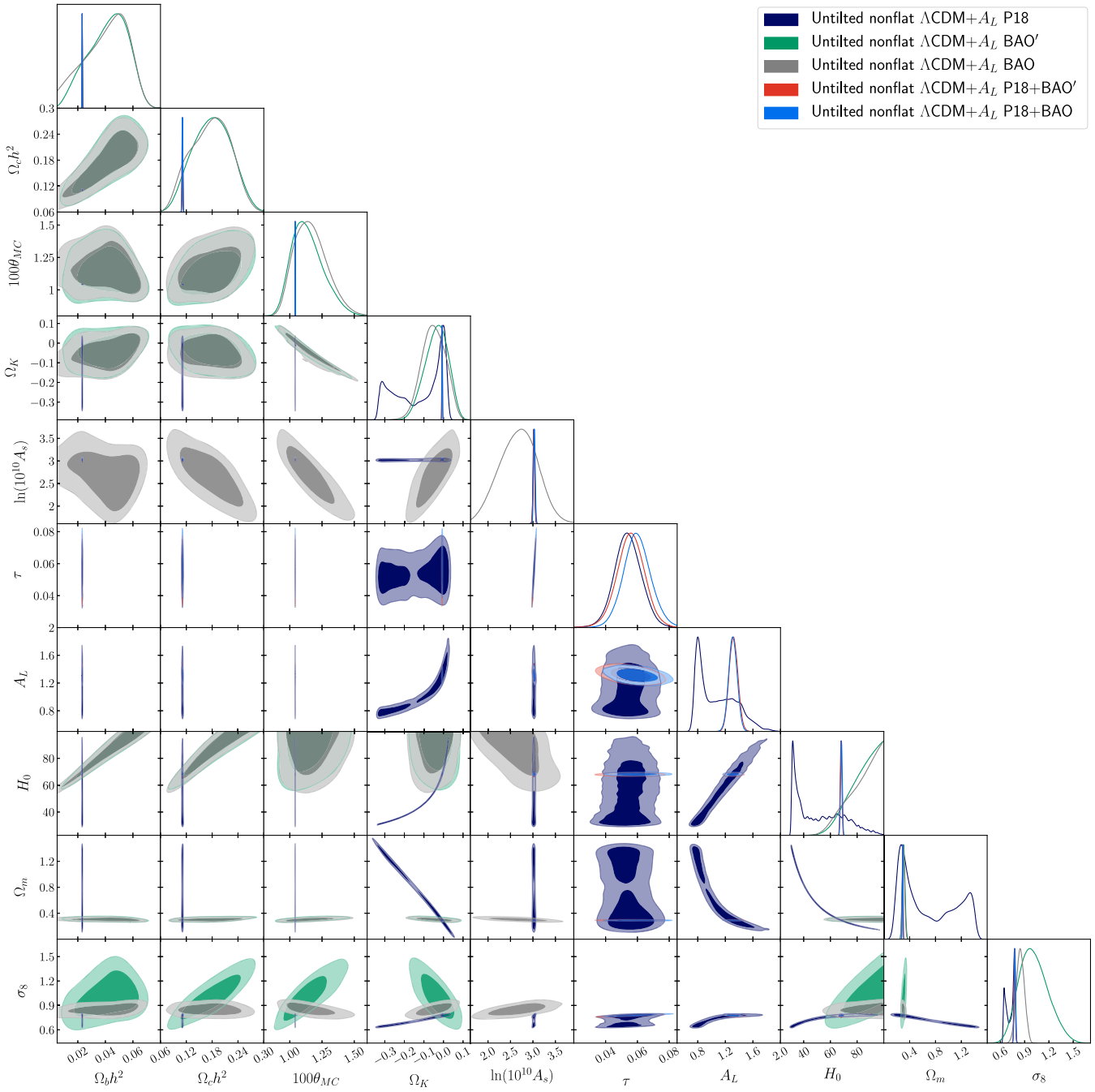

FIG. 19. Likelihood distributions constrained by the Planck 2018 TT, TE, EE + lowE (P18), BAO, and BAO′ datasets in the untilted nonflat ΛCDM + A_L model.

level of disagreement between P18 data cosmological constraints and non-CMB data cosmological constraints and one parameter in the tilted flat ΛCDM model with $A_L = 1$ and in the tilted nonflat ΛCDM + A_L model with the Planck $P(q)$ with a more than 2σ level of disagreement between P18 data cosmological constraints and non-CMB data cosmological constraints. From Tables XIII–XV, we see that both P18 data and non-CMB data favor negative values of the curvature parameter, with non-CMB data only weakly favoring closed spatial hypersurfaces, at 0.66σ to 0.71σ. However, we should take into account the geometrical degeneracy between H_0, Ω_k, and Ω_m and note that, like both BAO′ and BAO data, non-CMB data favor higher values of H_0 and lower values of Ω_m than do P18 data, and this is what causes the P18 and non-CMB cosmological constraint differences.

The dominant component of non-CMB data is BAO′/BAO data. This is why the cosmological constraints

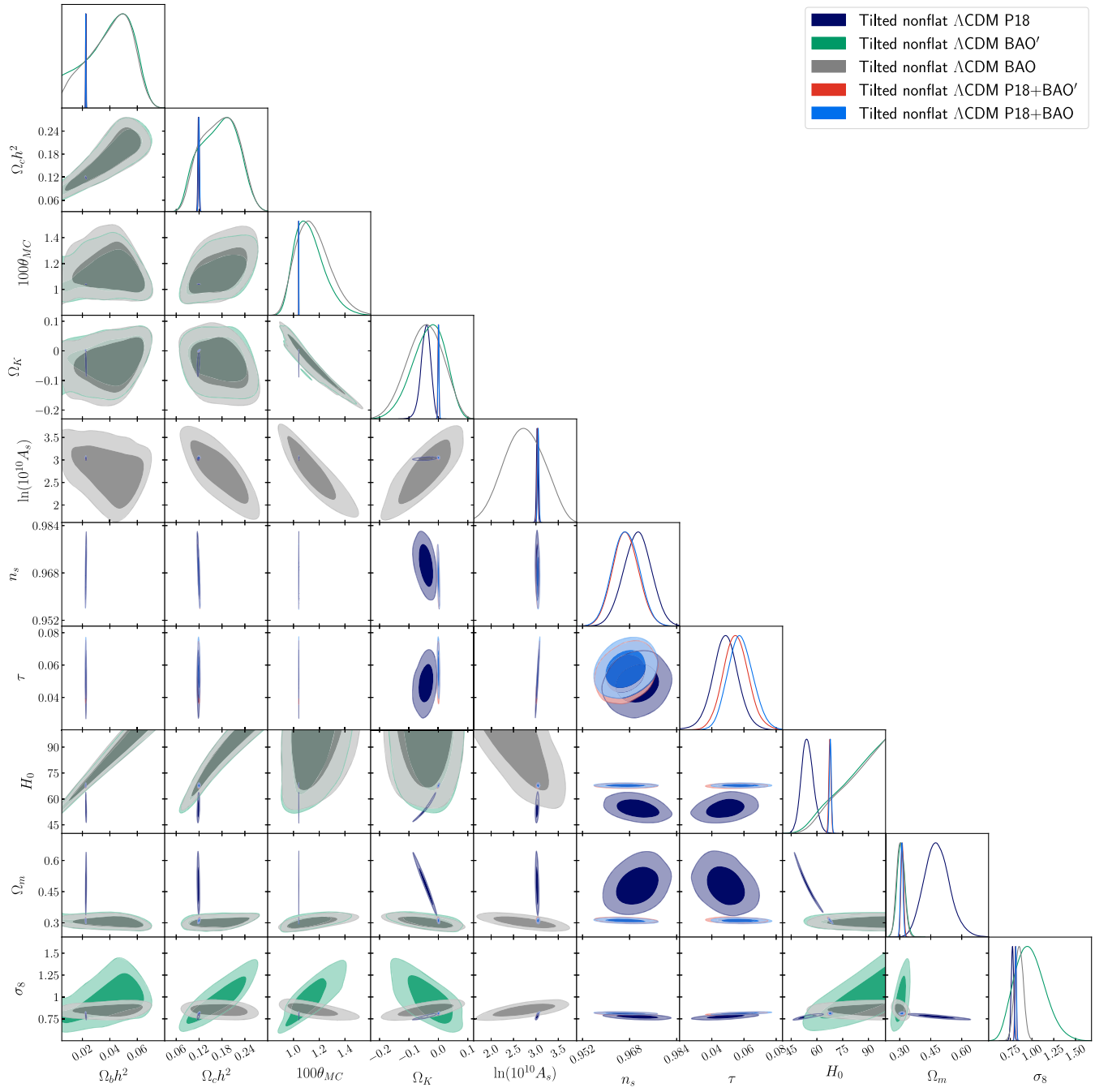

FIG. 20. Likelihood distributions constrained by the Planck 2018 TT, TE, EE + lowE (P18), BAO, and BAO′ datasets in the tilted nonflat ΛCDM model with the Planck $P(q)$.

obtained from BAO′/BAO data are similar to the ones obtained from the complete non-CMB low-redshift dataset. However, there are some differences between these sets of constraints that are worth mentioning. As expected, the error bars obtained considering non-CMB data are smaller than the ones from BAO′/BAO data. While similar values for Ω_m are found in both cases, the values of H_0 favored by non-CMB data are $\sim 1\sigma$ smaller than those favored by BAO′/BAO data. BAO′ data favor closed spatial hypersurfaces at 0.48σ–0.60σ, while BAO data favor them by 0.71σ–0.96σ, which are on either side of the 0.66σ–0.71σ favoring of closed spatial hypersurfaces from non-CMB data. We also find smaller values for the σ_8 parameter when non-CMB data are considered, with BAO′ data favoring 1.1σ–1.3σ larger values, while BAO data favor $\sim 1.3\sigma$ larger values in the nonflat models and a 1.9σ larger value in the tilted flat ΛCDM case. This might be because the non-CMB dataset contain additional $f\sigma_8$ data

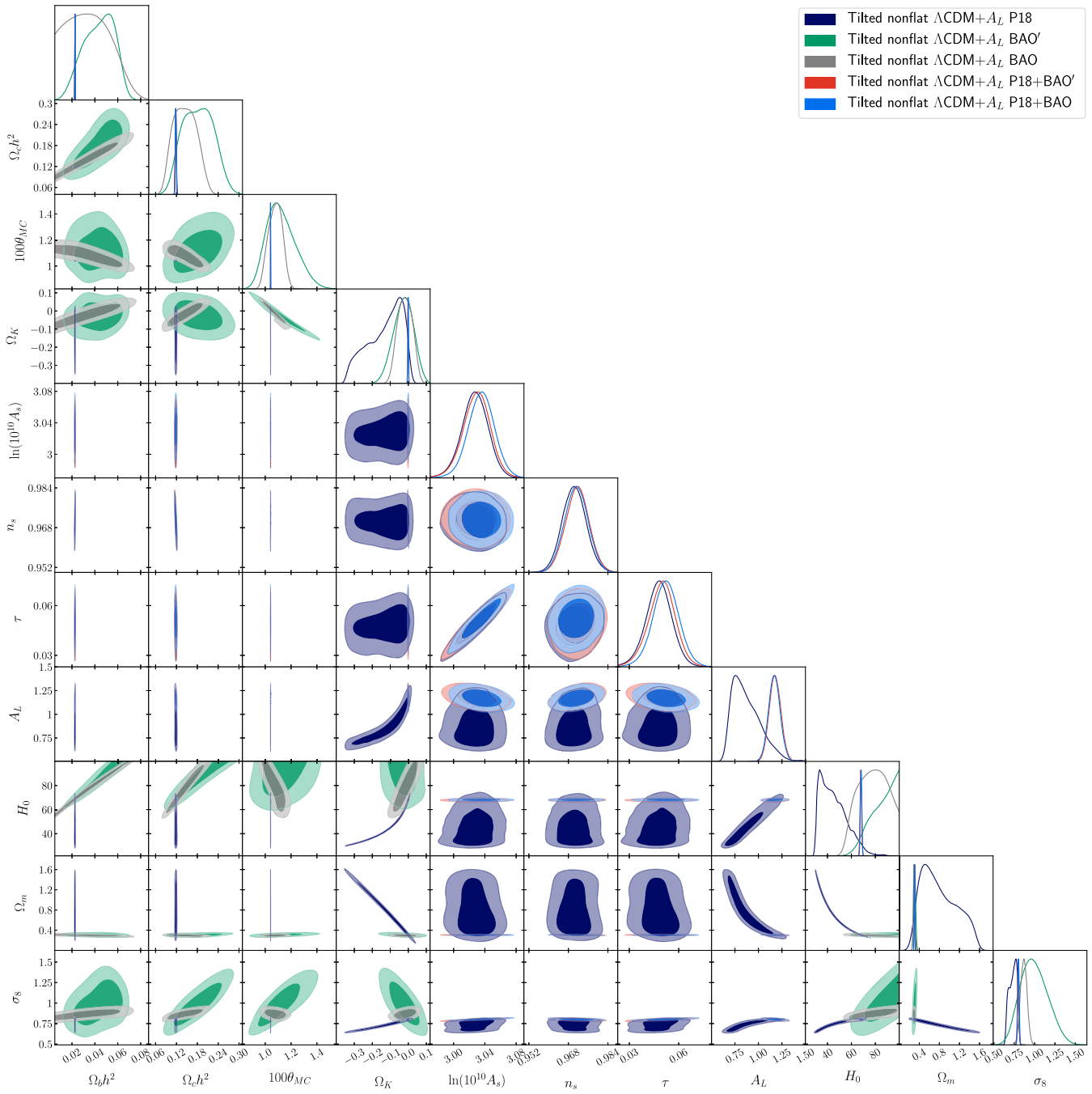

FIG. 21. Likelihood distributions constrained by the Planck 2018 TT, TE, EE + lowE (P18), BAO, and BAO′ datasets in the tilted nonflat ΛCDM + A_L model with the Planck $P(q)$.

points that favor lower values of σ_8 than those in the BAO dataset.

Comparing the six- and the four-parameter tilted flat ΛCDM model primary cosmological parameter constraints for P18 and non-CMB data, shown in the left half of Table XII, we see that the values of $\Omega_b h^2$, $\Omega_c h^2$, and $\theta_{\rm MC}$ are in mild disagreement at 1.3σ, 1.1σ, and 1.0σ, respectively. We also observe a more significant 2.2σ level of tension in the derived Ω_m values, the derived H_0 values differ by 1.4σ, and σ_8 values show a better agreement, disagreeing by only 0.89σ.

Comparing the seven- and the four-parameter tilted flat ΛCDM + A_L model primary cosmological parameter constraints for P18 and non-CMB data, shown in Table XII, we see that the values of $\Omega_b h^2$ and $\theta_{\rm MC}$ are in 1.2σ and 1.1σ tension, respectively. As for the derived parameters, we find Ω_m values differ by 1.2σ, while H_0 and σ_8 values are in only 0.81σ and 0.45σ disagreement. So unlike in the

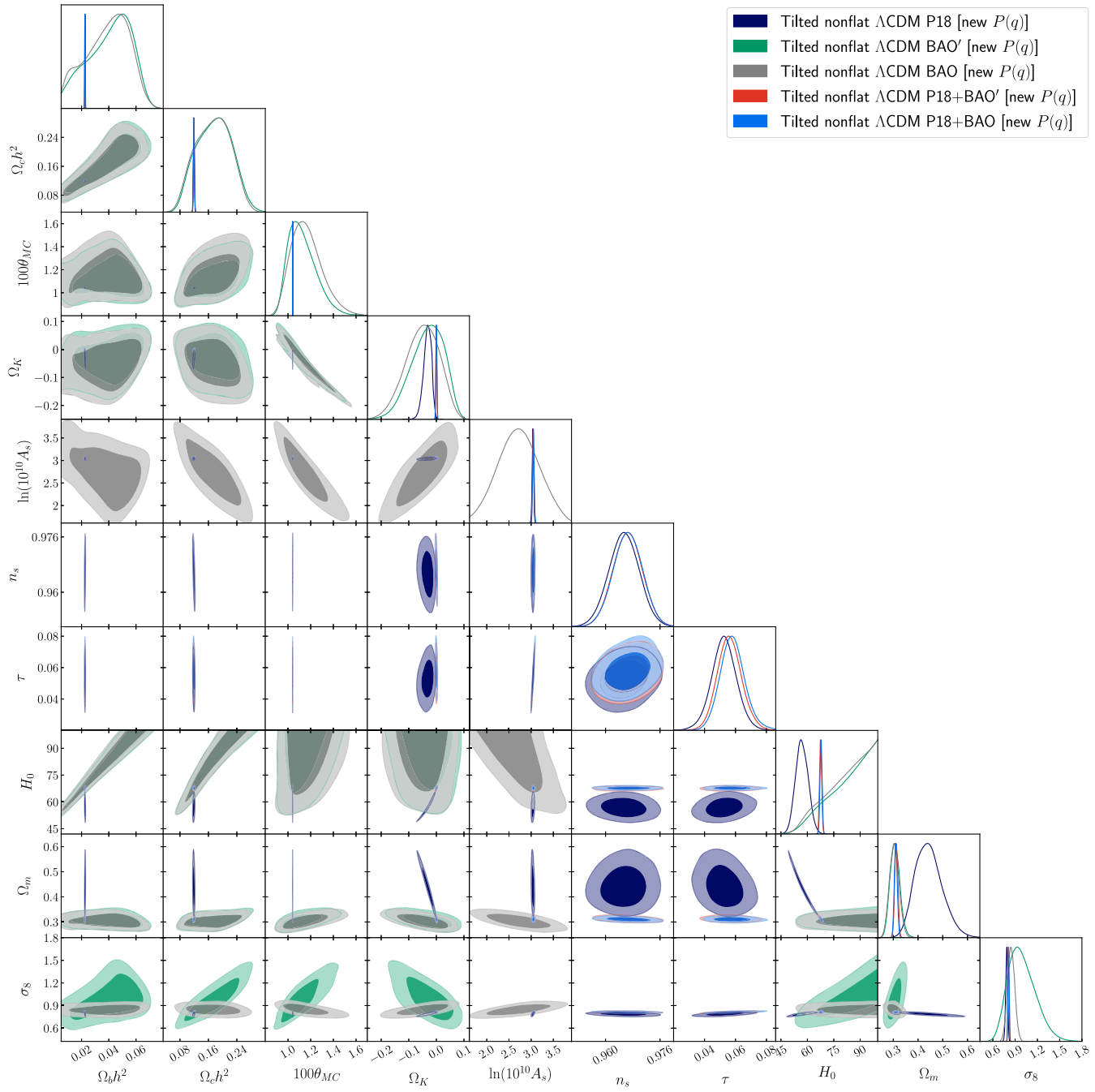

FIG. 22. Likelihood distributions constrained by the Planck 2018 TT, TE, EE + lowE (P18), BAO, and BAO′ datasets in the tilted nonflat ΛCDM model with the new $P(q)$.

BAO data and the BAO′ data comparisons with P18 data of Sec. IV A 5, the inclusion of a varying A_L reduces the disagreement for all three derived parameters, but less successfully for Ω_m in the non-CMB case here compared to the BAO/BAO′ cases there.

P18 and non-CMB data results obtained for the six- and the four-parameter untilted nonflat ΛCDM model, shown in the left half of Table XIII, indicate mostly less significant differences in primary parameters but more significant differences in derived parameters than found in the tilted flat ΛCDM model. The primary spatial curvature parameter value is $\Omega_k = -0.033 \pm 0.050$ for non-CMB data, which is 0.66σ away from flat and in 1.1σ tension with the P18 value $\Omega_k = -0.095 \pm 0.024$, which is 4.0σ away from flat. Regarding the derived parameters, we find that H_0, Ω_m, and σ_8 values are in 6.4σ, 3.8σ, and 1.1σ disagreement. These results probably mean that P18 and non-CMB data should not be jointly

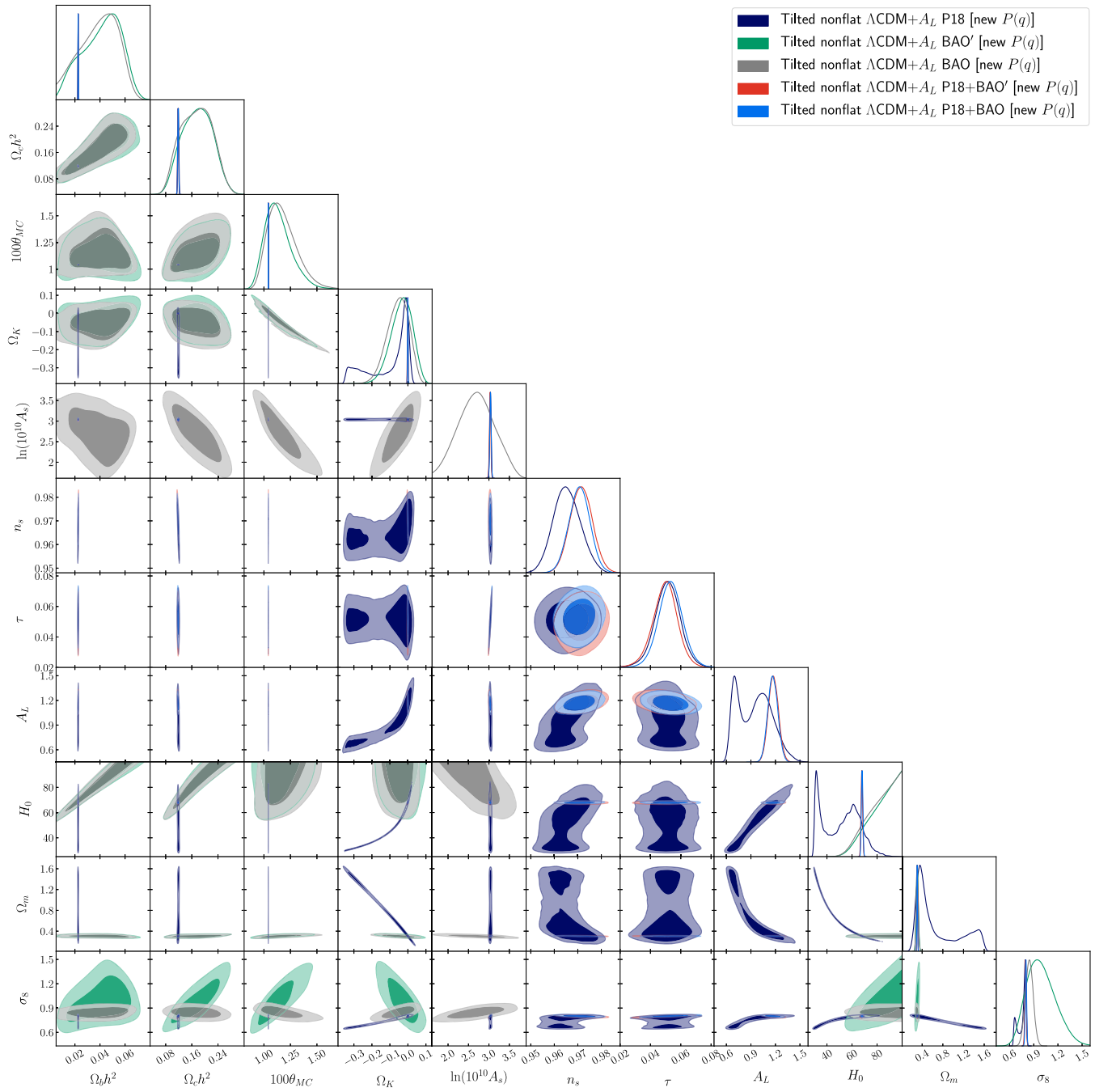

FIG. 23. Likelihood distributions constrained by the Planck 2018 TT, TE, EE + lowE (P18), BAO, and BAO′ datasets in the tilted nonflat ΛCDM + A_L model with the new $P(q)$.

analyzed in the context of the untilted nonflat ΛCDM model.

The results for the seven- and the four-parameter untilted nonflat ΛCDM + A_L model, obtained considering P18 and non-CMB data, are in Table XIII. There is a slight increase in the disagreement between the values of the primary spatial curvature parameter Ω_k (now 0.67σ) and decreases for the derived parameters H_0, Ω_m, and σ_8, which now disagree by 1.0σ, 0.97σ, and 0.79σ, respectively. This is caused by the larger error bars in the A_L-varying P18 case compared to the corresponding values obtained with $A_L = 1$. According to these results, unlike in the $A_L = 1$ case, in the A_L-varying case P18 and non-CMB data can probably be jointly analyzed in the context of the untilted nonflat ΛCDM model. Note that in this case a joint analysis of P18 + non-CMB data favors closed geometry at 4.4σ, with $\Omega_k = -0.0062 \pm 0.0014$, although because of the lack of the tilt (n_s) degree of freedom, this untilted nonflat

TABLE XII. Mean and 68.3% confidence limits of tilted flat ΛCDM ($+A_L$) model parameters constrained by non-CMB, P18, and P18 + non-CMB datasets. H_0 has units of km s^{-1} Mpc^{-1}.[a]

	Tilted flat ΛCDM			Tilted flat ΛCDM + A_L	
Parameter	Non-CMB	P18	P18 + non-CMB	P18	P18 + non-CMB
$\Omega_b h^2$	0.0256 ± 0.0025	0.02236 ± 0.00015	0.02250 ± 0.00012	0.02259 ± 0.00017	0.02265 ± 0.00014
$\Omega_c h^2$	0.1129 ± 0.0062	0.1202 ± 0.0014	0.11825 ± 0.00087	0.1180 ± 0.0015	0.11736 ± 0.00092
$100\theta_{\rm MC}$	1.0323 ± 0.0082	1.04090 ± 0.00031	1.04112 ± 0.00029	1.04114 ± 0.00032	1.04120 ± 0.00029
τ	0.0542	0.0542 ± 0.0079	0.0548 ± 0.0076	0.0496 ± 0.0082	0.0484 ± 0.0083
n_s	0.9649	0.9649 ± 0.0043	0.9692 ± 0.0036	0.9710 ± 0.0050	0.9726 ± 0.0038
$\ln(10^{10}A_s)$	3.10 ± 0.11	3.044 ± 0.016	3.041 ± 0.015	3.030 ± 0.017	3.026 ± 0.017
A_L	⋯	⋯	⋯	1.181 ± 0.067	1.201 ± 0.061
H_0	69.8 ± 1.7	67.28 ± 0.61	68.15 ± 0.39	68.31 ± 0.71	68.62 ± 0.43
Ω_m	0.286 ± 0.011	0.3165 ± 0.0084	0.3045 ± 0.0051	0.3029 ± 0.0093	0.2988 ± 0.0054
σ_8	0.787 ± 0.027	0.8118 ± 0.0074	0.8048 ± 0.0068	0.7997 ± 0.0088	0.7961 ± 0.0074
$\chi^2_{\rm min}$ (total)	1106.54	2765.80	3879.35	2756.12	3865.90
$\chi^2_{\rm min}$ (non-CMB)	1106.54	⋯	1111.57	⋯	1109.54
DIC	1114.45	2817.93	3931.02	2812.41	3922.11
ΔDIC	⋯	⋯	⋯	−5.52	−8.91
$\rm AIC_c$	1114.54	2819.80	3933.35	2812.1	3921.90
$\Delta\rm AIC_c$	⋯	⋯	⋯	−7.68	−11.45

[a]Note: ΔDIC ($\Delta\rm AIC_c$) indicates an excess value relative to that of the tilted flat ΛCDM model constrained with the same data.

ΛCDM + A_L model does not provide a good fit to smaller-angular-scale P18 data, which is reflected in the large ΔDIC and $\Delta\rm AIC_c$ values for the P18 + non-CMB case in the lower half of Table XIII.

Comparing the seven- and the five-parameter tilted nonflat ΛCDM Planck $P(q)$ model primary cosmological parameter constraints for P18 and non-CMB data, we see, in the left half of Table XIV, that the primary parameter values do not much disagree. The non-CMB data primary spatial curvature parameter value $\Omega_k = -0.032 \pm 0.051$ is 0.63σ away from flat and only in 0.20σ tension with the P18 value $\Omega_k = -0.043 \pm 0.017$, which is 2.5σ in favor of closed geometry. The derived parameters H_0, Ω_m, and σ_8 are in 3.9σ, 2.9σ, and 0.11σ tension. These results show that

TABLE XIII. Mean and 68.3% confidence limits of untilted nonflat ΛCDM ($+A_L$) model parameters constrained by non-CMB, P18, and P18 + non-CMB datasets. H_0 has units of km s^{-1} Mpc^{-1}.[a]

	Untilted nonflat ΛCDM			Untilted nonflat ΛCDM + A_L	
Parameter	Non-CMB	P18	P18 + non-CMB	P18	P18 + non-CMB
$\Omega_b h^2$	0.0243 ± 0.0033	0.02320 ± 0.00015	0.02300 ± 0.00014	0.02320 ± 0.00015	0.02320 ± 0.00015
$\Omega_c h^2$	0.120 ± 0.013	0.11098 ± 0.00088	0.11161 ± 0.00086	0.11097 ± 0.00087	0.11097 ± 0.00085
$100\theta_{\rm MC}$	1.10 ± 0.10	1.04204 ± 0.00030	1.04189 ± 0.00029	1.04202 ± 0.00030	1.04199 ± 0.00030
τ	0.0543	0.0543 ± 0.0091	0.0717 ± 0.0095	0.0540 ± 0.0087	0.0562 ± 0.0086
Ω_k	-0.033 ± 0.050	-0.095 ± 0.024	-0.0062 ± 0.0014	-0.12 ± 0.12	-0.0062 ± 0.0014
$\ln(10^{10}A_s)$	2.87 ± 0.34	3.021 ± 0.019	3.057 ± 0.019	3.020 ± 0.018	3.024 ± 0.018
A_L	⋯	⋯	⋯	1.08 ± 0.27	1.324 ± 0.063
H_0	70.2 ± 1.7	47.1 ± 3.2	68.07 ± 0.56	52 ± 18	68.45 ± 0.58
Ω_m	0.294 ± 0.018	0.617 ± 0.082	0.2920 ± 0.0050	0.70 ± 0.42	0.2878 ± 0.0050
σ_8	0.771 ± 0.034	0.730 ± 0.017	0.7921 ± 0.0085	0.721 ± 0.053	0.7759 ± 0.0078
$\chi^2_{\rm min}$ (total)	1106.53	2789.77	3926.27	2787.76	3895.24
$\chi^2_{\rm min}$ (non-CMB)	1106.53	⋯	1107.71	⋯	1107.45
DIC	1116.95	2847.14	3982.38	2846.45	3954.21
ΔDIC	2.50	29.21	51.36	28.52	23.19
$\rm AIC_c$	1116.53	2843.77	3980.27	2843.76	3951.24
$\Delta\rm AIC_c$	1.99	23.97	46.92	23.96	17.89

[a]Note: ΔDIC ($\Delta\rm AIC_c$) indicates an excess value relative to that of the tilted flat ΛCDM model constrained with the same data.

TABLE XIV. Mean and 68.3% confidence limits of Planck-$P(q)$-based tilted nonflat ΛCDM ($+A_L$) model parameters constrained by non-CMB, P18, and P18 + non-CMB datasets. H_0 has units of km s^{-1} Mpc^{-1}.[a]

	Tilted nonflat ΛCDM Planck $P(q)$			Tilted nonflat ΛCDM + A_L Planck $P(q)$	
Parameter	Non-CMB	P18	P18 + non-CMB	P18	P18 + non-CMB
$\Omega_b h^2$	0.0242 ± 0.0033	0.02260 ± 0.00017	0.02248 ± 0.00015	0.02258 ± 0.00017	0.02268 ± 0.00017
$\Omega_c h^2$	0.120 ± 0.012	0.1181 ± 0.0015	0.1185 ± 0.0013	0.1183 ± 0.0015	0.1170 ± 0.0014
$100\theta_{\rm MC}$	1.10 ± 0.11	1.04116 ± 0.00032	1.04107 ± 0.00031	1.04116 ± 0.00033	1.04125 ± 0.00032
τ	0.0483	0.0483 ± 0.0083	0.0543 ± 0.0077	0.0478 ± 0.0081	0.0485 ± 0.0087
Ω_k	-0.032 ± 0.051	-0.043 ± 0.017	0.0004 ± 0.0017	-0.130 ± 0.095	-0.0006 ± 0.0017
n_s	0.9706	0.9706 ± 0.0047	0.9687 ± 0.0043	0.9704 ± 0.0048	0.9735 ± 0.0046
$\ln(10^{10}A_s)$	2.90 ± 0.34	3.027 ± 0.017	3.040 ± 0.016	3.027 ± 0.017	3.025 ± 0.018
A_L	⋯	⋯	⋯	0.88 ± 0.15	1.203 ± 0.062
H_0	70.1 ± 1.7	54.5 ± 3.6	68.25 ± 0.56	45 ± 11	68.48 ± 0.56
Ω_m	0.294 ± 0.018	0.481 ± 0.062	0.3040 ± 0.0055	0.80 ± 0.35	0.2994 ± 0.0055
σ_8	0.771 ± 0.035	0.775 ± 0.015	0.8055 ± 0.0076	0.733 ± 0.045	0.7946 ± 0.0088
$\chi^2_{\rm min}$ (total)	1106.53	2754.73	3878.77	2754.99	3865.53
$\chi^2_{\rm min}$ (non-CMB)	1106.53	⋯	1111.36	⋯	1109.27
DIC	1116.92	2810.59	3933.33	2811.63	3924.07
ΔDIC	2.47	−7.34	2.31	−6.30	−6.95
AIC$_c$	1116.53	2810.73	3934.77	2812.99	3923.53
ΔAIC$_c$	1.99	−9.07	1.42	−6.81	−9.82

[a]Note: ΔDIC (ΔAIC$_c$) indicates an excess value relative to that of the tilted flat ΛCDM model constrained with the same data.

P18 and non-CMB data cosmological constraints are inconsistent in the tilted nonflat ΛCDM Planck $P(q)$ model and these data probably should not be used jointly to constrain this model.

Looking at Table XIV, we can compare results obtained for the eight- and the five-parameter tilted nonflat ΛCDM + A_L Planck $P(q)$ model from P18 and non-CMB data, respectively. Aside from Ω_k, the primary parameter disagreements do not change much compared to the $A_L = 1$ case. For the non-CMB data primary spatial curvature parameter, we have $\Omega_k = -0.032 \pm 0.051$, which is 0.63σ away from flat and in 0.91σ tension with the P18 value -0.130 ± 0.095, which is

TABLE XV. Mean and 68.3% confidence limits of new-$P(q)$-based tilted nonflat ΛCDM ($+A_L$) model parameters constrained by non-CMB, P18, and P18 + non-CMB datasets. H_0 has units of km s^{-1} Mpc^{-1}.[a]

	Tilted nonflat ΛCDM new $P(q)$			Tilted nonflat ΛCDM + A_L new $P(q)$	
Parameter	Non-CMB	P18	P18 + non-CMB	P18	P18 + non-CMB
$\Omega_b h^2$	0.0241 ± 0.0033	0.02255 ± 0.00017	0.02249 ± 0.00015	0.02257 ± 0.00017	0.02269 ± 0.00016
$\Omega_c h^2$	0.120 ± 0.013	0.1188 ± 0.0015	0.1184 ± 0.0013	0.1187 ± 0.0016	0.1170 ± 0.0013
$100\theta_{\rm MC}$	1.11 ± 0.11	1.04109 ± 0.00032	1.04108 ± 0.00031	1.04111 ± 0.00033	1.04125 ± 0.00032
τ	0.0525	0.0525 ± 0.0083	0.0549 ± 0.0077	0.0512 ± 0.0086	0.0490 ± 0.0086
Ω_k	-0.036 ± 0.051	-0.033 ± 0.014	0.0003 ± 0.0017	-0.10 ± 0.11	-0.0006 ± 0.0017
n_s	0.9654	0.9654 ± 0.0045	0.9684 ± 0.0041	0.9654 ± 0.0057	0.9730 ± 0.0043
$\ln(10^{10}A_s)$	2.88 ± 0.34	3.039 ± 0.017	3.042 ± 0.016	3.036 ± 0.018	3.026 ± 0.018
A_L	⋯	⋯	⋯	0.94 ± 0.20	1.204 ± 0.061
H_0	70.1 ± 1.8	56.9 ± 3.6	68.21 ± 0.55	51 ± 14	68.47 ± 0.56
Ω_m	0.295 ± 0.018	0.444 ± 0.055	0.3043 ± 0.0054	0.70 ± 0.43	0.2994 ± 0.0056
σ_8	0.770 ± 0.035	0.786 ± 0.014	0.8057 ± 0.0074	0.752 ± 0.052	0.7948 ± 0.0083
$\chi^2_{\rm min}$ (total)	1106.49	2757.38	3878.76	2756.33	3865.41
$\chi^2_{\rm min}$ (non-CMB)	1106.49	⋯	1111.36	⋯	1109.32
DIC	1117.31	2811.54	3932.56	2814.83	3923.86
ΔDIC	2.86	−6.39	1.54	−3.10	−7.16
AIC$_c$	1116.49	2813.38	3934.76	2814.33	3923.41
ΔAIC$_c$	1.95	−6.42	1.41	−5.47	−9.94

[a]Note: ΔDIC (ΔAIC$_c$) indicates an excess value relative to that of the tilted flat ΛCDM model constrained with the same data.

1.4σ away from flat. Regarding the derived parameters, we find that H_0, Ω_m, and σ_8 are in 2.3σ, 1.4σ, and 0.67σ disagreement. Compared to the $A_L = 1$ case, in the A_L-varying case we find significant reductions in the H_0 and Ω_m tensions, with both disagreements still being significant, which suggests that P18 and non-CMB data should not be jointly analyzed within the tilted nonflat $\Lambda\text{CDM} + A_L$ Planck $P(q)$ model.

Comparing the seven- and the five-parameter tilted nonflat ΛCDM new $P(q)$ model primary cosmological parameter constraints for P18 and non-CMB data, from the left half of Table XV, we see that the primary parameter values do not much disagree. The non-CMB data primary spatial curvature parameter value is $\Omega_k = -0.036 \pm 0.051$, which is only a 0.71σ deviation from flat and, similar to the Planck $P(q)$ model, is only in 0.057σ disagreement with the P18 value -0.033 ± 0.014, which is 2.4σ away from flat. Regarding the derived parameters H_0, Ω_m, and σ_8, we find that their values disagree at 3.3σ, 2.6σ, and 0.42σ, respectively. While the H_0 and Ω_m disagreements are a little smaller than the ones found in the tilted nonflat ΛCDM Planck $P(q)$ model, they still are large enough to require we more carefully test whether P18 and non-CMB data can be jointly used to constrain cosmological parameters in this model.

The results for the eight- and the five-parameter tilted nonflat $\Lambda\text{CDM} + A_L$ new $P(q)$ model are in Table XV, for P18 and non-CMB data, respectively. As happens in the Planck $P(q)$ model, when the A_L parameter is allowed to vary, the mild tensions found for the primary parameters, except for Ω_k, do not change much compared to the $A_L = 1$ case. For the non-CMB data primary spatial curvature parameter, we have $\Omega_k = -0.036 \pm 0.051$, which is 0.71σ away from flat hypersurfaces and now in 0.53σ tension with the P18 value $\Omega_k = -0.10 \pm 0.11$, which is 0.91σ away from flat. As for the value of the derived parameters H_0, Ω_m, and σ_8, we find disagreements at 1.4σ, 0.94σ, and 0.29σ, respectively. The tensions are reduced with respect to the case with $A_L = 1$, due to the increase of the error bars, but possibly the H_0 tension is still not small enough to allow the joint use of P18 + non-CMB data for constraining tilted nonflat $\Lambda\text{CDM} + A_L$ new $P(q)$ model cosmological parameters.

Figures 24–31 show one-dimensional likelihoods and two-dimensional contours for cosmological parameters obtained using P18, non-CMB, and P18 + non-CMB data. As mentioned above, non-CMB data constraints (shown with unfilled black lines) are comparatively less restrictive than P18 constraints (shown in gray), are unable to put tight constraints on the primary cosmological parameters (except on Ω_k in the three nonflat $\Lambda\text{CDM} + A_L$ models), and in many cases they at least partially overlap with the P18 data constraints.

Figures 24 and 25 are for tilted flat ΛCDM ($+A_L$) models. The $\sim 1\sigma$ disagreements between the non-CMB constraints and those obtained with P18 data, discussed above, can be clearly seen in the contour plots. For the tilted flat ΛCDM model, the larger disagreements are in panels for derived cosmological parameters, with the largest for Ω_m and the next largest for H_0. These disagreements decrease when the A_L parameter is allowed to vary.

Looking at the contour plots for the untilted nonflat ΛCDM ($+A_L$) models (see Figs. 26 and 27), we observe nonoverlapping contours in those panels that involve the derived parameters H_0 and Ω_m or the primary parameter Ω_k, especially in the Ω_k-$\theta_{\rm MC}$ subpanel of Fig. 26. These disagreements largely disappear when A_L is allowed to vary, except perhaps for the H_0 one. This may indicate that in the context of this cosmological model we may jointly analyze P18 data with non-CMB data only when A_L is allowed to vary.

Figures 28 and 29 show cosmological parameter constraints for the tilted nonflat ΛCDM ($+A_L$) Planck $P(q)$ models, while the ones for the tilted nonflat ΛCDM ($+A_L$) new $P(q)$ models are displayed in Figs. 30 and 31. As expected, considering the results discussed above in this subsubsection, the contour plots for these tilted nonflat models are quite similar. We see in the panels that involve the primary cosmological parameters that there is overlap at 1σ, not only when A_L is allowed to vary but also when $A_L = 1$. When $A_L = 1$, for the Planck $P(q)$ model, P18 and non-CMB data constraint contours that involve H_0 and Ω_m do not overlap even at 2σ. These disagreements are less severe for the new $P(q)$ model with $A_L = 1$, where overlap is reached in most cases at a little over 2σ.

In view of the results discussed in this subsubsection, further tests are needed to properly quantify the level of disagreement, in the context of nonflat models, between P18 data and non-CMB data cosmological constraints. We return to this issue in Sec. IV C.

7. *Comparing* P18 + lensing *data and non-CMB data cosmological constraints*

In the previous subsubsection we compared non-CMB data cosmological constraints to those obtained from P18 data. We found significant tensions in the nonflat models with $A_L = 1$ for the derived parameters H_0 and Ω_m and a 2.2σ tension between the two Ω_m values in the flat ΛCDM model with $A_L = 1$. In view of these results, additional tests are needed if one wants to know whether P18 and non-CMB data can be jointly analyzed to determine cosmological constraints. We study this in Sec. IV C. Interestingly, when the A_L parameter is allowed to vary, these tensions decrease significantly, with the largest tension being 2.3σ between the two H_0 values in the tilted nonflat Planck $P(q)$ model and the remaining tensions not exceeding 1.4σ, perhaps an indication that P18 and non-CMB data can be used jointly to constrain cosmological parameters when A_L is allowed to vary.

In Secs. IV A 1 and IV A 2 we discussed the cosmological constraints obtained from P18 data and from P18 + lensing data. We shall see in Sec. IV C that, in the nonflat

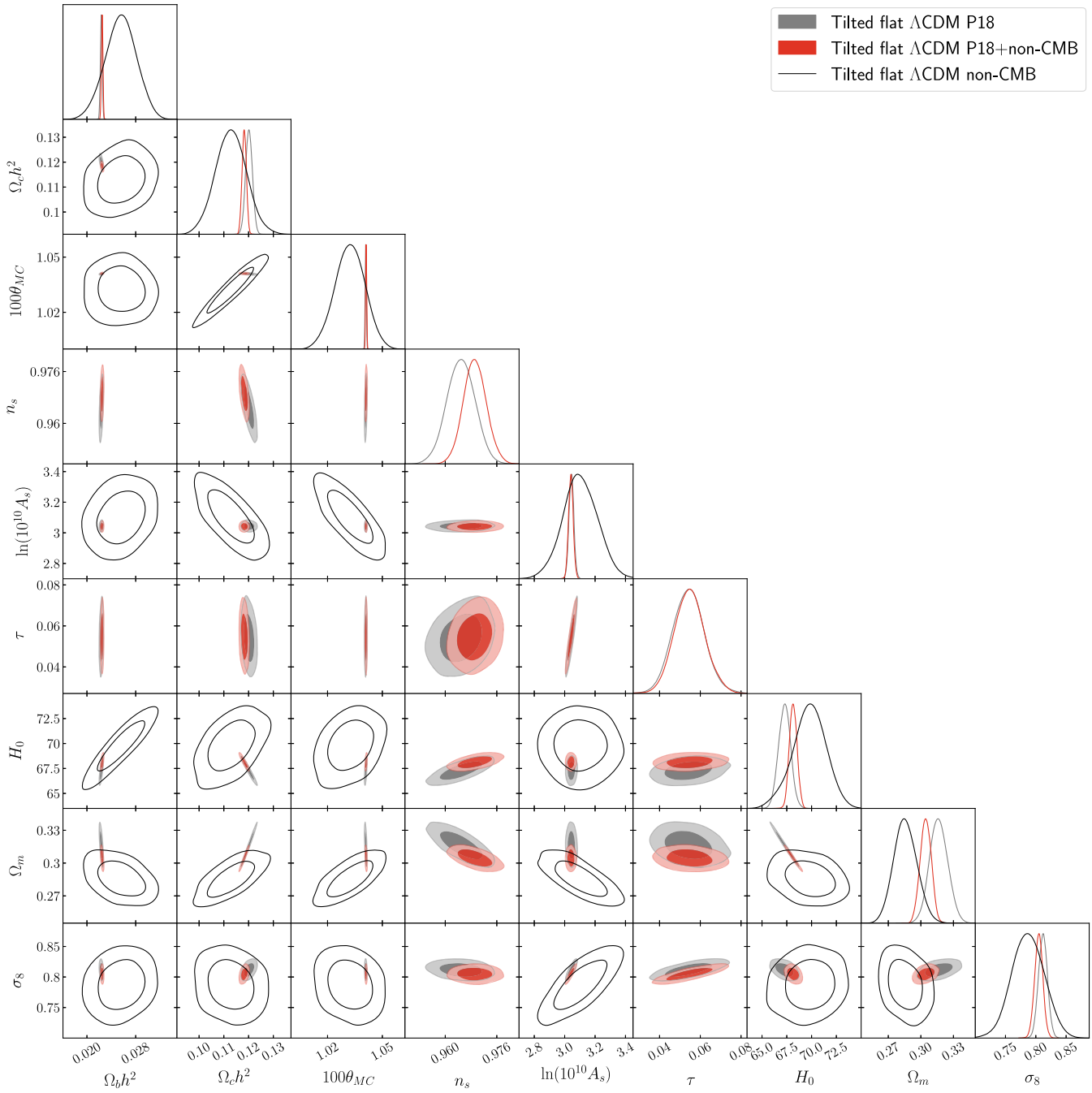

FIG. 24. Likelihoods of the tilted flat ΛCDM model parameters constrained by P18, non-CMB, and P18 + non-CMB datasets.

models, P18 data and lensing data are less mutually inconsistent than P18 data and non-CMB data are; however, it is necessary to perform an additional test to determine whether or not P18, lensing, and non-CMB data can be jointly analyzed to derive cosmological constraints in the nonflat models with $A_L = 1$.

In this subsubsection, we describe the results of this additional test that compares non-CMB data cosmological constraints to the ones obtained from P18 + lensing data. P18 + lensing + non-CMB data cannot be jointly used in the context of a given model unless the cosmological constraints obtained with P18 + lensing data and with non-CMB data are consistent. While in the previous subsubsection we labeled the study of P18 vs non-CMB as a study of high-redshift data cosmological constraints vs low-redshift data cosmological constraints, we cannot do that in this subsubsection since most of the information in the lensing data is from low-redshift data.

The cosmological parameter mean values and error bars favored by the P18 + lensing, non-CMB, and

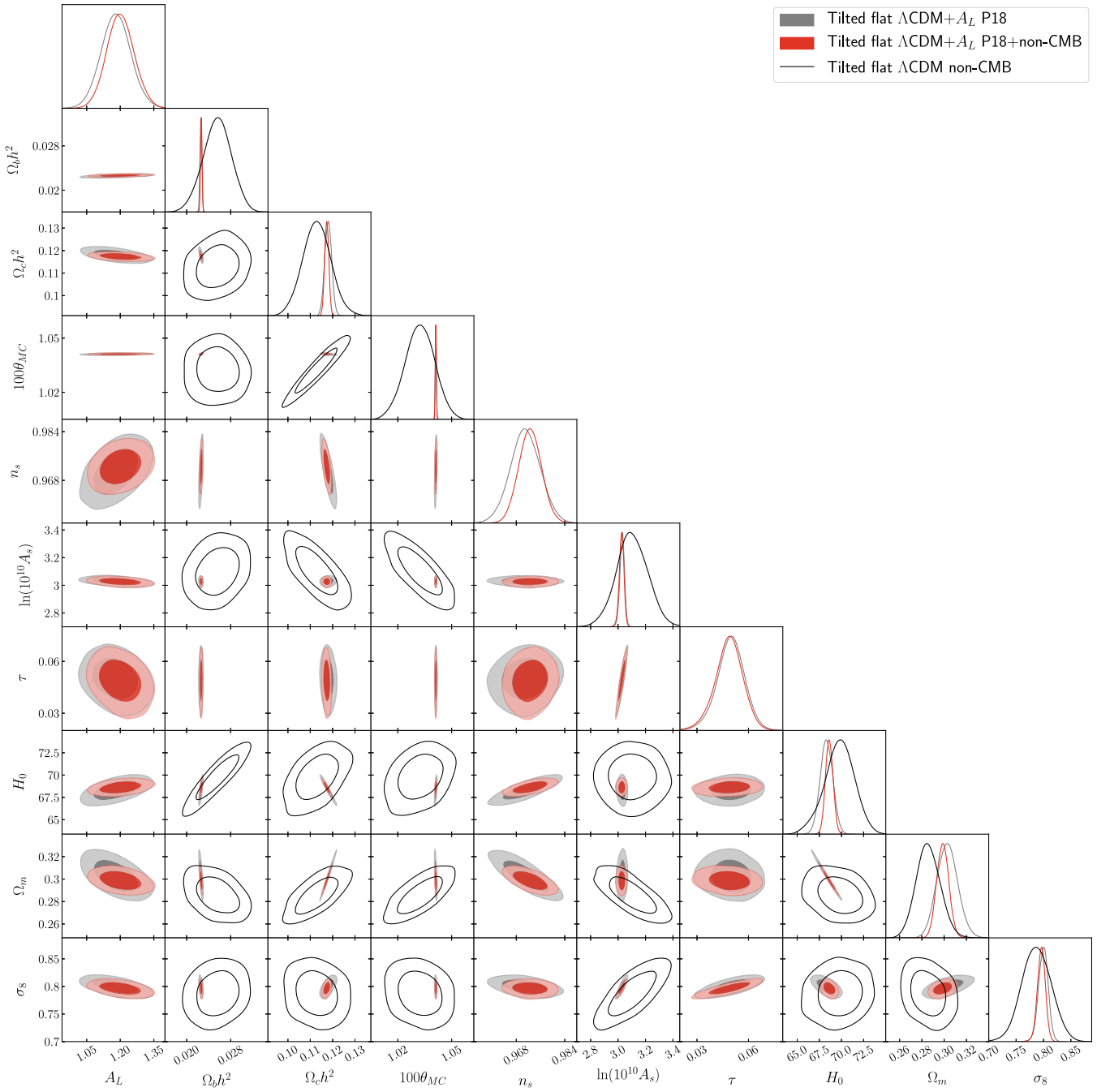

FIG. 25. Likelihoods of the tilted flat ΛCDM + A_L model parameters constrained by P18, non-CMB, and P18 + non-CMB datasets. The likelihoods for the non-CMB dataset, which do not depend on A_L, are the same as in Fig. 24.

P18 + lensing + non-CMB datasets are summarized in Tables XVI–XIX for the tilted flat ΛCDM ($+A_L$) model, the untilted nonflat ΛCDM ($+A_L$) model, the tilted nonflat ΛCDM ($+A_L$) Planck $P(q)$ model, and the tilted nonflat ΛCDM ($+A_L$) new $P(q)$ model. Likelihood distributions of cosmological parameters of the four models with $A_L = 1$ and with varying A_L are shown in Figs. 32–39 for the P18 + lensing, non-CMB, and P18 + lensing + non-CMB datasets.

Since non-CMB data do not have the ability to constrain τ or n_s, in this subsubsection we set their values in the non-CMB data only analyses to those found in the corresponding P18 + lensing data analyses. Note that, in the previous subsubsection, where the case of P18 data vs non-CMB data was studied, the values of τ and n_s in the non-CMB data only analyses were set to those found in the corresponding P18 data analyses; nevertheless, the cosmological parameter constraints from the two non-CMB data analyses

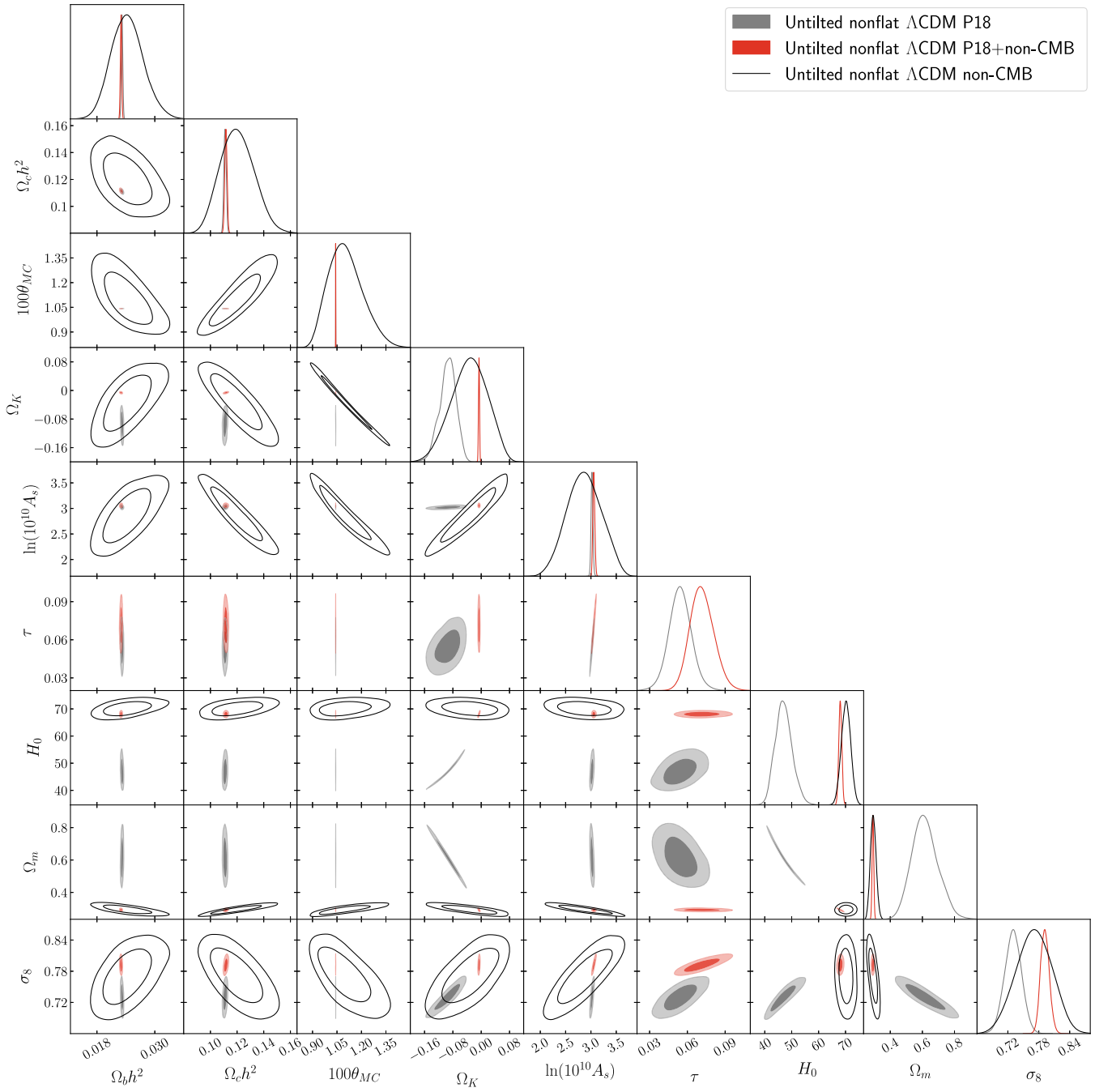

FIG. 26. Likelihoods of the untilted nonflat ΛCDM model parameters constrained by P18, non-CMB, and P18 + non-CMB datasets.

are practically identical. This indicates that non-CMB data are mostly insensitive to changes in the values of τ and n_s, as we have assumed. Again, we do not include the A_L parameter in the analyses when only non-CMB data are considered, since it does not play a role at low redshift.

Similar to what happens in the previous subsubsection, when we compare cosmological constraints from P18 data and from non-CMB data, by looking at Tables XVII–XIX we observe that, for the six nonflat ΛCDM ($+A_L$) models, the constraints imposed by non-CMB data on the H_0 and Ω_m parameters are tighter than the ones from P18 + lensing data. P18 + lensing data more restrictively constrain all other parameters in all eight cosmological models.

Comparing the six- and the four-parameter tilted flat ΛCDM model primary cosmological parameter constraints for P18 + lensing and non-CMB data, shown in the left part of Table XVI, we observe that the values of $\Omega_b h^2$, $\Omega_c h^2$, and $\theta_{\rm MC}$ are in mild disagreement, at 1.3σ, 1.2σ, and 1.1σ, respectively. We also see tensions in the derived parameters. In particular, for the nonrelativistic matter density

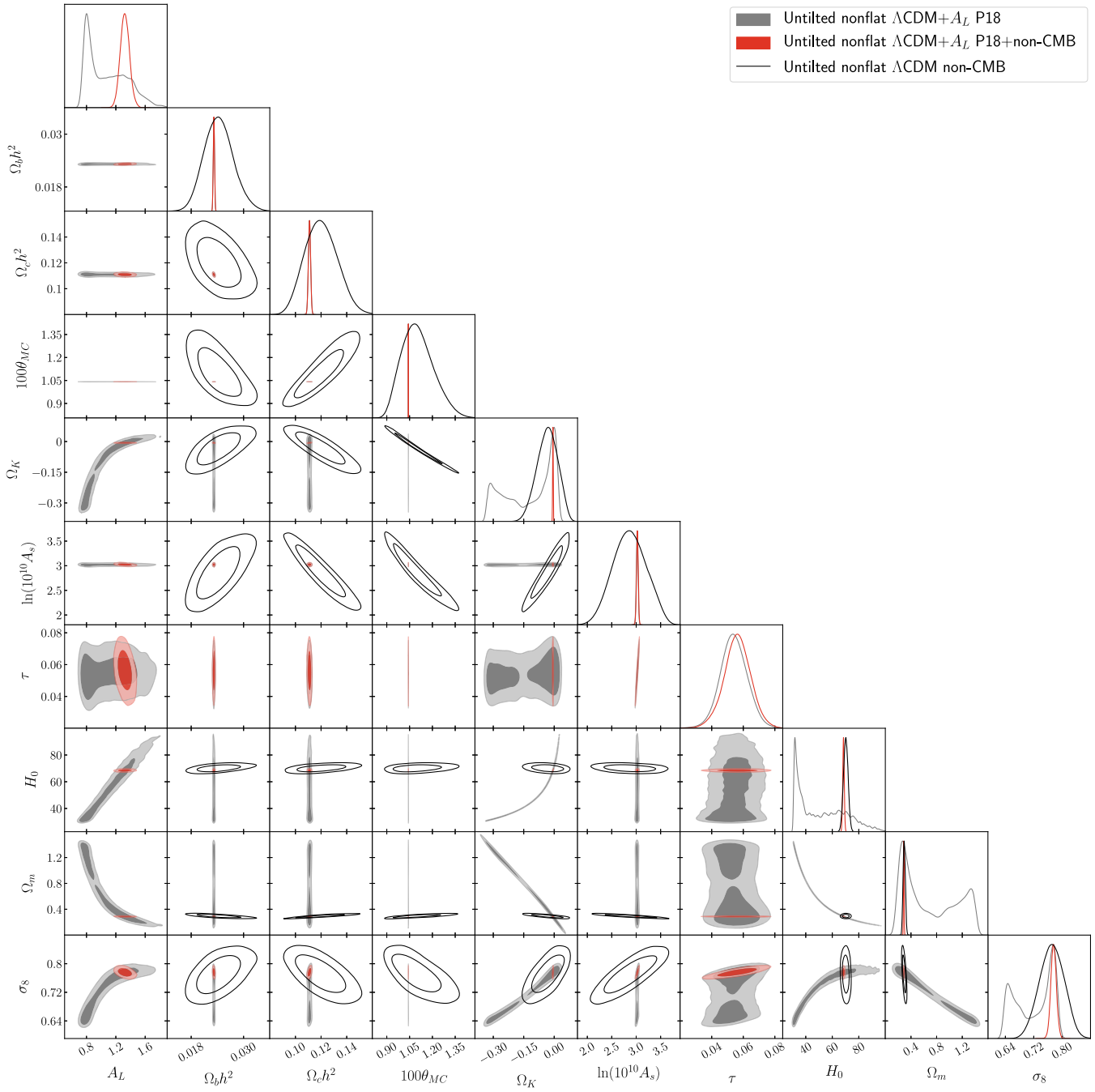

FIG. 27. Likelihoods of the untilted nonflat ΛCDM + A_L model parameters constrained by P18, non-CMB, and P18 + non-CMB datasets. The likelihoods for the non-CMB dataset, which do not depend on A_L, are the same as in Fig. 26.

parameter Ω_m, the level of tension reaches 2.3σ, whereas the values of H_0 disagree by 1.4σ.

From Table XVI, we can compare the seven- and the four-parameter tilted flat ΛCDM + A_L model cosmological parameter constraints for P18 + lensing data and for non-CMB data. Regarding the primary cosmological parameters, we see that the values of $\Omega_b h^2$ and $\theta_{\rm MC}$ disagree at 1.2σ and 1.1σ, respectively. The inclusion of the A_L-varying parameter reduces significantly the tension found in the $A_L = 1$ case for Ω_m and H_0, with them now disagreeing by only 1.4σ and 0.96σ. We do not find any clear evidence that prevents us from jointly analyzing P18 + lensing and non-CMB data, in the context of the tilted flat ΛCDM model, with and without a varying A_L parameter.

The results for the six- and the four-parameter untilted nonflat ΛCDM model obtained from P18 + lensing and non-CMB data are in Table XVII. While for the primary

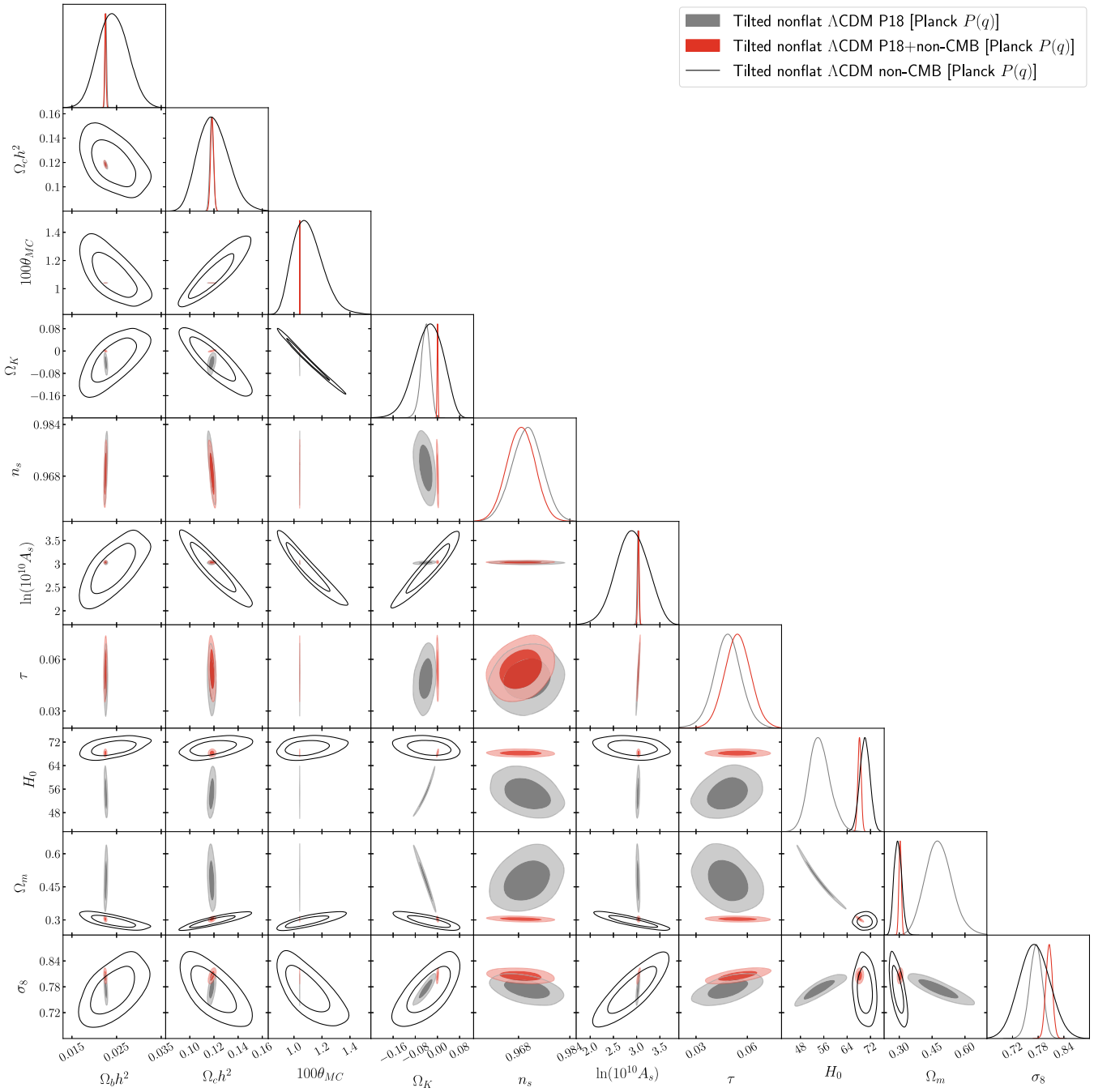

FIG. 28. Likelihoods of the tilted nonflat ΛCDM model [with Planck $P(q)$] parameters constrained by P18, non-CMB, and P18 + non-CMB datasets.

cosmological parameters we do not observe significant tensions, we do for the derived parameters. The primary spatial curvature parameter is $\Omega_k = -0.037 \pm 0.050$ for non-CMB data, which is 0.74σ away from flat hypersurfaces and in 0.095σ tension with the P18 + lensing analysis value $\Omega_k = -0.0322 \pm 0.0075$, which is 4.3σ away from flat. As for the derived parameters, we find that H_0, Ω_m, and σ_8 values are in 4.2σ, 2.9σ, and 0.11σ disagreement. The high levels of tensions reached for some of the parameters may indicate that P18 + lensing and non-CMB data should not be jointly analyzed in the context of the untilted nonflat ΛCDM model.

P18 + lensing and non-CMB data results obtained for the seven- and the four-parameter untilted nonflat ΛCDM + A_L model are shown in Table XVII. Regarding the values of the primary cosmological parameters, except for Ω_k (discussed next), as was observed in the $A_L = 1$ case, there are no significant tensions. The value of the curvature parameter is

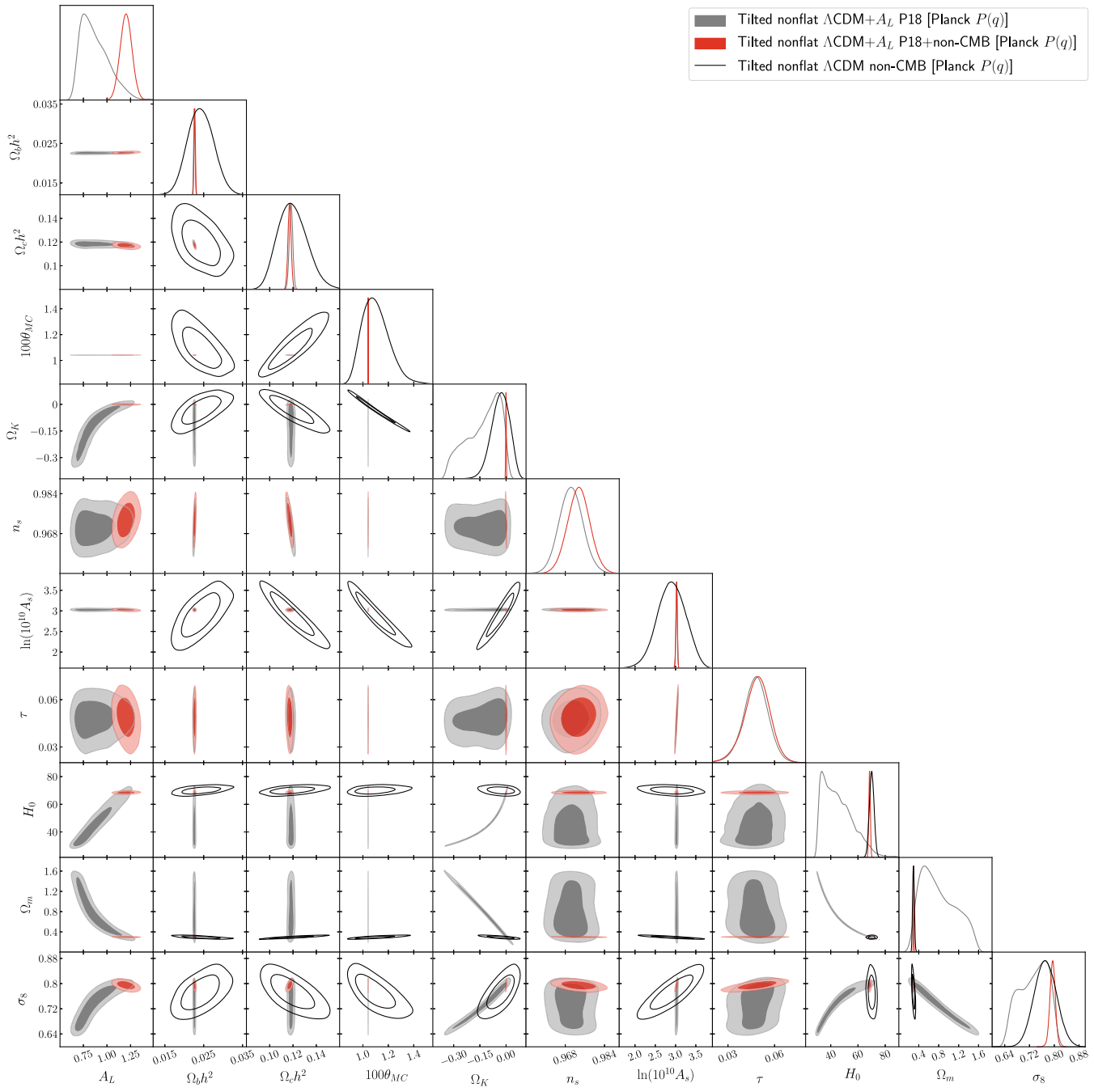

FIG. 29. Likelihoods of the tilted nonflat ΛCDM + A_L model [with Planck $P(q)$] parameters constrained by P18, non-CMB, and P18 + non-CMB datasets. The likelihoods for the non-CMB dataset, which do not depend on A_L, are the same as in Fig. 28.

$\Omega_k = -0.037 \pm 0.050$ (0.74σ away from flat) for the non-CMB data and $\Omega_k = 0.0161 \pm 0.0094$ for the P18 + lensing data, which indicates 1.7σ evidence in favor of an open spatial geometry. The two Ω_k values disagree at 1.0σ. The disagreement in the values of the derived parameters H_0, Ω_m, and σ_8 values are 1.8σ, 2.3σ, and 0.32σ, respectively, which clearly represents a reduction with respect to the $A_L = 1$ case. This is due to the elongation of the error bars in the varying A_L case compared to the $A_L = 1$ case. Given these results, the P18 + lensing and the non-CMB data should perhaps not be used together in the context of the untilted nonflat ΛCDM + A_L model. It may be noticed, however, that when we do so, namely in the P18 + lensing + non-CMB analysis, the obtained value for the curvature parameter is $\Omega_k = -0.0060 \pm 0.0014$, which is 4.3σ away from flat. Nonetheless, according to the AIC and DIC this model is strongly disfavored when it is compared with the tilted models, due to the lack of the degree of freedom contained in the n_s parameter.

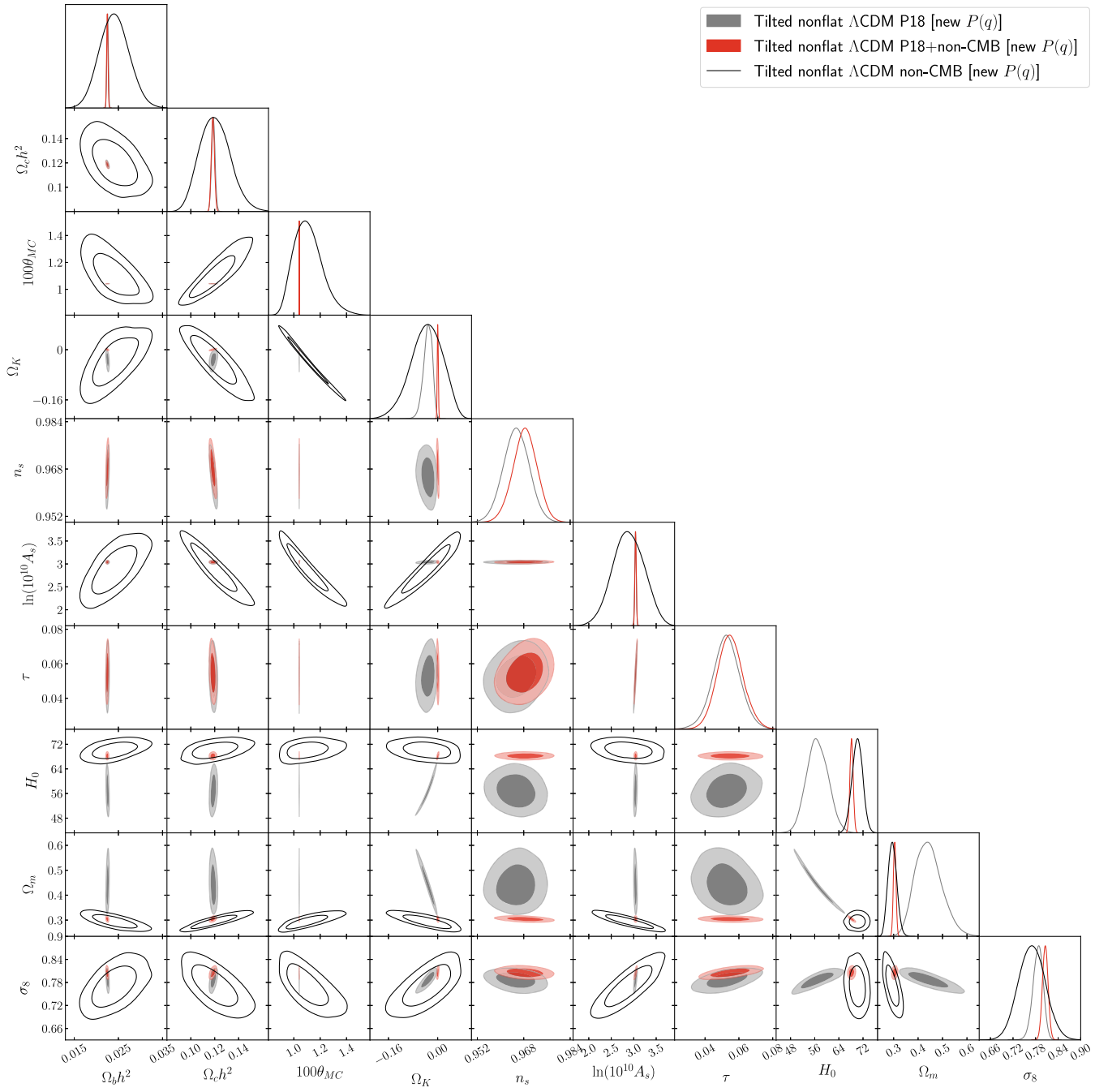

FIG. 30. Likelihoods of the tilted nonflat ΛCDM model [with new $P(q)$] parameters constrained by P18, non-CMB, and P18 + non-CMB datasets.

The results that allow us to compare the seven- and the five-parameter tilted nonflat ΛCDM Planck $P(q)$ model primary cosmological parameter constraints for P18 + lensing data and non-CMB data can be seen in Table XVIII. There are no significant tensions in the values of the primary cosmological parameters. The non-CMB data value of the spatial curvature parameter, $\Omega_k = -0.033 \pm 0.050$, is 0.66σ away from flat and in 0.45σ tension with the value found in the P18 + lensing analysis, namely $\Omega_k = -0.0103 \pm 0.0066$, which represents a 1.6σ deviation from flat hypersurfaces. As for the values of the derived parameters H_0, Ω_m, and σ_8, the tensions are 2.2σ, 1.9σ, and 0.66σ, respectively. Given these results, further tests are probably necessary in order to decide whether P18 + lensing and non-CMB data can be jointly analyzed in the context of the tilted nonflat ΛCDM Planck $P(q)$ model.

P18 + lensing and non-CMB data results obtained for the eight- and the five-parameter tilted nonflat

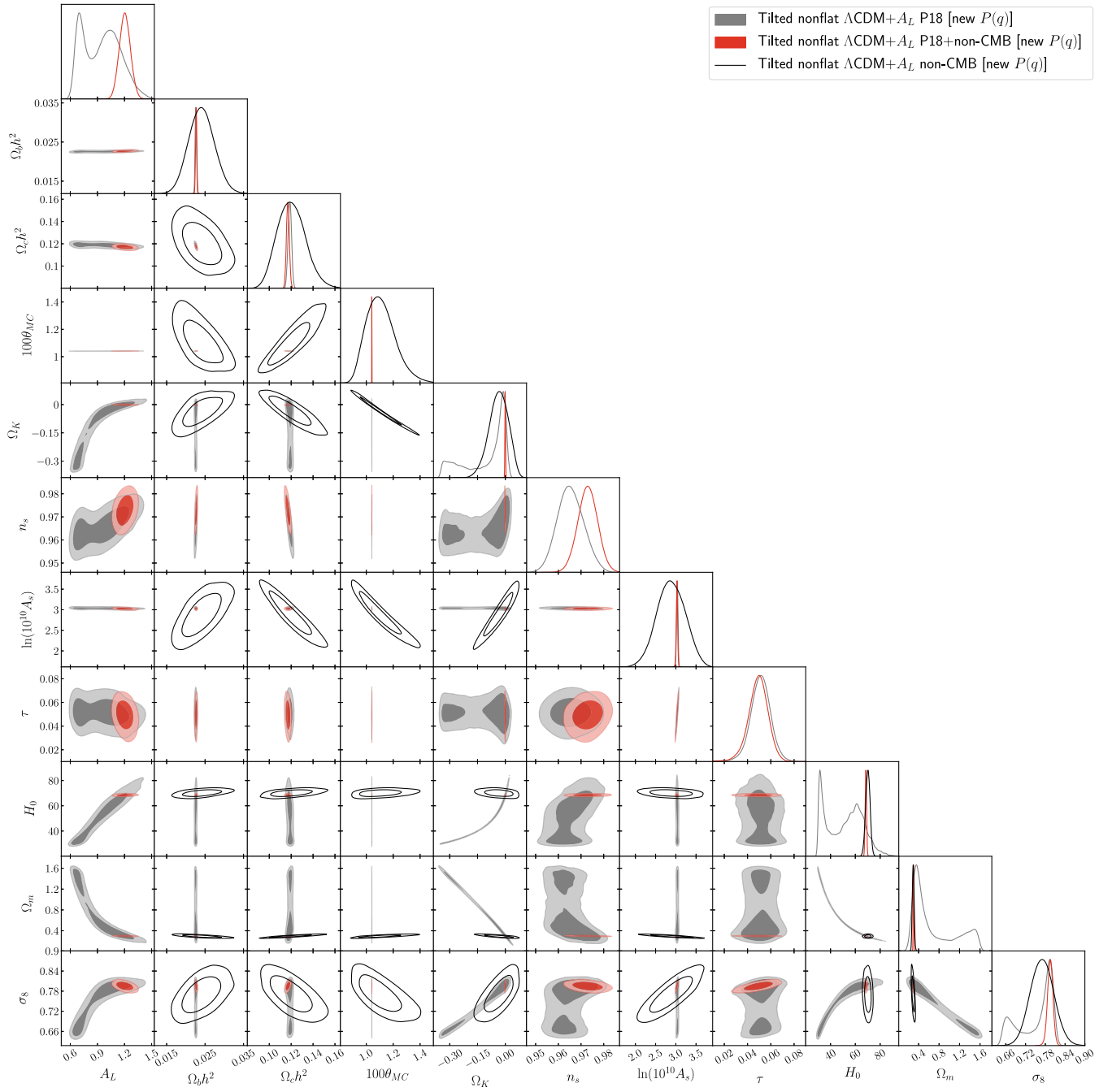

FIG. 31. Likelihoods of the tilted nonflat $\Lambda\mathrm{CDM} + A_L$ model [with new $P(q)$] parameters constrained by P18, non-CMB, and P18 + non-CMB datasets. The likelihoods for the non-CMB dataset, which do not depend on A_L, are the same as in Fig. 30.

$\Lambda\mathrm{CDM} + A_L$ Planck $P(q)$ model are shown in Table XVIII. Similar to the $A_L = 1$ case, we do not find significant disagreements in the values of the primary cosmological parameters. For the non-CMB data, the value of the curvature parameter is $\Omega_k = -0.033 \pm 0.050$, which is 0.66σ away from flat and in 0.49σ tension with the P18 + lensing value, $\Omega_k = -0.005 \pm 0.027$, which in turn is only 0.19σ in favor of a closed geometry. An important reduction in the disagreements found in the derived parameters, with respect to the $A_L = 1$ case, is observed. In particular, for H_0, Ω_m, and σ_8 the disagreement found is 0.099σ, 0.23σ, and 0.63σ. We may say that in the context of the tilted nonflat $\Lambda\mathrm{CDM} + A_L$ Planck $P(q)$ we are allowed to analyze together P18 + lensing data and non-CMB data. By doing so, we get for P18 + lensing + non-CMB data no evidence in favor of a nonflat geometry, $\Omega_k = -0.0002 \pm 0.0017$, but still a clear 2.5σ preference for $A_L \neq 1$, since $A_L = 1.090 \pm 0.036$.

TABLE XVI. Mean and 68.3% confidence limits of tilted flat ΛCDM ($+A_L$) model parameters constrained by non-CMB, P18 + lensing, and P18 + lensing + non-CMB datasets. The Hubble constant H_0 has a unit of km s^{-1} Mpc^{-1}.[a]

	Tilted flat ΛCDM			Tilted flat ΛCDM + A_L	
Parameter	Non-CMB	P18 + lensing	P18 + lensing + non-CMB	P18 + lensing	P18 + lensing + non-CMB
$\Omega_b h^2$	0.0257 ± 0.0026	0.02237 ± 0.00014	0.02250 ± 0.00013	0.02251 ± 0.00017	0.02258 ± 0.00014
$\Omega_c h^2$	0.1128 ± 0.0061	0.1200 ± 0.0012	0.11838 ± 0.00083	0.1183 ± 0.0015	0.11747 ± 0.00091
$100\theta_{\rm MC}$	1.0321 ± 0.0080	1.04091 ± 0.00031	1.04110 ± 0.00029	1.04109 ± 0.00032	1.04118 ± 0.00029
τ	0.0543	0.0543 ± 0.0073	0.0569 ± 0.0071	0.0487 ± 0.0087	0.0476 ± 0.0085
n_s	0.9649	0.9649 ± 0.0041	0.9688 ± 0.0036	0.9695 ± 0.0048	0.9715 ± 0.0038
$\ln(10^{10}A_s)$	3.10 ± 0.11	3.044 ± 0.014	3.046 ± 0.014	3.028 ± 0.018	3.023 ± 0.018
A_L	⋯	⋯	⋯	1.073 ± 0.041	1.089 ± 0.035
H_0	69.9 ± 1.7	67.34 ± 0.55	68.09 ± 0.38	68.14 ± 0.69	68.52 ± 0.42
Ω_m	0.285 ± 0.011	0.3155 ± 0.0075	0.3053 ± 0.0050	0.3048 ± 0.0091	0.2998 ± 0.0053
σ_8	0.787 ± 0.026	0.8112 ± 0.0059	0.8072 ± 0.0058	0.7996 ± 0.0089	0.7955 ± 0.0075
$\chi^2_{\rm min}$ (total)	1106.55	2774.71	3888.41	2771.24	3881.55
$\chi^2_{\rm min}$ (non-CMB)	1106.55	⋯	1112.05	⋯	1109.64
DIC	1114.38	2826.45	3940.70	2825.53	3935.15
ΔDIC	⋯	⋯	⋯	−0.92	−5.55
AIC$_c$	1114.55	2828.71	3942.41	2827.24	3937.55
ΔAIC$_c$	⋯	⋯	⋯	−1.47	−4.86

[a]Note: ΔDIC (ΔAIC$_c$) indicates an excess value relative to that of the tilted flat ΛCDM model constrained with the same data.

Comparing the seven- and the five-parameter tilted nonflat ΛCDM new $P(q)$ model primary cosmological parameter constraints for P18 + lensing data and non-CMB data, from the left part of Table XIX, we see no important differences in the values of the primary parameters. The value for the spatial curvature parameter is $\Omega_k = -0.033 \pm 0.050$ for non-CMB data, which represents a 0.66σ deviation from flat and it is in 0.48σ tension with the value obtained in the P18 + lensing analysis, $\Omega_k = -0.0086 \pm 0.0057$, which is 1.5σ away from flat hypersurfaces. Regarding the triad of derived parameters H_0, Ω_m, and σ_8, the disagreement found for each of them is 2.2σ, 1.9σ, and 0.75σ, respectively. In light of these results, we deem that more testing is required to decide whether the

TABLE XVII. Mean and 68.3% confidence limits of untilted nonflat ΛCDM ($+A_L$) model parameters constrained by non-CMB, P18 + lensing, and P18 + lensing + non-CMB datasets. The Hubble constant H_0 has a unit of km s^{-1} Mpc^{-1}.[a]

	Untilted nonflat ΛCDM			Untilted nonflat ΛCDM + A_L	
Parameter	Non-CMB	P18 + lensing	P18 + lensing + non-CMB	P18 + lensing	P18 + lensing + non-CMB
$\Omega_b h^2$	0.0241 ± 0.0033	0.02307 ± 0.00014	0.02301 ± 0.00014	0.02312 ± 0.00014	0.02310 ± 0.00014
$\Omega_c h^2$	0.121 ± 0.013	0.11108 ± 0.00086	0.11176 ± 0.00083	0.11092 ± 0.00087	0.11100 ± 0.00085
$100\theta_{\rm MC}$	1.11 ± 0.11	1.04196 ± 0.00029	1.04189 ± 0.00029	1.04193 ± 0.00029	1.04195 ± 0.00030
τ	0.0580	0.0580 ± 0.0087	0.0799 ± 0.0089	0.0554 ± 0.0097	0.0566 ± 0.0083
Ω_k	-0.037 ± 0.050	-0.0322 ± 0.0075	-0.0065 ± 0.0014	0.0161 ± 0.0094	-0.0060 ± 0.0014
$\ln(10^{10}A_s)$	2.84 ± 0.34	3.027 ± 0.018	3.075 ± 0.018	3.021 ± 0.020	3.024 ± 0.017
A_L	⋯	⋯	⋯	1.44 ± 0.15	1.162 ± 0.036
H_0	70.2 ± 1.7	58.9 ± 2.1	67.90 ± 0.56	85.7 ± 8.5	68.48 ± 0.58
Ω_m	0.295 ± 0.018	0.390 ± 0.027	0.2938 ± 0.0049	0.190 ± 0.043	0.2874 ± 0.0050
σ_8	0.769 ± 0.035	0.765 ± 0.011	0.7997 ± 0.0076	0.7805 ± 0.0094	0.7764 ± 0.0078
$\chi^2_{\rm min}$ (total)	1106.51	2813.13	3938.22	2807.91	3915.05
$\chi^2_{\rm min}$ (non-CMB)	1106.51	⋯	1108.60	⋯	1107.39
DIC	1117.24	2869.06	3992.71	2856.10	3973.55
ΔDIC	2.86	42.61	52.01	29.65	32.85
AIC$_c$	1116.51	2867.13	3992.22	2863.91	3971.05
ΔAIC$_c$	1.96	38.42	49.81	35.20	28.64

[a]Note: ΔDIC (ΔAIC$_c$) indicates an excess value relative to that of the tilted flat ΛCDM model constrained with the same data.

TABLE XVIII. Mean and 68.3% confidence limits of Planck-$P(q)$-based tilted nonflat ΛCDM ($+A_L$) model parameters constrained by non-CMB, P18 + lensing, and P18 + lensing + non-CMB datasets. The Hubble constant H_0 has a unit of km s^{-1} Mpc^{-1}.[a]

	Tilted nonflat ΛCDM Planck $P(q)$			Tilted nonflat ΛCDM + A_L Planck $P(q)$	
Parameter	Non-CMB	P18 + lensing	P18 + lensing + non-CMB	P18 + lensing	P18 + lensing + non-CMB
$\Omega_b h^2$	0.0242 ± 0.0033	0.02249 ± 0.00016	0.02249 ± 0.00015	0.02251 ± 0.00017	0.02259 ± 0.00016
$\Omega_c h^2$	0.120 ± 0.013	0.1186 ± 0.0015	0.1187 ± 0.0013	0.1183 ± 0.0015	0.1173 ± 0.0014
$100\theta_{\rm MC}$	1.10 ± 0.10	1.04107 ± 0.00032	1.04106 ± 0.00031	1.04110 ± 0.00032	1.04118 ± 0.00032
τ	0.0495	0.0495 ± 0.0082	0.0563 ± 0.0073	0.0489 ± 0.0085	0.0479 ± 0.0085
Ω_k	-0.033 ± 0.050	-0.0103 ± 0.0066	0.0004 ± 0.0017	-0.005 ± 0.027	-0.0002 ± 0.0017
n_s	0.9687	0.9687 ± 0.0046	0.9681 ± 0.0044	0.9696 ± 0.0049	0.9718 ± 0.0045
$\ln(10^{10} A_s)$	2.90 ± 0.34	3.030 ± 0.017	3.046 ± 0.014	3.028 ± 0.018	3.024 ± 0.017
A_L	…	…	…	1.09 ± 0.16	1.090 ± 0.036
H_0	70.1 ± 1.8	63.7 ± 2.3	68.17 ± 0.55	69 ± 11	68.49 ± 0.56
Ω_m	0.294 ± 0.018	0.351 ± 0.024	0.3051 ± 0.0053	0.32 ± 0.11	0.2998 ± 0.0055
σ_8	0.771 ± 0.036	0.796 ± 0.011	0.8080 ± 0.0066	0.796 ± 0.016	0.7952 ± 0.0085
$\chi^2_{\rm min}$ (total)	1106.51	2771.53	3887.99	2771.14	3881.37
$\chi^2_{\rm min}$ (non-CMB)	1106.51	…	1111.94	…	1110.31
DIC	1117.27	2826.17	3942.07	2827.14	3936.85
ΔDIC	2.89	−0.28	1.37	0.69	−3.85
$\rm AIC_c$	1116.51	2827.53	3943.99	2829.14	3939.37
$\Delta\rm AIC_c$	1.96	−1.18	1.58	0.43	−3.04

[a]Note: ΔDIC ($\Delta\rm AIC_c$) indicates an excess value relative to that of the tilted flat ΛCDM model constrained with the same data.

P18 + lensing and non-CMB data can be jointly analyzed in the context of the tilted nonflat ΛCDM new $P(q)$ model.

In Table XIX we provide the results for the eight- and the five-parameter tilted nonflat ΛCDM + A_L new $P(q)$ model when P18 + lensing data and non-CMB data are considered. The tensions found for the values of primary cosmological parameters are not significant, as in the $A_L = 1$ case. When non-CMB data are considered, we find $\Omega_k = -0.033 \pm 0.050$, which shows a 0.66σ evidence in favor of a closed geometry and is in 0.69σ tension with the

TABLE XIX. Mean and 68.3% confidence limits of new-$P(q)$-based tilted nonflat ΛCDM ($+A_L$) model parameters constrained by non-CMB, P18 + lensing, and P18 + lensing + non-CMB datasets. The Hubble constant H_0 has a unit of km s^{-1} Mpc^{-1}.[a]

	Tilted nonflat ΛCDM new $P(q)$			Tilted nonflat ΛCDM + A_L new $P(q)$	
Parameter	Non-CMB	P18 + lensing	P18 + lensing + non-CMB	P18 + lensing	P18 + lensing + non-CMB
$\Omega_b h^2$	0.0242 ± 0.0033	0.02248 ± 0.00016	0.02248 ± 0.00015	0.02252 ± 0.00017	0.02260 ± 0.00016
$\Omega_c h^2$	0.120 ± 0.013	0.1188 ± 0.0014	0.1186 ± 0.0013	0.1183 ± 0.0015	0.1174 ± 0.0013
$100\theta_{\rm MC}$	1.10 ± 0.10	1.04104 ± 0.00032	1.04106 ± 0.00031	1.04108 ± 0.00032	1.04118 ± 0.00032
τ	0.0515	0.0515 ± 0.0081	0.0566 ± 0.0074	0.0495 ± 0.0093	0.0486 ± 0.0086
Ω_k	-0.033 ± 0.050	-0.0086 ± 0.0057	0.0003 ± 0.0017	0.003 ± 0.016	-0.0002 ± 0.0017
n_s	0.9654	0.9661 ± 0.0043	0.9679 ± 0.0042	0.9688 ± 0.0053	0.9713 ± 0.0042
$\ln(10^{10} A_s)$	2.89 ± 0.34	3.035 ± 0.016	3.046 ± 0.014	3.030 ± 0.019	3.025 ± 0.017
A_L	…	…	…	1.13 ± 0.15	1.088 ± 0.035
H_0	70.1 ± 1.8	64.2 ± 2.0	68.13 ± 0.54	72.0 ± 9.2	68.48 ± 0.56
Ω_m	0.295 ± 0.017	0.345 ± 0.021	0.3054 ± 0.0051	0.287 ± 0.076	0.2999 ± 0.0055
σ_8	0.771 ± 0.036	0.799 ± 0.010	0.8079 ± 0.0067	0.801 ± 0.011	0.7956 ± 0.0082
$\chi^2_{\rm min}$ (total)	1106.49	2771.75	3887.55	2770.45	3880.69
$\chi^2_{\rm min}$ (non-CMB)	1106.49	…	1111.65	…	1109.43
DIC	1117.14	2825.74	3942.22	2827.29	3937.52
ΔDIC	2.76	−0.71	1.52	0.84	−3.18
$\rm AIC_c$	1116.49	2827.75	3943.55	2828.45	3938.69
$\Delta\rm AIC_c$	1.94	−0.96	1.14	−0.26	−3.72

[a]Note: ΔDIC ($\Delta\rm AIC_c$) indicates an excess value relative to that of the tilted flat ΛCDM model constrained with the same data.

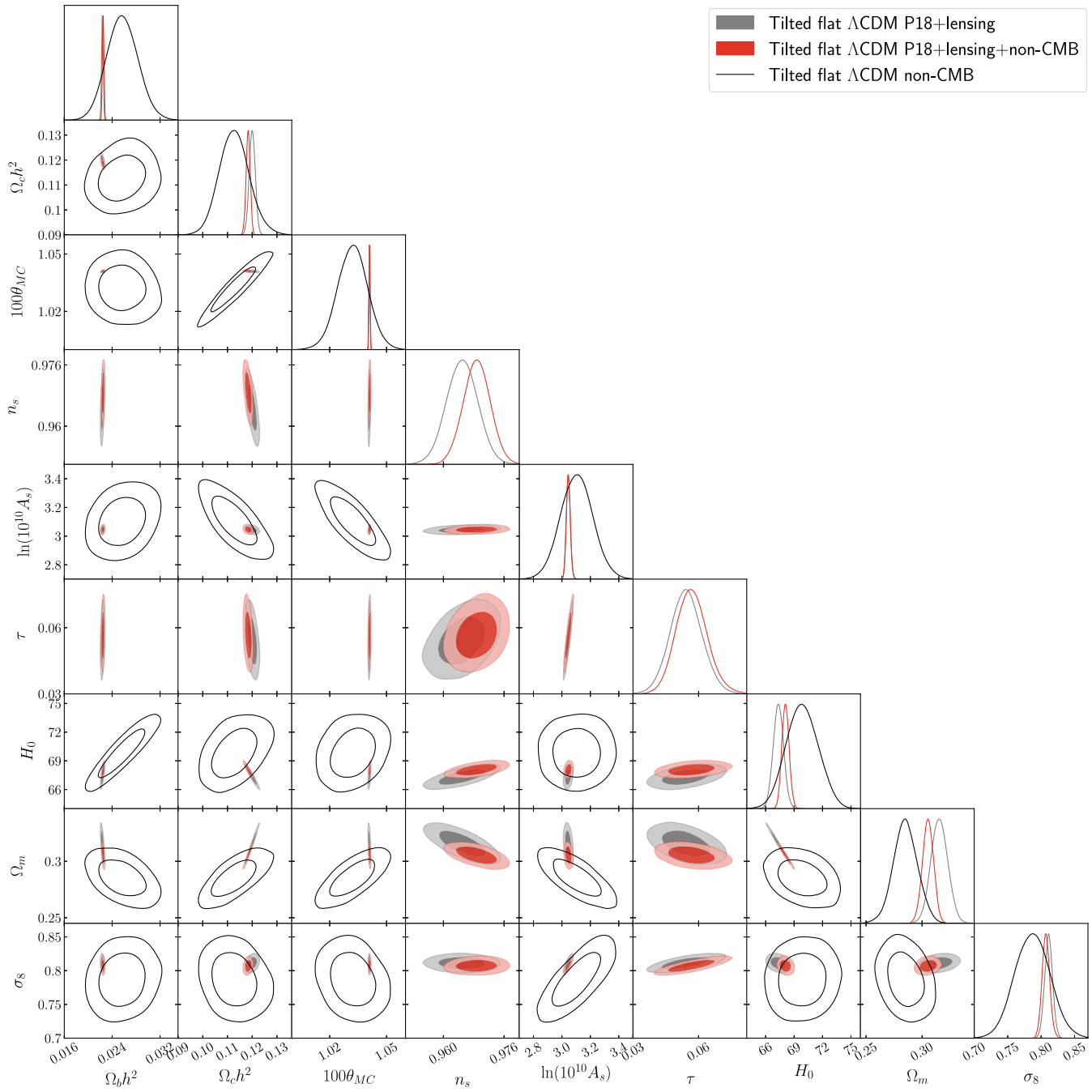

FIG. 32. Likelihoods of the tilted flat ΛCDM model parameters constrained by P18 + lensing, non-CMB, and P18 + lensing + non-CMB datasets.

P18 + lensing data value, $\Omega_k = 0.003 \pm 0.016$, which shows only a 0.19σ preference for an open geometry. As for the derived parameters H_0, Ω_m, and σ_8, the level of agreement is really good, with the corresponding values only in 0.20σ, 0.10σ, and 0.80σ tension, respectively. These results seem to indicate that in the context of the tilted nonflat $\Lambda\text{CDM} + A_L$ new $P(q)$ model, P18 + lensing data and non-CMB data can be jointly analyzed. In the P18 + lensing + non-CMB analysis we find $\Omega_k = -0.0002 \pm 0.0017$, so no clear preference for an open or a closed geometry. On the other hand, we find $A_L = 1.088 \pm 0.035$, which is 2.5σ away from the predicted value $A_L = 1$.

In Figs. 32–39 we show the one-dimensional likelihoods and the two-dimensional contours for cosmological parameters obtained using P18 + lensing, non-CMB, and P18 + lensing + non-CMB data. The constraints coming from non-CMB data (shown with unfilled black lines) are less

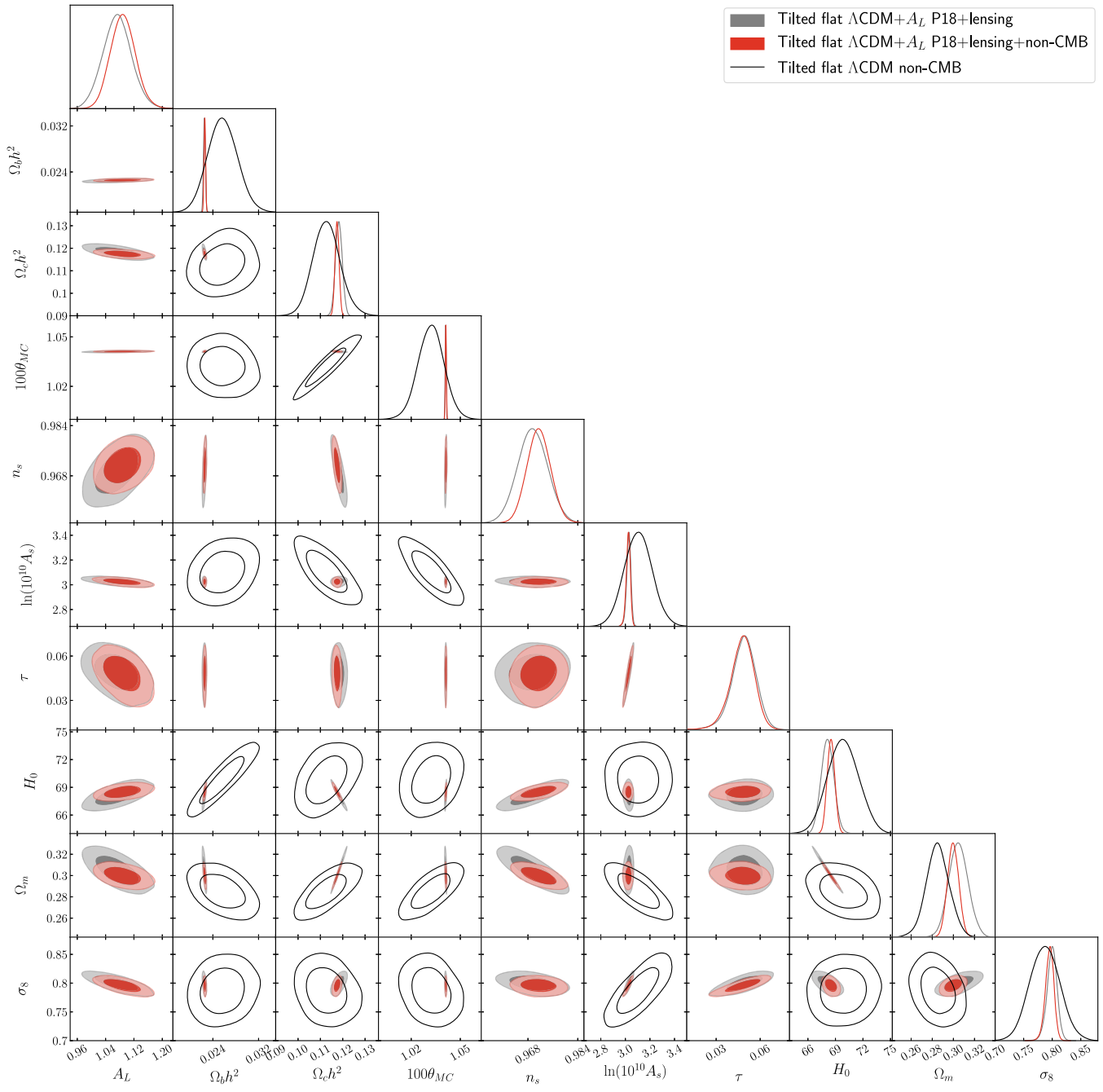

FIG. 33. Likelihoods of the tilted flat ΛCDM + A_L model parameters constrained by P18 + lensing, non-CMB, and P18 + lensing + non-CMB datasets. The likelihoods for the non-CMB dataset, which do not depend on A_L, are the same as in Fig. 32.

restrictive than P18 + lensing constraints (shown in gray), except for the H_0 and Ω_m constraints in the six nonflat models. Except for the untilted nonflat model with $A_L = 1$, we observe at least partial overlaps between the three sets of contours even when the A_L parameter is not allowed to vary.

The contour plots for the tilted flat ΛCDM ($+A_L$) models are in Figs. 32 and 33. The aforementioned $\sim 1\sigma$ disagreements (and the $\sim 2\sigma$ Ω_m disagreement in the $A_L = 1$ case) found when we compared the one-dimensional likelihood P18 + lensing and non-CMB results can also be observed here. The largest tensions are seen in the panels containing one of the derived parameters and the inclusion in the analysis of the varying A_L parameter clearly reduces them.

Looking at the contour plots for the untilted nonflat ΛCDM ($+A_L$) models displayed in Figs. 34 and 35, we observe significantly nonoverlapping contours, either when the primary parameter Ω_k is involved or when the derived

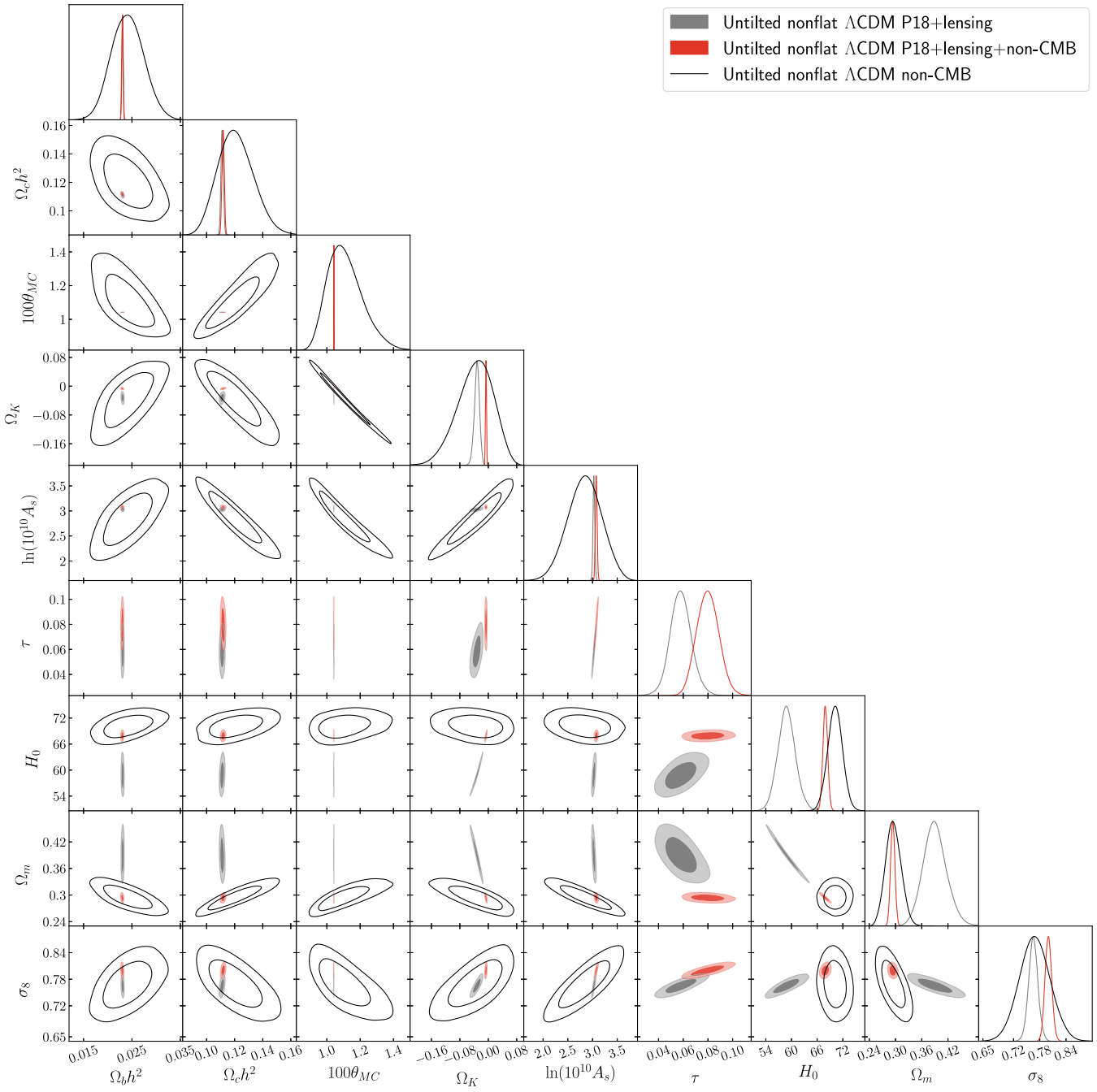

FIG. 34. Likelihoods of the untilted nonflat ΛCDM model parameters constrained by P18 + lensing, non-CMB, and P18 + lensing + non-CMB datasets.

parameter H_0 or Ω_m is involved. This reinforces the idea that when A_L is not allowed to vary the P18 + lensing and non-CMB datasets cannot be analyzed together in the untilted nonflat ΛCDM model. Quite different results are found when we do allow A_L to vary. The disagreements observed in the $A_L = 1$ case largely disappear. Therefore, we may say that in the context of this varying A_L cosmological model we can jointly analyze P18 + lensing and non-CMB data.

Figures 36 and 37 show cosmological parameter constraints for the tilted nonflat ΛCDM ($+A_L$) models, while the ones for the tilted nonflat ΛCDM ($+A_L$) new $P(q)$ models are displayed in Figs. 38 and 39. The contour plots for these tilted nonflat models are very similar, something that was not unexpected given the results discussed above in this subsubsection. In both cases, when A_L is not allowed to vary and when it is allowed to vary, we observe overlaps between the primary parameter panels contours at 1σ.

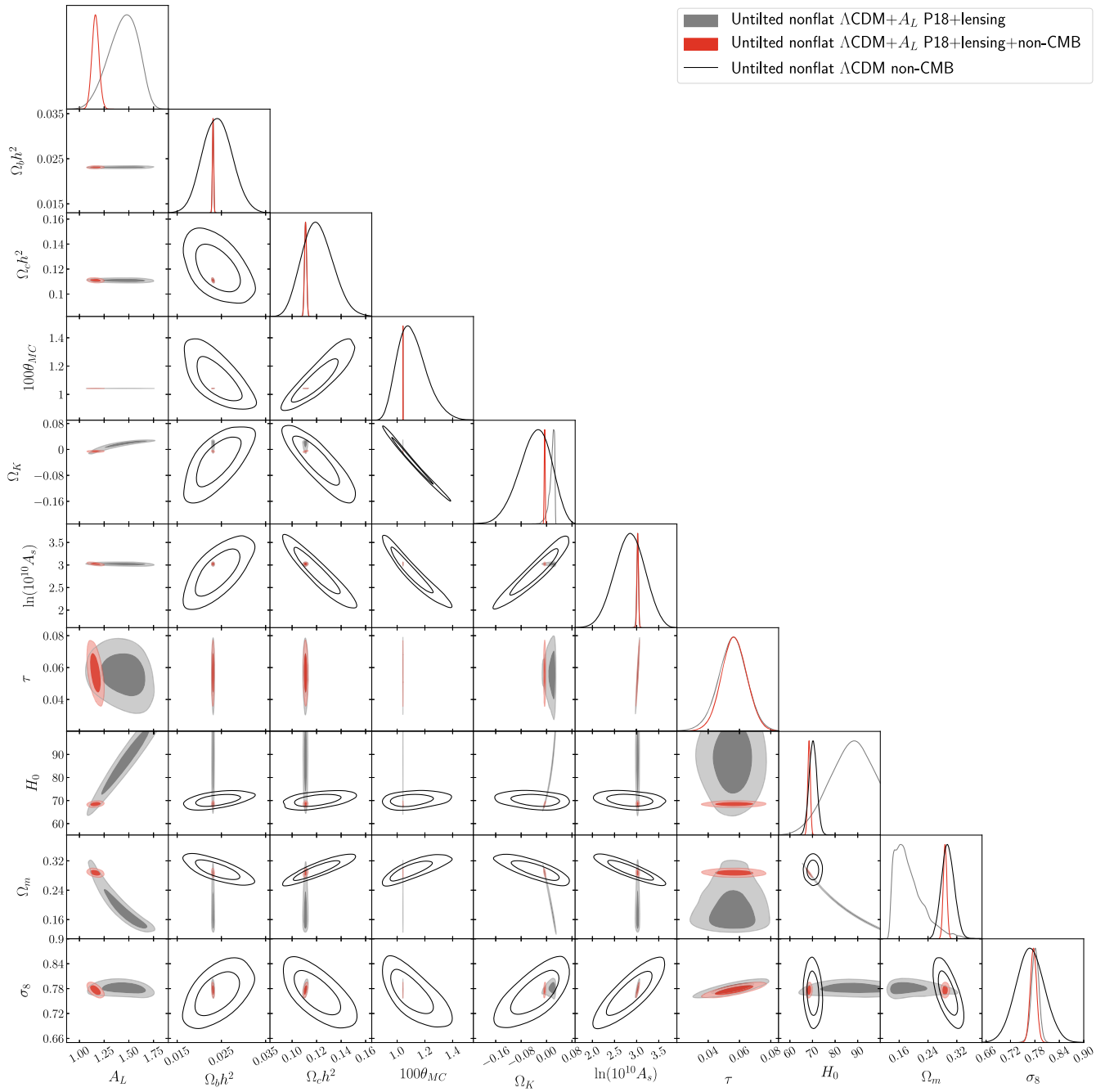

FIG. 35. Likelihoods of the untilted nonflat ΛCDM + A_L model parameters constrained by P18 + lensing, non-CMB, and P18 + lensing + non-CMB datasets. The likelihoods for the non-CMB dataset, which do not depend on A_L, are the same as in Fig. 34.

When $A_L = 1$, we observe an improvement in the overlapping in the current P18 + lensing data vs non-CMB data case compared to the P18 data vs non-CMB data case of the previous subsubsection, where now for both the Planck $P(q)$ model and the new $P(q)$ model the contours do overlap at 2σ. On the other hand, in the varying A_L case, we observe overlaps, even in those panels that involve some of the derived parameters, at 1σ.

As in the P18 data vs non-CMB data cosmological constraints comparison discussed in the previous subsubsection, further tests are needed to determine whether or not P18 + lensing data and non-CMB data can be jointly analyzed in the context of the nonflat models under study. We discuss this issue in detail in Sec. IV C.

B. Model selection

In Sec. IV A, we determined and discussed the cosmological parameter mean values and error bars in eight cosmological models (with $A_L = 1$ and with varying A_L) from P18, P18 + lensing, and P18 + lensing + non-CMB

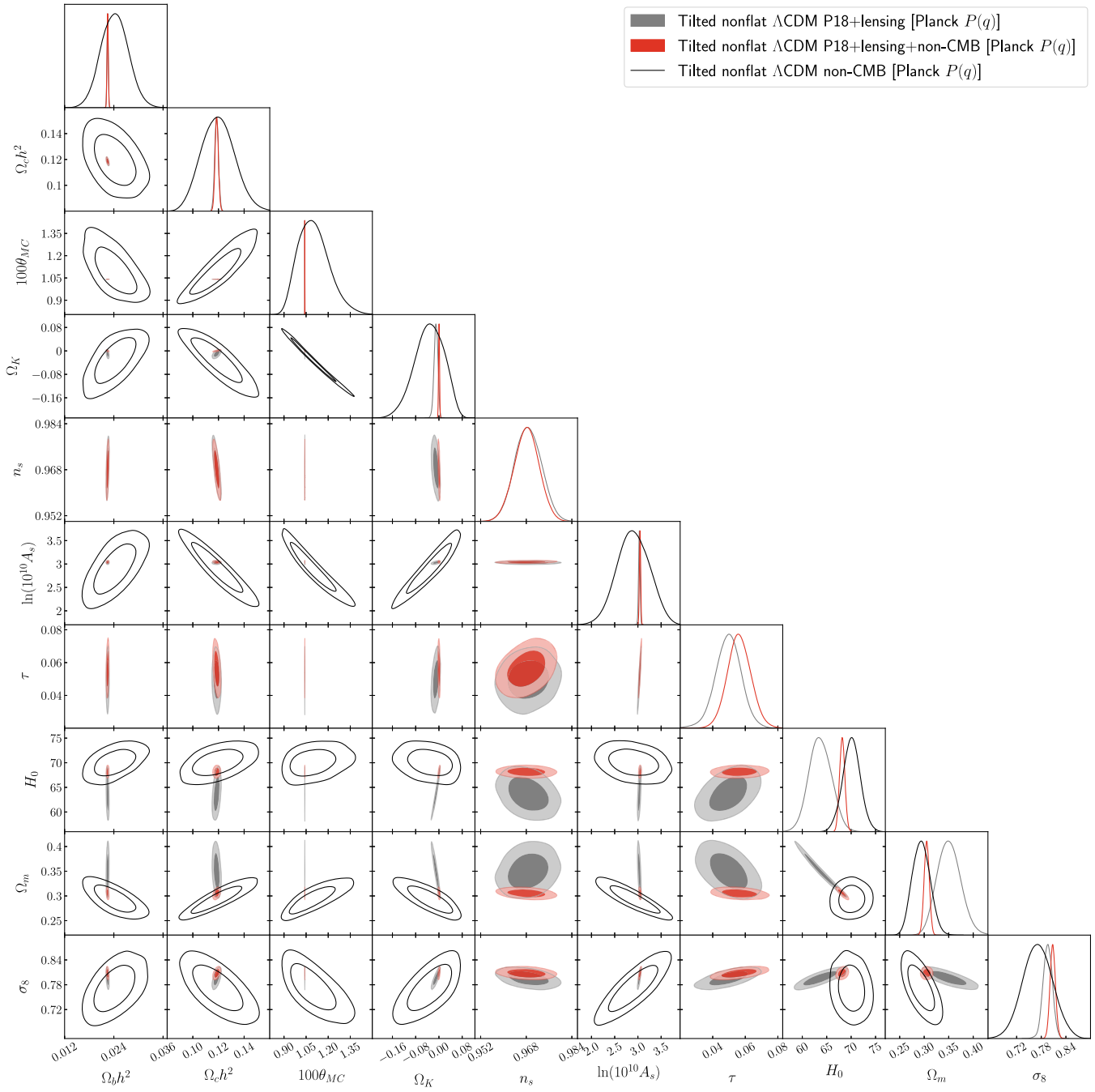

FIG. 36. Likelihoods of the tilted nonflat ΛCDM model [with Planck $P(q)$] parameters constrained by P18 + lensing, non-CMB, and P18 + lensing + non-CMB datasets.

data, as well as the differences in the values of the cosmological parameters obtained from P18 data and BAO/BAO′ data, from P18 data and non-CMB data, and from P18 + lensing data and non-CMB data. In this subsection, we utilize the DIC, Eq. (23), to determine which of these models best fit some combinations of these datasets.

For the P18, P18 + lensing, and P18 + lensing + non-CMB datasets, the values of ΔAIC_c, ΔDIC, and the individual contributions to the χ^2_{total} for each model are in Table XX. Here the Planck CMB data χ^2's are as follows: χ^2_{plik} from the TT data power spectra $30 \leq \ell \leq 2508$ multipoles, the TE data $30 \leq \ell \leq 1996$ multipoles, and the EE data $30 \leq \ell \leq 1996$ multipoles; χ^2_{lowl} from the TT data power spectra $2 \leq \ell \leq 29$ multipoles; χ^2_{smallI} from the EE data power spectra $2 \leq \ell \leq 29$ multipoles; χ^2_{lensing} from the lensing potential data power spectrum; and χ^2_{prior} from

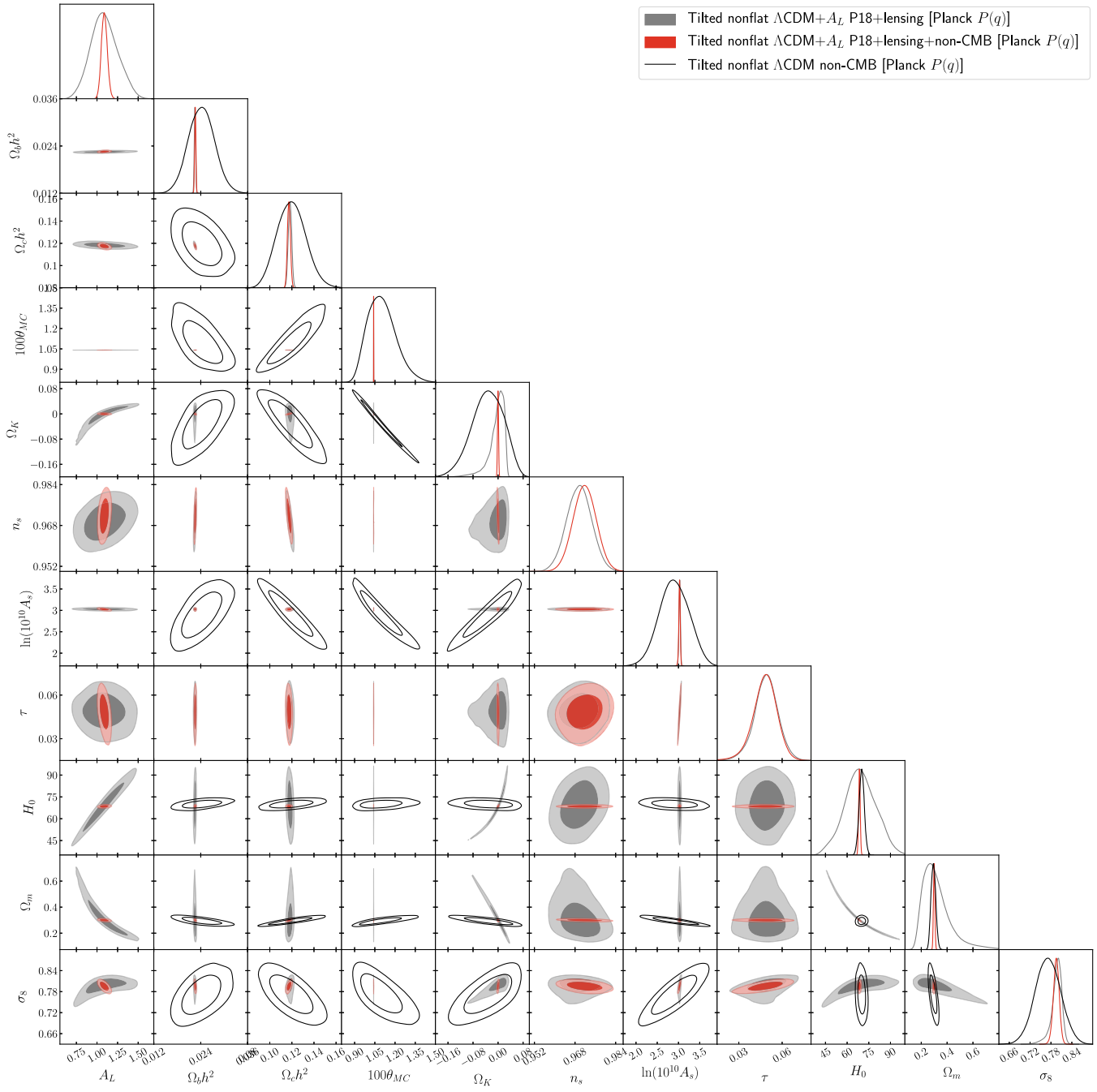

FIG. 37. Likelihoods of the tilted nonflat ΛCDM + A_L model [with Planck $P(q)$] parameters constrained by P18 + lensing, non-CMB, and P18 + lensing + non-CMB datasets. The likelihoods for the non-CMB dataset, which do not depend on A_L, are the same as in Fig. 36.

the priors for the Planck calibration and dust foreground emission. The P18 + BAO/BAO′ data values of ΔAIC_c and ΔDIC are provided in Tables VIII–XI, whereas the corresponding P18 + non-CMB data results can be found in Tables XII–XV.

In this subsection, we do not discuss the results obtained for the untilted nonflat ΛCDM models, without and with a varying A_L, since as seen in the results presented in Tables XIII, IX, and XX this model is not able to fit CMB data as well as the other (tilted) models do. According to the statistical criteria we use, the untilted nonflat ΛCDM model is very strongly disfavored when it is compared with the rest of the models that allow for a tilt (n_s) degree of freedom.

We also do not discuss results obtained when only BAO′, BAO, (P18) lensing (but see Table XXII and the brief

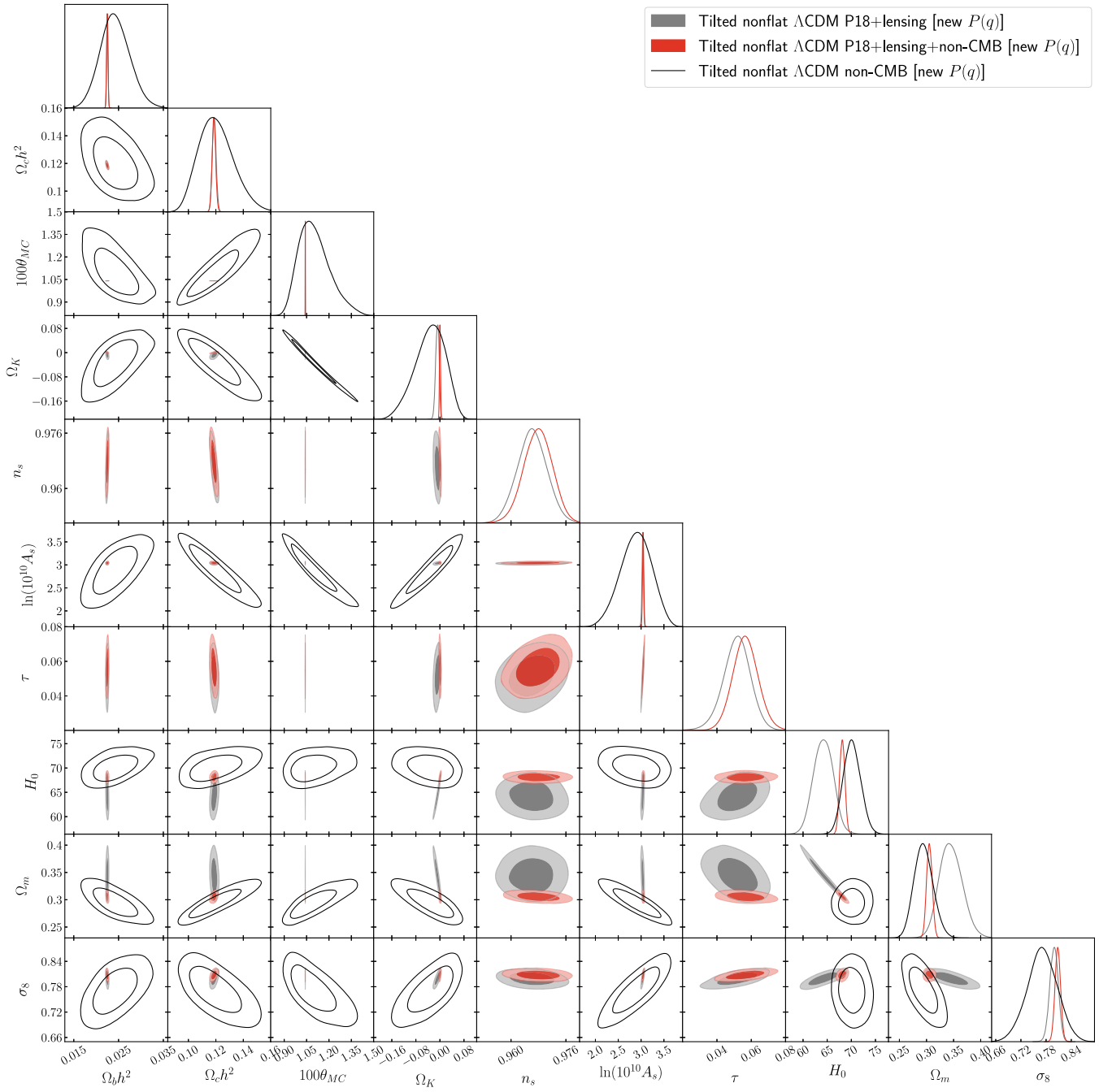

FIG. 38. Likelihoods of the tilted nonflat ΛCDM model [with new $P(q)$] parameters constrained by P18 + lensing, non-CMB, and P18 + lensing + non-CMB datasets.

related discussion in the third paragraph in Sec. IV C), or non-CMB data are considered, because these datasets do not much discriminate between models. From Tables VIII–XV, one sees that for these three datasets the DIC values for all models, including the untilted nonflat ΛCDM model, are very similar. In order to find more significant differences among the models under study, we must include CMB data.

In what follows, we summarize results we find in a number of different combinations of datasets for the three tilted models. For clarity, we focus on DIC results, since this is a more reliable indicator [159,160]. The tables also list the AIC_c values.

P18.—The results for these data are listed in Table XX. When $A_L = 1$, the nonflat Planck $P(q)$ and the nonflat new $P(q)$ models are strongly favored over the tilted flat model, while the Planck $P(q)$ model is weakly favored over the new $P(q)$ model. When A_L is allowed to vary, the nonflat Planck $P(q)$ model is weakly favored over the flat model,

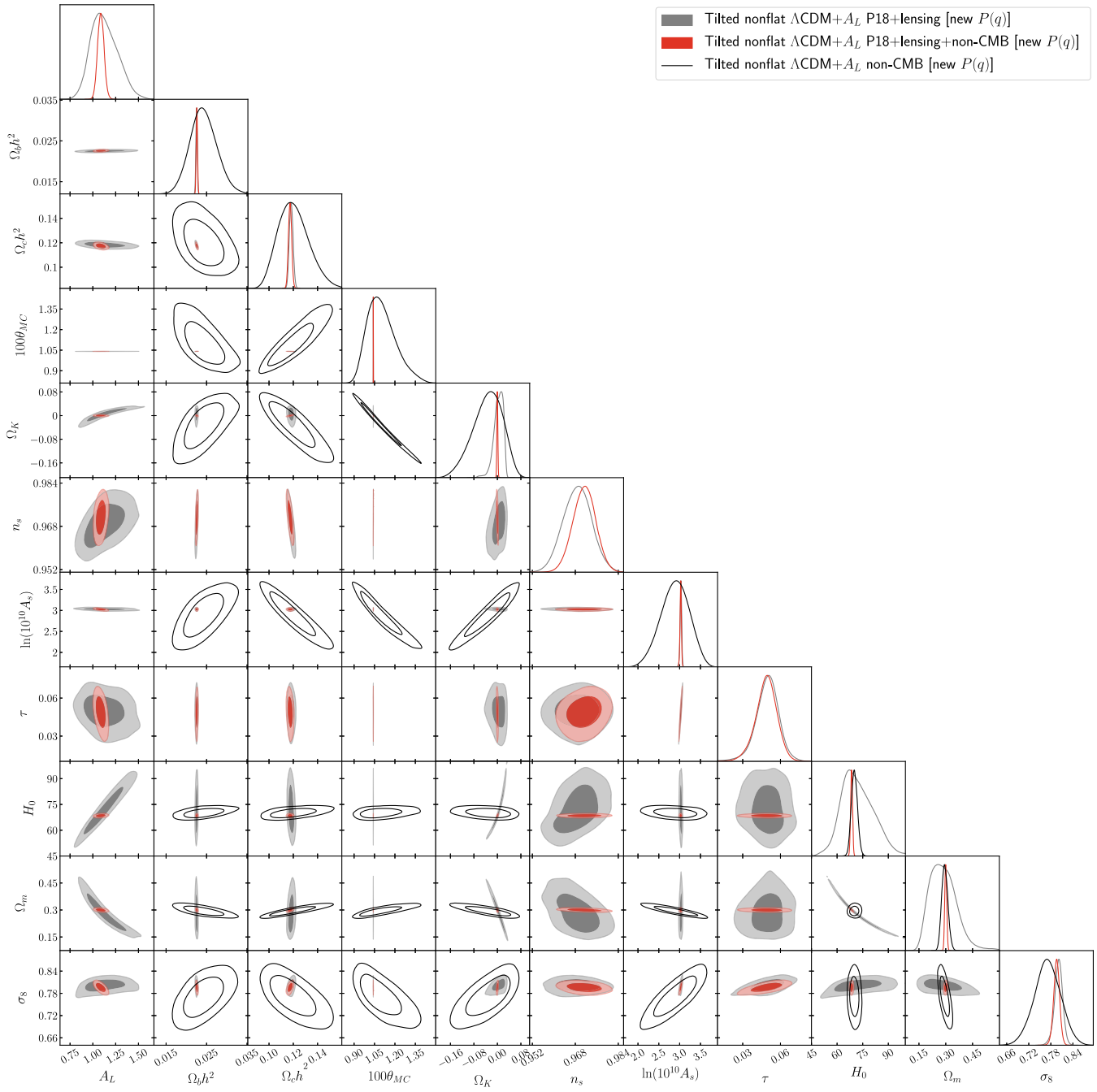

FIG. 39. Likelihoods of the tilted nonflat ΛCDM + A_L model [with new $P(q)$] parameters constrained by P18 + lensing, non-CMB, and P18 + lensing + non-CMB datasets. The likelihoods for the non-CMB dataset, which do not depend on A_L, are the same as in Fig. 38.

with both models being positively favored over the nonflat new $P(q)$ model. The flat + A_L model is positively favored over the flat one, the Planck $P(q)$ model is weakly favored over the Planck $P(q) + A_L$ one, and the new $P(q)$ model is positively favored over the new $P(q) + A_L$ one. It is interesting that, compared to the varying A_L case, when $A_L = 1$ both tilted nonflat models are strongly favored over the tilted flat ΛCDM model.

P18 + lensing.—The results for these data are listed in Table XX. These data provide only weak discrimination between models. When $A_L = 1$, the nonflat new $P(q)$ model is weakly favored over the nonflat Planck $P(q)$ model and both are weakly favored over the flat model. When A_L is allowed to vary, the tilted flat model is weakly favored over both nonflat models, while the nonflat Planck $P(q)$ model is weakly favored over the nonflat new $P(q)$

TABLE XX. Individual and total χ^2 values for the best-fit flat and nonflat ΛCDM inflation models. The deviance information criterion and the Akaike information criterion are also listed.[a]

Datasets	$\chi^2_{\rm plik}$	$\chi^2_{\rm lowl}$	$\chi^2_{\rm smallA}$	$\chi^2_{\rm lensing}$	$\chi^2_{\rm prior}$	$\chi^2_{\rm SN}$	$\chi^2_{\rm BAO}$	$\chi^2_{H(z)}$	$\chi^2_{f\sigma_8}$	$\chi^2_{\rm total}$	$\Delta\chi^2$	DIC	ΔDIC	$\Delta{\rm AIC}_c$
Tilted flat ΛCDM model														
P18	2344.71	23.39	396.05		1.66					2765.80		2817.93		
P18 + lensing	2344.66	23.39	396.06	8.79	1.82					2774.71		2826.45		
P18 + lensing + non-CMB	2346.61	22.64	396.34	8.94	1.84	1058.99	20.10	14.76	18.20	3888.41		3940.70		
Tilted flat ΛCDM + A_L model														
P18	2337.23	21.92	395.66		1.31					2756.12	−9.68	2812.41	−5.52	−7.68
P18 + lensing	2341.62	22.29	395.68	9.94	1.71					2771.24	−3.47	2825.53	−0.92	−1.47
P18 + lensing + non-CMB	2342.43	21.99	395.68	9.74	2.06	1059.14	21.46	14.73	14.31	3881.55	−6.86	3935.15	−5.55	−4.86
Untilted nonflat ΛCDM model														
P18	2369.95	22.22	395.69		1.92					2789.77	23.97	2847.14	29.21	23.97
P18 + lensing	2383.06	20.88	396.13	10.63	2.43					2813.13	38.42	2869.06	42.61	38.42
P18 + lensing + non-CMB	2396.21	19.89	399.59	11.65	2.28	1059.51	20.65	15.68	12.77	3938.22	49.81	3992.71	52.01	49.81
Untilted nonflat ΛCDM + A_L model														
P18	2369.32	20.34	395.87		2.23					2787.76	21.96	2846.45	28.52	23.96
P18 + lensing	2378.87	20.09	395.65	11.25	2.05					2807.91	33.20	2856.10	29.65	35.20
P18 + lensing + non-CMB	2379.11	19.95	395.82	10.72	2.06	1060.16	22.50	15.47	9.26	3915.05	26.64	3973.55	32.85	28.64
Tilted nonflat ΛCDM model [Planck $P(q)$]														
P18	2336.45	21.29	395.60		1.38					2754.73	−11.07	2810.59	−7.34	−9.07
P18 + lensing	2342.29	21.86	395.66	10.09	1.63					2771.53	−3.18	2826.17	−0.28	−1.18
P18 + lensing + non-CMB	2345.82	22.90	396.53	8.92	1.88	1059.00	20.09	14.70	18.15	3887.99	−0.42	3942.07	1.37	1.58
Tilted nonflat ΛCDM + A_L model [Planck $P(q)$]														
P18	2336.57	21.51	395.61		1.29					2754.99	−10.81	2811.63	−6.30	−6.81
P18 + lensing	2341.32	22.55	395.71	9.44	2.12					2771.14	−3.57	2827.14	0.69	0.43
P18 + lensing + non-CMB	2341.91	22.16	395.77	9.62	1.60	1059.06	20.61	14.74	15.90	3881.37	−7.04	3936.85	−3.85	−3.04
Tilted nonflat ΛCDM model [new $P(q)$]														
P18	2338.26	21.42	396.28		1.42					2757.38	−8.42	2811.54	−6.39	−6.42
P18 + lensing	2342.99	21.18	395.90	9.92	1.76					2771.75	−2.96	2825.74	−0.71	−0.96
P18 + lensing + non-CMB	2346.63	22.53	396.30	8.91	1.53	1058.99	20.12	14.75	17.79	3887.55	−0.86	3942.22	1.52	1.14
Tilted nonflat ΛCDM + A_L model [new $P(q)$]														
P18	2337.56	21.31	395.93		1.52					2756.33	−9.47	2814.83	−3.10	−5.47
P18 + lensing	2341.21	22.62	395.75	9.49	1.37					2770.45	−4.26	2827.29	0.84	−0.26
P18 + lensing + non-CMB	2342.85	21.35	395.81	9.72	1.53	1059.13	21.27	14.77	14.27	3880.69	−7.72	3937.52	−3.18	−3.72

[a]Note: $\Delta\chi^2$, ΔDIC, and $\Delta{\rm AIC}_c$ indicate the values relative to those of the tilted flat ΛCDM model for the same combination of datasets. For the tilted flat ΛCDM model, ${\rm AIC}_c = 2819.8$ (P18), 2828.7 (P18 + lensing), and 3942.4 (P18 + lensing + non-CMB). All χ^2 values are computed at the corresponding model best-fit cosmological parameter values.

model. The flat + A_L model is weakly favored over the flat one, the Planck $P(q)$ model is weakly favored over the Planck $P(q) + A_L$ one, and the new $P(q)$ model is weakly favored over the new $P(q) + A_L$ one.

P18 + BAO/P18 + BAO′.—The results for these data are listed in Tables VIII, X, and XI. We discuss the P18 + BAO data and P18 + BAO′ data results together since the conclusions are very similar. When $A_L = 1$, the tilted flat model is weakly (positively) favored over the nonflat Planck and new $P(q)$ models with the nonflat new $P(q)$ model weakly (weakly) favored over the nonflat Planck $P(q)$ model for P18 + BAO (P18 + BAO′) data. When A_L is allowed to vary, the tilted flat model is positively (weakly) favored over the nonflat Planck (new) $P(q)$ model, and the nonflat new $P(q)$ model is weakly favored over the nonflat Planck $P(q)$ model, for P18 + BAO data, while for P18 + BAO′ data the tilted flat model is weakly favored over both nonflat Planck and new $P(q)$ models, and the nonflat new $P(q)$ model is weakly favored over the nonflat Planck $P(q)$ model. The flat + A_L model is strongly (positively) favored over the flat one, the Planck $P(q) + A_L$ model is positively (strongly) favored over the Planck $P(q)$ one, and the new $P(q) + A_L$ model is positively (strongly) favored over the new $P(q)$ one for P18 + BAO (P18 + BAO′) data.

P18 + non-CMB.—The results for these data are listed in Tables XII, XIV, and XV. Since the dominant component of non-CMB data is BAO/BAO′ data, in the P18 + non-CMB case here we find similar conclusions to the ones presented in the P18 + BAO/P18 + BAO′ cases above. When $A_L = 1$, the tilted flat model is positively (weakly) favored over the nonflat Planck (new) $P(q)$ model with the nonflat new $P(q)$ model weakly favored over the nonflat Planck $P(q)$ model. When A_L is allowed to vary, the

TABLE XXI. $\log_{10}\mathcal{I}$ and tension (σ and p) parameters for P18 data vs lensing data, P18 data vs BAO (BAO′) data, P18 data vs non-CMB data, and P18 + lensing data vs non-CMB data in the six tilted flat and nonflat ΛCDM models. Table III lists our, Handley, and Handley + Ω_k priors.[a]

Tilted flat ΛCDM model							
Data:	P18 vs lensing	P18 vs lensing	P18 vs lensing	P18 vs BAO	P18 vs BAO′	P18 vs non-CMB	P18 + lensing vs non-CMB
Prior:	Our	Handley	Handley + Ω_k	Our	Our	Our	Our
$\log_{10}\mathcal{I}$	1.240	1.166	…	0.132	0.707	0.296	0.029
σ	0.718	0.390	…	1.533	0.426	1.749	1.747
p (%)	47.3	69.7	…	12.5	67.0	8.03	8.06
Tilted flat ΛCDM + A_L model							
Data:	P18 vs lensing	P18 vs lensing	P18 vs lensing	P18 vs BAO	P18 vs BAO′	P18 vs non-CMB	P18 + lensing vs non-CMB
Prior:	Our	Handley	Handley + Ω_k	Our	Our	Our	Our
$\log_{10}\mathcal{I}$	…	…	…	0.286	0.810	1.033	1.033
σ	…	…	…	1.402	0.371	0.835	0.774
p (%)	…	…	…	16.1	71.0	40.4	43.9
Tilted nonflat ΛCDM model [Planck $P(q)$]							
Data:	P18 vs lensing	P18 vs lensing	P18 vs lensing	P18 vs BAO	P18 vs BAO′	P18 vs non-CMB	P18 + lensing vs non-CMB
Prior:	Our	Handley	Handley + Ω_k	Our	Our	Our	Our
$\log_{10}\mathcal{I}$	−0.486	−0.316	−0.360	−1.236	−0.891	−1.263	0.297
σ	2.479	2.411	2.403	3.000	2.478	3.005	1.837
p (%)	1.32	1.59	1.63	0.270	1.32	0.265	6.62
Tilted nonflat ΛCDM + A_L model [Planck $P(q)$]							
Data:	P18 vs lensing	P18 vs lensing	P18 vs lensing	P18 vs BAO	P18 vs BAO′	P18 vs non-CMB	P18 + lensing vs non-CMB
Prior:	Our	Handley	Handley + Ω_k	Our	Our	Our	Our
$\log_{10}\mathcal{I}$	…	…	…	0.182	0.847	0.972	1.641
σ	…	…	…	1.460	0.465	0.793	0.516
p (%)	…	…	…	14.4	64.2	42.8	60.6
Tilted nonflat ΛCDM model [new $P(q)$]							
Data:	P18 vs lensing	P18 vs lensing	P18 vs lensing	P18 vs BAO	P18 vs BAO′	P18 vs non-CMB	P18 + lensing vs non-CMB
Prior:	Our	Handley	Handley + Ω_k	Our	Our	Our	Our
$\log_{10}\mathcal{I}$	−0.062	−0.089	−0.057	−0.880	−0.526	−0.806	0.143
σ	2.201	1.887	1.843	2.604	2.108	2.577	1.886
p (%)	2.77	5.91	6.54	0.922	3.50	0.996	5.93
Tilted nonflat ΛCDM + A_L model [new $P(q)$]							
Data:	P18 vs lensing	P18 vs lensing	P18 vs lensing	P18 vs BAO	P18 vs BAO′	P18 vs non-CMB	P18 + lensing vs non-CMB
Prior:	Our	Handley	Handley + Ω_k	Our	Our	Our	Our
$\log_{10}\mathcal{I}$	…	…	…	1.066	1.655	1.798	1.500
σ	…	…	…	1.052	0.145	0.402	0.573
p (%)	…	…	…	29.3	88.4	68.7	56.7

[a]Note: The statistical estimator values in the tilted flat ΛCDM model for the Handley + Ω_k priors are the same as for the Handley priors because $\Omega_k = 0$ in the flat model.

tilted flat model is weakly favored over the nonflat Planck $P(q)$ and nonflat new $P(q)$ models, with the nonflat new $P(q)$ model weakly favored over the nonflat Planck $P(q)$ model. The flat + A_L model is strongly favored over the flat one, the Planck $P(q) + A_L$ model is strongly favored over the Planck $P(q)$ one, and the new $P(q) + A_L$ model is strongly favored over the new $P(q)$ one.

P18 + lensing + non-CMB.—The results for these data are listed in Table XX. When $A_L = 1$, the tilted flat model is weakly favored over the nonflat Planck $P(q)$ and nonflat new $P(q)$ models with the nonflat Planck $P(q)$ model weakly favored over the nonflat new $P(q)$ model. When A_L is allowed to vary, the tilted flat model is weakly (positively) favored over the nonflat Planck (new) $P(q)$ model, with the nonflat Planck $P(q)$ model weakly favored over the nonflat new $P(q)$ model. The flat + A_L model is positively favored over the flat one, the Planck $P(q) + A_L$ model is positively favored over the Planck $P(q)$ one,

TABLE XXII. Mean and 68.3% confidence limits of tilted flat and nonflat ΛCDM model parameters constrained by lensing data alone. Table III lists our, Handley, and Handley + Ω_k priors. The Hubble constant H_0 has units of km s^{-1} Mpc^{-1}.[a]

	Lensing data constraints with Our priors		
Parameter	Tilted flat ΛCDM	Tilted nonflat ΛCDM [Planck $P(q)$]	Tilted nonflat ΛCDM [new $P(q)$]
$\Omega_b h^2$	0.049 ± 0.023	0.052 ± 0.027	0.048 ± 0.026
$\Omega_c h^2$	0.125 ± 0.032	0.120 ± 0.023	0.116 ± 0.022
$100\theta_{\rm MC}$	1.016 ± 0.022	1.41 ± 0.33	1.47 ± 0.27
τ	0.0542	0.0483	0.0525
Ω_k	…	-0.26 ± 0.11	-0.279 ± 0.095
n_s	0.9649	0.9706	0.9654
$\ln(10^{10}A_s)$	3.23 ± 0.11	3.10 ± 0.19	3.13 ± 0.16
H_0	83 ± 10	65 ± 17	66 ± 16
Ω_m	0.255 ± 0.070	0.54 ± 0.48	0.48 ± 0.36
σ_8	0.779 ± 0.082	0.85 ± 0.16	0.88 ± 0.15
$\chi^2_{\rm min}$	3.67	3.12	3.38
DIC (lensing)	14.2	13.3	13.9
AIC (lensing)	13.7	15.1	15.4
DIC (P18)	2817.9	2810.6	2811.5
DIC (P18 + lensing)	2826.5	2826.2	2825.7
$\log_{10}\mathcal{I}$	1.240	−0.486	−0.062
	Lensing data constraints with Handley priors		
Parameter	Tilted flat ΛCDM	Tilted nonflat ΛCDM [Planck $P(q)$]	Tilted nonflat ΛCDM [new $P(q)$]
$\Omega_b h^2$	0.0220 ± 0.0018	0.0221 ± 0.0017	0.0220 ± 0.0017
$\Omega_c h^2$	0.1121 ± 0.0093	0.1117 ± 0.0099	0.1134 ± 0.0097
$100\theta_{\rm MC}$	1.0397 ± 0.0058	1.0395 ± 0.0058	1.0395 ± 0.0059
τ	0.21 ± 0.11	0.20 ± 0.11	0.21 ± 0.11
Ω_k	…	-0.032 ± 0.040	-0.029 ± 0.040
n_s	0.957 ± 0.043	0.954 ± 0.043	0.939 ± 0.033
$\ln(10^{10}A_s)$	3.26 ± 0.15	3.20 ± 0.16	3.21 ± 0.16
H_0	69.7 ± 3.9	62 ± 14	63 ± 14
Ω_m	0.281 ± 0.050	0.40 ± 0.15	0.39 ± 0.15
σ_8	0.869 ± 0.064	0.826 ± 0.083	0.836 ± 0.084
$\chi^2_{\rm min}$	6.81	6.89	6.79
DIC (lensing)	13.9	14.1	13.8
AIC (lensing)	20.8	22.9	22.8
DIC (P18)	2817.9	2810.6	2811.5
DIC (P18 + lensing)	2826.5	2826.2	2825.7
$\log_{10}\mathcal{I}$	1.166	−0.316	−0.088
	Lensing data constraints with Handley + Ω_k priors		
Parameter	Tilted flat ΛCDM	Tilted nonflat ΛCDM [Planck $P(q)$]	Tilted nonflat ΛCDM [new $P(q)$]
$\Omega_b h^2$	⋯	0.0221 ± 0.0017	0.0221 ± 0.0017
$\Omega_c h^2$	⋯	0.1088 ± 0.0088	0.1104 ± 0.0089
$100\theta_{\rm MC}$	⋯	1.0395 ± 0.0058	1.0396 ± 0.0059
τ	⋯	0.20 ± 0.11	0.20 ± 0.11
Ω_k	⋯	-0.123 ± 0.095	-0.122 ± 0.096
n_s	⋯	0.951 ± 0.041	0.939 ± 0.032
$\ln(10^{10}A_s)$	⋯	3.11 ± 0.16	3.11 ± 0.16
H_0	⋯	48 ± 15	48 ± 15
Ω_m	⋯	0.70 ± 0.33	0.71 ± 0.33
σ_8	⋯	0.745 ± 0.096	0.75 ± 0.10

(Table continued)

TABLE XXII. *(Continued)*

	Lensing data constraints with Our priors		
Parameter	Tilted flat ΛCDM	Tilted nonflat ΛCDM [Planck $P(q)$]	Tilted nonflat ΛCDM [new $P(q)$]
$\chi^2_{\rm min}$	···	6.79	6.77
DIC (lensing)	···	13.9	13.9
AIC (lensing)	···	22.8	22.8
DIC (P18)	···	2810.6	2811.5
DIC (P18 + lensing)	···	2826.2	2825.7
$\log_{10}\mathcal{I}$	···	−0.360	−0.057

[a]Note: $\mathcal{I} = \exp(-\mathcal{F}/2)$ where $\mathcal{F} = \text{DIC(P18 + lensing)} - \text{DIC(P18)} - \text{DIC(lensing)}$. The cosmological parameter values in the tilted flat ΛCDM model for the Handley + Ω_k priors are the same as for the Handley priors because $\Omega_k = 0$ in the flat model.

and the new $P(q) + A_L$ model is positively favored over the new $P(q)$ one.

In summary, P18 data and P18 + non-CMB data both strongly disfavor the tilted flat ΛCDM model with $A_L = 1$ relative to some of the tilted $\Omega_k < 0$ or varying A_L options, P18 + lensing data are largely agnostic, and P18 + lensing + non-CMB data, P18 + BAO data, and P18 + BAO′ data all positively favor the varying A_L options over the $A_L = 1$ cases.

C. Dataset tensions

In this subsection, we check whether there is concordance (discordance) between pairs of some of the datasets we study (in the context of a given cosmological model), as well as whether or not this concordance (discordance) is model independent. To do this, we use the two Sec. III statistical estimators, in Eq. (26) and in Eqs. (35) and (37). The values of these statistical estimators for the six tilted flat and nonflat ΛCDM ($+A_L$) models are listed in Table XXI; we do not compute these estimators in the untilted nonflat ΛCDM model that does not include the tilt (n_s) degree of freedom that is strongly favored by data. As in Sec. IV B, here we only study pairs of datasets in which one of the datasets is or includes the P18 dataset. Conclusions based on either of the two statistical estimators qualitatively agree, for the five pairs of datasets we compare in this subsection, as discussed next.

(i) *P18 vs lensing.*—Since, as mentioned earlier, lensing data (see Sec. II) alone do not place significant constraints on cosmological parameters (even if we fix the values of some of them), the role played by the priors is more important in lensing data alone analyses than in other cases. Therefore, in this case, we use three different sets of priors (see Table III) in order to determine whether and how the lensing data alone cosmological parameter constraints and statistical estimator values depend on the priors used. In all three cases, we report results obtained from converged chains. Because of the weak constraining power of lensing data alone, it is not possible to reach convergence when the A_L parameter is allowed to vary. Consequently, we provide results only for the $A_L = 1$ cases.

Here we first briefly comment on the lensing data alone cosmological parameter constraints, which do depend on the set of priors used, see Table XXII. For instance, if we look at the value of the curvature parameter Ω_k (which is most affected by the choice of prior) obtained by employing Our priors, for the tilted nonflat ΛCDM Planck (new) $P(q)$ model, $\Omega_k = -0.26 \pm 0.11$ ($\Omega_k = -0.279 \pm 0.095$), we find a 1.9σ (2.4σ) difference with the Handley priors analysis value $\Omega_k = -0.032 \pm 0.040$ ($\Omega_k = -0.029 \pm 0.040$) and a 0.94σ (1.2σ) difference with the Handley + Ω_k priors analysis value $\Omega_k = -0.123 \pm 0.095$ ($\Omega_k = -0.122 \pm 0.096$). Reassuringly, we find that when we broaden the prior for Ω_k, as we do when we move from Handley priors to Handley + Ω_k priors, the results get closer to those obtained with Our priors, the broadest priors we use. Additionally, our lensing data alone analysis (and cosmological parameter constraints) differ from those of the Planck team (Sec. 3.2.1 of Ref. [36]) in that we fix n_s and vary $\Omega_b h^2$ freely, whereas the Planck team uses Gaussian priors for n_s and $\Omega_b h^2$. Also, in our analysis $0.2 < h < 1.0$ was chosen as the prior, while the Planck team used $0.4 < h < 1.0$. One notable difference is that when Our priors are used the value we find for $\Omega_b h^2$ is larger than the Gaussian prior value ($\Omega_b h^2 = 0.0222 \pm 0.0005$) adopted by the Planck team. In the tilted flat ΛCDM model, we find $\Omega_b h^2 = 0.049 \pm 0.023$, and similar results are seen in the tilted nonflat models with the Planck and the new $P(q)$. However, when the Handley priors and the Handley + Ω_k priors are used, due to the very narrow range of $\Omega_b h^2$ (between 0.019 and 0.025) in these priors, such a deviation disappears, and $\Omega_b h^2$ is constrained with very consistent values in the tilted flat and the two tilted nonflat ΛCDM models and is also consistent with the Gaussian prior value adopted by the Planck team. Given the significant dependence on priors of the lensing data alone cosmological constraints, it is not

possible to compare lensing data alone cosmological constraints to cosmological constraints we have derived from the other datasets.

On the other hand, looking at Table XXI, we do not see significant differences in the statistical estimator values from lensing only data analyses for the three different priors. This being the case, in the following, for the sake of consistency with our other discussions, we discuss only the lensing data alone results obtained using Our priors.

For the tilted flat ΛCDM model, we do not find discordance between P18 data and lensing data. We find $\log_{10}\mathcal{I} = 1.240$, which indicates a strong consistency between the two datasets. A similar conclusion is indicated by the other statistical estimator, $\sigma = 0.718$ and $p = 47.3\%$. We conclude that P18 and lensing data can be jointly analyzed in the context of the tilted flat ΛCDM model.

Looking at the results for the tilted nonflat ΛCDM Planck $P(q)$ model, for the first statistical estimator $\log_{10}\mathcal{I} = -0.486$, which is on the verge of indicating a substantial discordance, while for the second one $\sigma = 2.479$ and $p = 1.32\%$, which indicate a moderate tension. These results, however, may not be significant enough to conclude that P18 and lensing data cannot be used together in an analysis of the tilted nonflat ΛCDM Planck $P(q)$ model.

In the tilted nonflat new $P(q)$ ΛCDM model, the two statistical estimators considered here point to somewhat different conclusions. While for the first one we get $\log_{10}\mathcal{I} = -0.062$, which indicates neither consistency nor inconsistency between the two datasets, the second one, $\sigma = 2.201$ and $p = 2.77\%$, indicates a moderate tension between the two datasets. Taken together, these results indicate that there is at most moderate inconsistency between P18 and lensing data within the tilted flat new $P(q)$ ΛCDM model.

(ii) *P18 vs* BAO′.—In the context of the tilted flat ΛCDM model, there is no sign of discordance between these two datasets. We find $\log_{10}\mathcal{I} = 0.707$, which indicates a substantial consistency. The other statistical estimator points to a similar conclusion, with $\sigma = 0.426$ and $p = 67\%$. Very similar results are found for the tilted flat $\Lambda\text{CDM} + A_L$ model. The value $\log_{10}\mathcal{I} = 0.810$, once again, indicates a substantial consistency between P18 and BAO′ data, whereas for the second estimator we find $\sigma = 0.371$ and $p = 71\%$. The P18 and BAO′ datasets are mutually consistent and can be jointly analyzed in the tilted flat ΛCDM ($+A_L$) models.

On the other hand, the opposite is true in the tilted nonflat ΛCDM models (with $A_L = 1$). The comparison of P18 and BAO′ data in the tilted nonflat Planck $P(q)$ model results in $\log_{10}\mathcal{I} = -0.891$, which indicates a substantial disagreement between these two datasets. Reassuringly, the second statistical estimator points to the same conclusion, in particular, $\sigma = 2.478$ and $p = 1.32\%$. As expected (see Sec. IV A 5), inclusion of the varying A_L parameter reduces the tensions with respect to the $A_L = 1$ case. For the Planck $P(q) + A_L$ model, we find $\log_{10}\mathcal{I} = 0.847$, which indicates a substantial degree of consistency between the two datasets, and $\sigma = 0.465$ and $p = 64.2\%$, therefore, there is no tension between P18 data and BAO′ data in this model.

We noted in Sec. IV A 5 that the tilted nonflat ΛCDM new $P(q)$ model better accommodates P18 and BAO′ data than does the tilted nonflat ΛCDM Planck $P(q)$ model. In particular, in the tilted nonflat ΛCDM new $P(q)$ model when $A_L = 1$, we find $\log_{10}\mathcal{I} = -0.526$, which is just in the range of substantial inconsistency. According to the values obtained for the other statistical estimator, $\sigma = 2.108$ and $p = 3.50\%$, there is a moderate tension between the two datasets. The inclusion of a varying A_L parameter in the analysis completely changes the conclusions with respect to the $A_L = 1$ case. For the new $P(q) + A_L$ model, we find $\log_{10}\mathcal{I} = 1.655$, indicating strong agreement. The values $\sigma = 0.145$ and $p = 88.4\%$ support this conclusion.

(iii) *P18 vs BAO.*—We comment now on the results obtained when the tension between P18 data and BAO data is studied in the context of the different cosmological models. We note that the BAO dataset includes some $f\sigma_8$ data points which, as we shall see, induces some changes in the results with respect to the P18 data and BAO′ data case.

Both statistical estimators do not indicate significant disagreement between P18 data and BAO data for the tilted flat ΛCDM model with $A_L = 1$. For the first one, we have $\log_{10}\mathcal{I} = 0.132$, which neither indicates consistency nor inconsistency, and this is supported by the second one for which we obtain $\sigma = 1.533$ and $p = 12.5\%$. It is important to note that in this case the statistical estimators are closer to indicating a moderate tension than they are in the P18 data vs BAO′ data case. This is related to the previously mentioned σ_8 tension. We get similar results for the tilted flat $\Lambda\text{CDM} + A_L$ model, in which case we find $\log_{10}\mathcal{I} = 0.286$, which again neither indicates an agreement nor a disagreement, while for the second estimator $\sigma = 1.402$ and $p = 16.1\%$, and again no tension is revealed. In view of these results, we find no evidence that P18 and BAO data cannot be considered together in the analysis of the tilted flat ΛCDM ($+A_L$) models.

Given the P18 data vs BAO′ data comparison results in the tilted nonflat ΛCDM models, it should not come as a surprise that we find tensions when P18 data and BAO data are compared. In the tilted nonflat Planck $P(q)$ ΛCDM model with $A_L = 1$ we find for the first estimator $\log_{10}\mathcal{I} = -1.236$, and

$\sigma = 3.000$ and $p = 0.27\%$ for the second one. Both results indicate a strong inconsistency between the two datasets. This level of tension fades when the A_L parameter is allowed to vary. For the Planck $P(q) + A_L$ model, we obtain $\log_{10}\mathcal{I} = 0.182$, which does not indicate consistency or inconsistency, and $\sigma = 1.460$ and $p = 14.4\%$. The P18 and BAO data can be jointly used in the Planck $P(q) + A_L$ model. As happens in the case of the P18 data vs BAO′ data comparison, the tilted nonflat new $P(q)$ ΛCDM model performs better than the Planck $P(q)$ when it comes to accommodating the P18 and BAO datasets. For the $A_L = 1$ case, we find $\log_{10}\mathcal{I} = -0.880$, revealing substantial disagreement, while for the other estimator $\sigma = 2.604$ and $p = 0.922\%$, which indicates a moderate tension. Once again, the tensions observed when $A_L = 1$, in the context of nonflat models, disappear when this parameter is allowed to vary. For the tilted nonflat ΛCDM + A_L new $P(q)$ model, we find $\log_{10}\mathcal{I} = 1.066$, which points to a strong consistency between the two datasets, and for the other estimator we obtain $\sigma = 1.052$ and $p = 29.3\%$. The P18 and BAO data can be jointly used in the new $P(q) + A_L$ model.

In summary, in the tilted nonflat models, in the Planck $P(q)$ model P18 and BAO data should not be jointly analyzed unless the A_L parameter is allowed to vary, while in the new $P(q)$ models these two datasets can be considered together to put constraints on the cosmological parameters even when $A_L = 1$.

(iv) *P18 vs non-CMB.*—We now discuss whether or not there is tension between P18 data and non-CMB data in the context of the different cosmological models. Similar results to the ones obtained in the P18 data and BAO′/BAO data comparisons are expected, since BAO′ data and BAO data are dominant components of non-CMB data.

For the tilted flat ΛCDM model with $A_L = 1$, we find $\log_{10}\mathcal{I} = 0.296$, which neither indicates agreement nor disagreement, and $\sigma = 1.749$ together with $p = 8.03\%$, with neither of the two estimators pointing to tension between P18 and non-CMB data in this model. Including a varying A_L in the model improves the agreement between the two datasets. For the tilted flat ΛCDM + A_L model, we find $\log_{10}\mathcal{I} = 1.033$, which points to strong consistency between the two datasets, and for the other estimator we get $\sigma = 0.835$ and $p = 40.4\%$, a result consistent with the first. There is no tension that prevents us from jointly analyzing P18 data and non-CMB data in the tilted flat ΛCDM ($+A_L$) models.

In the case of the tilted nonflat Planck $P(q)$ ΛCDM model with $A_L = 1$, the value $\log_{10}\mathcal{I} = -1.263$ indicates a strong inconsistency between the P18 and non-CMB datasets. The second statistical estimator provides similar results, $\sigma = 3.005$ and $p = 0.265\%$. In light of these results, we conclude that P18 data and non-CMB data should not be jointly analyzed in the context of this tilted nonflat $A_L = 1$ model. For the Planck $P(q) + A_L$ model, we get $\log_{10}\mathcal{I} = 0.972$, so substantial agreement is observed between P18 data and non-CMB data in this case. In agreement with the result obtained employing the first statistical estimator, for the second one we find $\sigma = 0.793$ and $p = 42.8\%$, which again does not indicate any tension.

Once again, the tilted nonflat ΛCDM new $P(q)$ model does better in jointly accommodating P18 and non-CMB data than does the tilted nonflat ΛCDM Planck $P(q)$ model. In the new $P(q)$ case with $A_L = 1$, the values obtained for both statistical estimators, $\log_{10}\mathcal{I} = -0.806$ and $\sigma = 2.577$ and $p = 0.996\%$, indicate a substantial discordance between P18 data and non-CMB data in the context of this model. Allowing A_L to vary reduces the tension found in the $A_L = 1$ cases. For the new $P(q) + A_L$ model, we get $\log_{10}\mathcal{I} = 1.798$, which points to a strong agreement between the two datasets, whereas for the second estimator we find $\sigma = 0.402$ and $p = 68.7\%$ and no tension. Therefore, we may say that, in the context of the tilted nonflat ΛCDM ($+A_L$) new $P(q)$ models, P18 and non-CMB data can be jointly analyzed.

(v) P18 + lensing *vs non-CMB.*—In the previous cases, we have detected some tensions in the context of the nonflat models. Here we study the possible disagreement between P18 + lensing data and non-CMB data.

For the tilted flat ΛCDM model with $A_L = 1$, both statistical estimators, with values $\log_{10}\mathcal{I} = 0.029$ and $\sigma = 1.747$ and $p = 8.06\%$, shed no light on a possible consistency or inconsistency between P18 + lensing data and non-CMB data. For the tilted flat ΛCDM + A_L model, we find $\log_{10}\mathcal{I} = 1.033$, which indicates a strong consistency between the two datasets. On the other hand, the second statistical estimator provides $\sigma = 0.774$ and $p = 43.9\%$, which do not indicate consistency or inconsistency. As we noted at the beginning of this subsection, we do not always expect a perfect match in the conclusions from the two estimators.

In the tilted nonflat ΛCDM Planck $P(q)$ model with $A_L = 1$, we find $\log_{10}\mathcal{I} = 0.297$, which neither indicates consistency nor inconsistency between P18 + lensing data and non-CMB data, whereas for the second estimator we find $\sigma = 1.837$ and $p = 6.62\%$, which does not reveal inconsistency. The consistency between P18 + lensing and non-CMB data improves considerably in the context of the Planck $P(q) + A_L$ model. We get $\log_{10}\mathcal{I} = 1.641$ indicating a strong consistency between the two datasets, while the second one gives $\sigma = 0.516$ and

$p = 60.6\%$, in agreement with the conclusion provided by the first estimator.

Very similar conclusions are found for the new $P(q)$ $(+A_L)$ and the Planck $P(q)$ $(+A_L)$ models. When the A_L parameter is not allowed to vary for the new $P(q)A_L = 1$ model, we find $\log_{10}\mathcal{I} = 0.143$, which does not reveal either an inconsistency or a consistency, with the second estimator giving $\sigma = 1.886$ and $p = 5.927\%$, and again no tension is revealed. On the other hand, in the context of the new $P(q) + A_L$ model, we get $\log_{10}\mathcal{I} = 1.50$ indicating a strong consistency between the two datasets and, reassuringly, we find similar conclusions from the second statistical estimator, $\sigma = 0.573$ and $p = 56.7\%$.

Unlike in the comparisons of P18 data and BAO′/BAO data and the comparisons of P18 data and non-CMB data, we do not find tensions in the context of the nonflat models between P18 + lensing data and non-CMB data, even when the A_L parameter is not allowed to vary. This may be suggesting that, if we want to jointly analyze P18 data and a low-redshift dataset, such as BAO′/BAO data or non-CMB data, we should either consider a varying A_L parameter or include (P18) lensing data in the mix.

We have studied the tensions between pairs of datasets, in the context of a given cosmological model, in three different ways based on Bayesian statistics. In Secs. IV A 5–IV A 7, we quantified the level of tension by comparing the (one- and two-dimensional) cosmological parameter constraints favored by each of the pair of datasets. In the one-dimensional cases, we estimated the tension by considering the quadrature sum of the two error bars for each parameter, while in the two-dimensional cases, we looked at whether or not the two sets of contours shared a common parameter space area. In this subsection, we study tensions between dataset pairs by using the two more precise statistical estimators of Sec. III, see Eqs. (26), (35), and (37). Reassuringly, all three techniques employed result in similar conclusions in most cases.

Among all the dataset comparisons we study, there are two with significant enough discordances to be ruled out: we find in the tilted nonflat ΛCDM Planck $P(q)$ $A_L = 1$ model that P18 data and BAO data, as well P18 data and non-CMB data, are not mutually consistent. In the first case, when P18 and BAO data are compared, we observe a 2.7σ tension between the derived cosmological parameter values of Ω_m and of H_0, obtained with P18 data and with BAO data. Additionally, in Fig. 20, contour plot panels that contain one of these derived parameters show nonoverlapping regions at more than 2σ. As for the P18 vs non-CMB case, the tensions are even greater than for P18 vs BAO. Comparing the derived cosmological parameter values of Ω_m and of H_0, obtained with P18 data and non-CMB data, we observe a disagreement at 2.9σ and 3.9σ, respectively. Again the contour plot panels in Fig. 28 containing Ω_m and/or H_0 show a nonoverlapping region at more than 2σ.

For the two statistical estimators of Sec. III, if we choose to say two datasets are mutually inconsistent (in a given model) when $\log_{10}\mathcal{I} \leq -1$ or $\sigma \geq 3$, then this is true only in the two cases discussed in the previous paragraph. For the tilted nonflat ΛCDM Planck $P(q)$ $A_L = 1$ model, in the P18 vs BAO case, we find $\log_{10}\mathcal{I} = -1.236$ (meaning a strong disagreement between the two datasets) and $\sigma = 3.000$ $(p = 0.270\%)$, while in the P18 vs non-CMB analysis, we find $\log_{10}\mathcal{I} = -1.263$ (again a strong disagreement between the two datasets) and $\sigma = 3.005$ $(p = 0.265\%)$. These results are qualitatively consistent with those of the previous paragraph. They mean that P18 data and BAO data, as well as P18 data and non-CMB data, cannot be jointly analyzed in this model; alternatively, it means that the tilted nonflat ΛCDM Planck $P(q)$ $A_L = 1$ model is inconsistent with these data and ruled out at approximately 3σ by them. We note that the level of tensions seen in the P18 vs BAO and P18 vs non-CMB comparisons are less severe in the context of the new $P(q)$ model, which does not strongly rule out the joint analyses of P18 data and BAO data, as well as P18 data and non-CMB data, in the tilted nonflat ΛCDM new $P(q)$ $A_L = 1$ model. What is more, none of the other combinations studied, namely, P18 data vs lensing data, P18 data vs BAO′ data, and P18 + lensing data vs non-CMB data, are strongly mutually inconsistent in the tilted nonflat ΛCDM new $P(q)$ model, even when the A_L parameter is not allowed to vary.

We now turn to a comparison between some of our results in Table XXI and results presented in Refs. [30,31]. We emphasize that these are only semiquantitative comparisons, since the datasets used are not identical and the priors used also differ.

Reference [30] compares P18 data and lensing data, as well P18 data and BAO data (note that while we refer to both datasets as BAO there are some significant differences between the BAO data points used in Ref. [30] and the updated BAO data we use here), in the tilted flat ΛCDM model and in the tilted nonflat ΛCDM Planck $P(q)$ model. As described in Sec. III, we use the same (p, σ) statistical estimator as Ref. [30] does, and so these are the results we compare. For the tilted flat ΛCDM model, from the P18 vs lensing analysis, Ref. [30] Fig. 2 reports $\sigma \simeq 0.19$ and $p \simeq 85\%$, while we get $\sigma = 0.72$ and $p = 47\%$ (for our priors) and $\sigma = 0.39$ and $p = 70\%$ (for Handley priors). Some differences are expected due to the different set of data and priors used and this is reflected in these results. Reassuringly, when we employ the same priors for the lensing data (but not for P18 data) as used in Ref. [30], the results get closer. From the P18 vs BAO analysis in the tilted flat ΛCDM model, Ref. [30] finds $\sigma \simeq 0.95$ and $p \simeq 65\%$, while we get $\sigma = 1.5$ and $p = 13\%$; consequently, the qualitative conclusions are the same, indicating that no tension is found. As for the tilted nonflat ΛCDM Planck $P(q)$ model, from the P18 vs lensing analysis, Ref. [30] reports $\sigma \simeq 2.5$ and $p \simeq 1.2\%$ and we find $\sigma = 2.5$

and $p = 1.3\%$ (for Our priors) and $\sigma = 2.4$ and $p = 1.6\%$ (for Handley priors), so there is very good agreement between the results. Finally, in the tilted nonflat ΛCDM Planck $P(q)$ model, from a comparison of P18 data and BAO data, Ref. [30] finds $\sigma \simeq 3.0$ and $p \simeq 0.3\%$, whereas we get $\sigma = 3.0$ and $p = 0.3\%$. Considering all results, and the fact that somewhat different BAO data and priors are used in the two analyses, there is good agreement between the results and conclusions of Ref. [30] and our results and conclusions.

Reference [31] uses $\log_{10}\mathcal{I}$ to quantify tensions, so here we compare our and their results for this statistical estimator. Reference [31] compares P18 data and lensing data, as well as P18 and BAO′ data (note that while we refer to both datasets as BAO′ there are significant differences between the BAO′ data used in Ref. [31] and the updated BAO′ data we use here), in the tilted flat ΛCDM model and in the tilted nonflat ΛCDM Planck $P(q)$ model. For the tilted flat ΛCDM model and the P18 data vs lensing data analysis, Ref. [31] finds $\log_{10}\mathcal{I} = 0.6$ (substantial concordance), while we get $\log_{10}\mathcal{I} = 1.24$ (strong concordance). For the P18 data vs BAO′ data analysis in the tilted flat ΛCDM model, Ref. [31] reports $\log_{10}\mathcal{I} = 0.2$ (neither a concordance nor a discordance) and we find $\log_{10}\mathcal{I} = 0.7$ (substantial concordance). On the other hand, in the tilted nonflat ΛCDM Planck $P(q)$ model, for the P18 vs lensing data analysis, Ref. [31] provides $\log_{10}\mathcal{I} = -0.84$ (substantial discordance), while we obtain $\log_{10}\mathcal{I} = -0.49$, which is on the verge of also indicating a substantial discordance between the two datasets. Finally, from the P18 vs BAO′ analysis in the tilted nonflat ΛCDM Planck $P(q)$ model, Ref. [31] reports $\log_{10}\mathcal{I} = -1.8$ (strong discordance), whereas we get $\log_{10}\mathcal{I} = -0.89$ (substantial discordance).

As can be appreciated from the preceding discussion, the agreement between our results and the results presented in Ref. [31] is not as good as the one obtained from a comparison of our results and those of Ref. [30]. It is important to note that the (p, σ) statistical estimator of Eqs. (35) and (37) is not as dependent on the priors as is the $\log_{10}\mathcal{I}$ statistical estimator of Eq. (26). This may explain the differences found in the comparisons of our results to those of Refs. [30,31]. All in all, we consider that there is reasonable, and so reassuring, agreement between our results and results available in the literature.

V. DISCUSSION

We have used P18 data, (P18) lensing data, BAO′ data, BAO data, and non-CMB data to constrain cosmological parameters in eight cosmological models, the tilted flat ΛCDM $(+A_L)$ model, the untilted nonflat ΛCDM $(+A_L)$ model, the tilted nonflat ΛCDM $(+A_L)$ Planck $P(q)$ model, and the tilted nonflat ΛCDM $(+A_L)$ new $P(q)$ model, and to determine the goodness-of-fit of these models to the datasets. We have also used the models to examine whether or not pairs of datasets are mutually consistent, studying five cases: P18 data vs lensing data, P18 data vs BAO′/BAO data, P18 data vs non-CMB data, and P18 + lensing data vs non-CMB data.

Assuming these data are correct and that there are no unaccounted systematic errors, three of the eight models we consider may be rejected because they are incompatible with some of these data at levels of significance discussed in Sec. IV and summarized next. These rejected models are the two untilted nonflat ΛCDM $(+A_L)$ models and the tilted nonflat ΛCDM Planck $P(q)$ model.

When P18 data are included in the analyses, the untilted nonflat ΛCDM $(+A_L)$ models are, according to the DIC, very strongly disfavored when compared with the tilted models. This is because the untilted models lack the degree of freedom encapsulated in the power spectrum tilt (n_s) parameter that is strongly favored by P18 data, and so the untilted models are incompatible with P18 data.

When we use the tilted nonflat ΛCDM Planck $P(q)$ model to compare cosmological parameter values from P18 data and BAO′/BAO data, as well as from P18 data and non-CMB data, we find disagreements in the one-dimensional values of the H_0 and Ω_m derived parameters of 2.3σ and 2.7σ (BAO′), 2.3σ and 2.7σ (BAO), and 2.9σ and 2.9σ (non-CMB). In Figs. 20 and 28, in those panels containing H_0 and Ω_m, the two-dimensional contours do not overlap even at more than 2σ significance. Additionally, in the P18 data vs BAO data case, we find $\log_{10}\mathcal{I} = -1.236$ (meaning a strong disagreement between the two datasets) and $\sigma = 3.000$ $(p = 0.27\%)$, while in the P18 data vs non-CMB data analysis, we get $\log_{10}\mathcal{I} = -1.263$ (again a strong disagreement between the two datasets) and $\sigma = 3.005$ $(p = 0.265\%)$. At their levels of significance, these results mean that the tilted nonflat ΛCDM Planck $P(q)$ model is unable to simultaneously accommodate P18 data and non-CMB data and so is ruled out at 3σ. Note that non-CMB data include BAO′/BAO data and Refs. [30,31] have previously noted the incompatibility of P18 data and older BAO′/BAO data in the tilted nonflat ΛCDM Planck $P(q)$ model. We return to this point below.

The six-parameter tilted flat ΛCDM model is the simplest (largely, see below) observationally consistent, general-relativistic cosmological model. It assumes the existence of cold dark matter, a nonevolving dark energy density Λ, flat spatial hypersurfaces $(\Omega_k = 0)$, and $A_L = 1$. This is the current standard cosmological model. We have found that this model passes all the consistency tests we use. The largest dataset we have used is the P18 + lensing + non-CMB dataset. These data provide the most restrictive constraints on the parameters of this model, and if the tilted flat ΛCDM model is a reasonably good approximation of the Universe, the cosmological parameters values measured in this model from these data provide a reasonably good description of parameters of the Universe. From P18 + lensing + non-CMB data we find, for the six primary cosmological parameters, $\Omega_b h^2 = 0.02250 \pm 0.00013$,

$\Omega_c h^2 = 0.11838 \pm 0.00083$, $100\theta_{\rm MC} = 1.04110 \pm 0.00029$, $\tau = 0.0569 \pm 0.0071$, $n_s = 0.9688 \pm 0.0036$, and $\ln(10^{10} A_s) = 3.046 \pm 0.014$. We also provide the values of three derived parameters, $\Omega_m = 0.3053 \pm 0.0050$, $H_0 = 68.09 \pm 0.38$ km s^{-1} Mpc^{-1}, and $\sigma_8 = 0.8072 \pm 0.0058$. The least well-determined parameters are the reionization optical depth τ at 8.0σ and the scalar spectral index n_s, which deviates from unity at 8.7σ. As we discuss below, the values of the cosmological parameters determined using any of the six tilted models we study are relatively independent of the cosmological model used, indicating that the values of the cosmological parameters listed above for the tilted flat ΛCDM model are relatively model independent.

It is interesting that the Hubble constant value measured using P18 + lensing + non-CMB data in the tilted flat ΛCDM model, $H_0 = 68.09 \pm 0.38$ km s^{-1} Mpc^{-1}, is consistent with that from an early estimate from a median statistics analysis of a large compilation of Hubble constant measurements, $H_0 = 68 \pm 2.8$ km s^{-1} Mpc^{-1}, see Refs. [166–168], as well as with some local measurements, e.g., $H_0 = 69.8 \pm 1.7$ km s^{-1} Mpc^{-1} (quadrature sum of statistical and systematic uncertainties) from Ref. [169], but not with some other local measurements, e.g., $H_0 = 73.04 \pm 1.04$ km s^{-1} Mpc^{-1} from Ref. [170].

As for the other derived parameter employed to quantify another tension affecting the tilted flat ΛCDM model, the σ_8 parameter, there are differences in its value depending on the dataset considered. In the tilted flat ΛCDM model, using P18 data, we get $\sigma_8 = 0.8118 \pm 0.0074$, whereas non-CMB data give $\sigma_8 = 0.787 \pm 0.027$, with the two values differing by 0.89σ. In the P18 + lensing + non-CMB data analysis case, we obtain $\sigma_8 = 0.8072 \pm 0.0058$, which is between the P18 value and the non-CMB value.

The shifts in the cosmological parameter values obtained by jointly analyzing non-CMB data with P18 + lensing data, compared to the cosmological parameter values obtained from "Planck" P18 + lensing data, for the tilted flat ΛCDM are as follows: -0.68σ ($\Omega_b h^2$), 1.1σ ($\Omega_c h^2$), -0.45σ ($100\theta_{\rm MC}$), -0.26σ (τ), -0.71σ (n_s), -0.10σ [$\ln(10^{10} A_s)$], -1.1σ (H_0), 1.1σ (Ω_m), and 0.48σ (σ_8), with the largest shifts being 1.1σ, suggesting again that in this model non-CMB data and P18 + lensing data are not inconsistent. As for the reduction in the error bars obtained by jointly analyzing non-CMB data with P18 + lensing data, compared to the error bars obtained from Planck P18 + lensing data, we find 7.1% ($\Omega_b h^2$), 31% ($\Omega_c h^2$), 6.5% ($100\theta_{\rm MC}$), 2.7% (τ), 12% (n_s), 0% [$\ln(10^{10} A_s)$], 31% (H_0), 33% (Ω_m), and 1.7% (σ_8), with the biggest reductions being the 33% Ω_m one and the 31% $\Omega_c h^2$ and H_0 ones; adding non-CMB data to the mix does quite significantly improve the constraints on some cosmological parameters.

We mentioned above that P18 data and non-CMB data are incompatible in the seven-parameter tilted nonflat ΛCDM Planck $P(q)$. When this model is used to analyze P18 data, it favors a closed geometry at 2.5σ with $\Omega_k = -0.043 \pm 0.017$, when it is used to analyze P18 + lensing data it favors a closed geometry at 1.6σ with $\Omega_k = -0.0103 \pm 0.0066$, and when it is used to analyze non-CMB data, it favors a closed geometry at 0.63σ with $\Omega_k = -0.032 \pm 0.051$. However, since P18 data and non-CMB data are incompatible in this model, the model is ruled out at the relevant levels of significance and so cannot be used to measure the geometry of spatial hypersurfaces from P18 + lensing + non-CMB data.

On the other hand, the seven-parameter tilted nonflat ΛCDM new $P(q)$ model is not ruled out. According to the statistical estimators presented in Sec. III (see values in Table XXI) for all the cases studied using the new $P(q)$ model, in none are our conditions to rule out a model, $\log_{10}\mathcal{I} \leq -1$ or $\sigma \geq 3$, fulfilled. For the new $P(q)$ model, in the P18 data analysis, we find $\Omega_k = -0.033 \pm 0.014$, which favors closed geometry at 2.4σ. When the new $P(q)$ model is used to analyze P18 + lensing data, the results indicate a 1.5σ preference for closed geometry with $\Omega_k = -0.0086 \pm 0.0057$, and when non-CMB data is analyzed alone we find $\Omega_k = -0.036 \pm 0.051$, which is 0.71σ in favor of closed geometry. Contrary to what happens in the case of the Planck $P(q)$ model, in the new $P(q)$ model it is reasonable to jointly analyze P18 data, (P18) lensing data, and non-CMB data. And in the P18 + lensing + non-CMB and P18 + non-CMB analysis cases we obtain $\Omega_k = 0.0003 \pm 0.0017$ favoring open geometry by only 0.18σ in both cases. It may come as a surprise that, even though each dataset individually favors a closed geometry, some even with a somewhat significant level of evidence, the joint consideration of all three (or just two) of them reveals a result consistent with flat spatial hypersurfaces and also more consistent with open than with closed geometry. This is because of the H_0-Ω_k-Ω_m degeneracy and the fact that, in the nonflat models, non-CMB data favor higher H_0 values and lower Ω_m values than do P18 data and P18 + lensing data.

We have found that with $A_L = 1$, the six-parameter untilted nonflat and the seven-parameter tilted nonflat ΛCDM Planck $P(q)$ models are incompatible with some data we consider. If these data are correct, these models are ruled out. On the other had, we find that the most restrictive data compilation we consider, the P18 + lensing + non-CMB dataset, indicates that the seven-parameter tilted nonflat ΛCDM new $P(q)$ model has flat (or very close to flat) spatial hypersurfaces. Yes, P18 data alone favor closed geometry at 2.4σ, and while it would be valuable to have a much better understanding of this result than is currently available, at this point we feel that the P18 + lensing + non-CMB data support for flat geometry should be given more credence. Perhaps more and better future non-CMB might alter this conclusion, however, current data are consistent with flat spatial hypersurfaces when $A_L = 1$.

In the seven-parameter tilted flat ΛCDM + A_L model, A_L is allowed to vary and is constrained by data. In this model, P18 data favor $A_L = 1.181 \pm 0.067$, $A_L > 1$ at

2.7σ; P18 + non-CMB data favor $A_L = 1.204 \pm 0.061$, $A_L > 1$ at 3.3σ; P18 + lensing data favor $A_L = 1.073 \pm 0.041$, $A_L > 1$ at 1.8σ; and P18 + lensing + non-CMB data favor $A_L = 1.089 \pm 0.035$, $A_L > 1$ at 2.5σ. With P18 + lensing + non-CMB data resulting in $\Delta\text{DIC} = -5.55$ in favor of $A_L > 1$ over $A_L = 1$, just a little bit below the strongly favoring threshold of -6, the 2.5σ $A_L > 1$ value indicates a more serious CMB weak lensing consistency issue than the preference for closed spatial geometry exhibited by some of the datasets. If these data are correct, these results are somewhat uncomfortable for the six-parameter tilted flat ΛCDM model—the standard cosmological model. New, and better, data should help to clarify this issue.

When A_L is allowed to vary, the eight-parameter tilted nonflat ΛCDM + A_L Planck $P(q)$ model is not ruled out by datasets' incompatibilities, unlike what happens in the $A_L = 1$ seven-parameter tilted nonflat ΛCDM Planck $P(q)$ model. The eight-parameter tilted nonflat ΛCDM + A_L new $P(q)$ model also does not suffer from datasets' incompatibilities, similar to the $A_L = 1$ seven-parameter tilted nonflat ΛCDM new $P(q)$ model case. In the eight-parameter tilted nonflat ΛCDM + A_L Planck (new) $P(q)$ model, P18 data favor $A_L = 0.88 \pm 0.15$ and $A_L < 1$ at 0.8σ ($A_L = 0.94 \pm 0.20$ and $A_L < 1$ at 0.3σ) and $\Omega_k = -0.130 \pm 0.095$ and closed at 1.4σ ($\Omega_k = -0.10 \pm 0.11$ and closed at 0.91σ); P18 + non-CMB data favor $A_L = 1.203 \pm 0.062$ and $A_L > 1$ at 3.3σ ($A_L = 1.204 \pm 0.061$ and $A_L > 1$ at 3.3σ) and $\Omega_k = -0.0006 \pm 0.0017$ and closed at 0.35σ ($\Omega_k = -0.0006 \pm 0.0017$ and closed at 0.35σ); P18 + lensing data favor $A_L = 1.089 \pm 0.16$ and $A_L > 1$ at 0.56σ ($A_L = 1.13 \pm 0.15$ and $A_L > 1$ at 0.87σ) and $\Omega_k = -0.005 \pm 0.027$ and closed at 0.19σ ($\Omega_k = 0.003 \pm 0.0016$ and open at 0.19σ); and P18 + lensing + non-CMB data favor $A_L = 1.090 \pm 0.036$ and $A_L > 1$ at 2.5σ ($A_L = 1.088 \pm 0.035$ and $A_L > 1$ at 2.5σ) and $\Omega_k = -0.0002 \pm 0.0017$ and closed at 0.12σ ($\Omega_k = -0.0002 \pm 0.0017$ and open at 0.12σ). With P18 + lensing + non-CMB data in the eight-parameter tilted nonflat ΛCDM + A_L Planck (new) $P(q)$ model resulting in $\Delta\text{DIC} = -5.22$ (-4.70), again (as in the seven-parameter tilted flat ΛCDM + A_L model) positively favoring $A_L > 1$ over $A_L = 1$, there is a bit more evidence supporting the existence of a CMB weak lensing consistency issue, in all tilted, flat as well as nonflat, models, although the resulting Ω_k values in both nonflat cases are quite consistent with flat geometry.

In the eight-parameter tilted nonflat ΛCDM + A_L new $P(q)$ model, which unlike the Planck $P(q)$ model is not ruled out, allowing A_L to vary reduces support for closed geometry. Compared to the seven-parameter new $P(q)$ model with $A_L = 1$, for P18 data, support for closed spatial hypersurfaces drops from 2.4σ to 0.91σ, while for P18 + lensing data the 1.5σ support for closed geometry becomes 0.19σ support for open geometry. We also note, from comparing P18 data results given in the two previous paragraphs for the seven-parameter tilted flat ΛCDM + A_L model and for the eight-parameter tilted nonflat ΛCDM + A_L Planck and new $P(q)$ models, as one goes from the first to either of the second models, A_L values becomes consistent with unity, while Ω_k values deviate from flat by only 1.4σ and 0.91σ. So for P18 data both the tilted nonflat models cannot be ruled out, while the seven-parameter tilted flat model with $A_L > 1$ at 2.7σ and a lower DIC value indicates that the standard six-parameter tilted flat ΛCDM model with $A_L = 1$ is somewhat uncomfortably observationally squeezed. These and other results from our more comprehensive analyses and updated and more expansive data here support and extend the earlier results of Refs. [25,30,31] that indicate that P18 data support either a closed geometry with $\Omega_k < 0$ or $A_L > 1$, both of which make the amount of CMB weak lensing higher than in the tilted flat ΛCDM model. We recall here the discussion in Sec. I about the differences found in the values of the A_L parameter from Planck data, ACT CMB anisotropy data [26], and from SPT CMB anisotropy data [34]. Therefore, the possibility that CMB data employed in our paper are not completely correct remains open.

References [25,30,31] have also noted that in the tilted nonflat Planck $P(q)$ model, when P18 data and BAO′/BAO data are jointly analyzed, evidence for closed geometry dissipates, as we have found here for updated BAO′/BAO data as well as for non-CMB data (even though, as we have found here, P18 data and to a lesser extent BAO′/BAO data and non-CMB data are all by themselves not inconsistent with closed geometry). References [30,31] have suggested that this might be because of a problem (possibly undetected systematic errors) with BAO′/BAO data (and so also with non-CMB data) and so these results (from combinations of these data and P18 data) should not be taken to mean that spatial hypersurfaces are flat. Along these lines, we note that Ref. [171] present results from a full-shape analysis (instead of the compressed BAO and $f\sigma_8$ data points analysis here) of the 6dFGS, BOSS, and eBOSS catalogs and find $\Omega_k = -0.0041^{+0.0026}_{-0.0021}$ (see their Table 6) when P18 data (not exactly the same P18 data used here) are jointly analyzed with the full-shape galaxy sample data, which is still in favor of a closed geometry, contrary to the conclusions we present here. New and better data and improved analysis techniques will help to shed some light on this issue.

It is useful to determine which of the datasets we use are able to set model-independent constraints on the cosmological parameter values. Here we only consider the P18, P18 + lensing, P18 + non-CMB, and P18 + lensing + non-CMB datasets, as the other datasets we study have less constraining power. In our analyses here we consider only the six tilted models, flat and nonflat, with $A_L = 1$ and varying A_L. In order to determine whether the constraints are model independent, we compute the shifts in the cosmological parameter value between pairs of models and say that the cosmological constraints are model independent if almost all the shifts are $< 1\sigma$.

Neither P18 data nor P18 + lensing data are able to place model-independent constraints on the cosmological parameter values. In the case of P18 data, when we compare the flat model with the flat + A_L model, we observe disagreements in the values of the derived parameters H_0, Ω_m, and σ_8 at $\sim 1\sigma$ confidence level. More significant are the discrepancies found when the flat model is compared with the tilted nonflat models. In particular for the Planck (new) $P(q)$ models, we get for H_0 a shift of -3.5σ (-2.8σ), for Ω_m a shift of 2.6σ (2.3σ), and for σ_8 a shift of -2.2σ (-1.7σ). As expected, when the flat model is compared with the tilted nonflat models with varying A_L, the differences are smaller, though still significant. Comparing the flat model cosmological parameter values with the Planck (new) $P(q) + A_L$ cosmological parameter values, we find for H_0 a shift of -2.0σ (-1.2σ), for Ω_m a shift of 1.4σ (0.89σ), and for σ_8 a shift of -1.7σ (-1.1σ). Similar results are found when the flat + A_L model is compared with the tilted nonflat models with and without a varying A_L parameter. On the other hand, we do not find significant disagreements when we compare the cosmological parameter values of the four tilted nonflat models, the Planck $P(q)$ ($+A_L$) and the new $P(q)$ ($+A_L$) models, with each other, with the shifts always remaining below 1σ. The joint consideration of P18 data and (P18) lensing data reduces the disagreements discussed above, though it is not possible to claim that P18 + lensing data impose model-independent constraints. In this case, when the cosmological parameter constraints for the flat and the flat + A_L models are compared, the largest disagreement found is -1.1σ for σ_8. When the flat model is compared with the Planck (new) $P(q)$ model, we get for H_0 a shift of -1.5σ (-1.5σ), for Ω_m a shift of 1.4σ (1.3σ), and for σ_8 a shift of -1.2σ (-1.1σ), while when the flat model is compared with the Planck (new) $P(q) + A_L$ model, all differences remain $< 1\sigma$. When we compare the cosmological parameter values obtained for the flat + A_L model with those obtained for the Planck (new) $P(q)$ model, we observe disagreements at -1.9σ (-1.9σ) for H_0 and 1.8σ (1.8σ) for Ω_m. As happens in the P18 analysis, in the P18 + lensing analysis no significant differences are observed when we compare the Planck $P(q)$ ($+A_L$) and new $P(q)$ ($+A_L$) models with each other.

It is the inclusion of non-CMB data that results in model-independent constraints. When P18 data are jointly analyzed with non-CMB data, we do not find discrepancies $> 1\sigma$. The most important differences in this case, in absolute value, are 0.78σ–0.96σ ($\Omega_b h^2$) and 0.87σ–0.98σ (σ_8) that are found when the results for models with a varying A_L parameter are compared with the results obtained when $A_L = 1$. In the P18 + lensing + non-CMB data case, almost no significant model-to-model discrepancies are found. The largest ones are found when the varying A_L models are compared with those with $A_L = 1$. In particular, the two largest shifts are in $\ln(10^{10} A_s)$ (the largest one being in absolute value 1σ) and in σ_8 (the largest one being in absolute value 1.3σ). We note that P18 + non-CMB data cosmological parameter constraints are slightly more model independent than those determined using P18 + lensing+ non-CMB data. This is partly because (P18) lensing data changes the A_L parameter value, which in turn causes small shifts in some of the other parameter values. Consequently, when (P18) lensing data are included in the mix, we observe larger differences between the cosmological parameter values of the varying A_L models and those of the $A_L = 1$ models. Also, P18 + lensing + non-CMB cases error bars are smaller than the ones found in the P18 + non-CMB analyses, and this contributes to increasing the significance of the differences in some of the cosmological parameter values in the P18 + lensing + non-CMB cases. We may say that, as long as at least P18 + non-CMB data are considered, if we start from the tilted flat ΛCDM and then vary A_L and/or Ω_k [which implies the consideration of one of the nonflat $P(q)$'s we have used in this work], we obtain model-independent constraints as a result, since the shifts in the cosmological parameter values remain within or just slightly above 1σ. In light of these results, we can conclude that the P18 + lensing + non-CMB dataset is powerful enough to result in model-independent cosmological parameter constraints and, if these data are correct and include all systematic errors, this dataset is able to accurately measure these parameters of the (reasonably accurate tilted flat ΛCDM approximation of the) real Universe.

VI. CONCLUSION

In what follows we summarize our main conclusions.

If the datasets we use are correct and free from unknown systematics, three of the eight cosmological models are ruled out due to incompatibilities with some of the datasets employed in the analyses. The untilted nonflat ΛCDM ($+A_L$) models are unable to properly fit the P18 data, while the tilted nonflat ΛCDM Planck $P(q)$ model is ruled out at 3σ because it is not able to simultaneously accommodate P18 data and non-CMB (or some subset of these) data.

Interestingly, the new $P(q)$ tilted nonflat inflation ΛCDM cosmological model, characterized by the primordial power spectrum in Eq. (13), does better than the Planck $P(q)$ model in being able to simultaneously accommodate P18 data and non-CMB data. In Sec. IV C, we study the mutual compatibility of pairs of datasets and in none of the cases studied is the level of tension high enough to rule out this model. The same holds true for the flat ($+A_L$) models and the Planck and new $P(q) + A_L$ models.

P18 data do not break the geometrical Ω_m-H_0-Ω_k-A_L degeneracy present in the Planck and the new $P(q)$ ($+A_L$) models. In the tilted nonflat ΛCDM new $P(q)$ model, the P18 data analysis reveals a 2.4σ evidence in favor of closed geometry with $\Omega_k = -0.033 \pm 0.014$ and this model is strongly favored over the tilted flat ΛCDM model. In the tilted nonflat models when the A_L parameter is allowed to vary, the evidence in favor of closed geometry

subsides, yet they are either strongly favored [Planck $P(q)+A_L$] or positively favored [new $P(q)+A_L$] over the tilted flat model. The tilted flat $\Lambda\mathrm{CDM}+A_L$ model better fits P18 data, compared to the tilted flat ΛCDM model fit, with an A_L parameter value 2.7σ larger than the theoretically expected value of $A_L=1$. These results update and strengthen those presented in Refs. [30,31]; both options $\Omega_k<0$ and $A_L>1$ appear more indicative of a CMB weak lensing consistency issue.

The joint consideration of P18 data and (P18) lensing data does not result in significant changes in the values of most primary cosmological parameters with respect to those from the P18 data alone analysis, the exceptions being Ω_k and A_L. From P18 + lensing data in the seven-parameter tilted nonflat new $P(q)$ model, we find 1.5σ evidence in favor of closed geometry with $\Omega_k=-0.0086\pm0.0057$, while in the seven-parameter tilted flat $\Lambda\mathrm{CDM}+A_L$ model, we find that $A_L>1$ is favored by 1.8σ with $A_L=1.073\pm0.041$. In these single parameter extensions of the tilted flat ΛCDM model, the addition of (P18) lensing data to P18 data does not favor $\Omega_k<0$ over $A_L>1$ or vice versa. However, in the eight-parameter tilted nonflat Planck (new) $P(q)$ $\Lambda\mathrm{CDM}+A_L$ models, we find from P18 + lensing data that $\Omega_k=-0.005\pm0.027$ closed at 0.19σ ($\Omega_k=0.003\pm0.016$ open at 0.19σ), and $A_L=1.09\pm0.16$ ($A_L=1.13\pm0.15$) favoring $A_L>1$ at 0.56σ (0.87σ), highlighting, if anything, the CMB weak lensing consistency issue. On the other hand, the values of the derived parameters Ω_m and H_0 are greatly affected by the inclusion of lensing data and the geometrical degeneracy, when $A_L=1$, is partially broken. According to the DIC values, P18 + lensing data do not strongly discriminate between models. The two statistical estimators ($\log_{10}\mathcal{I}$ and σ) tell us that there are only moderate tensions between P18 data and lensing data in the tilted nonflat models and even less tension in the tilted flat model.

Comparing the constraints from P18 data and non-CMB data allows for a robust test of the consistency of cosmological parameter values determined from high- and low-redshift data, respectively. For these data, the statistical estimators we consider do not show tensions between P18 data and non-CMB data, in the tilted flat model and in the varying A_L models. Also, in the new $P(q)$ model with $A_L=1$, we find $\log_{10}\mathcal{I}=-0.806$ and $\sigma=2.577$, which indicates a non-negligible tension between P18 data results and non-CMB data results, but this is not high enough to rule out this model. No significant evidence is found in favor of nonflat hypersurfaces within the nonflat models. On the other hand, when the A_L parameter is allowed to vary, the $A_L>1$ option is strongly preferred over the $A_L=1$ one. From P18 + non-CMB data, for the flat $+A_L$ model we get $A_L=1.201\pm0.061$ (3.3σ), for the Planck $P(q)+A_L$ model we find $A_L=1.203\pm0.062$ (3.3σ), and for the new $P(q)+A_L$ model we obtain $A_L=1.204\pm0.061$ (3.3σ).

Among the datasets we consider in this paper, the P18 + lensing + non-CMB dataset provides the tightest constraints on cosmological parameters and pins down the cosmological parameter values of the standard tilted flat ΛCDM model with impressive precision. (We emphasize that in most of the discussion in this paper we assume these data are accurate.) In fact, due to the great constraining power of this dataset, almost all cosmological parameter values determined using this dataset in the six tilted models considered are compatible at 1σ (actually at slightly above 1σ for the σ_8 parameter). Therefore, we may say that the cosmological parameter values determined using P18 + lensing + non-CMB data are very close to being model independent. From the P18 + lensing + non-CMB analysis, it is clear that the evidence in favor of $A_L>1$ remains, while the evidence in favor of nonflat hypersurfaces subsides. We get $A_L=1.089\pm0.035$ for the flat $+A_L$ model, $A_L=1.090\pm0.036$ for the Planck $P(q)+A_L$ model, and $A_L=1.088\pm0.035$ for the new $P(q)+A_L$ model, with a 2.5σ deviation from $A_L=1$ in all cases.

It is interesting that the large (in absolute value) negative Ω_k values demanded by P18 data in order to deal with the lensing anomaly are not supported by non-CMB data (although the non-CMB data do mildly favor a closed geometry), and the larger H_0 and smaller Ω_m favored by non-CMB data (compared to those favored by P18 data) result in P18 + lensing + non-CMB data favoring flat spatial hypersurfaces. This is at the heart of the tensions found, in the context of the tilted nonflat models, when comparing P18 data and BAO′/BAO data cosmological parameter constraints and P18 data and non-CMB data constraints. It is interesting that the Hubble constant value measured using P18 + lensing + non-CMB data in the tilted flat ΛCDM model, $H_0=68.09\pm0.38\ \mathrm{km\,s^{-1}\,Mpc^{-1}}$, is consistent with that from a median statistics analysis of a large compilation of Hubble constant measurements, as well as with some local measurements.

More and better cosmological data are needed in order to shed additional light on the issues studied in this paper. In the meantime, the P18 + lensing + non-CMB dataset looks like the most reliable among all those considered and, consequently, we conclude that current observational data do not favor curved spatial geometry—consistent with the standard tilted flat ΛCDM model—but do favor $A_L>1$ and so somewhat uncomfortably squeeze the standard tilted flat ΛCDM model.

ACKNOWLEDGMENTS

We thank Héctor Gil-Marín for useful discussions about BAO data. J. d. C. P. was supported by a FPI fellowship associated with the project FPA2016-76005-C2-1-P (MINECO) with reference BES-2017-081892. C.-G. P. was supported by National Research Foundation of Korea (NRF) grant funded by the Korea government (MSIT) (No. 2020R1F1A1069250). B. R. was supported by DOE Award No. DE-SC0011840.

[1] A. Einstein and W. de Sitter, Proc. Natl. Acad. Sci. U.S.A. **18**, 213 (1932).
[2] P. J. E. Peebles, Astrophys. J. **284**, 439 (1984).
[3] A. H. Guth, Phys. Rev. D **23**, 347 (1981).
[4] K. Sato, Mon. Not. R. Astron. Soc. **195**, 467 (1981).
[5] K. Sato, Phys. Lett. **99B**, 66 (1981).
[6] D. Kazanas, Astrophys. J. Lett. **241**, L59 (1980).
[7] J. R. Gott, Nature (London) **295**, 304 (1982).
[8] S. W. Hawking, Nucl. Phys. **B239**, 257 (1984).
[9] B. Ratra, Phys. Rev. D **31**, 1931 (1985).
[10] A. G. Riess *et al.* (Supernova Search Team), Astron. J. **116**, 1009 (1998).
[11] S. Perlmutter *et al.* (Supernova Cosmology Project Collaboration), Astrophys. J. **517**, 565 (1999).
[12] P. J. E. Peebles and B. Ratra, Astrophys. J. Lett. **325**, L17 (1988).
[13] B. Ratra and P. J. E. Peebles, Phys. Rev. D **37**, 3406 (1988).
[14] E. Di Valentino, O. Mena, S. Pan, L. Visinelli, W. Yang, A. Melchiorri, D. F. Mota, A. G. Riess, and J. Silk, Classical Quantum Gravity **38**, 153001 (2021).
[15] L. Perivolaropoulos and F. Skara, New Astron. Rev. **95**, 101659 (2022).
[16] E. Abdalla *et al.*, J. High Energy Astrophys. **34**, 49 (2022).
[17] B. Ratra and P. J. E. Peebles, Astrophys. J. Lett. **432**, L5 (1994).
[18] B. Ratra and P. J. E. Peebles, Phys. Rev. D **52**, 1837 (1995).
[19] M. Bucher, A. S. Goldhaber, and N. Turok, Phys. Rev. D **52**, 3314 (1995).
[20] K. Yamamoto, M. Sasaki, and T. Tanaka, Astrophys. J. **455**, 412 (1995).
[21] M. Kamionkowski, B. Ratra, D. N. Spergel, and N. Sugiyama, Astrophys. J. Lett. **434**, L1 (1994).
[22] K. M. Gorski, B. Ratra, R. Stompor, N. Sugiyama, and A. J. Banday, Astrophys. J. Suppl. Ser. **114**, 1 (1998).
[23] B. Ratra, R. Stompor, K. Ganga, G. Rocha, N. Sugiyama, and K. M. Gorski, Astrophys. J. **517**, 549 (1999).
[24] G. Hinshaw *et al.* (WMAP Collaboration), Astrophys. J. Suppl. Ser. **208**, 19 (2013).
[25] N. Aghanim *et al.* (Planck Collaboration), Astron. Astrophys. **641**, A6 (2020); **652**, C4(E) (2021).
[26] S. Aiola *et al.* (ACT Collaboration), J. Cosmol. Astropart. Phys. 12 (2020) 047.
[27] L. Balkenhol *et al.* (SPT-3G Collaboration), Phys. Rev. D **104**, 083509 (2021).
[28] A. Lewis and A. Challinor, Phys. Rep. **429**, 1 (2006).
[29] E. Calabrese, A. Slosar, A. Melchiorri, G. F. Smoot, and O. Zahn, Phys. Rev. D **77**, 123531 (2008).
[30] W. Handley, Phys. Rev. D **103**, L041301 (2021).
[31] E. Di Valentino, A. Melchiorri, and J. Silk, Nat. Astron. **4**, 196 (2019).
[32] E. Di Valentino, W. Giarè, A. Melchiorri, and J. Silk, Mon. Not. R. Astron. Soc. **520**, 210 (2023).
[33] W. Yang, W. Giarè, S. Pan, E. Di Valentino, A. Melchiorri, and J. Silk, arXiv:2210.09865.
[34] J. W. Henning *et al.* (SPT Collaboration), Astrophys. J. **852**, 97 (2018).
[35] F. Bianchini *et al.* (SPT Collaboration), Astrophys. J. **888**, 119 (2020).
[36] N. Aghanim *et al.* (Planck Collaboration), Astron. Astrophys. **641**, A8 (2020).
[37] S. W. Hawking, Phys. Lett. **115B**, 295 (1982).
[38] A. A. Starobinsky, Phys. Lett. **117B**, 175 (1982).
[39] A. H. Guth and S. Y. Pi, Phys. Rev. Lett. **49**, 1110 (1982).
[40] J. M. Bardeen, P. J. Steinhardt, and M. S. Turner, Phys. Rev. D **28**, 679 (1983).
[41] W. Fischler, B. Ratra, and L. Susskind, Nucl. Phys. **B259**, 730 (1985); **B268**, 747(E) (1986).
[42] E. R. Harrison, Phys. Rev. D **1**, 2726 (1970).
[43] P. J. E. Peebles and J. T. Yu, Astrophys. J. **162**, 815 (1970).
[44] Y. B. Zeldovich, Mon. Not. R. Astron. Soc. **160**, 1P (1972).
[45] F. Lucchin and S. Matarrese, Phys. Rev. D **32**, 1316 (1985).
[46] B. Ratra, Phys. Rev. D **40**, 3939 (1989).
[47] B. Ratra, Phys. Rev. D **45**, 1913 (1992).
[48] B. Ratra, Phys. Rev. D **96**, 103534 (2017).
[49] A. Guth, M. H. Namjoo, and B. Ratra (to be published).
[50] B. Ratra, Phys. Rev. D **106**, 123524 (2022).
[51] A. Lasenby and C. Doran, Phys. Rev. D **71**, 063502 (2005).
[52] E. Masso, S. Mohanty, A. Nautiyal, and G. Zsembinszki, Phys. Rev. D **78**, 043534 (2008).
[53] A. A. Asgari and A. H. Abbassi, Eur. Phys. J. C **75**, 544 (2015).
[54] B. Bonga, B. Gupt, and N. Yokomizo, J. Cosmol. Astropart. Phys. 10 (2016) 031.
[55] W. Handley and P. Lemos, Phys. Rev. D **100**, 043504 (2019).
[56] A. Thavanesan, D. Werth, and W. Handley, Phys. Rev. D **103**, 023519 (2021).
[57] C. Kiefer and T. Vardanyan, Gen. Relativ. Gravit. **54**, 30 (2022).
[58] L. T. Hergt, F. J. Agocs, W. J. Handley, M. P. Hobson, and A. N. Lasenby, Phys. Rev. D **106**, 063529 (2022).
[59] D. M. Scolnic *et al.*, Astrophys. J. **859**, 101 (2018).
[60] H. Yu, B. Ratra, and F.-Y. Wang, Astrophys. J. **856**, 3 (2018).
[61] S. Alam *et al.* (eBOSS Collaboration), Phys. Rev. D **103**, 083533 (2021).
[62] A. L. González-Morán, R. Chávez, R. Terlevich, E. Terlevich, F. Bresolin, D. Fernández-Arenas, M. Plionis, S. Basilakos, J. Melnick, and E. Telles, Mon. Not. R. Astron. Soc. **487**, 4669 (2019).
[63] S. Cao, J. Ryan, and B. Ratra, Mon. Not. R. Astron. Soc. **497**, 3191 (2020).
[64] S. Cao, J. Ryan, N. Khadka, and B. Ratra, Mon. Not. R. Astron. Soc. **501**, 1520 (2021).
[65] J. P. Johnson, A. Sangwan, and S. Shankaranarayanan, J. Cosmol. Astropart. Phys. 01 (2022) 024.
[66] A. Mehrabi *et al.*, Mon. Not. R. Astron. Soc. **509**, 224 (2022).
[67] S. Cao, X. Zheng, M. Biesiada, J. Qi, Y. Chen, and Z.-H. Zhu, Astron. Astrophys. **606**, A15 (2017).
[68] J. Ryan, Y. Chen, and B. Ratra, Mon. Not. R. Astron. Soc. **488**, 3844 (2019).
[69] Y. Lian, S. Cao, M. Biesiada, Y. Chen, Y. Zhang, and W. Guo, Mon. Not. R. Astron. Soc. **505**, 2111 (2021).
[70] S. Cao, J. Ryan, and B. Ratra, Mon. Not. R. Astron. Soc. **509**, 4745 (2022).
[71] Z. Yu *et al.* (OzDES Collaboration), Mon. Not. R. Astron. Soc. **507**, 3771 (2021).

[72] N. Khadka, Z. Yu, M. Zajaček, M. L. Martinez-Aldama, B. Czerny, and B. Ratra, Mon. Not. R. Astron. Soc. **508**, 4722 (2021).
[73] N. Khadka, M. L. Martínez-Aldama, M. Zajaček, B. Czerny, and B. Ratra, Mon. Not. R. Astron. Soc. **513**, 1985 (2022).
[74] N. Khadka, M. Zajaček, S. Panda, M. L. Martínez-Aldama, and B. Ratra, Mon. Not. R. Astron. Soc. **515**, 3729 (2022).
[75] S. Cao, M. Zajaček, S. Panda, M. L. Martínez-Aldama, B. Czerny, and B. Ratra, Mon. Not. R. Astron. Soc. **516**, 1721 (2022).
[76] Z. Yu *et al.* (OzDES Collaboration), arXiv:2208.05491.
[77] B. Czerny *et al.*, Astrophys. Space Sci. **368**, 8 (2023).
[78] G. Risaliti and E. Lusso, Nat. Astron. **3**, 272 (2019).
[79] N. Khadka and B. Ratra, Mon. Not. R. Astron. Soc. **492**, 4456 (2020).
[80] N. Khadka and B. Ratra, Mon. Not. R. Astron. Soc. **497**, 263 (2020).
[81] E. Lusso *et al.*, Astron. Astrophys. **642**, A150 (2020).
[82] N. Khadka and B. Ratra, Mon. Not. R. Astron. Soc. **502**, 6140 (2021).
[83] N. Khadka and B. Ratra, Mon. Not. R. Astron. Soc. **510**, 2753 (2022).
[84] M. Rezaei, J. Solà Peracaula, and M. Malekjani, Mon. Not. R. Astron. Soc. **509**, 2593 (2021).
[85] M. G. Dainotti, G. Bardiacchi, A. L. Lenart, S. Capozziello, E. O. Colgain, R. Solomon, D. Stojkovic, and M. M. Sheikh-Jabbari, Astrophys. J. **931**, 106 (2022).
[86] V. Petrosian, J. Singal, and S. Mutchnick, Astrophys. J. Lett. **935**, L19 (2022).
[87] N. Khadka, M. Zajaček, R. Prince, S. Panda, B. Czerny, M. L. Martínez-Aldama, V. K. Jaiswal, and B. Ratra, arXiv:2212.10483.
[88] F. F. Dirirsa, S. Razzaque, F. Piron, M. Arimoto, M. Axelsson, D. Kocevski, F. Longo, M. Ohno, and S. Zhu, Astrophys. J. **887**, 13 (2019).
[89] N. Khadka and B. Ratra, Mon. Not. R. Astron. Soc. **499**, 391 (2020).
[90] N. Khadka, O. Luongo, M. Muccino, and B. Ratra, J. Cosmol. Astropart. Phys. 09 (2021) 042.
[91] F. Y. Wang, J. P. Hu, G. Q. Zhang, and Z. G. Dai, Astrophys. J. **924**, 97 (2022).
[92] J. P. Hu, F. Y. Wang, and Z. G. Dai, Mon. Not. R. Astron. Soc. **507**, 730 (2021).
[93] S. Cao, N. Khadka, and B. Ratra, Mon. Not. R. Astron. Soc. **510**, 2928 (2022).
[94] O. Luongo and M. Muccino, Galaxies **9**, 77 (2021).
[95] S. Cao, M. Dainotti, and B. Ratra, Mon. Not. R. Astron. Soc. **512**, 439 (2022).
[96] Y. Liu, F. Chen, N. Liang, Z. Yuan, H. Yu, and P. Wu, Astrophys. J. **931**, 50 (2022).
[97] M. G. Dainotti, V. Nielson, G. Sarracino, E. Rinaldi, S. Nagataki, S. Capozziello, O. Y. Gnedin, and G. Bargiacchi, Mon. Not. R. Astron. Soc. **514**, 1828 (2022).
[98] S. Cao, M. Dainotti, and B. Ratra, Mon. Not. R. Astron. Soc. **516**, 1386 (2022).
[99] C.-G. Park and B. Ratra, Astrophys. Space Sci. **364**, 134 (2019).
[100] S. Cao, J. Ryan, and B. Ratra, Mon. Not. R. Astron. Soc. **504**, 300 (2021).
[101] S. Cao and B. Ratra, Mon. Not. R. Astron. Soc. **513**, 5686 (2022).
[102] S. Vagnozzi, A. Loeb, and M. Moresco, Astrophys. J. **908**, 84 (2021).
[103] R. Arjona and S. Nesseris, Phys. Rev. D **103**, 103539 (2021).
[104] S. Dhawan, J. Alsing, and S. Vagnozzi, Mon. Not. R. Astron. Soc. **506**, L1 (2021).
[105] J. E. Gonzalez, M. Benetti, R. von Marttens, and J. Alcaniz, J. Cosmol. Astropart. Phys. 11 (2021) 060.
[106] C.-Q. Geng, Y.-T. Hsu, and J.-R. Lu, Astrophys. J. **926**, 74 (2022).
[107] J.-J. Wei and F. Melia, Astrophys. J. **928**, 165 (2022).
[108] P. Mukherjee and N. Banerjee, Phys. Rev. D **105**, 063516 (2022).
[109] P.-J. Wu, J.-Z. Qi, and X. Zhang, arXiv:2209.08502.
[110] S. Baumgartner and J. Yoo, J. Cosmol. Astropart. Phys. 08 (2022) 077.
[111] S. Anselmi, M. F. Carney, J. T. Giblin, S. Kumar, J. B. Mertens, M. ODwyer, G. D. Starkman, and C. Tian, arXiv:2207.06547.
[112] R. Jimenez, A. R. Khalife, D. F. Litim, S. Matarrese, and B. D. Wandelt, arXiv:2210.10102.
[113] A. Gómez-Valent and J. Solà Peracaula, Mon. Not. R. Astron. Soc. **478**, 126 (2018).
[114] J. Ooba, B. Ratra, and N. Sugiyama, Astrophys. Space Sci. **364**, 176 (2019).
[115] J. Ryan, S. Doshi, and B. Ratra, Mon. Not. R. Astron. Soc. **480**, 759 (2018).
[116] J. Sola Peracaula, A. Gomez-Valent, and J. de Cruz Pérez, Phys. Dark Universe **25**, 100311 (2019).
[117] A. Singh, A. Sangwan, and H. K. Jassal, J. Cosmol. Astropart. Phys. 04 (2019) 047.
[118] C.-G. Park and B. Ratra, Phys. Rev. D **101**, 083508 (2020).
[119] A. Gómez-Valent, V. Pettorino, and L. Amendola, Phys. Rev. D **101**, 123513 (2020).
[120] C. Moreno-Pulido and J. Solà, Eur. Phys. J. C **80**, 692 (2020).
[121] S. Sinha and N. Banerjee, J. Cosmol. Astropart. Phys. 04 (2021) 060.
[122] L. A. Ureña López and N. Roy, Phys. Rev. D **102**, 063510 (2020).
[123] J. Solà Peracaula, A. Gómez-Valent, J. de Cruz Perez, and C. Moreno-Pulido, Europhys. Lett. **134**, 19001 (2021).
[124] T. Xu, Y. Chen, L. Xu, and S. Cao, Phys. Dark Universe **36**, 101023 (2022).
[125] J. F. Jesus, R. Valentim, A. A. Escobal, S. H. Pereira, and D. Benndorf, J. Cosmol. Astropart. Phys. 11 (2022) 037.
[126] C. Moreno-Pulido and J. Sola Peracaula, Eur. Phys. J. C **82**, 551 (2022).
[127] A. Adil, A. Albrecht, and L. Knox, arXiv:2207.10235.
[128] H. Gil-Marin *et al.*, Mon. Not. R. Astron. Soc. **498**, 2492 (2020).
[129] J. E. Bautista *et al.*, Mon. Not. R. Astron. Soc. **500**, 736 (2020).
[130] J. Hou *et al.*, Mon. Not. R. Astron. Soc. **500**, 1201 (2020).
[131] R. Neveux *et al.*, Mon. Not. R. Astron. Soc. **499**, 210 (2020).
[132] P. Carter, F. Beutler, W. J. Percival, C. Blake, J. Koda, and A. J. Ross, Mon. Not. R. Astron. Soc. **481**, 2371 (2018).

[133] T. M. C. Abbott *et al.* (DES Collaboration), Mon. Not. R. Astron. Soc. **483**, 4866 (2019).
[134] H. du Mas des Bourboux *et al.*, Astrophys. J. **901**, 153 (2020).
[135] S. J. Turnbull, M. J. Hudson, H. A. Feldman, M. Hicken, R. P. Kirshner, and R. Watkins, Mon. Not. R. Astron. Soc. **420**, 447 (2012).
[136] M. J. Hudson and S. J. Turnbull, Astrophys. J. Lett. **751**, L30 (2013).
[137] K. Said, M. Colless, C. Magoulas, J. R. Lucey, and M. J. Hudson, Mon. Not. R. Astron. Soc. **497**, 1275 (2020).
[138] F. Shi *et al.*, Astrophys. J. **861**, 137 (2018).
[139] F. Simpson, C. Blake, J. A. Peacock, I. Baldry, J. Bland-Hawthorn, A. Heavens, C. Heymans, J. Loveday, and P. Norberg, Phys. Rev. D **93**, 023525 (2016).
[140] C. Blake *et al.*, Mon. Not. R. Astron. Soc. **436**, 3089 (2013).
[141] F. G. Mohammad *et al.*, Astron. Astrophys. **619**, A17 (2018).
[142] T. Okumura *et al.*, Publ. Astron. Soc. Jpn. **68**, 38 (2016).
[143] T. M. C. Abbott *et al.* (DES Collaboration), Astrophys. J. Lett. **872**, L30 (2019).
[144] C.-G. Park and B. Ratra, Astrophys. J. **882**, 158 (2019).
[145] A. Challinor and A. Lasenby, Astrophys. J. **513**, 1 (1999).
[146] A. Lewis, A. Challinor, and A. Lasenby, Astrophys. J. **538**, 473 (2000).
[147] A. Lewis and S. Bridle, Phys. Rev. D **66**, 103511 (2002).
[148] D. Blas, J. Lesgourgues, and T. Tram, J. Cosmol. Astropart. Phys. 07 (2011) 034.
[149] B. Audren, J. Lesgourgues, K. Benabed, and S. Prunet, J. Cosmol. Astropart. Phys. 02 (2013) 001.
[150] J. Ooba, B. Ratra, and N. Sugiyama, Astrophys. J. **864**, 80 (2018).
[151] J. Ooba, B. Ratra, and N. Sugiyama, Astrophys. J. **869**, 34 (2018).
[152] J. Ooba, B. Ratra, and N. Sugiyama, Astrophys. J. **866**, 68 (2018).
[153] C.-G. Park and B. Ratra, Astrophys. Space Sci. **364**, 82 (2019).
[154] C.-G. Park and B. Ratra, Astrophys. J. **868**, 83 (2018).
[155] J. Lesgourgues and T. Tram, J. Cosmol. Astropart. Phys. 09 (2014) 032.
[156] A. Lewis (2019), arXiv:1910.13970.
[157] H. Akaike, IEEE Trans. Autom. Control **19**, 716 (1974).
[158] K. P. Burnham and D. R. Anderson, *Model Selection and Multimodel Inference* (Springer, New York, 2002).
[159] D. J. Spiegelhalter, N. G. Best, B. P. Carlin, and A. van der Linde, J. R. Stat. Soc. **64**, 583 (2002).
[160] A. R. Liddle, Mon. Not. R. Astron. Soc. **377**, L74 (2007).
[161] S. Joudaki *et al.*, Mon. Not. R. Astron. Soc. **465**, 2033 (2017).
[162] W. Handley and P. Lemos, Phys. Rev. D **100**, 023512 (2019).
[163] A. Heavens, Y. Fantaye, E. Sellentin, H. Eggers, Z. Hosenie, S. Kroon, A. Mootoovaloo, Phys. Rev. Lett. **119**, 101301 (2017).
[164] C. E. Shannon, Bell Syst. Tech. J. **27**, 379 (1948).
[165] E. Di Valentino, A. Melchiorri, and J. Silk, Astrophys. J. Lett. **908**, L9 (2021).
[166] G. Chen and B. Ratra, Publ. Astron. Soc. Pac. **123**, 1127 (2011).
[167] J. R. Gott III, M. S. Vogeley, S. Podariu, and B. Ratra, Astrophys. J. **549**, 1 (2001).
[168] E. Calabrese, M. Archidiacono, A. Melchiorri, and B. Ratra, Phys. Rev. D **86**, 043520 (2012).
[169] W. L. Freedman, Astrophys. J. **919**, 16 (2021).
[170] A. G. Riess *et al.*, Astrophys. J. Lett. **934**, L7 (2022).
[171] A. Glanville, C. Howlett, and T. M. Davis, Mon. Not. R. Astron. Soc. **517**, 3087 (2022).